MECHANOBIOLOGY OF STEM CELLS: IMPLICATIONS FOR VASCULAR TISSUE ENGINEERING

by

Timothy Maul

Bachelor of Science, University of Pittsburgh, 2001

Submitted to the Graduate Faculty of

School of Engineering in partial fulfillment

of the requirements for the degree of

Doctor of Philosophy

University of Pittsburgh

2007

UNIVERSITY OF PITTSBURGH

SCHOOL OF ENGINEERING

This dissertation was presented

by

Timothy M. Maul

It was defended on

October 1st, 2007

and approved by

Dr. William R. Wagner, PhD, Professor, Departments of Surgery and Bioengineering

Dr. Johnny Huard, PhD, Associate Professor, Departments of Orthopaedic Surgery and Bioengineering

Dr. Satdarshan Monga, MD, Associate Professor, Department of Pathology

Dissertation Director: Dr. David A. Vorp, PhD, Associate Professor, Departments of Surgery and Bioengineering

MECHANOBIOLOGY OF STEM CELLS: IMPLICATIONS FOR VASCULAR TISSUE ENGINEERING

Timothy M. Maul, PhD

University of Pittsburgh, 2007

Current challenges in vascular medicine (e.g., bypass grafting, stenting, and angioplasty.) have driven the field of vascular regenerative medicine. Bone marrow-derived mesenchymal stem cells (BMMSCs) are adult stem cells which may be a suitable cell source for vascular regenerative medicine applications. While it is well known that BMMSCs readily differentiate into musculoskeletal cells, recent studies have provided evidence for their differentiation into smooth muscle cells (SMCs) and endothelial cells (ECs). We and others have demonstrated the ability of the mechanical stimulus of cyclic stretch to drive BMMSC differentiation towards SMCs *in vitro*, but a rigorous, systematic analysis of other relevant forces is lacking. The working hypothesis that this work addressed is that mechanical stimuli relevant to the vasculature will guide BMMSC differentiation towards SMCs and ECs.

To test this hypothesis, rat BMMSCs were exposed to physiologically relevant magnitudes and frequencies of a Mechanical Panel, which consisted of cyclic stretch, cyclic pressure, and shear stress, each applied in parallel to subcultures of BMMSCs. Quantitative changes in morphology, proliferation, and gene and protein expression were assessed to determine the differential effect of each stimulus in a dose- and frequency-dependant manner. Next, we investigated the importance of the duration of applied stimulation to BMMSC differentiation as well as tissue commitment (i.e., cell plasticity) following mechanical stimulation.

Our results demonstrate that mechanical stimulation differentially altered BMMSC morphology, proliferation, and gene and protein expression towards the cardiovascular lineage while limiting expression for other lineages including bone, fat, and chondrocyte. This was particularly evident for cyclic stretch, which caused an elongated, spindle-shape and expression of the SMC proteins α-actin, calponin, and myosin heavy chain. Furthermore, we found that cyclic pressure and shear stress tended to increase endothelial gene expression when these stimuli are applied to confluent BMMSCs. While our findings as a whole tended to support our hypothesis, our data indicate that SMC protein expression is more readily increased by mechanical stimulation, and is highly variable, even without associated changes in gene expression. Future work employing systems biology approaches that take into consideration the resulting transcriptional and proteomic changes in BMMSCs from these mechanical stimuli will be necessary to more accurately identify how mechanical stimulation can be used as a tool for regenerative medicine.

TABLE OF CONTENTS

ACKNOWLEDGEMENTS XXXIV

1.0 INTRODUCTION 1

1.1 VASCULAR DISEASE 1

1.1.1 Vascular conduits 2

1.1.2 Angioplasty and vascular stenting 3

1.1.3 Regenerative medicine 4

1.2 SMOOTH MUSCLE CELLS 5

1.2.1 Development and basic biology 5

1.2.1.1 Smooth muscle α-actin 8

1.2.1.2 Calponin 8

1.2.1.3 SM22α 9

1.2.1.4 Caldesmon 10

1.2.1.5 Smoothelin 10

1.2.1.6 Myosin Heavy Chain 11

1.2.1.7 Myocardin 11

1.2.2 Response to biological factors 12

1.2.2.1 Platelet derived growth factor (PDGF) 12

1.2.2.2 Transforming growth factor beta (TGF-β) 14

1.2.2.3 Fibroblast growth factor (FGF) 17

1.2.3 Response to mechanical stimuli 18

1.2.3.1 Stretch 22

1.2.3.2 Pressure 25

1.2.3.3 Shear stress 26

1.3 ENDOTHELIAL CELLS 27

1.3.1 Development and basic biology 27

1.3.1.1 Flk-1 28

1.3.1.2 Platelet-endothelial cell adhesion molecule (PECAM) 29

1.3.1.3 Tie Receptors 30

1.3.1.4 Vascular endothelial cadherin (VE-Cadherin) 30

1.3.1.5 von Willebrand factor (vWF) 31

1.3.2 Response to biological factors 32

1.3.2.1 Vascular endothelial growth factor (VEGF) 32

1.3.2.2 TGF-β 35

1.3.2.3 FGF 37

1.3.2.4 PDGF 38

1.3.3 Response to mechanical stimuli 39

1.3.3.1 Stretch 39

1.3.3.2 Pressure 41

1.3.3.3 Shear 43

1.4 ADULT STEM CELLS 48

1.4.1 Definition of stem cells 48

1.4.2 Differentiation of BMMSCs 49
1.4.2.1 Biological and biochemical factors 50
1.4.2.2 Mechanical stimulation 52
1.5 SUMMARY AND LIMITATIONS OF PREVIOUS RESEARCH 60
1.6 HYPOTHESIS AND SPECIFIC AIMS 61
2.0 DEVELOPMENT OF A CYCLIC PRESSURE BIOREACTOR 63
2.1 INTRODUCTION 63
2.1.1 Overall goals 63
2.1.2 Prior art and limitations 64
2.2 METHODS 66
2.2.1 Design considerations 66
2.2.1.1 Minimal size 66
2.2.1.2 Environmental stability 67
2.2.1.3 Maximum accessibility 67
2.2.1.4 Versatility 68
2.2.1.5 Humidifier designs 71
2.2.2 Computational fluid dynamics 74
2.2.2.1 Mesh development 74
2.2.2.2 Boundary conditions 76
2.2.2.3 Solution Parameters 76
2.2.3 Biological validation 77
2.2.3.1 Cell source 78
2.2.3.2 BMMSC characterization 79

2.2.3.3 Pressure conditions 80
2.2.3.4 Dissolved gas measurements 80
2.2.3.5 Relative humidity calculation 81
2.2.3.6 Viability analysis 81
2.2.3.7 Glycosaminoglycan staining 82
2.2.3.8 Morphology analysis 82
2.2.3.9 Proliferation Analysis 82
2.2.3.10 Statistical analysis 83
2.3 RESULTS 83
2.3.1 Pressure waveforms 83
2.3.2 CFD results 85
2.3.3 Dissolved gas and relative humidity results 89
2.3.4 AHC viability 91
2.3.5 GAG production in AHCs 91
2.3.6 BMMSC morphology and proliferation, and differentiation 92
2.4 DISCUSSION 94
2.4.1 Limitations 95
2.5 CONCLUSIONS 96
3.0 THE MECHANICAL PANEL 97
3.1 INTRODUCTION 97
3.1.1 Definition and advantages of the Mechanical Panel 97
3.2 METHODS 99
3.2.1 Cell source 99

3.2.1.1 Assessment of the multipotentiality of tBMMSCs 99
3.2.2 Device descriptions 101
3.2.2.1 Cyclic stretch apparatus 101
3.2.2.2 Shear stress apparatus 102
3.2.2.3 Cyclic pressure apparatus 103
3.2.3 Experimental Design 104
3.2.3.1 Substrate 104
3.2.3.2 Dose-response of tBMMSCs to mechanical stimulation 105
3.2.4 Endpoint assessment 107
3.2.4.1 Morphology 107
3.2.4.2 Proliferation 108
3.2.4.3 Histology 109
3.2.4.4 Immunohistochemistry (IHC) 109
3.2.4.5 RNA isolation and PCR 112
3.2.5 Data storage and statistical analysis 120
3.2.5.1 Database design and utilization 120
3.2.5.2 Statistical analysis from database contents 120
3.3 RESULTS 124
3.3.1 Multipotentiality of tBMMSC 124
3.3.2 Morphology 125
3.3.2.1 Area changes 125
3.3.2.2 Major axis changes 129
3.3.2.3 Shape index changes 132

3.3.2.4 Tortuosity index changes 135
3.3.2.5 Changes in angle of alignment 138
3.3.3 Proliferation 142
3.3.4 Histology 145
3.3.5 Immunohistochemistry 147
3.3.6 Gene expression 156
3.3.6.1 Muscle-related genes 158
3.3.6.2 Endothelial-related genes 160
3.3.6.3 Soluble factor- and apoptosis-related gene expression 162
3.3.6.4 Extracellular matrix-related gene expression 163
3.3.6.5 Stem-cell related gene expression 164
3.3.6.6 Osteoblast-related gene expression 165
3.3.6.7 Chondrocyte- and adipocyte-related gene expression 166
3.4 DISCUSSION 167
3.4.1 Differential morphology and proliferation changes 167
3.4.2 Differential protein expression 172
3.4.3 Differential gene expression 174
3.4.4 Limitations 176
3.5 CONCLUSION 179
4.0 TEMPORAL RESPONSE TO MECHANICAL STIMULATION 180
4.1 INTRODUCTION 180
4.2 METHODS 181
4.2.1 Experimental design 181

4.2.1.1 Time points 181

4.2.1.2 Cell source 181

4.2.1.3 Mechanical panel parameters 182

4.2.2 Endpoints 183

4.2.2.1 RNA isolation and qualitative assessment 183

4.2.2.2 TaqMan® RT-PCR Low Density Array 184

4.2.2.3 Protein isolation and quantification 188

4.2.2.4 Western blotting 190

4.2.3 Statistical analysis 193

4.3 RESULTS 194

4.3.1 Determination of endogenous control gene 194

4.3.2 Gene Expression 196

4.3.2.1 Muscle related genes 196

4.3.2.2 Endothelial Related Genes 198

4.3.2.3 Soluble factor-related genes 199

4.3.2.4 Extracellular matrix-related gene expression 200

4.3.2.5 Stem cell-related gene expression 201

4.3.2.6 Osteoblast-related gene expression 202

4.3.2.7 Chondrocyte-related gene expression 203

4.3.2.8 Adipocyte-related gene expression 205

4.3.2.9 Proliferation-related gene expression 205

4.3.3 Protein expression 206

4.3.3.1 Calponin 207

4.4 DISCUSSION 208
4.4.1 The importance of choosing an appropriate endogenous control gene 208
4.4.2 Temporal changes in gene expression 210
4.4.3 Temporal changes in calponin expression 216
4.4.4 Limitations 217
4.5 CONCLUSION 218
5.0 LINEAGE COMMITMENT FOLLOWING MECHANICAL STIMULATION .. 220
5.1 INTRODUCTION 220
5.2 METHODS 221
5.2.1 Experimental Design 221
5.3 RESULTS 221
5.3.1 Gene expression 221
5.3.1.1 Muscle related genes 221
5.3.1.2 Endothelial Related Genes 222
5.3.1.3 Soluble factor -related genes 223
5.3.1.4 Extracellular matrix-related gene expression 224
5.3.1.5 Stem-cell related gene expression 225
5.3.1.6 Osteoblast-related gene expression 226
5.3.1.7 Chondrocyte-related gene expression 226
5.3.1.8 Adipocyte-related gene expression 227
5.3.1.9 Proliferation-related gene expression 228
5.3.2 Protein expression 228
5.4 DISCUSSION 230

5.4.1 Limitations 232
5.5 CONCLUSION 232
6.0 DISCUSSION 234
6.1 SUMMARY OF RESULTS 234
6.1.1 Specific aim 1 234
6.1.2 Specific Aim 2 235
6.1.3 Specific Aim 3 237
6.1.4 Specific Aim 4 238
6.2 APPLICATIONS FOR VASCULAR REGENERATIVE MEDICINE 239
6.3 ADVANTAGES OF METHODOLOGY 240
6.4 LIMITATIONS OF METHODOLOGY 241
6.5 FUTURE WORK 243
APPENDIX A 245
APPENDIX B 247
APPENDIX C 251
APPENDIX D 252
APPENDIX E 259
APPENDIX F 273
APPENDIX G 276
APPENDIX H 278
APPENDIX I 281
APPENDIX J 282
BIBLIOGRAPHY 292

LIST OF TABLES

Table 1.1: Comparison of SMC contractile proteins, their exclusivity to SMCs, and presence in different SMC phenotypes. ++ indicates definitively positive expression; +/- indicates transient expression or conflicting reports; and -- indicates definitively negative expression. Table adapted from [66]..... 7

Table 1.2: Multiple cell types express different isoforms of PDGF and PDGF receptor (PDGFR) [109]. 13

Table 1.3: The effects of shear stress on EC gene and protein expression. Solid arrows indicate up (↑), down (↓), or no change (→) in gene or protein expression of each factor. Double arrows indicate the sustainability of the signal as up (⇑), down (⇓), or returning to baseline (⇔). The type and magnitude (in parenthesis) of each shear stress is indicated in the magnitude column. L=laminar; T=turbulent; I=impulse;O=oscillatory; P=pulsatile. Table adapted from [244]. 46

Table 1.4: Differentiation of BMMSCs can be induced by a variety of biological and biochemical agents. 51

Table 1.5: Effects of mechanical stimulation of BMMSCs and ESCS. Solid arrows indicate up (↑), down (↓), or no change (↔) in each factor. Double arrows indicate signal sustainability as up (⇑), down (⇓), or returning to baseline (⇔). CS=cyclic stretch,

PF=pulsatile flow; LSS=laminar shear stress; CP=cyclic pressure; OFF=oscillatory fluid flow; UN=uniaxial; EQ=equiaxial; OI=osteo-inductive media; AI=adipo-inductive media; IM=intermittent/ <0.5 Hz; Magnitudes listed in parenthesis % for CS; dynes/cm^2 for LSS, PF, and OFF; and mmHg for CP. 59

Table 2.1: Physical properties of the air and water used in the CFD model of the cyclic pressure chamber. 77

Table 3.1: Applied stimuli for Mechanical Panel experiments to determine the dose-response of tBMMSCs to different magnitudes and frequencies of mechanical stimulation. See text for further detail about stimulus headings. Parenthetical terms denote abbreviations for each of the stimuli. For example, CS-1 denotes 1% 1 Hz cyclic stretch, and LSS-1 denotes 1 dyne/cm^2 laminar shear stress. CS-1HF denotes cyclic stretch at 1% at 2.75 Hz stimulation (high frequency)..... 107

Table 3.2: Antibodies and dilutions for IHC 111

Table 3.3: Thermal cycler protcol used for RT reaction..... 115

Table 3.4: List of TaqMan® PCR primers, their classifications and catalog numbers for the first custom-designed TLDA 117

Table 3.5: Fold changes in muscle-related gene expression relative to control for each component of the Mechanical Panel as analyzed by the low density qPCR. Green and red highlights indicate an average fold change greater than 1.3 or less than 0.7 (considered biologically relevant), respectively. Data are presented as the mean ± SD with sample numbers. + $p<0.10$, *$p<0.05$, and ND=No detectable transcripts. 159

Table 3.6: Fold changes in endothelial-related gene expression relative to control for each component of the Mechanical Panel as analyzed by the low density qPCR. Green and

red highlights indicate an average fold change greater than 1.3 or less than 0.7 (considered biologically relevant), respectively. Data are presented as the mean ± SD with sample numbers. + p<0.10, *p<0.05, compared to controls, and ND=No detectable transcripts. 161

Table 3.7: Fold changes in soluble factor and apoptosis-related gene expression relative to control for each component of the Mechanical Panel as analyzed by the low density qPCR. Green and red highlights indicate an average fold change greater than 1.3 or less than 0.7 (considered biologically relevant), respectively. Data are presented as the mean ± SD with sample numbers. + p<0.10, *p<0.05 compared to controls, and ND=No detectable transcripts. 163

Table 3.8: Fold changes in extracellular matrix-related gene expression relative to control for each component of the Mechanical Panel as analyzed by the low density qPCR. Green and red highlights indicate an average fold change greater than 1.3 or less than 0.7 (considered biologically relevant), respectively. Data are presented as the mean ± SD with sample numbers. + p<0.10, *p<0.05, compared to controls, and ND=No detectable transcripts. 164

Table 3.9: Fold changes in stem cell-related gene expression relative to control for each component of the Mechanical Panel as analyzed by the low density qPCR. Green and red highlights indicate an average fold change greater than 1.3 or less than 0.7 (considered biologically relevant), respectively. Data are presented as the mean ± SD with sample numbers. + p<0.10, *p<0.05, compared to controls. 165

Table 3.10: Fold changes in osteoblast-related gene expression relative to control for each component of the Mechanical Panel as analyzed by the low density qPCR. Green and

red highlights indicate an average fold change greater than 1.3 or less than 0.7 (considered biologically relevant), respectively. Data are presented as the mean ± SD with sample numbers. + $p<0.10$, *$p<0.05$ compared to controls, and ND=No detectable transcripts. 166

Table 3.11: Fold changes in chondrocyte and adipocyte-related gene expression relative to control for each component of the Mechanical Panel as analyzed by the low density qPCR. Green and red highlights indicate an average fold change greater than 1.3 or less than 0.7 (considered biologically relevant), respectively. Data are presented as the mean ± SD with sample numbers. + $p<0.10$, *$p<0.05$ compared to controls, and ND=No detectable transcripts. 167

Table 3.12: Summary of the morphology and proliferation results for the 5 day Mechanical Panel experiments. Double arrows indicate a significant increase or decrease ($p<0.05$) in the measured parameter from control values. Single arrows denote a moderate ($p<0.10$) change in the measured parameter. $\perp$ and || indicate significant perpendicular and parallel alignment ($p<0.05$), respectively..... 168

Table 3.13: Linear regression output from SPSS for proliferation regressed against area and shape index. Despite the weak correlation between shape index and area, they do not exhibit colinearity, and are therefore suitably compatible in the linear regression model. 171

Table 3.14: Summary of IHC results for Mechanical Panel experiments. ++ indicates strong homogenous staining intensity. + indicates a moderate to weak homogeneous staining intensity. +/- indicates heterogenous staining. – indicates no staining was evident. 172

Table 4.1: Stimulation regimens used for Mechanical Panel experiments to determine the temporal response of tBMMSCs to mechanical stimulation. tBMMSCs were exposed to these conditions for 24 hours or 3 days. 183

Table 4.2: List of TaqMan® PCR primers, classifications, and catalog numbers for the second custom-designed TLDA card. Many of the genes listed in the first card (see Table 3.4) that are not found on the second card were removed because of their lack of expression, or were moved to single assays because we wished to examine the primer in conjunction with a non-inventoried primer that could not be placed on a TLDA. 185

Table 4.3: Sample list analyzed by the endogenous control TLDA. The samples were chosen to represent each component of the Mechanical Panel at different magnitudes, frequencies, times of exposure, and confluence..... 187

Table 4.4: List of the endogenous control genes used in the Endogenous Control TLDA. Each of these endogenous control genes have been commonly employed in research involving gene expression..... 188

Table 4.5: Transfer solutions and settings for each protein endpoint interrogated by Western blotting. 191

Table 4.6: Reagent details for each of the endpoints interrogated by Western blotting..... 192

Table 4.7: Table depicting the average and variance of the C_T for each of the potential endogenous control genes. 196

Table 4.8: Fold changes in muscle-related gene expression relative to control for each component of the Mechanical Panel. Green and red highlights indicate an average fold change greater than 1.3 or less than 0.7 (considered biologically relevant),

respectively. Data are presented as the mean ± SD with sample numbers. + p<0.10, *p<0.05, vs. controls. 197

Table 4.9: Fold changes in endothelial-related gene expression relative to control for each component of the Mechanical Panel. Green and red highlights indicate an average fold change greater than 1.3 or less than 0.7 (considered biologically relevant), respectively. Data are presented as the mean ± SD with sample numbers. + p<0.10, *p<0.05 vs. controls. 199

Table 4.10: Fold changes in soluble factor-related gene expression relative to control for each component of the Mechanical Panel. Green highlights indicate an average fold change greater than 1.3 (considered biologically relevant), respectively. Data are presented as the mean ± SD with sample numbers. + p<0.10, *p<0.05 vs. controls. 200

Table 4.11: Fold changes in ECM-related gene expression relative to the control for each component of the Mechanical Panel. Green and red highlights indicate an average fold change greater than 1.3 or less than 0.7 (considered biologically relevant), respectively. Data are presented as the mean ± SD with sample numbers. + p<0.10, *p<0.05 vs. controls. 201

Table 4.12: Fold changes in stem cell-related gene expression relative to control for each component of the Mechanical Panel. Green and red highlights indicate an average fold change greater than 1.3 or less than 0.7 (considered biologically relevant), respectively. Data are presented as the mean ± SD with sample numbers. + p<0.10, *p<0.05 vs. controls. 202

Table 4.13: Fold changes in osteoblast-related gene expression relative to control for each component of the Mechanical Panel. Green and red highlights indicate an average

fold change greater than 1.3 or less than 0.7 (considered biologically relevant), respectively. Data are presented as the mean ± SD with sample numbers. + $p<0.10$, *$p<0.05$ vs. controls. 203

Table 4.14: Fold changes in chondrocyte-related gene expression relative to control for each component of the Mechanical Panel. Green and red highlights indicate an average fold change greater than 1.3 or less than 0.7 (considered biologically relevant), respectively. Data are presented as the mean ± SD with sample numbers. + $p<0.10$, *$p<0.05$ vs. controls. 204

Table 4.15: Fold changes in PPAR-γ expression relative to control for each component of the Mechanical Panel. Green and red highlights indicate an average fold change greater than 1.3 or less than 0.7 (considered biologically relevant), respectively. Data are presented as the mean ± SD with sample numbers. No significant differences were found compared to controls. 205

Table 4.16: Fold changes in cyclin B1-related gene expression relative to control for each component of the Mechanical Panel. Green and red highlights indicate an average fold change greater than 1.3 or less than 0.7 (considered biologically relevant), respectively. Data are presented as the mean ± SD with sample numbers. + $p<0.10$, *$p<0.05$ vs. controls. 206

Table 4.17: Summary of the changes in gene expression for phenotypic groups by mechanical stimulation. To give some global sense to the data, a change index (CI) was calculated by averaging a score of 0 for no change, +/- 1 for a biological or statistical ($p<0.1$) trend, and +/- 2 for a biologically relevant and statistically significant change for each of the genes in that category. ↑↑ and ↓↓ indicate a majority increase or decrease

(CI>0.75) in the overall gene expression for that group from control values. Single arrows denote a moderate change (0.25≤CI≤0.75) in the majority of the genes for a particular phenotype, and ↔ indicates no change (CI<0.25). 210

Table 5.1: Fold changes in muscle-related gene expression relative to control for CS or DeDiff samples. Green highlights indicate an average fold change greater than 1.3 (considered biologically relevant). Data are presented as the mean ± SD with sample numbers. +p<0.10, vs. controls. 222

Table 5.2: Fold changes in endothelial-related gene expression relative to control for CS and DeDiff samples. Green and red highlights indicate an average fold change greater than 1.3 or less than 0.7 (considered biologically relevant), respectively. Data are presented as the mean ± SD with sample numbers. + p<0.10, *p<0.05 vs. controls.223

Table 5.3: Fold changes in soluble factor-related gene expression relative to control for CS and DeDiff samples. Green highlights indicate an average fold change greater than 1.3 (considered biologically relevant). Data are presented as the mean ± SD with sample numbers. No statistically significant differences were found for CS-10 or DeDiff when compared to controls. 224

Table 5.4: Fold changes in extracellular matrix-related gene expression relative to control for CS and DeDiff samples. Green and red highlights indicate an average fold change greater than 1.3 or less than 0.7 (considered biologically relevant), respectively. Data are presented as the mean ± SD with sample numbers. No statistically significant differences were found for CS-10 or DeDiff when compared to controls. 225

Table 5.5: Fold changes in stem cell-related gene expression relative to control for CS and DeDiff samples. Green highlights indicate an average fold change greater than 1.3

(considered biologically relevant). Data are presented as the mean ± SD with sample numbers. *p<0.05 vs. controls. 225

Table 5.6: Fold changes in osteoblast-related gene expression relative to control for CS and DeDiff samples. Green highlights indicate an average fold change greater than 1.3 (considered biologically relevant). Data are presented as the mean ± SD with sample numbers. *p<0.05 vs. controls. 226

Table 5.7: Fold changes in chondrocyte-related gene expression relative to control for CS and DeDiff samples. Green indicate an average fold change greater than 1.3 (considered biologically relevant). Data are presented as the mean ± SD with sample numbers. No statistically significant differences were found for CS-10 or DeDiff when compared to controls. 227

Table 5.8: Fold changes in PPAR-γ expression relative to control for CS and DeDiff samples. Data are presented as the mean ± SD. No biologically relevant (±1.3 fold change) or statistically significant changes were found for CS-10 or DeDiff compared to controls. 227

Table 5.9: Fold changes in cyclin B1-related gene expression relative to control for CS and DeDiff samples. Green highlights indicate an average fold change greater than 1.3 (considered biologically relevant). Data are presented as the mean ± SD. No statistically significant differences were found for CS-10 or DeDiff when compared to controls. 228

Table 5.10: Summary of the statistically significant changes in gene expression following removal of the cyclic stretch stimulation in the tBMMSCs. 231

LIST OF FIGURES

Figure 1.1: SMC phenotypic switching occurs from various external stimuli. Reprinted with permission from [62]. 7

Figure 1.2: Mechanical stimulation plays an important role in vascular biology because blood vessels undergo multiple types of mechanical stimulation throughout each cardiac cycle. Reprinted with permission from IOS Press [188]. 19

Figure 1.3: Schematic of cellular mechanisms for sensing mechanical signals which are relevant to vascular SMCs and ECs. Figure adapted from [191]. 21

Figure 1.4: Various levels of cyclic stretch can induce multiple phenotypic changes in SMCs. Adapted from [189]. 24

Figure 1.5: VEGF signaling in ECs is mediated through two VEGF receptors to increase survival, proliferation, migration, and production of vasoactive agents including NO and PGI_2. Figure adapted from [253]. 34

Figure 1.6: TGF-β signaling in ECs can elicit two different responses depending upon the type of receptor the ligands bind. This may account for the multiple phenotypes seen with embryonic TGF-β knockouts [325] as well as reports of transdifferentiation to SMCs [77, 78, 326]. 36

Figure 1.7: The effects of shear stress on ECs depend upon the temporal exposure and type of shear stress. Chronic exposure to laminar shear is atheroprotective while both acute

and chronic exposure to disturbed shear stress leads to atherogenesis. Acute changes in the laminar shear region lead to adaptive changes such as vascular remodeling and arteriogenesis. Reprinted with permission from Elsevier [360]..... 47

Figure 1.8: The application of cyclic uniaxial stretch to BMMSCs leads to the production of smooth muscle proteins (A) SMA and (B) h1-calponin. Control cultures (C-D) were negative for (C) SMA and (D) h1-calponin. Figure adapted from [526]..... 54

Figure 2.1: Schematic of the cyclic hydrostatic pressure system designed during the execution of Specific Aim 1. A constant pressure source (a) provides the bulk airflow that powers the cyclic pressure system, and consists of an in-house air pump and pure CO_2 blended together to achieve 5% CO_2, 20% O_2, and 75% N_2. A heated passover circuit (b) humidifies the air to ~100% before it passes through a resistor that controls the mean pressure (c). The air then passes through a sterile filter (d) before it enters the culture chamber (e) and builds a static pressure in the dead space above the culture media. Two stainless steel bars (f) deflect the incoming air and provide weight to stabilize the culture surface. An injection port (g) provides access for media sampling or chemical injection. The air then passes through a second sterile filter (h) on its way to a solenoid valve (i). When the valve is closed, pressure builds inside the system. When the valve is open, the pressure is released through a second resistor (j) that controls the diastolic pressure. Two pressure transducers (k) and their associated monitor (m) display the pressure inside the cyclic pressure chamber. A check valve (l), which has a cracking pressure of 250mmHg, allows the system to release built-up pressure in the event that one of the filters becomes obstructed. The dashed box represents the interior of the incubator. Figure reproduced with permission from ASME [1]..... 69

Figure 2.2: A three-dimensional exploded view (to scale) of the cyclic hydrostatic pressure chamber (see Figure 2.1e) depicting the lid with the inlet, outlet, and sampling ports, 6 culture slides, o-ring groove, and stainless steel bars. Figure reproduced with permission from ASME [1]..... 70

Figure 2.3: Progression of humidification system design for the cyclic pressure system. (A) Simple bubble humidifier kept at 37^{o}C. (B) The simple bubble humidifier with the added heating element (callout) to increase the air temperature prior to entry into the bubble humidifier. (C) Adding a bubbling stone increased the surface area available to pick up moisture. (D) Increasing the volume of the bubble humidifier increased the residence time for air. (E) The MR730 respiratory humidifier finally chosen as the best possible humidification system. (F) Table depicting the increased humidity achieved with each successive improvement to the humidification system. The increase in volume did not add any increase in relative humidity. The heated passover humidifier achieved the optimal humidity for the cyclic pressure system..... 73

Figure 2.4: A 2-D CFD model of the pressure chamber using linear quadratic elements. Two boundary layers were created, one at the air/liquid interface (+), and the other at the base of the chamber where the cells would be located (*). A sealed box (arrow) with an equivalent 2-D volume to the volume of the circuit between the chamber and the solenoid valve was used at the outlet. The x- and y-axes depict positional information (in meters) relevant to the velocity, pressure, and shear stress plots in subsequent figures. Figure reproduced with permission from ASME [1]. 75

Figure 2.5: Pressure waveforms collected with the solenoid valve frequency set to (a) 0.5 Hz, (b) 1.0 Hz, and (c) 2.75 Hz. Figure reproduced with permission from ASME [1]..... 84

Figure 2.6: Results for CFD analysis revealing a uniform pressure distribution across the length of the chamber. There is a slidght increase in pressure in the fluid layer progressing down towards the base of the chamber (inset), which is consistent with the expected increase in pressure from the weight of the fluid. The dashed line represents the slice through which the velocity field (shown in Figure 2.8) along the y-axis was extracted. Figure reproduced with permission from ASME [1]. 86

Figure 2.7: Results for the pressure vs. time vs. the X-position across the bottom of the cyclic pressure chamber indicate a smooth, continuous increase in pressure over the course of the simulation and a uniform distribution along the length of the chamber. Figure reproduced with permission from ASME [1]..... 87

Figure 2.8: A three-dimensional spatial velocity profile over time extracted from the dashed line shown in Figure 1.1 shows the development of parabolic flow in the air space, and that the velocity is zero in the liquid space (air-liquid interface located at y=0.063 m). Figure reproduced with permission from ASME [1]. 88

Figure 2.9: ABL readings demonstrate similar values between the cyclic pressure (○) and control experiments (■) for (a) pH, (b) pCO2, and (c) HCO-3. (n=8) Dashed lines indicate the upper and lower limits for acceptable values for each measured variable. The stability in the HCO-3 values indicates sufficient humidification. (d) pO2 values for pressure were elevated over controls throughout the experiments due to the increase in ambient pressure. These values, although statistically different ($p<0.05$), had similar FiO2 values when adjusted for ambient pressure and are not considered biologically significant. Figure reproduced with permission from ASME [1]. 90

Figure 2.10: Representative Live/Dead images from AHCs exposed to (a) Control and (b) 120/80 mmHg, 0.5 Hz cyclic pressure for 5 days. (c) Averaged percentage of dead cells in 10 fields of view indicates no difference in cell death following exposure to 5 days of cyclic pressure. Bars indicate mean ± SEM. 91

Figure 2.11: GAG production is evident in controls (A) but inhibited under cyclic pressure (B) as evidenced by Safranin O staining (n=3). 92

Figure 2.12: (a) Quantification of BMMSC proliferation via cell counts revealed a 1.8 fold increase in cells exposed to cyclic pressure for 7 days compared to controls. (b) BMMSCs exposed to cyclic pressure demonstrated a significant reduction in their total area. (c) Shape index measurements indicated a more rounded morphology for BMMSCs under cyclic pressure. (d) Coomassie blue stained images of pressure (left) and control (right) reflect the measured differences in morphology and proliferation that occurred upon stimulation with cyclic pressure. Images taken at 10x magnification. Figure reproduced with permission from ASME [1]. 93

Figure 3.1: The Mechanical Panel applies mechanical stimulation in parallel from a single population of cells to determine a differential response to each of the stimuli..... 98

Figure 3.2: Cyclic stretch in the FX4000T is controlled by the FlexCentral® computer, which opens valves in the FlexLink® controller that shuttle vacuum in and out of the Baseplate (far left). The applied vacuum from below pulls the deformable culture surface downward. Rigid pots constrain the deformation to achieve uniaxial tension (far right). Figure adapted from Error! Hyperlink reference not valid.. 102

Figure 3.3: The Streamer® consists of six identical parallel plate chambers (inset). Fluid flow is imparted by a computer-controlled roller pump, and two serial pulse dampeners that

ensures a steady laminar flow is delivered to the shear stress chamber. The entire setup can be contained in a standard CO_2 incubator, as shown. Figure adapted from Error! Hyperlink reference not valid.. 103

Figure 3.4: Images of the cyclic pressure system (left) and cyclic pressure chamber (right) during an experiment. As detailed in Chapter 2.0, the respiratory humidifier is fed with a pressurized sterile IV water source, and a clinical pressure monitor displays the pressure of both the cyclic pressure chamber and the humidifier. The cyclic pressure system was designed to take up minimal space in the incubator to allow the Streamer® to fit into the same incubator (seen in lower part of the right image) for the Mechanical Panel experiments. 104

Figure 3.5: (A) Alizarin Red staining of tBMMSCs following osteogenic induction under defined media conditions confirms matrix mineralization. (B) Oil Red O staining of tBMMSCs following adipogenic induction under defined media conditions confirms lipid formation within the cells. Taken together, these images demonstrate that the tBMMSCs are multipotent. Represenative images taken at 100x. 124

Figure 3.6: Representative images of coomassie brilliant blue stained tBMMSCs following 5 days of exposure to the Mechanical Panel. All images taken at 100X. 126

Figure 3.7 Surface area measurements for tBMMSCs exposed to 5 days of mechanical stimulation. (A) Raw measurements for all experiments. (B) Area measurements for each component of the Mechanical Panel normalized by division by the experimental control. The dashed line represents control values. All data presented as the average ± standard error of the mean (SEM). * denotes $p<0.05$ compared to controls. + denotes $p<0.1$ compared to controls. † denotes $p<0.01$ for means within each

stimulus. (1), (2), (3) denote p<0.05 for means between stimuli of corresponding bar color where (1)=CS, (2)=CP, and (3)=LSS..... 128

Figure 3.8: Major axis measurements for tBMMSCs exposed to 5 days of mechanical stimulation. (A) Raw measurements for all experiments. (B) Major axis measurements normalized by division by the experimental control for each of the components of the Mechanical Panel. The dashed line represents control values. All data presented as the average ± standard error of the mean (SEM). * denotes p<0.05 compared to controls. + denotes p<0.1 compared to controls. † denotes p<0.01 for means within each stimulus. (1), (2), (3) denote p<0.05 for means between stimuli of corresponding bar color where (1)=CS, (2)=CP, and (3)=LSS..... 131

Figure 3.9: Shape Index measurements based upon the area perimeter measurements for tBMMSCs exposed to 5 days of mechanical stimulation. (A) Raw shape index calculations. (B) Shaped indices normalized by subtraction of the experimental control for each of the components of the Mechanical Panel. All data presented as the average ± SEM. * denotes p<0.05 compared to controls. + denotes p<0.1 compared to controls. † denotes p<0.01 for means within each stimulus. (1), (2), (3) denote p<0.05 for means between stimuli of corresponding bar color where (1)=CS, (2)=CP, and (3)=LSS. 134

Figure 3.10: Tortuosity Index calculated from the perimeter and major axis measurement of tBMMSCs exposed to 5 days of mechanical stimulation. (A) Raw tortuosity index calculations. (B) Tortuosity indices normalized by subtraction of each component of the Mechanical Panel by their respective experimental control. All data presented as the average ± SEM. * denotes p<0.05 compared to controls. + denotes p<0.1

compared to controls. † denotes $p<0.01$ for means within each stimulus. (1), (2), (3) denote $p<0.05$ for means between stimuli of corresponding bar color where (1)=CS, (2)=CP, and (3)=LSS. 137

Figure 3.11: Normalized histograms for cellular of orientation in CP experiments. The error bars represent the standard error of the mean for the averaged normalized frequencies. Non-parametric analysis against a uniform distribution resulted in no statistical significant differences with any of the cyclic pressure regimens, which is in agreement with the normalized histogram for the control. 139

Figure 3.12: Normalized histograms for cellular orientation in tBMMSCs exposed to LSS. The error bars represent the standard error of the mean for the averaged normalized frequencies. Non-parametric analysis against a uniform distribution resulted in no statistical difference for 1 dyne/cm^2 and 5 dynes/cm^2. However, at 10 dynes/cm^2 and 20 dynes/cm^2, a preferred orientation begins to develop around 90^o, which is in the direction of flow. The histogram from control samples is provided to represent random orientation. 140

Figure 3.13: Normalized histograms for cellular orientation in tBMMSCs exposed to CS. The error bars represent the standard error of the mean for the averaged normalized frequencies. Non-parametric analysis against a uniform distribution did not demonstrate any significant changes for 1% 2.75 Hz and 1% 1 Hz cyclic stretch. However, higher magnitudes of stretch (5% 1 Hz and 10% 1 Hz) demonstrate a significant change from a uniform distribution centered on 90^o, which is perpendicular to the direction of stretch. 141

Figure 3.14: Cell density of tBMMSCs following 5 days of mechanical stimulation. (A) Raw cell density measurements for each component of the Mechanical Panel (B) Cell density for each component of the Mechanical Panel normalized by division by the experimental control. The dashed line represents control values. All data presented as the average ± SEM. * denotes $p<0.05$ compared to controls. + denotes $p<0.1$ compared to controls. † denotes $p<0.01$ for means within each stimulus. (1), (2), (3) denote $p<0.05$ for means between stimuli of corresponding bar color where (1)=CS, (2)=CP, and (3)=LSS. 144

Figure 3.15: Representative histology images from a 5 day Mechanical Panel experiment stained for Alizarin Red and Oil Red O All images taken at 100x. 146

Figure 3.16: Representative immunohistochemistry images for smooth muscle α-actin. Arrows indicate the direction of applied stimulation, if applicable. All images taken at 200x. 148

Figure 3.17: Representative immunohistochemistry images for calponin. Arrows indicate the direction of applied stimulation, if applicable. All images taken at 200x..... 149

Figure 3.18: Representative immunohistochemistry images for myosin heavy chain. Arrows indicate the direction of applied stimulation, if applicable. All images taken at 200x. 152

Figure 3.19: Representative immunohistochemistry images for flk-1. Arrows indicate the direction of applied stimulation, if applicable. All images taken at 200x..... 153

Figure 3.20: Representative immunohistochemistry images for PECAM. Arrows indicate the direction of applied stimulation, if applicable. All images taken at 200x..... 154

Figure 3.21: Representative immunohistochemistry images for vWF. Arrows indicate the direction of applied stimulation, if applicable. All images taken at 200x..... 155

Figure 3.22: RT-PCR reaction products curves. (A) Osteocalcin reaction products for RT-negative samples do not show an exponential increase, demonstrating no genomic amplification. (B) Osteocalcin reaction products for experimental samples show the appropriate exponential increase indicating proper amplification. 157

Figure 3.23: Non-normalized regression model fit for cell density with cellular area and shape index as independent variables. Observed values for cell density (cell/cm^2) are plotted against values predicted by the model in Equation (3.15). 171

Figure 4.1: Plot of the stability index calculated from the variance in gene expression as a function of the stepwise removal of each of the genes listed on the X-axis. 195

Figure 4.2: Western blot stained for calponin (upper band) with 40μg of the A-10 cell lysate serving as a positive control. The membrane was stripped and reprobed for GAPDH (lower band) to serve as an endogenous loading control. 207

Figure 4.3: Time-dependent changes in calponin expression in tBMMSCs following mechanical stimulation. Data are presented as the mean ± SD. † $p<0.05$ compared to CS and *$p<0.05$ compared to controls. 208

Figure 5.1: Changes in normalized calponin expression as determined by Western blot. Data are presented as the mean ± SD. 229

Figure 5.2: Representative Western blot for calponin (top) and GAPDH (bottom) for two experiments (separated by dashed line). A-10 cell lysates were used as a positive control. 230

ACKNOWLEDGEMENTS

John Donne's phrase "No man is an island.." holds meaning for me both in my life and research. Although I am proud of the work that I have accomplished as part of this independent research project, I cannot say "thank you" enough to all the people who have contributed to not only this project, but also to my personal and professional development that have lead me down the path towards a lifetime of learning.

To Dr. Vorp, I owe you more than I can repay for giving me the opportunity and the environment in which I could explore, grow, and succeed. Thank you for all the guidance, patience, and respect that you have given me. You were not only an outstanding mentor, but a good friend as well.

To Dr. Borovetz and the department of Bioengineering, I want to say thank you for all the hard work and dedication it took to create this department. I feel privileged to have been among the first go through the undergraduate program and to have had the wonderful opportunity to work as a clinical engineer at Children's Hospital. Because of your efforts, the doors of opportunity were always open to anyone who wanted them.

Thank you to Dr. Wagner, Dr. Huard, and Dr. Monga for volunteering your time as members of my committee. I have benefited from your instruction and comments.

Thank you to the members of the Center for Biological Imaging for all the training and expertise necessary to complete the antibody and fluorescent imaging. Thank you to Dr.

Badylak and the members of his laboratory for the use of their Kodak Image station for the Western blots. The members of the Genomics and Proteomics Core facility at the University of Pittsburgh, and Vai Pathak and Dr. Patrick Leahy at the Gene Expression and Genotyping Facility of the Case Comprehensive Cancer Center have my sincere thanks for your expedited RNA work and analysis.

To all the members of the Vorp Laboratory – both past and present – thank you for providing your unique expertise whenever I had a problem to solve, for the hours spent polishing conference presentations, and for all the fun we shared in and out of the lab. Thank you to Dr. Hamilton ushering me into the realm of cell biology and sharing your appreciation of good music. Thank you to Doug Chew for helping me to grow as a molecular biologist and helping me to accept that there is voodoo in what we do. You are perhaps one of the finest instructors in the biological sciences, and I am fortunate to have had you as a teacher and a friend. Thank you to Deb Cleary, Renee Laspin, and Paul Wallenberg for your hours of help isolating all my protein samples. Special thanks to Melissa Morgan for being the queen of the Westerns and sharing in the voodoo by letting Yoda watch over our blots.

On a personal level, I want to thank Alex Nieponice, Scott Van Epps, Doug Chew, and Donna Haworth for being such great friends. From lunches and dinners to golfing and conference free-time, I have enjoyed every minute of your company and you have definitely made my time here more enjoyable. I have the highest respect for each of you, both personally and professionally.

A special thanks to my family – mom, dad, Jason, Adam, and Cyndi. Thank you for encouraging me to explore science, always believing in me, and showing me the value of hard work and seeing everything through to the end. Above all, I want to thank my wife and my best

friend, Stephanie. Thank you for putting up with the long hours, countless nights on-call, and for never letting me take work on vacation. Your patience, love, and support are without parallel, and I could not have done it without you.

Finally, I would like to acknowledge the funding sources that have made this research possible. This work was funded by the NIH BRP grant # R01 HL069368, NIH training grant # T32 EB001026, Ruth L. Kirschstein predoctoral fellowship #F31 EB004791, and American Heart Association predoctoral fellowship #0415437U.

1.0 INTRODUCTION

1.1 VASCULAR DISEASE

Cardiovascular disease continues to be the number one cause of death in this country, affecting more than 79 million Americans at an average cost of more than $283 billion [2]. One of the most life-threatening cardiovascular diseases is coronary artery disease, in which the blood vessels feeding the heart become obstructed due to atherosclerotic lesions, depriving the heart muscle of much needed oxygen and leading to myocardial infarction. In 2004, more than 6.3 million cardiovascular procedures were performed, including 427,000 coronary bypass surgeries in 249,000 patients, 615,000 stent placements, and 1.6 million angioplasties [2]. Another, related sub-type of cardiovascular disease is peripheral vascular disease, which although not as life-threatening as coronary artery disease, causes significant morbidity including loss of limbs. Each year approximately 150,000 additional patients receive peripheral bypass grafts to relieve perfusion deficits in the leg [3]. In 2002, approximately 400,000 patients underwent surgical placement of a vascular access graft for dialysis [3, 4]. Currently accepted treatments for coronary artery and peripheral vascular disease include surgical bypass with native or synthetic grafts, as well as stenting.

Bypass grafting is the surgical implantation of a biocompatible conduit for shunting blood around a blocked segment of a blood vessel. In nearly all instances, an autologous vein or

artery or prosthetic graft is employed to provide circulation or vascular access. While vascular grafting has been around since the early twentieth century, cardiovascular surgeons still face many challenges when bypassing small diameter (<6mm) blood vessels [5]. Currently, the majority of patients receive the left internal mammary artery as a graft for the left anterior descending coronary artery bypass and the saphenous vein for all other bypass positions [6]. Research has indicated that 30% of vein grafts become occluded in the first year and one half of those occlusions occur within the first month [7]. Moreover, only 60-70% of patients can reach a 10–12 yr period free of reoperations or angioplasty [6, 8]. Other, less common autologous grafting materials include the radial artery and the gastro-epiploic artery [5]. Complications from vascular access grafts, including infection, thrombosis, and intimal hyperplasia, account for nearly 25% of all hospital admissions each year [9-13].

1.1.1 Vascular conduits

Much effort has been focused on creating an ideal bypass or access graft. Moderate success has been achieved with expanded polytetrafluoroethylene (ePTFE) and polyethylene-teraphthalate (Dacron) in large diameter applications, but small diameter graft performance has been unacceptable [14-21]. Newer grafting materials, including polyurethanes [18], decellularized extracellular matrix (ECM) [22, 23], and cryopreserved allografts [24] show some promise for improving long-term patency, but are still in the experimental stages.

1.1.2 Angioplasty and vascular stenting

Angioplasty, which involves the use of a balloon or other mechanical device to open a stenosed or occluded artery – either by physical expansion of the lumen, or compression or removal of atherosclerotic plaque – is often employed as a first step approach because of it low immediate risk and relative non-invasiveness. The major drawback to this simple procedure is that it causes damage to the endothelial lining, leading to subsequent platelet adhesion and/or SMC proliferation and intimal hyperplasia [25]. Subsequently, stenting, which is the placement of a metal scaffold to prop open the vessel, is often employed to hold open an artery that cannot maintain its lumen following angioplasty or was not a suitable candidate for angioplasty [26]. The major drawbacks to stenting are the thrombotic events that can occur from blood contacting the metal struts of the stent, as well as vessel restenosis via intimal hyperplasia as the vessel grows over the stent struts and into the lumen of the vessel [27]. Second-generation stents are beginning to employ controlled-release of certain drugs, such as Tacrolimus and Paclitaxel, which are intended to prevent cellular division and therefore reduce intimal hyperplasia [28-30]. Anti-platelet drugs, such as Plavix, are also being employed in drug-eluting stents to provide local anti-platelet activity instead of the systemic dosing that many patients typically undergo. However, the use of these types of stents often still requires additional anti-thrombotic agents, such as thienopyridine, of which one-in-seven patients requires premature discontinuation, leading to increased mortality [31]. Recent reports also suggest that stenting may increase peripheral thrombotic events, also leading to increased morbidity and mortality [28, 29, 32].

1.1.3 Regenerative medicine

In addition to advances in bypass grafting and stenting, a new field of regenerative medicine has been developing as a potential treatment for a number of diseases, including cardiovascular disease. Regenerative medicine, which includes tissue engineering and cellular therapy, aims to replace damaged vessels with living, functional tissues instead of synthetic devices which cannot mimic the complex biological function of blood vessels. Additionally, in pediatric cardiovascular surgery, regenerative medicine promises replacement materials that will grow with the child. The first attempts at tissue engineering were endothelialization of ePTFE and Dacron grafts [33-35]. While research is still ongoing in this area [16, 36, 37], more attention is being focused on a complete vascular equivalent [38-42]. However, no tissue-engineered vascular graft has progressed beyond the experimental stage [39, 43-45], with animal studies demonstrating lower patency rates than synthetic materials [39, 46].

One of the biggest challenges for vascular regenerative medicine is finding an appropriate cell source for populating the vessel with smooth muscle (SMCs) and endothelial cells (ECs)[43]. It is widely believed that autologous cells are most appropriate for tissue engineering applications to avoid the use of anti-rejection therapies, but terminally differentiated cells derived from vascular tissue may be predisposed to the same pathology as the diseased tissue. Additionally, quick expansion of fully differentiated cells to the numbers required for tissue engineering is difficult and often results in cellular transformation [47, 48]. Clearly, an alternative cell source is needed, and autologous progenitor cells have been identified as a plausible candidate [43].

Progenitor cells have the capability of becoming any of a number of cell types given the right environment. Of the tissues containing adult progenitor cells, the bone marrow is viewed

by many as having the greatest potential for providing progenitor cells for clinical therapy because it is a site of rapid cellular turnover [49, 50]. Bone marrow progenitor cells have become widely used in cellular therapy [51-54] and are thought to have many applications in cardiovascular tissue engineering [43, 55]. Bone marrow presents a readily available source of autologous progenitor cells that have the ability to become many types of tissue, provided they receive the proper cues [56-58]. However, in order to effectively apply the necessary stimuli for the generation of functional smooth muscle and endothelial cells, an understanding of the developmental paths and basic biology for these cells is necessary.

1.2 SMOOTH MUSCLE CELLS

1.2.1 Development and basic biology

Smooth muscle cells (SMCs) are spindle-shaped cells found in the walls of almost every hollow organ in the body [59]. They arise primarily from the mesodermal layer during embryonic development [60]. SMCs play a fundamental role in many tissue types where the organism requires rhythmic slow or sustained contraction. Across an organism, SMCs in different tissue beds have many unique characteristics, including expression of contractile protein isoforms and response to adrenergic agents. Even within a single tissue, SMCs exhibit many different phenotypes, ranging from a prototypical fibroblast that contains very few contractile proteins and produces and organizes ECM, to an intermediate myofibroblast that contains some contractile proteins and continues, to participate in matrix production to a fully-differentiated SMC expressing the complete assortment of contractile proteins, intercellular signaling molecules

(e.g.,, connexins), and responding to biological agents including epinephrine, nitric oxide, and acetylcholine [61].

The state of the SMC depends heavily upon the local biochemical and biomechanical milieu, each regulating the cellular state in a continuum between a synthetic fibroblast-like phenotype and the fully contractile phenotype found in the vessel media. The possibility for stem cells to enter into this cycle has been hypothesized, initially becoming a fibroblast-like cell with potential to differentiate to the fully contractile phenotype (**Figure 1.1**) [62]. Of the variety of proteins expressed by SMCs (including SM22α, myocardin, smooth muscle α-actin, smoothelin, calponin, caldesmon, and myosin heavy chain), only myosin heavy chain (isoform SM-2) and smoothelin appear to be exclusive to SMCs (**Table 1.1**) [61, 63-65]. However, the presence of myosin heavy chain and smoothelin does not necessarily imply functionality. A functional SMC requires abundant K+ and Ca2+ ion channels, as well as the receptors for vasoconstrictors and -dilators. To determine the true contractile/functional state of a presumed SMC, one needs to perform a multitude of protein and functional assays to elucidate the true phenotype [66]. The proceeding sections describe the various proteins involved in SMC development and their restriction to the SMC phenotype.

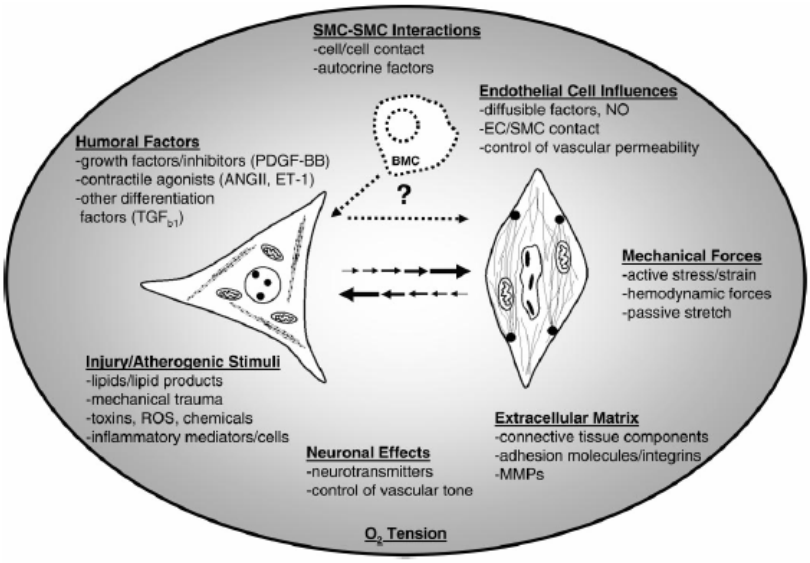

Figure 1.1: SMC phenotypic switching occurs from various external stimuli. Reprinted with permission from [62].

Table 1.1: Comparison of SMC contractile proteins, their exclusivity to SMCs, and presence in different SMC phenotypes. ++ indicates definitively positive expression; +/- indicates transient expression or conflicting reports; and -- indicates definitively negative expression. Table adapted from [66].

Protein	Exclusive to SMCs	Contractile	Synthetic/ developmental	Expression in other cells
SMA	N	++	++	Fibroblasts, myoblasts, inducible in ECs *in vitro*
SM22α	N	++	++	Inducible by stretch, TGF-β, and loss of cell-cell contact in ECs *in vitro*
Caldesmon	N	++	+/-	Inducible skeletal myoblasts *in vitro*
h1-Calponin	N	++	+/-	Myoepithelium, inducible in ECs *in vitro*
Myosin heavy chain (SM-1 and SM-2)	Y	++	--	
Smoothelin	Y	++	--	

1.2.1.1 Smooth muscle α-actin

Smooth muscle cells arise during vasculogenesis as early as two days into development (in chicken and quail embryos), enveloping the newly formed aortic tube [61, 67, 68]. These cells are morphologically different from the rounded endothelial cells lining the newly formed vessel, and are distinct from the surrounding mesoderm by the expression of smooth muscle α-actin (SMA) [61]. SMA is a 42 kDa protein and is one of many forms of actin expressed throughout the body in addition to cardiac α-, skeletal α-, smooth muscle γ-, nonmuscle γ-, and β-actin [61, 69]. These isoforms are the product of different genes, but only differ from each other in the first ten amino acids, suggesting a highly conserved and efficient protein utilized for contraction, cellular locomotion, and intracellular transport [61]. Only SMA and γ–actin are considered to be contractile associated proteins, while the other isoforms part of the non-contractile cytoskeleton [70-73]. The amount of SMA produced in the early SMCs continues to increase as the cells mature, eventually making up 40% of the total protein produced and 70% of the actin isoforms produced by the SMC [61, 69]. Although the expression of SMA was once thought to be highly specific for SMCs, since its expression in the normal adult organism is relatively restrictive, studies in wound healing and tumorigenesis, as well as other cell types treated with specific growth factors, have shown that non-SMCs can express SMA [61, 74-78]. Thus, SMA does not appear to be sufficient to positively identify SMCs (contractile or synthetic); other proteins are necessary.

1.2.1.2 Calponin

Calponin is a 34kDa regulatory protein that is associated with actin and tropomyosin binding [79]. Several isoforms of calponin are known to exist, but only h1-calponin is found in

vascular SMCs [61]. A more recently discovered isoform, h2-calponin, is the product of a separate gene and is found in skeletal muscle and other non-muscle cells including platelets and fibroblasts [79]. The functional significance of calponin is demonstrated by its ability to bind actin in the same stoichiometry as tropomyosin, suggesting that it acts as an inhibitory protein to SMC contraction. Indeed, addition of calponin to a simple contractile system consisting of free actin, myosin, tropomyosin, calmodulin, and myosin light chain kinase reduces ATP consumption by more than 80% [80].

The expression of h1-calponin occurs early in the development of the aorta and is maintained in adult, contractile SMCs [61]. Although h1-calponin is relatively restricted to SMCs in the normal adult, calponin expression has been reported in platelets and tumor cells. However, the h1 isoform has not been confirmed in these studies, lending the possibility that it is in fact the non-muscle h2-calponin isoform [61, 81, 82]. Additionally, h1-calponin expression has been noted in ECs subjected to cyclic stretch [83], to fibroblast growth factor [84], or to transforming growth factor-β stimulation [85] *in vitro*.

1.2.1.3 SM22α

SM22α is a 22kDa protein of similar structure and developmental specificity to calponin [68, 86]. Although SM22α and calponin share certain homologous regions, SM22α has had conflicting reports on its ability to bind actin, and the functional importance is still in dispute [72, 87, 88]. SM22α appears developmentally after day 4 (in chicken and quail embryos), but before other late markers of differentiation such as calponin and myosin heavy chain [61, 72]. There are reports that SM22α is identical, both in mRNA and amino acid sequence, to transgelin, which is an actin-polymerization chaperone protein [89, 90]. Knockouts of the SM22α gene

develop normally but show changes in actin cytoskeletal arrangement, further supporting the theory that it participates in actin polymerization [91]. Although SM22α is inducible in ECs *in vitro* [83, 85], it has yet to be found in non-muscle cells *in vivo* [86].

1.2.1.4 Caldesmon

Caldesmon is a calmodulin, tropomyosin, and actin-binding protein found in SMCs and some non-muscle cells [64]. Two isoforms, h-caldesmon (120kDa) and l-caldesmon (70kDa), exist, with h-caldesmon restricted primarily to SMCs. Neither isoform is found in skeletal or cardiac muscle cells *in vivo* [61], but, h-caldesmon can be induced by serum deprivation in skeletal myoblast culture [92]. Caldesmon's primary function is to regulate actin-myosin interactions during contraction, and it is localized in the thin filaments of SMCs and along stress-fibers in non-muscle cells [65]. It appears as a later marker than calponin and SM22α but prior to myosin heavy chain [61].

1.2.1.5 Smoothelin

Smoothelin has been proposed as protein restricted to muscular arteries of the vasculature [93]. Since its discovery, two isoforms, smoothelin-A (59kDA) and smoothelin-B (100kDa), have been identified that are predominantly found in the visceral and vascular SMCs, respectively, but only one gene has been identified thus far [94, 95]. It appears relatively late in development (around 10 weeks in humans) in the blood vessels surrounding the placenta. In the adult, smoothelin is found in only 10% of the aorta SMCs, more than 50% of the muscular arteries, but not in veins or capillaries [95]. Smoothelin is also found in developing atherosclerotic lesions, usually isoform –B [96], and is usually co-expressed with desmin [97]. Upon explant, transcription of the smoothelin gene ceases very quickly [93]. Smoothelin

expression is essential for normal contractile function in SMCs of the vasculature and gut, suggesting it is part of the contractile apparatus along with actin and myosin heavy chain [96, 98].

1.2.1.6 Myosin Heavy Chain

Myosin is a hexameric protein principally responsible for cellular contraction and is found in nearly every muscle and nonmuscle cell [61]. Myosin heavy chain (MHC), one of the subunits of myosin, is expressed in several isoforms across muscle and nonmuscle cells, but there are two isoforms, SM-1 (204kDa) and SM-2 (200kDa), that are believed to be exclusively expressed by SMCs [61, 99]. A third isoform, SMemb (198kDa), is found in most developing and cultured SMCs as well as atherosclerotic lesions. It can be induced in other cell types, such as fibroblasts, with mechanical or growth factor stimulation [100] and during wound repair [101]. However, in mature functional SMCs, SMemb is typically replaced by SM-2 late in development, thus making SM-2 the latest marker for SMC differentiation [102]. SM-2 expression continues to increase postnatally, which may be related to the increasingly sustained or rhythmic contraction that is a hallmark of SMCs.

1.2.1.7 Myocardin

Like its relatives, skeletal and cardiac muscle, many researchers have postulated that SMC differentiation should be governed by a specific family of transcription factors that control a significant portion of the transcription of contractile proteins. There has been much difficulty in identifying such a master switch, but the best candidate to date is myocardin. It plays a significant role in both SMC and cardiac muscle differentiation and has been used as an indicator of SMC potential [103]. Myocardin is part of a complex set of transcription factors that

transcribe numerous SMC-specific genes. Knockout studies of myocardin have demonstrated embryonic lethality by day 10.5 in mice with no evidence of any SMC differentiation [104]. Ectopic expression of myocardin has demonstrated the ability to turn on SMC proteins in non-muscle cells [105, 106]. Although many of the SMC-restricted genes are under the promotion of myocardin, there are a few exceptions. In particular, smoothelin-B, the isoform specific for vascular SMCs, does not appear to be regulated by myocardin [107, 108]. Although relying on a single transcription factor to promote the expression of most of the necessary proteins for contraction seems fairly intuitive, the functional purpose for this separation of transcriptional control for smoothelin is not yet understood.

1.2.2 Response to biological factors

Because SMCs provide such an important function in all major organ systems, they need to develop and adapt to changing demands and injury. As part of this development and remodeling process, SMCs are exposed to a variety of growth factors that alter their proliferation rates, matrix production, and differentiation (see **Figure 1.1**). Four key growth factors in SMC development and biology – platelet derived growth factor, transforming growth factor β, fibroblast growth factor, and vascular endothelial growth factor- are discussed here.

1.2.2.1 Platelet derived growth factor (PDGF)

PDGF is a ~30kDa growth factor expressed by numerous cells types (**Table 1.2**) [109, 110]. There are four known isoforms - PDGF-A, PDGF-B, PDGF-C, and PDGF-D – that exist as homo-dimers. Only PDGF-A and PDGF-B are known to exist naturally as a hetero-dimer [111]. Each PDGF isoform is transcribed from a separate gene, meaning that cells transcribing

PDGF-A and PDGF-B can produce equal amounts of PDGF-AA, PDGF-BB, and PDGF-AB [109, 111]. PDGF acts upon a receptor (either the α- or β-isoform) on the cell surface belonging to the tyrosine kinase family of growth factor receptors.

Table 1.2: Multiple cell types express different isoforms of PDGF and PDGF receptor (PDGFR) [109].

Cell Type	PDGF-A	PDGF-B	PDFGR-α	PDGFR-β
Fibroblast	+	+	+	+
Skeletal myoblast	+			+
Vascular SMC	+	+	+	+
Vascular EC	+	+		+
Macrophages	+	+		+
Platelets	+	+	+	

The expression of PDGF and its receptor varies depending upon the cell type (**Table 1.2**) and local milleu, especially in development and disease states. For instance, PDGFR expression is increased in vascular SMCs following injury to increase mitosis and accelerate tissue repair and regeneration [112-114]. Likewise, PDGF expression by newly forming vascular ECs rises and falls during vasculogenesis and angiogenesis to attract pericytes expressing PDGFRs [109]. Normal SMCs do not express high levels of PDGF-Rα, but do increase their levels in response to hypertension, mechanical stimulation [110, 115-117], inflammation states such as injury or atherosclerosis [110, 118], and fibroblast growth factor stimulation [119].

During development, PDGF plays an important role in the formation of the vasculature as knockouts of the PDGF-A and -B isoforms as well as their receptors are either embryonic lethal or suffer severe growth retardation and poor vascular development [111]. PDGFR stimulation induces myocardin expression, which in turn activates the gene expression of calponin, SM22α,

and smooth muscle γ-actin [61, 120]. Hellstrom et al. [121] developed a two-stage theory on the role of PDGF in vascular development that describes a temporal-spatial signaling between PDGFR-β positive pericytes and ECs. This model of induction followed by co-proliferation is also evident during the epithelial to mesenchymal transition of coronary artery development [120]. In addition to the direct effects on SMCs during vasculogenesis and angiogenesis, PDGF has also been shown to have indirect effects on vessel growth through an increase vascular endothelial growth factor (VEGF) and basic fibroblast growth factor (bFGF) expression in SMCs (see Section 1.2.2.3)[122, 123].

In adult quiescent SMCs, PDGF plays a very different role. As stated previously, expression of PDGF-Rβ in arterial SMCs is low until acted on by an external mechanical or biological stimulus, or placement into tissue culture [109, 124]. Once these conditions are met, PDGFR expression increases, and the cells are primed for stimulation by PDGF, which has been shown to cause increased proliferation [125-127], decreased expression of contractile protein expression in SMCs including SMA, calponin, and SM-α tropomyosin, and MHC (SM-1) [120, 125, 127-132], suppression of collagen synthesis [133, 134], and increased production of matrix metalloproteinases -2 and -9 [135, 136]. These processes are important for both normal vascular remodeling and pathology.

1.2.2.2 Transforming growth factor beta (TGF-β)

TGF-β is a 25 kDa polypeptide in a superfamily also containing activins, inhibins, myostatin, bone morphogenic proteins (BMPs), and others that play an important role in mitogenesis and morphogenesis throughout the body in both development and tissue remodeling [137-140]. There are three isoforms of TGF-β, each is differentially expressed in almost every

cell type in the body. TFGβ is produced as a latent inactive dimer, which is activated in the extracellular space and binds to receptors forming a dimeric complex consisting of two subunits, TGF-βR-I and TGF-βR-II, to activate intracellular signaling [137, 139, 141]. TGF-βR-II is the predominantly expressed in normal SMCs, whereas TGF-βR-I is found in atherosclerotic plaques [139, 142]. A third receptor, TFGβR-III (also known as endoglin) found predominantly in ECs (see Section 1.3.2.2) does not appear to have signaling capability, but may aide in chaperoning active TGF-β to TGF-β receptors [138, 139].

During vascular development, TGF-β is expressed by ECs and SMCs participating in vasculogenesis and angiogenesis [139, 143, 144]. Knockouts of TGF-β, its co-receptors (including Alk1 and endoglin) [145], or the downstream TGF-β signaling molecule SMAD5 [146, 147], result in embryonic lethality from widespread hemorrhage due to a lack of mature SMCs surrounding the newly forming blood vessels [138, 139, 144]. This evidence has led to the hypothesis that TGF-β is essential for the induction and maturation of SMCs during vasculogenesis and angiogenesis [138, 148]. Recently, an embryoid body culture system has definitively shown that TGF-β contributes SMC differentiation and maturation in development [149].

In adult SMCs, TGF-β alters SMC proliferation in a biphasic manner. Low concentrations of TGF-β (1-2 fg/ml) induce SMC proliferation through PDGF-AA and PDGFR production (similar to developmental processes) [139, 144, 150, 151]. The effects of TGF-β at lower concentrations are consistent with reports that TGF-β and PDGF-A are increased in damaged vessels, leading to the initiation of intimal hyperplasia through SMC proliferation and matrix production [114, 119, 152]. Further evidence of this phenomenon has been found through increases in both vascular endothelial growth factor [122] (an EC mitogen; see Section 1.3.2.1)

and bFGF [122, 123] (both an EC and SMC mitogen; see Sections 1.2.2.3 and 1.3.2.3) following treatment of SMCs with TGF-β.

Higher concentrations (10 pg/ml-10 μg/ml) of TGF-β have been shown to inhibit SMC proliferation by downregulating PDGFRβ protein synthesis [139, 144, 150, 151] and extending the G_2 phase of the cell cycle [153, 154]. TGF-β also inhibits proliferation by downregulating FGF binding proteins, thus reducing the effective binding capacity and mitogenic effects of FGF [155]. Additionally, at these concentrations TGF-β has been shown to help maintain SMCs in their differentiated states through production of α-SMA, SM22α, calponin, and MHC (SM-1) [127, 139, 156-158]. TGF-β has also been shown to induce α-SMA and other contractile proteins including calponin in non-muscle cells such as fibroblasts (converting them to myofibroblasts) [78, 159, 160], 10T1/2 SMC precursor cells [160, 161], macrophages [162], and neural crest cells [160, 163].

In addition to changes in proliferation and contractile markers, TGF-β has been shown to be a potent inductor of ECM production. TGF-β promotes the expression of α2 type I collagen, reduces the activity of matrix metalloproteinases (MMPs) [139, 154, 164, 165], and upregulates inhibitors of MMPs (TIMPs) [166]. There are, however, reports that show an increase in MMP expression when TGF-β is induced by mechanical stretch *in vitro* [167] or when low doses of TGF-β accompany PDGF [135]. These two opposing effects may demonstrate a unique balancing act by TGF-β in normal vessel homeostasis, and this balance may depend upon amount of TGF-β and the other signaling mediators involved [135, 139, 142, 168].

1.2.2.3 Fibroblast growth factor (FGF)

FGF is a 16-34 kDa polypeptide that is a strong mitogen and morphogen for most cell types, including SMCs and ECs, which plays a critical role in developmental processes and in tissue growth and remodeling in adults [156, 169, 170]. There are at least 23 members of this polypeptide family binding to four receptor isoforms. Two isoforms, acidic and basic FGF (aFGF and bFGF, respectively) play large roles most cellular processes [171, 172]. FGF is localized to heparin sulfate proteoglycan molecules on the cellular surface and the ECM, which protects it from proteolytic degradation and acts as a co-receptor for FGF receptors [171, 173]. Although it lacks a secretory peptide for packaging and release outside the cell, FGF is predominantly found in the basement membrane of blood vessels where it is released following vessel injury [169, 174, 175]. Current theory postulates that the extracellular FGF is derived from apoptotic cells, possibly a byproduct of developmental processes of cell regression following tissue formation [174].

In early development, bFGF plays a role in differentiation and patterning for multiple structures, including the induction of the vasculature from the mesoderm [169, 176-178]. Furthermore, FGF has demonstrated different effects depending upon concentration and embryologic timing. For instance, high concentrations of bFGF are more chemotactic than mitogenic, and bFGF can either delay or accelerate myogenesis depending upon cellular state and the timing of the stimulation [179, 180]. Additionally, during angiogenesis, bFGF increases the secretion of VEGF from SMCs leading to increased vessel sprouting [174]. This model of bFGF's role in angiogenesis has been further demonstrated in developing cardiac muscle explants where bFGF antibodies inhibited VEGF-dependent vessel sprouting [181].

Postnatally, the effect of bFGF on vascular cells appears to be mainly mitogenic [60]. bFGF has been shown to play a role in the upregulation of autocrine PDGF-induced mitosis by increasing the mRNA and protein production of PDGF-A [182], and PDGFRα without affecting PDGFRβ [119]. Without the induction of PDGFRα by bFGF, PDGF-AA is a poor SMC mitogen. This signaling paradigm is supported by *in vivo* evidence that shows increased PDGFRα and PDGF-A levels in injured and atherosclerotic arteries [114, 119, 125], and administration of antibodies to bFGF decreases SMC proliferation. In addition, bFGF plays a role in the migration of SMCs after injury by inhibiting collagen I and III production and increasing MMP-1 production in vascular SMCs [183].

1.2.3 Response to mechanical stimuli

Vascular cells, both SMCs and ECs, exist in a mechanically dynamic environment (**Figure 1.2**). In the vasculature, these can be broken down into three separate mechanical stimuli – pressure, shear, and stretch – that result from the flowing blood in the vessels. These forces arise from the pulsatile flow of blood through the arteries and veins. Each pulse of blood from the left ventricle causes a hydrostatic pressure increase inside the vessel. This hydrostatic pressure can be though of as an outward normal force distributed evenly over the lumen. The change in pressure over the cardiac cycle acts mainly on the ECs lining the vessels, but there is also a transmural pressure distribution where it acts on SMCs residing in the medial layers of the vessel. In addition to imparting a normal force on the vessel, the cyclic pressure changes lead to the forward flow of blood through the vessel, which results in a drag force, or shear stress, acting along the lumen of each vessel. The magnitude and direction of this shear force is governed by the local geometry, pressure, and flow distribution and varies throughout the vasculature. Because the vessel wall is

an elastic material, the cyclic pressure also causes a cyclic change in diameter in arteries. This change in diameter imparts a cyclic circumferential stretch on the SMCs and ECs making up the vessel. The magnitude of stretch imparted by the blood depends heavily on the ECM constituents of the blood vessel, mostly collagen I and elastin. For instance, in the large arteries close to the heart, there is high elastin content causing these vessels to experience a greater change in diameter. In the smaller arteries and arterioles, which are responsible for maintaining vascular tone, the ECM composition favors collagen I and an increased smooth muscle component that makes these vessels less compliant, therefore receiving a lower circumferential stretch over the cardiac cycle [184-187].

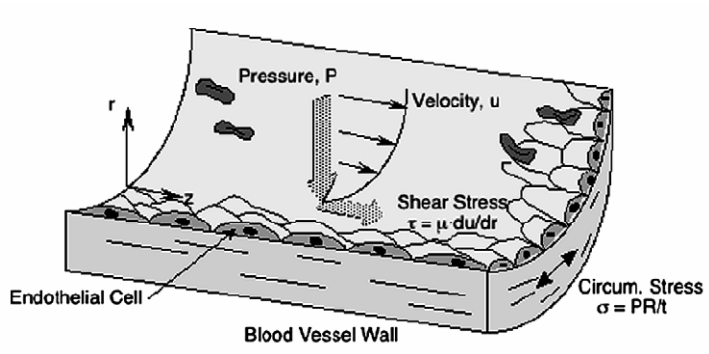

Figure 1.2: Mechanical stimulation plays an important role in vascular biology because blood vessels undergo multiple types of mechanical stimulation throughout each cardiac cycle. Reprinted with permission from IOS Press [188].

These forces have significant effects on the functionality, proliferation, and protein expression of vascular cells. The alteration of the mechanical environment is thought to play a role in development and disease states, such as hypertension where the average magnitude of wall stretch can be increased by more than 15% [189, 190]. Many researchers have investigated

the effects of mechanical forces on vascular cells, attempting to elucidate mechanisms for the maintenance of functionality as well as early signals of pathology (**Figure 1.3**). Cells within a tissue can sense mechanical stimuli, such as compression, tension and shear stress, through various mechanisms including stretch activated ion channels, GTP-coupled proteins, integrins, and receptor tyrosine kinases (not shown in the figure). These sensors trigger secondary signaling that can include prostacyclin, cAMP, changes in membrane potential, Src, the mitogen activated protein kinase (MAPK) cascade, phospholipases, and protein kinase C (PKC). The secondary pathways converge upon the nucleus, and depending upon other environmental factors, initiate gene transcription leading to alterations in proliferation, survival, and protein synthesis. Additionally, the spatial and temporal gradients of the magnitude and frequency for a given mechanical stimulus within a tissue can influence the secondary signaling, ultimately impacting the final cellular response [191]. The following is a brief discussion of how SMCs respond to their mechanical environment, specifically stretch, pressure, and shear.

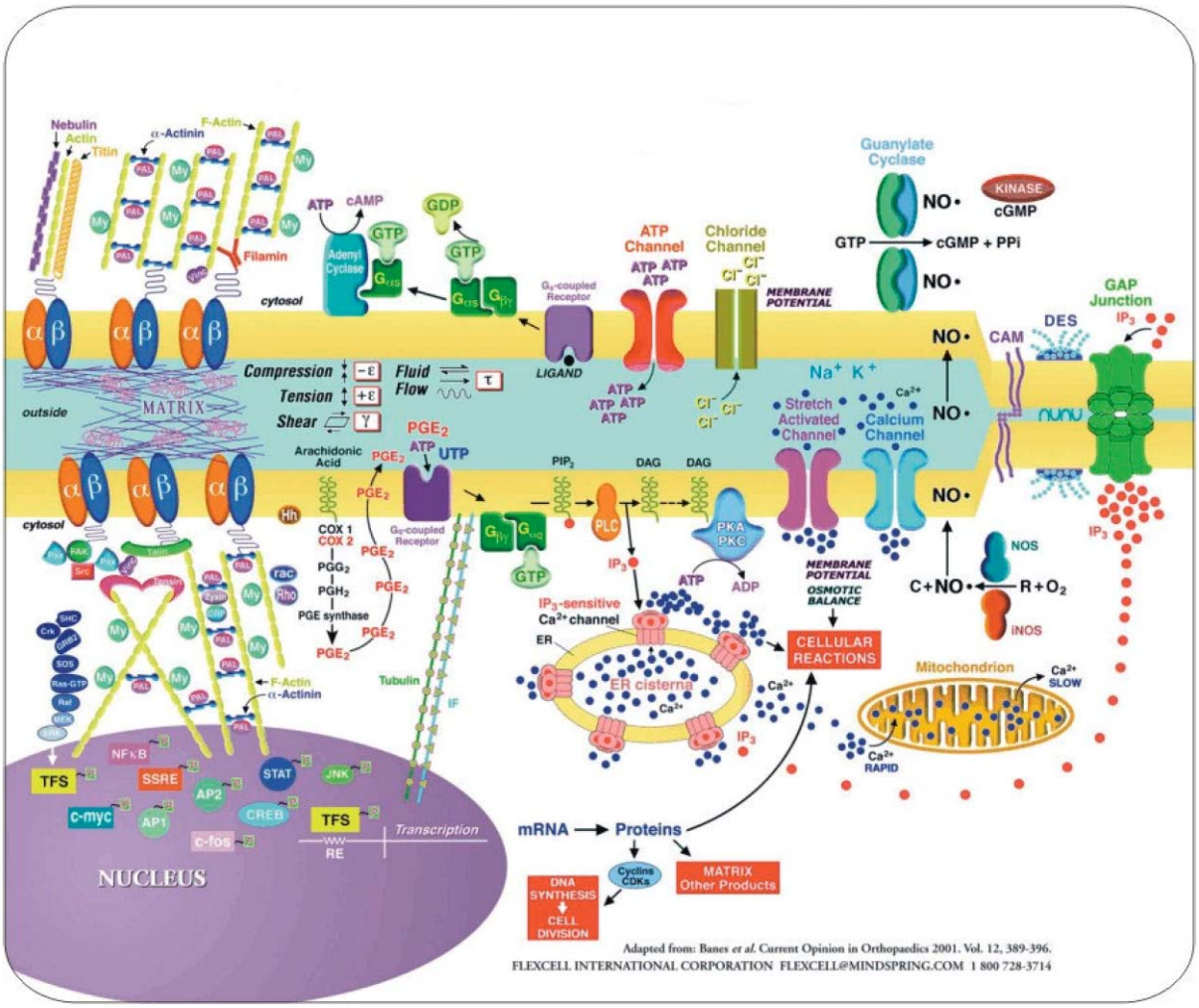

Figure 1.3: Schematic of cellular mechanisms for sensing mechanical signals which are relevant to vascular SMCs and ECs. Figure adapted from [191].

1.2.3.1 Stretch

The cyclic circumferential stretching that SMCs experience with each cardiac cycle due to the elastic properties of the blood vessels typically ranges from 5%-15% depending upon the position in the vascular tree and local mechanical properties [192]. The effects of cyclic stretch on SMCs have been widely studied as this stimulus is believed to play a major role in SMC differentiation and pathology (see **Figure 1.1**) [127, 130, 167, 193-195].

Upon explant, isolation, and *in vitro* culture in a static environment, SMCs begin to take on a synthetic phenotype by downregulating their expression of contractile proteins, such as myosin heavy chain (MHC) and calponin, producing more extracellular matrix proteins, and proliferating at higher rates than SMCs with a contractile phenotype [189, 196-198]. Cyclic stretch has been shown to alter proliferation [116, 117, 127, 131, 199-202], increase the production of several biological factors (PDGF-A and -B [116, 117, 131, 183, 201, 202], IGF [203], VEGF [204], TGF-β [167, 205, 206], and FGF[207]), matrix components (collagen I [167, 205, 208-210], collagen III [208], collagen IV [206], elastin [211, 212], and fibronectin [167]), and contractile proteins (SMA, calponin, caldesmon, SM-1, and SM-2) [130, 189, 213-215].

Overall, the response of SMCs to stretch appears to be highly dependent upon several factors including extracellular matrix [130, 194, 213, 216, 217], the magnitude and frequency of stretch [116, 117, 127, 131, 201, 202, 210], cellular state , and soluble factors [189]. Wilson et al. [216] demonstrated that stretch increased DNA synthesis on collagen, fibronectin and vitronectin, but not laminin or elastin. They went on to further demonstrate the response to stretch was inhibited by β_3 and $\alpha_v\beta_5$ but not β_1 antibodies, thus defining a link between integrins

and mechanotransduction and demonstrating the importance of ECM in cellular responses to their environment.

Stretch magnitude and frequency also play important roles in the response of SMCs to mechanical stimulation (**Figure 1.4**) Stretch frequency has been demonstrated to have an effect on ECM production and turnover with physiologic adult (1 Hz) and neonatal (2.65 Hz) frequencies both stimulating collagen I and MMP-1 production, but only neonatal frequency stimulation increases TIMP-1 [127, 210]. Proliferation increases have consistently been demonstrated at lower stretch magnitudes (1-7%). This process has been shown to be mediated by autocrine signaling loops involving angiotensin II, PDGF, and PDGF receptors [116, 131, 201], which can be auto-phosphorylated directly through integrin-mediated mechanosensing [117, 202].

Physiologic stretch magnitudes (5-15%) help maintain SMCs in a contractile, quiescent phenotype [189], and may also prevent calcification of tissues *in vivo* [218]. Nikolovski et al. [218] demonstrated that without stretch, osteoblast genes including osteopontin, matrix gla protein, and alkaline phosphatase are increased as is calcium uptake. Although contractile protein expression is consistently increased with physiologic levels of stretch [130, 213, 219], changes in proliferation have been reported to vary [127, 199, 200, 202]. The variance in proliferation as a result of cyclic stretch is likely due to differences in the starting cell population or ECM and may be mediated through a balance between PDGF [130, 220] and TGF-β signaling [127, 167, 221] that can result from the application of cyclic stretch.

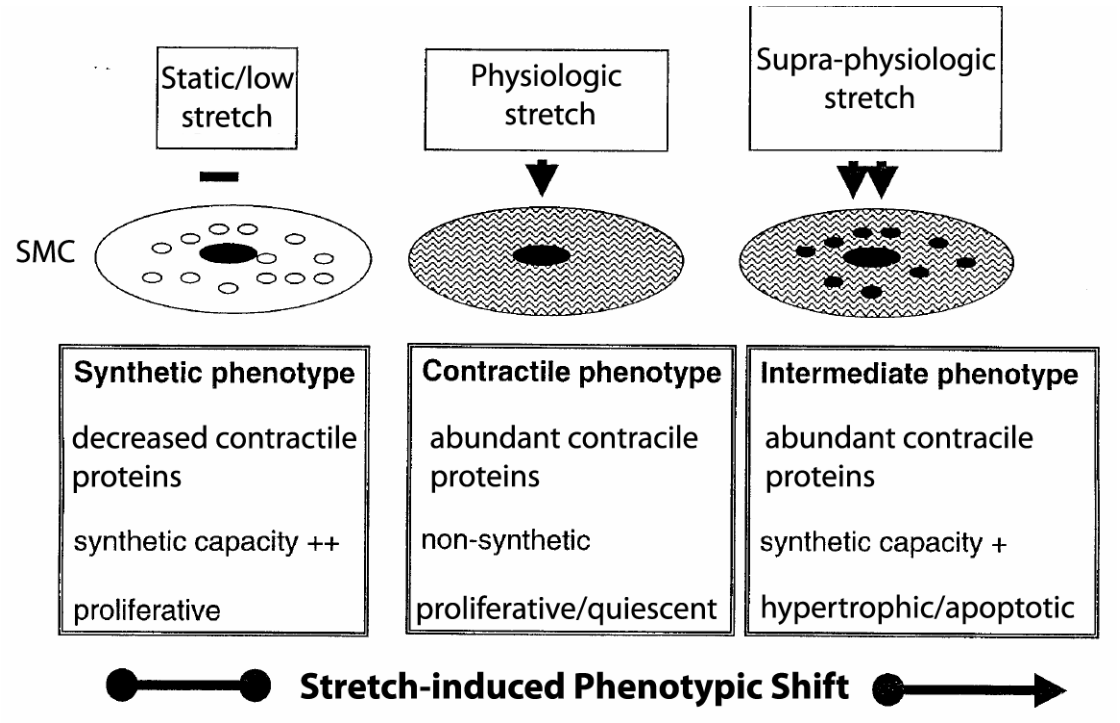

Figure 1.4: Various levels of cyclic stretch can induce multiple phenotypic changes in SMCs. Adapted from [189].

Supra-physiologic magnitudes (>15%) tend to increase proliferation, apoptosis, matrix production, and some contractile protein expression in SMCs, most of which are mediated by TGF-β signaling [167, 189, 209, 213, 221]. These higher stretch magnitudes have also been shown to cause FGF2 release as a response to vessel damage, which may in turn activate proliferative mechanisms (see Section 1.2.2.3) leading to intimal hyperplasia [207, 222]. Indeed, there is evidence that these higher stretch magnitudes induce apoptosis in mature SMCs through decreases in the pro-survival protein, Bcl-2, and increases in Bcl-2 associated death protein (BAD) [223]. This process was demonstrated by Wernig et al. [217] to be mediated through p38 MAPK pathways and required collagen I matrix, thus demonstrating that the same signaling mechanism can lead to very different results depending upon the type of matrix, level of stretch, and the state of the SMC. This mixture of contractile and synthetic states produced by higher

levels of stretch may reflect local imbalances in TGF-β and PDGF signaling, leading the tissue towards a pathologic state [189, 220].

While species variability, age of SMC source (adult vs. neonatal), matrix content, exogenous signaling, magnitude and frequency of stimulation, and contractile state may account for much of the variability seen in SMC response to stretch, there is also an apparent paradox resulting from increased ECM production, proliferation, and contractile proteins in some SMCs as a result of stretch [189, 220]. One possible reason for this is the hypothesis that growth and differentiation may not be mutually exclusive events in adult animals, but rather SMCs are capable of returning to developmental processes in order to repair and maintain homeostasis in the vessel wall [68, 189].

1.2.3.2 Pressure

SMCs also experience cyclic pressure through transmural pressure gradients as a result of the pulsatile blood flow. While most experiments dealing with models of hypertension have studied increased stretch as an indirect effect of the increased hydrostatic pressure, little research has been conducted on the direct influence of pressure on SMCs. The overall effects of hypertension are reported to be increased cellular and matrix components as well as increased matrix remodeling [194, 224].

Watase et al. [225] appear to be the first to expose SMCs to direct hydrostatic pressure. Using a custom-built apparatus, they exposed aortic SMCs to control, 105mmHg static pressure, and 120/90mmHg cyclic pressure at 1Hz. They found that the increased pressure, whether constant or cyclic, increased SMC proliferation beginning at day 5 and increasing through day 9, with no effect on cellular viability. In addition, cyclic pressure altered the morphology of SMCs, leading to a more elongated phenotype, characteristic of the contractile phenotype found *in vivo*.

In a related study, Ozaki et al. [226] demonstrated that steady atmospheric pressures above 140 mmHg stimulated dose-dependent DNA synthesis in SMCs within 3 hours, while lower pressures showed no change. Other research *in vivo* has demonstrated that the pulse-pressure instead of a mean pressure elevation was critical for the initiation of hypertension-mediated vessel remodeling [227].

Cappadona et al. [228] have shown that increased pressure in a capillary perfusion model can increase contractile, but not synthetic, SMC proliferation. Subsequent research by Birney et al. [229] has demonstrated that transmural pressure pulses result in time- and pressure-dependent increases in apoptosis as measured by activated caspase-3. Lower pulse pressures (6mmHg) were significantly less apoptotic than higher pulse pressures (>34mmHg). While EC signaling (either pro-survival or pro-apoptotic) was shown to have no influence on SMC apoptosis, the pressure-induced apoptosis was dependant on the differentiation status of the SMCs. More differentiated cells were prone to pressure-induced apoptosis while embryonic or immature SMCs demonstrated decreased FasL and p53 expression upon exposure to pressure. The fact that the contractile phenotype of SMCs is capable of rapid proliferation and is susceptible to apoptosis may be related to insufficient time spent in the G0/G1 cycle resulting in insufficient DNA repair [229, 230].

1.2.3.3 Shear stress

While shear stress is predominantly associated with ECs lining the lumen, SMCs can exposed to this force through interstitial fluid flow and because of EC denudation following vessel injury [231]. SMCs react very differently to shear stress by orienting perpendicular to the direction of flow [232, 233], whereas ECs align parallel [233]. Hu et al. [117] have demonstrated that 5 dynes/cm^2 shear stress increased proliferation, most likely through a direct

activation of growth factor receptors by shear stress similar to cyclic stretch (see 1.2.3.1) because supernatant from shear stimulated cells failed to increase proliferation. The increased proliferation of SMCs had been previously reported [117, 234, 235] and is a common response mechanism to endothelial injury or denudation *in vivo* [125, 236]. Higher levels of shear stress (>10 dynes/cm^2) have been shown to initiate SMC contraction [237] as well as inhibit proliferation [232, 238, 239] and migration [240]. These responses appear to be in line with theories that sub-physiologic and oscillatory shear stresses contribute to atherosclerotic plaque formation [241, 242], and are similar to the responses of ECs under shear (see Section 1.3.3.3). In a recent study, Wang et al.[243] discovered that a murine SMC cell line (P53LMAC01) exposed to 15 dynes/cm^2 shear stress induced the mRNA expression of EC markers (CD31, von Willebrand factor and VE-cadherin) and proteins while decreasing the expression of SMA, h1-calponin, and MHC. While the use of a cell line may not be representative of SMCs *in vivo*, it raises the possibility that SMCs are capable of transdifferentiation into ECs through mechanical stimulation; an exciting possibility for regenerative medicine.

1.3 ENDOTHELIAL CELLS

1.3.1 Development and basic biology

Epithelial cells are polarized cells that line the cavities of all hollow organs in the body and perform many important functions. Vascular endothelial cells (ECs) are a specialized sub-type of epithelial cells that line blood vessels and are responsible for providing a permeability barrier between flowing blood and the surrounding tissue as well as the production, secretion and

metabolism of bioactive substances, and the maintenance of hemostasis and vascular tone [244]. Even throughout the vasculature, ECs in different vessels exhibit very different morphologies and functions in accordance with their particular role in that environment [245]. During development, simultaneous with cardiac formation, the vasculature develops through a process known as vasculogenesis. Vasculogenesis is the *de novo* development of blood vessels in separate parallel structures. The process begins as small islands of specialized cells, known as angioblasts, are derived from the mesoderm. The development of the circulatory system is believed to begin as the embryo's size begins to limit diffusion, and a new method of transporting nutrients and waste throughout the embryo is necessary [246]. These islands form throughout the embryo proper, creating the first vessel structures that begin to coalesce, forming larger and larger vessel structures. SMCs are recruited to stabilize these new vessels, and a continual process of vessel merging, branching, and apoptosis continues throughout the rest of development and adult life in a process known as angiogenesis. The progression from angioblasts to endothelial cell is marked by the expression of several key proteins distinguishing ECs and their precursors from surrounding SMCs and other cells that also have functional significance [246-249]. What follows here is a brief description of these proteins and their role during developmental and post-developmental endothelial biology.

1.3.1.1 Flk-1

The first protein to be expressed by differentiating angioblasts during development is the vascular endothelial growth factor receptor 2 (VEGFR2), also known as flk-1 [246, 250-252]. Flk-1 is a 150-230 kDa tyrosine kinase receptor that is one of several VEGF receptors, and is crucial for the vasodilation, destabilization of mature vessels, migration, inhibition of apoptosis, proliferation, and differentiation response seen in ECs and EC precursors following VEGF

stimulation (see **Figure 1.5**)[246, 253-255]. Flk-$1^{-/-}$ knockout mice are embryonic lethal very early in development from a complete lack of vascular and hematopoietic development [251, 256]. Flk-1 expression is believed to be specific for ECs and EC precursors and persists throughout EC maturation as VEGF is an important signaling molecule for angiogenesis and normal vascular function [245, 246]. However, there have been reports of flk-1 expression in other cell types including neural cells [245, 257-259] and pericytes [260-262]. Flk-1 expression in ECs continues, albeit in a downregulated fashion, throughout adulthood in stable, mature vessels. However, flk-1 upregulation is a hallmark of angiogenesis and tumor formation [245, 263, 264].

1.3.1.2 Platelet-endothelial cell adhesion molecule (PECAM)

PECAM (130kDa) is one of several molecules expressed very early in angioblasts development [247, 265]. It is present in the yolk sac immediately upon implantation and is also found in the developing heart structure as well as intestinal portals [266]. There is some evidence that PECAM precedes flk-1, but is later downregulated and then returns following flk-1 expression [267]. The functional significance of PECAM is that it plays a role in homotypic cell-cell adhesions necessary for lumen formation, cell polarity, and vascular permeability [247, 266, 268]. PECAM expression during development proceeds in thread-like projections down the dorsal aorta as ECs are differentiated from their surrounding mesoderm, resembling primitive vascular networks [266]. Although PECAM is present in some megakaryocytes and other cells, it is still considered an EC-specific molecule as it is expressed in every adult EC [247, 266, 268-270]. PECAM is required for neutrophil and macrophage movement across ECs, and PECAM binding causes integrin clustering on lymphocytes [266, 271, 272].

1.3.1.3 Tie Receptors

Tie receptors (Tie-1 and Tie-2) are 117-125kDa tyrosine kinase receptors that are primarily involved in vessel stabilization and EC survival [245, 249, 273]. Tie receptors have extracellular domains with immunoglobulin-, fibronectin, and EGF-like repeating elements. They appear very early in vascular development and persist through adult-hood in an EC-specific manner [245, 274]. While the ligand for Tie-1 is unknown, angiopoietins have been identified as the ligands for Tie-2 receptors. Ang1 and 3 act as Tie-2 agonists while Ang2 and Ang4 act as Tie-2 antagonists. Ang1 binding to Tie-2 causes autophosphorylation of the receptor leading to vessel stabilization through recruitment of pericytes [245, 275, 276]. In fact, overexpression of Ang1 in the adult leads to hypervascularization in the form of many small, stable vessels[245, 277] in an opposing manner to VEGF overexpression, which leads to hypervascularization with multiple leaky, immature vessels [245, 278].

1.3.1.4 Vascular endothelial cadherin (VE-Cadherin)

VE-cadherin is a 140kDa calcium-dependent intercellular adhesion protein that is specific for ECs [279, 280]. Its expression is limited to confluent cultures and is downregulated under the influence of vascular permeability enhancing molecules such as tumor necrosis factor-α and interferon-γ [247, 280]. VE-cadherin functions to control vascular permeability to neutrophils and solutes as well as provide adhesive structure to the blood vessel through homotypic cell-cell interactions [280, 281]. During development, VE-cadherin appears in close conjunction with flk-1 in angioblasts, specifically in a subset of angioblasts that are flk-1^+ and GATA-1^- [282-284]. VE-cadherin has been shown to be exclusively expressed in ECs that have formed the first primitive vascular plexus [282, 285]. Indeed, VE-cadherin knockouts fail to form the primary

vascular plexus, indicating the importance of this cell-cell binding molecule in the formation of vascular structures [286]. VE-cadherin$^+$ cells go on to produce flk-1$^+$, VE-cadherin$^+$, and CD31$^+$ ECs in *in vitro* embryonic stem cell models. These differentiated ECs are also capable of acetylated low density lipoprotein (Ac-LDL) uptake, a hallmark of EC functionality [282, 287, 288].

After the formation of the vascular plexus, VE-cadherin is necessary for the continued expansion, maturation, branching, and prevention of vascular regression [254, 279]. VE-cadherin is also responsible for mediating contact inhibition of EC growth [289, 290]. Mutant VE-cadherin mice surviving through the plexus formation demonstrate disintegration of EC cell contacts as well as vessel regression, EC apoptosis, and tissue necrosis [254, 279]. The fact that VE-cadherin is not necessary for the initial induction of vasculogenesis and early vessel formation, but is necessary for subsequent angiogenesis and EC survival implies that VE-cadherin plays a role in maintaining cell-cell contacts under the mechanical load of more developed circulation and helps mediate VEGF-dependent survival signaling [279].

1.3.1.5 von Willebrand factor (vWF)

von Willebrand Factor (vWF) is an 250-270 kDa protein that is expressed almost exclusively by mature ECs [291]. vWF can be expressed at low levels on megakaryocytes, but has traditionally been used as a functional marker of ECs [291-293]. vWF has binding sites for a number of haemostatic molecules including Factor VIII and heparin, thus implicating its role in thrombosis [291]. It is found in three regions *in vivo*- free plasma, bound to blood vessel basement membranes, or stored within ECs [294]. vWF bound to the basement membrane has been shown to assist EC binding in intact and injured vessels where it increases microtubule and focal adhesion formation [295, 296].

Embryologically, vWF appears only after large vessel formation has occurred and precedes the onset of blood flow. In fact, vWF does not co-localize with other proteins that are expressed during the angioblast stage of vascular development. The expression of vWF is spatially and temporally restricted to a subset of ECs in large vessels, specifically those cells destined to form the dorsal aorta and its major branches, but the reasons for this are as yet unknown [292]. This continues in the adult where the total expression of vWF varies depending upon the tissue bed [292, 297, 298]. vWF expression in adults *in vivo* is controlled by a variety of stimuli including inflammatory cytokines, hypoxia, thrombin, compliment, and histamines [291, 292, 294].

1.3.2 Response to biological factors

Like SMCs, ECs have a long history of research with biological stimulation. ECs respond to various growth factors and cytokines during development and adult life that are directly related to their ability to participate in vasculogenesis and angiogenesis. In addition to growth factors, ECs produce and respond to a variety of other biological chemicals including nitric oxide, carbon monoxide, and prostaglandins [299]. Although these factors are important in their own right for their roles in EC biology, their discussion will be limited to within the context of the major growth factors including VEGF, FGF, PDGF, and TGF-β [256].

1.3.2.1 Vascular endothelial growth factor (VEGF)

VEGF is among the most important growth factors in the study of EC biology and pathology throughout the lifespan of the organism. The activity of VEGF in vascular ECs is mediated primarily through VEGF receptor 2 (VEGFR2 / flk-1), whereas VEGF receptor 1

(VEGFR1 / Flt-1) is believed to be an agonist for VEGF-mediated cell behavior [245, 300] (**Figure 1.5**)

VEGF is of critical importance to vascular formation as evidenced in the early embryonic lethality of VEGF and flk-1 knockouts due lack of vasculogenesis and complete vascular disorganization [251, 253]. Although VEGF is not responsible for the initial differentiation of angioblasts from the mesoderm during development [301, 302], it is required for differentiation into the mature EC phenotype [301, 303] as well as EC survival through expression of the anti-apoptotic protein Bcl-2 [300, 304]. In addition, VEGF induces dose-dependent increases in nitric oxide (NO) and prostacyclin (PGI_2), both powerful vasodilators [289, 305, 306]. VEGF production is regulated by several factors including hypoxia [264, 307] and mechanical stimulation [204, 308].

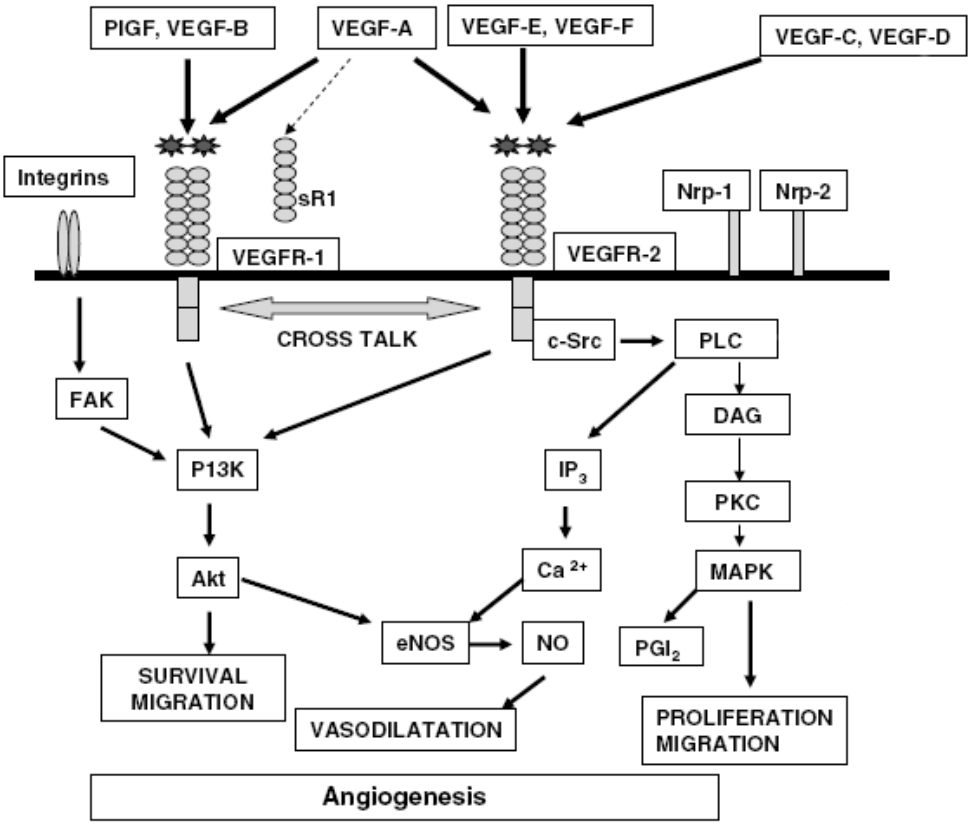

Figure 1.5: VEGF signaling in ECs is mediated through two VEGF receptors to increase survival, proliferation, migration, and production of vasoactive agents including NO and PGI_2. Figure reproduced with permission from [253].

Throughout vasculogenesis and angiogenesis, VEGF is responsible for EC cell junction disassembly, proliferation, sprouting, migration, and tube formation [253, 279, 287, 289, 309, 310]. Cell junction disassembly allows for the extravasation of plasma into the surrounding tissue, providing a fibronectin substrate for EC migration [309]. Indeed, fibronectin has been shown to increase EC proliferation and migration *in vitro* and *in vivo* [311-313]. Sprouting and migration are also mediated through VEGF-induced increases in MMP, tissue-type and urokinase-type plasminogen activators (tPA and uPA, respectively) and decreases in TIMP production in ECs [309, 314-317].

1.3.2.2 TGF-β

TGF-β signaling in ECs is important for vasculogenesis and angiogenesis. In addition to the standard TGF-β receptors (Type I and Type II) found on other cell types, ECs also have a Type III receptor (endoglin). This receptor is believed to be an agonist for TGF-β signaling [245, 318, 319]. Targeted mutations of TGF-β and its various receptors display major, but subtly different vascular malformations, underlining the importance of TGF-β and its downstream signaling targets to vasculogenesis and angiogenesis [145, 245, 320-323]. The small differences in mutant phenotype have led to the hypothesis that there are two distinct signaling mechanisms that result from activation of different TGF-β receptor groups, and that these somehow balance TGF-β signaling in ECs [324] (**Figure 1.6**). Overall, TGF-β appears to be responsible for EC differentiation [323] and vessel stabilization [145, 321, 322] as well as capillary fusion and vessel remodeling [324].

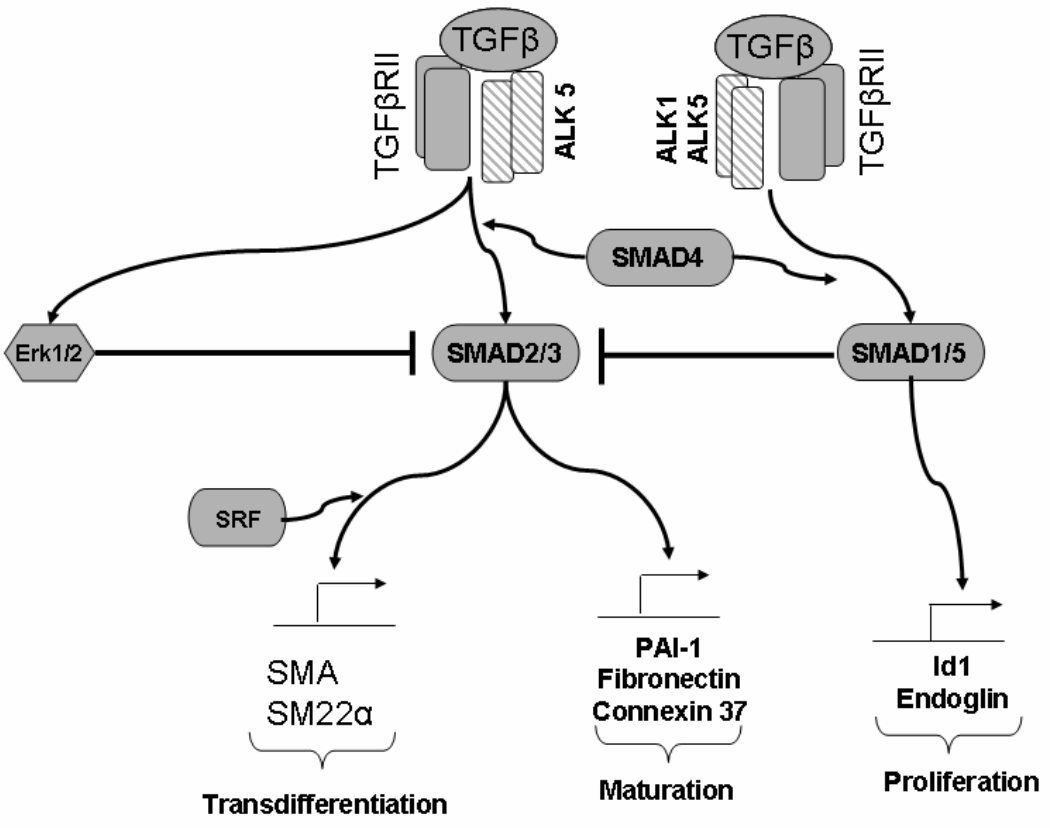

Figure 1.6: TGF-β signaling in ECs can elicit two different responses depending upon the type of receptor the ligands bind. This may account for the multiple phenotypes seen with embryonic TGF-β knockouts [325] as well as reports of transdifferentiation to SMCs [77, 78, 326]...

Like the genetic studies, the response of adult ECs to TGF-β has proven difficult to unravel because of the opposing results demonstrated in the literature. In general TGF-β tends to slow angiogenesis by reducing proliferation [323, 327, 328] and migration [329, 330] and increasing matrix production [245], TIMPs, and plasminogen activator inhibitors (PAIs) [245]. However, there appear to be specific conditions that cause the opposite effect, such as increasing vascular permeability [331] and proliferation [139], thus implying TGF-β has a biphasic response that may be dependant on TGF-β concentration and competing intracellular signaling cascades [139, 245, 332]. This concept is illustrated in studies from Li et al. [333] and Schwarte-Waldhoff et al. [334] where they found that TGF-β inhibited angiogenesis early during stages of oncogenesis, but promoted angiogenesis in later stages [245].

In addition to effects on vascular formation and angiogenesis, TGF-β may play a role in epithelial-mesenchymal transformations [77, 85]. Although this process is relatively restricted to embryonic processes (specifically heart formation) [335], Arciniegas et al. [77] have demonstrated that aortic ECs exposed to TGF-β can downregulate their expression of vWF and begin to express the SMC-like protein SMA and appear to be most similar to contractile SMCs by their ultrastructure [336]. This process was partially reversible, with vWF returning in some cells within 5 days of TGF-β removal and may have implications in atherosclerosis where injured vessels release large amounts of TGF-β, potentially converting ECs to contractile SMCs during plaque formation [77, 180, 337, 338].

1.3.2.3 FGF

FGF is necessary for the induction of angioblasts from the mesoderm both *in vitro* and *in vivo* [247, 301, 339]. Mutations in FGF or its receptors lead to embryonic death prior to

gastrulation [339-341]. The role of FGF in vascular development is mainly an inductor of the angioblast into an flk-1^{+} cell, with flk-1 becoming maximally expressed within 24h of FGF stimulation [247, 342]. However, following angioblast induction, embryonic ECs do not contain detectable levels of FGF receptor mRNA, suggesting that they are not utilizing FGF signaling for the remainder of vascular morphogenesis [247, 343, 344].

In adult ECs, the FGF receptor expression returns, suggesting its importance for repair and regeneration [247, 344, 345]. FGF has been shown to be an important inductor of angiogenesis [175, 289, 346] and is found in the ECM, although FGF has no known mechanisms for extracellular export (see Section 1.2.2.3) [175, 340]. FGF induces EC proliferation [347], survival [348], migration [349], and matrix degrading proteins including MMPs and plasminogen activators [346, 350]. The effect of FGF on ECs is also dependant upon their ECM. Kanda et al. [348] have demonstrated that ECs exposed to FGF on fibronectin proliferate and spread, but do not differentiate (form tubes). Conversely, on collagen ECs do not proliferate or spread, but instead immediately differentiate and form capillary tubes. This result further implies an interaction between growth factor receptors and integrin-mediated signaling that plays such a crucial role in vascular biology [351-353].

1.3.2.4 PDGF

Although PDGF has been demonstrated to promote angiogenesis, early studies could not delineate whether its effects were directly related to ECs or indirect through SMCs and pericytes [247, 354, 355]. While the expression of PDGF receptors are well documented on SMCs and pericytes (see Section 1.2.2.1), only microvascular ECs appear to express the PDGF receptors, specifically PDGFRβ (see **Table 1.2**) and are capable of proliferation and angiogenic sprouting in response to PDGF [289, 355, 356]. Battegay et al. [355] have demonstrated the expression of

PDGFRβ is restricted to microvascular ECs undergoing angiogenesis, specifically those ECs within chords and sprouts, and this expression increases over time as chord formation continues. They further demonstrated that PDGF-BB was released from the non-angiogenic ECs that did not express PDGFRβ, and that the growth factor release increased the proliferation of angiogenic ECs. However, PDGF-BB was not sufficient to drive sprouting, suggesting that the other factors such as FGF and/or VEGF are the major players in EC growth and differentiation [355, 357].

1.3.3 Response to mechanical stimuli

ECs throughout the vasculature experience various degrees of all three mechanical stimuli (see **Figure 1.2**). The magnitude of each stimulus (pressure, stretch, and shear) that ECs experience depends upon their position in the vasculature. ECs in the major vessels (aorta and first major branches), which have more elastic content and larger diameters, experience higher stretch magnitudes and lower shear magnitudes. In more muscular arteries, shear magnitudes increase and stretch magnitudes decrease as the caliber and composition have changed. In the venous system, the magnitudes of pressure, stretch, and shear are greatly diminished [185-188, 358, 359]. Of the possible mechanical stimuli, the effects of shear stress on ECs have received the most attention because of the established role of shear stress in atherosclerosis [188, 193, 358, 360, 361]. The following is a brief discussion of how ECs respond to their mechanical environment, specifically stretch, pressure, and shear.

1.3.3.1 Stretch

The effects of cyclic stretch on ECs have shown many different effects depending upon the magnitude of stretch as well as the species and tissue bed origin of the ECs. Iba et al.[359]

demonstrated that ECs from the aorta, pulmonary artery, and vena cava display different proliferation, alignment, and prostaglandin production when exposed to stretch. Only the vena cava ECs oriented perpendicular to the direction of stretch, while only the aortic ECs increase proliferation and prostaglandin production.

Another series of studies have demonstrated that stretch causes oxidative stress (as measured by superoxide release) and associated responses by arterial ECs [362-364]. These responses to oxidative stress include increases in endothelial nitric oxide synthase (eNOS), which releases NO to scavenge superoxides)[364-366], monocyte chemotactic protein (MCP-1)[367], interleukin-6 (IL-6)[368], endothelin-1 (ET-1)[369-371], intercellular adhesion molecule (ICAM-1)[372, 373], and tissue plasminogen activator inhibitor (PAI-1)[372]. Some of these responses, such as NOS production, are highly dependent on the magnitude of stretch [366]. Concomitant with the increase in ICAM-1, Barron et al.[373] demonstrated a decrease in vascular cell adhesion molecule-1 (VCAM-1), indicating that ECs exposed to stretch might increase their permeability which is another response to oxidative stress [374]. MCP-1, IL-1 and ICAM-1 have been identified as participants in the development of atherosclerosis [375]. However, in another study, Iba et al.[376] found that saphenous vein ECs increase expression of tissue plasminogen activator (tPA), but not PAI-1, upon exposure to 24% cyclic stretch, again demonstrating the importance of tissue source on the response of ECs to mechanical stimulation.

Other studies have demonstrated that cyclic stretch has an important effect on the way that ECs function. Matsumoto et al.[377] have demonstrated that cyclic stretch increases EC proliferation in 2D and 3Dculture. Stretch also inhibited EC sprouting in 3D culture leading to fewer, but larger caliber capillaries. The increase in EC proliferation as a response to stretch has been reported in ECs from other tissue sources as well [366, 378]. The increased proliferation

may be resulting from changes in cell-cell contacts, which are controlled by the intercellular adhesion protein VE-cadherin [289, 290, 377]. Thus, vessels that are experiencing stretch may have a tendency to enlarge in an attempt to improve compliance or reduce stress. This is borne out in other studies that demonstrate that cyclic stretch is necessary for the sustained release of vasodilating agents such as NO and PGI_2 [365, 366, 379]. Cyclic stretch also increases Ang-2 and Tie-2 receptors, which are important for maintaining vessel stability and are angiogenesis inhibitors [380], and promotes EC survival by phosphorylation of the anti-apoptotic protein Bad [381]. These studies all point to the importance of cyclic stretch in maintaining ECs in a normal functional state and leading to the prevention of atherosclerosis [381].

Cyclic stretch can also have other effects on ECs, including a possible phenotypic switch towards an SMC phenotype. Cevallos et al. [83] have shown that 10% cyclic stretch causes umbilical vein ECs to express SMA and SM22α, two molecules typically restricted to SMCs. These results are similar to the epithelial-mesenchymal transitions in ECs resulting from TGF-β stimulation (see Section 1.3.2.2) [77, 85]. However, the expression of these two markers is not sufficient to claim a complete SMC phenotype and further work is necessary to verify the resultant phenotype.

1.3.3.2 Pressure

ECs in the lumen of a blood vessel are exposed to the cyclic pressure wave that propagates down the length of the vessel during fluid flow. Although studies have demonstrated the importance of pressure to vascular health [115, 224, 382, 383], pressure is the least-studied physical stimulus on vascular cells *in vitro.*

Tokunaga et al. [384, 385] were among the first to examine the differential effects of pressure on both aortic ECs (AECs) and umbilical vein ECs (UVECs). They reported an increase in UVEC proliferation between 0 and 80 mmHg with an inverse relationship to PGI_2 release. Pressure between 80 and 160 mmHg caused AEC damage with continual increases in PGI_2 release. These studies were followed by others that showed similar trends in proliferation [384-390] and PGI_2 [391] release that also varied depending upon where in the vasculature the ECs were derived. Additionally, these studies have identified other molecules, including MMP-1 [387], ET-1 [392], NO [392], and ZO-1 [393], are regulated by pressure in a manner consistent with the hypothesis that higher pressures may be damaging to ECs and lead towards atherosclerotic processes. Although ZO-1 is regulated by pressure to increase EC permeability, VE-cadherin does not appear to be affected by pressure [393].

The proliferation changes in ECs in response to pressure may be mediated through changes in growth factor release that include VEGF [394] and bFGF [395] but not TGF-β [388]. Ohashi et al. [396] have recently shown that increased proliferation from pressure (up to 150 mmHg) resulted from a decreased in VE-cadherin leading to a loss of contact inhibition. The decreases in proliferation reported at higher pressures [384-390] may be a result of apoptosis [390]. Hasel et al. [390] have reported that pressures outside of physiologic ranges (200/100mmHg) initially induce apoptosis through Fas and FasL interactions within 24 hours. However, the ECs seem to recover after 48 hours, and this phenomenon appeared to be independent of the EC cell source (UVEC and AEC). This paradoxical relationship may be related to the potential dual role of Fas, which can increase proliferative and pro-survival paracrine signaling [397].

1.3.3.3 Shear

Shear stresses are arguably the most important mechanical stimuli for ECs. During development, the induction of blood flow is critically important to the continued development of the vasculature [247]. Only after connection of the vascular plexus to the vitelline arteries and veins does the enlargement of the major vessels occur. Without this connection, the vasculature completely regresses [247, 398]. In several elegant studies on cardiovascular development, Hogers at al. [399-401] have demonstrated that altering vitelline blood flow leads to heart and major vessel malformations in chick embryos. In adult physiology, it is well documented that systemic vascular diseases such as atherosclerosis have lesion formation in geometrically distinct points, namely at branches and bifurcations in the arterial tree [358, 360]. The shear stresses along the straight portions of vessels can be considered laminar, while branching points, bifurcations, and stenotic areas have complex fluid profiles that typically involve recirculation and turbulent profiles [402]. These features are evident in EC morphology, which is ellipsoid and aligned with the flow in the straight portions of arteries, and more polygonal and randomly oriented near bifurcations [402, 403]. Studies on shear stress are numerous and varied, depending upon the types of shear stress studied (laminar, oscillatory, turbulent, and complex flow patterns) as well as magnitude, temporal effects, and EC cell source.

Although the data presented in **Table 1.3** comes from a variety of different EC sources, shear regimes and shear apparatuses, several trends begin to appear depending upon the type of shear stress, i.e., laminar vs. disturbed (which includes turbulent, impulse, step, and oscillatory). Laminar shear stress has consistently demonstrated decreases in EC proliferation [402, 404-406] and increases survival (Tie-2) as well as angiogenic (flk-1 and MMP-1) gene expression [244, 407]. Another common response by ECs to laminar shear stress is that several genes tend to be

initially upregulated (0-12 hours) followed by downregulation (12+ hours) to baseline or lower levels [402]. These genes include PDGF [408, 409], bFGF [410], tPA [411], MCP-1 [412],and ICAM-1 [413, 414]. This appears to be an adaptive process for ECs since their initial state in culture is without shear stress [360] (see **Figure 1.7**). Vasodilators (NOS, NO), SMC proliferation inhibitors (TGF-β), anti-oxidants (heme oxygenase, cyclooxensase-2, cytochrome 1B1 and 1A1) and anti-thrombogenic factors (thrombomodulin, TFPI) seem to have sustained expression while vasoconstrictors (ET-1), pro-coagulation proteins (PAR-1 and vWF), and inflammatory proteins (MCP-1, ICAM-1, VCAM-1) display a sustained decrease. Those factors that are initially increased, then decreased may be under the control of immediate early genes (ERK, JNK), which can be activated within a few minutes and peak by one hour followed by downregulation [415, 416]. In fact, shear stress response elements (SSREs) have been identified as an intermediary between these early genes and other genes such as PDGF [402, 417, 418]. In contrast to these early responders, the vasoactive, anti-thrombogenic, and anti-oxidant factors remain at elevated levels with sustained shear stress. Therefore, it would seem that immediate early genes are needed for a short-term response to injury while the vasoactive, anti-thrombogenic genes are maintained for hemostasis [363, 419].

Low magnitude, oscillatory, impulse, and turbulent shear stress profiles favor higher EC proliferation [402, 406, 420, 421] as well as increased levels of adhesive, chemotactic, and growth factors [184, 420]. Decreased shear stress induced by coronary ligation has shown increased uptake of low density lipoprotein (LDL) and monocyte adhesion through increases in VCAM-1 [360, 422] as well as increased apoptosis [423-425]. This apoptotic response to low magnitude and oscillatory shear stress is in contrast to anti-apoptotic responses of ECs to higher magnitude laminar shear stresses [426-428]. Vasoactive factors, such as eNOS, while increased

under laminar flow, are held constant or decreased in turbulent flow [429], and oscillatory flow has been shown to increase oxidative-stress in ECs leading to increases in VCAM expression [430-432]. In experiments involving disturbed non-laminar shear stress, EC response has shown to be heterogeneous depending upon what region of flow they fall in, such as increased proliferation, migration, and apoptosis at the flow-reattachment site [425, 433]. This may indicate an activated EC state that is more susceptible to other stimuli (such as oxidative stress) and can lead to further progression towards atherosclerosis (see **Figure 1.7**). This hypothesis is validated studies where VCAM-1 expression is increased by lipopolysaccharide (LPS) stimulation only in regions of the aorta predisposed to atherosclerosis [427, 428]. ECs at the reattachment point of disturbed flow also express increased levels of VCAM-1 [360] as well as repression of cell cycle inhibitors and survival genes [434]. Computational modeling has shown that increased cardiac output shifts these disturbed regions to different parts of the vessel, thus not allowing a single position to be constantly exposed to this fluid profile and potentially inhibiting atherosclerosis development in that region [358, 435].

Table 1.3: The effects of shear stress on EC gene and protein expression. Solid arrows indicate up (↑), down (↓), or no change (→) in gene or protein expression of each factor. Double arrows indicate the sustainability of the signal as up (⇑), down (⇓), or returning to baseline (⇔). The type and magnitude (in parenthesis) of each shear stress is indicated in the magnitude column. L=laminar; T=turbulent; I=impulse;O=oscillatory; P=pulsatile. Table adapted from [244].

Factor	Change	Shear Stress Magnitude (dynes/cm^2)	Reference
Vasoactivity			
eNOS	↑ ⇑	L(6-25), P(8-12)	[436-438]
	→	T(8)	[429]
ET-1	↓ ⇓	L(8-25), P(12-18), T(15)	[439-443]
	↑ ⇔	L(1.8-5)	[444]
PGI_2	↑ ⇔	L(10), P(8-12)	[445-447]
Growth			
PDGF-A	↑ ⇔	L(6-51), S(16), I (16)	[408, 409, 416, 420]
	→	L(15-36),P(15),T(15)	[410, 420]
PDGF-B	↑ ⇔	L(3-51)	[448-450]
	↑ ⇓	L(15-36), P(15), T(15)	[410]
bFGF	↑ ⇔	L(15-36), P(15), T(15)	[410]
	→	L(25)	[411]
TGF-β	↑ ⇑	L(5-40)	[451, 452]
	→	L(<5)	[451]
Proliferation	↑ ⇑	T(1.5-15), I(16),	[404, 406, 420, 421]
	→	L(1-30)	[405, 406]
Adhesion			
ICAM-1	↑ ⇔	L(2.5-46), T(10)	[413, 414, 422, 453]
VCAM-1	→	L(2.5-46)	[414, 422]
	↓ ⇓	L(<7.2)	[422, 431]
MCP-1	↑ ⇓	L(16)	[412, 454]
	↑ ⇑	I(16), S(16)	[420]
PECAM	↓ ⇔	L(12)	[455]
	↑	L(14)	[456]
VE-Cadherin	↑ ⇑	L(12-15)	[455, 457, 458]
Coagulation			
TF	↑	L(12)	[459]
tPA	↑	L(15-25)	[411, 455]
Thrombomodulin	↑ ⇔	L(15-36), P(12-18), T(15)	[460, 461]
	→	L(4)	[460]
TFPI	↑ ⇑	L(0.27-19)	[462]
vWF	↓	L(12)	[455]
Anti-oxidant			
COX-2	↑ ⇑	L(1-30)	[419, 463]
	→	T(10)	[419]
HO-1	↑ ⇔	L(5)	[432]
	↑ ⇑	O(5)	[432]
SOD	↑ ⇑	L(0.6-15)	[419, 432, 464]
	→	T(10)	[419]
Cytochrome 1A1/1B1	↑ ⇑	L(25)	[443]

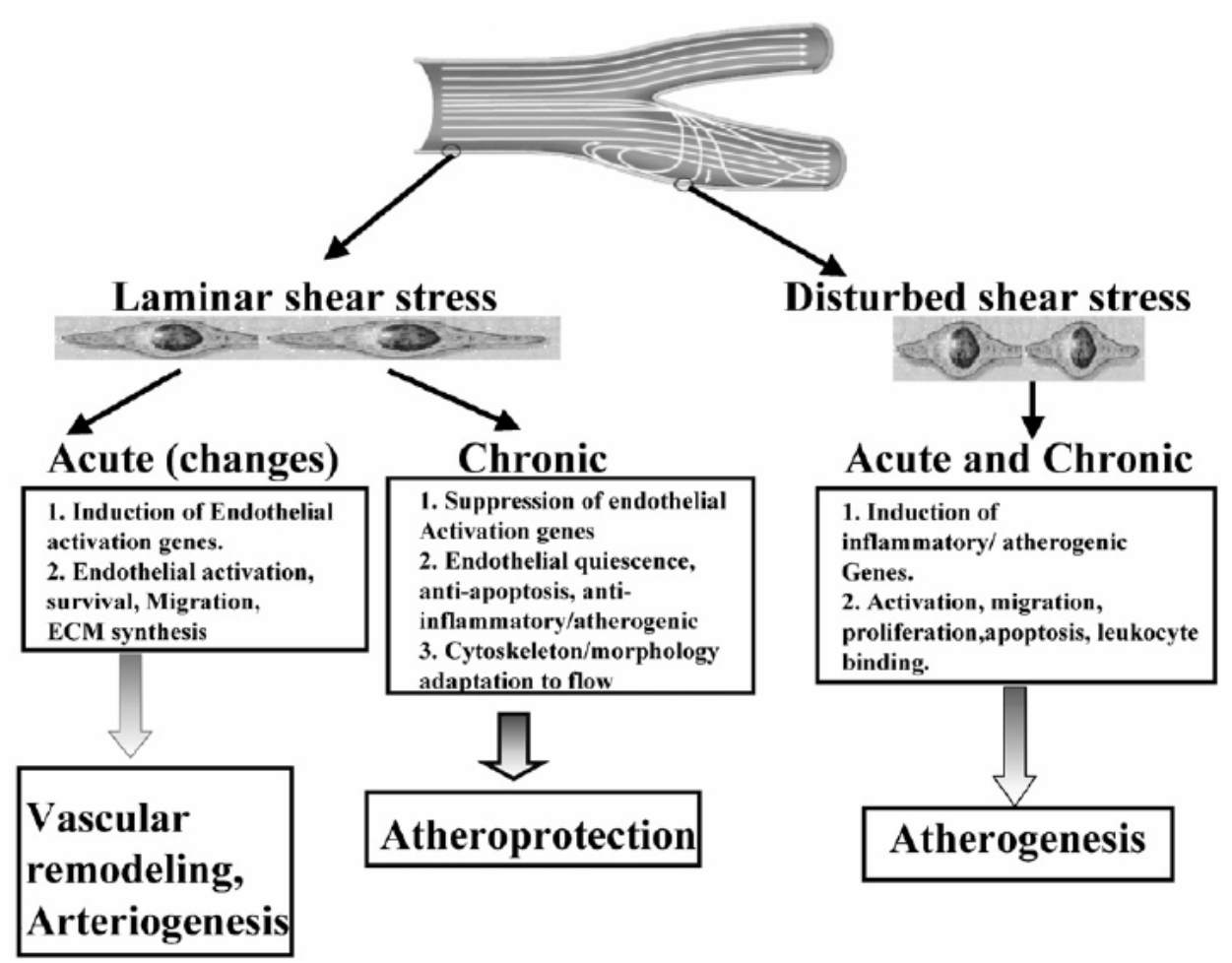

Figure 1.7: The effects of shear stress on ECs depend upon the temporal exposure and type of shear stress. Chronic exposure to laminar shear is atheroprotective while both acute and chronic exposure to disturbed shear stress leads to atherogenesis. Acute changes in the laminar shear region lead to adaptive changes such as vascular remodeling and arteriogenesis. Reprinted with permission from Elsevier [360].

1.4 ADULT STEM CELLS

1.4.1 Definition of stem cells

The notion that primitive stem cells exist in adult humans was first suggested in 1867 by Cohnheim [465]. Further work pioneered by Friedenstein [466-469] and Dexter [470-472] confirmed the presence of hematopoietic and mesenchymal stem cells in the bone marrow. Since then, adult stem cells have also been isolated from striated muscle [57, 473, 474], peripheral blood [475-479], umbilical cord blood [480, 481], adipose [482-485], placenta [486, 487], and the neuronal system [488, 489]. More recently, the embryonic aortic wall was reported to contain mesangial-like stem cells that also share common traits with the skeletal muscle derived stem cell {Tavian, 2005 #3890}. Because of this diversity in stem cell sources, future discussion will be limited to stem cells derived from the bone marrow with limited reference to cells from other sources (including embryonic) where the experimental data for bone marrow-derived stem cells is lacking.

Bone marrow-derived hematopoietic stem cells are the best-characterized stem cells due to the focus on treating bone marrow-associated diseases. Research in recent years has been devoted to purification of the bone marrow to find multipotent stem cells, particularly the bone marrow derived mesenchymal stem cells (BMMSCs), which could be used for other medical applications. Bone marrow has been sorted based upon density and the expression of many different cluster designation markers and membrane receptors [57]. The main division for bone marrow has been along the marker for CD34, with $CD34^{+}$ cells being considered the hematopoietic stem cells (HSCs) and the $CD34^{-}$ being considered mesenchymal stem cells [57]. However, separation into the hematopoietic and mesenchymal cell types may not restrict the

progenitor cells to certain germ lines. For example, research has shown that $CD34^+$ HSCs can generate cardiomyocytes [490]. BMMSCs have traditionally been identified as being positive for SH3 (CD71), SH2 (CD105/endoglin), activated leukocyte adhesion molecule (ALCAM/CD166), phagocytic glycoprotein I (CD44), Thy1 (CD90), integrin β1 (CD29), STRO-1, and HOP26 (CD63) and negative for CD14, CD34, and leukocyte common antigen (LCA/CD45) [56, 491, 492]. BMMSCs have also been shown to express CD59, CD117, and CD90, and have been sorted accordingly using fluorescent activated cell sorting [493-498]. A newer marker, CD133 (a.k.a. AC133), has also been used as an indicator for endothelial progenitor cells [499-501].

1.4.2 Differentiation of BMMSCs

As detailed in Sections 1.2.2-1.2.3 and 1.3.2-1.3.3, it is well established that SMCs and ECs, and indeed many other cell types, are sensitive to biomechanical and/or biochemical stimulation [214, 215, 219, 502-508], and data is continuously emerging to suggest that BMMSCs are no different. Primary cultures of BMMSCs have consistently demonstrated multiple differentiation capacities [56, 58, 477, 509-513]. Specifically, *in vitro* biochemical and biomechanical conditions have been identified which stimulate the differentiation of these stem cells towards adipocytes [56, 514], osteoblasts [56, 466, 514, 515], stroma [516, 517], chondrocytes [56, 518, 519], cardiomyocytes,[520-525], SMCs [42, 526-531], and ECs [49, 499, 501, 520, 532-534]. The various chemical and mechanical stimuli that drive BMMSC differentiation will be further discussed in the proceeding sections.

1.4.2.1 Biological and biochemical factors

As knowledge has increased about growth factors, cytokines and other bioactive molecules that induce cell phenotypic changes *in vivo*, conditions have been identified which may guide the *in vitro* differentiation of BMMSCs to specified cell lineages (see **Table 1.4**). For example, researchers have defined conditions which lead to the derivation of osteoblasts using ascorbic acid, dexamethasone and β-glycerophosphate [56]; to chondrocytes using transforming growth factor-β (TGF-β) and pellet culture [56]; to adipocytes using isobutyl methylxanthine, dexamethasone and insulin [56]; to neural cells using basic fibroblastic growth factor (bFGF) [535] or epidermal growth factor (EGF) [536]; and to cardiac cells using 5-azacytidine [523, 525, 537] or insulin, dexamethasone, and ascorbic acid [524]. It is important to note that several common chemicals, such as dexamethasone, insulin, and ascorbic acid have been utilized to produce varying differentiation patterns [524, 529, 538-540].

Extensive research also has been performed on the differentiation of BMMSCs towards ECs using various combinations of vascular endothelial growth factor (VEGF) alone or in conjunction with insulin-like growth factor (IGF), stem cell growth factor (SCF), or bFGF [501, 541-543]. Although many researchers have utilized different growth factor cocktails, VEGF is the common biochemical addition for the differentiation of stem cells towards ECs [54, 493, 501, 542, 544, 545], and it is also known that BMMSCs express the VEGF receptor, flk-1 [493, 546-549]. VEGF is also known to be a potent inducer of mature EC functions such as nitric oxide and prostaglandin production [306, 550]. Work performed by Kim et al. [551] has shown that differentiation to ECs is possible with other chemicals such as β-mercaptoethanol and dexamethasone when BMMSCs are cultured in Iscove's modified Eagle's medium.

Previous research has also focused on utilizing BMMSCs as a source of SMCs. Observations by Charbord et al. [552] indicate that long-term culture of bone marrow results in cells whose cytoskeleton resembles that of SMCs. Furthermore, Arakawa et al. [529] have demonstrated that a clonal cell line mouse BMMSCs can be induced to express h1-caldemson, calponin, and myosin heavy chain (all of which are markers for SMCs; recall Section 1.2), in the presence of β-mercaptoethanol and ascorbic acid. Other research has shown the importance of several cytokines such as PDGF-BB [42, 120], bFGF [553], TGF-β [42, 554], and retinoic acid [555] in the formation of SMCs from BMMSCs. One interesting finding related to competing signals has shown that TGF-β appears to cause an increase of BMMSC proliferation by synergizing with effects of PDGF [42].

Table 1.4: Differentiation of BMMSCs can be induced by a variety of biological and biochemical agents.

Phenotype	Biological and Biochemical Factors	Reference
Adipocytes	Insulin, isobutyl-methylxanthine, indomethacin, dexamethasone	[56]
Osteoblasts	Ascorbic acid, dexamethasone, β-glycerophosphate	[56]
Chondrocytes	TGF-β, pellet culture	[56, 556]
Neurocytes	bFGF	[535]
	EGF	[536]
Cardiomyocytes	5-azacytidine	[523, 525]
	Insulin, dexamethasone, and ascorbic acid	[524]
SMCs	PDGF-BB	[42, 120]
	TGF-β	[42, 554]
	bFGF	[553]
	Retinoic acid	[555]
ECs	VEGF	[54, 493, 501, 533, 544, 545]
	VEGF, IGF, bFGF	[542]
	VEGF, SCF	[501]

1.4.2.2 Mechanical stimulation

Although the effects of mechanical stimuli on fully differentiated SMCs and ECs has been extensively studied and demonstrated to be important for the normal physiologic function of these cells (recall Sections 1.2.3 and 1.3.3), the use of physiologically-relevant biomechanical stimuli have only recently begun to be employed, not only for BMMSC differentiation, but other stem cell sources as well.. Therefore, the powerful potential of biomechanical forces on their own, or in combination with biological factors, has not been fully elucidated and has gone underutilized in the field of vascular regenerative medicine. There have been few reports evaluating the effect of biomechanical forces on BMMSC differentiation which are outlined here.

1.4.2.2.1 Stretch

Our lab [526] was among the first to demonstrate that cyclic uniaxial stretch was sufficient to promote SMC protein production in BMMSCs (**Figure 1.8**) while inhibiting division. These results were confirmed in a three dimensional model showing that BMMSCs to produce SMC-specific proteins under static tension or cyclic stretch, and decreased proliferation (as measured by MTT) under cyclic stretch [557]. These results may be related to the redirection of the cells towards differentiation instead of proliferation, a concept that has previously been proposed for differentiated SMCs [336]. Park et al. [527] further showed that uniaxial stretch, but not equiaxial stretch, is necessary for the increase in SMC gene transcription and protein production. Their results, however, depicted a transient increase in SMC gene expression as the BMMSCs oriented perpendicular to the direction of strain. In a follow-up study, Kurpinski et al. [558] showed that by forcing the alignment of the BMMSCs in the direction of stretch, they

could achieve a stronger increase in the expression of SMC markers as well as increase proliferation. Song et al. [559] have also reported increased proliferation under uniaxial stretch.

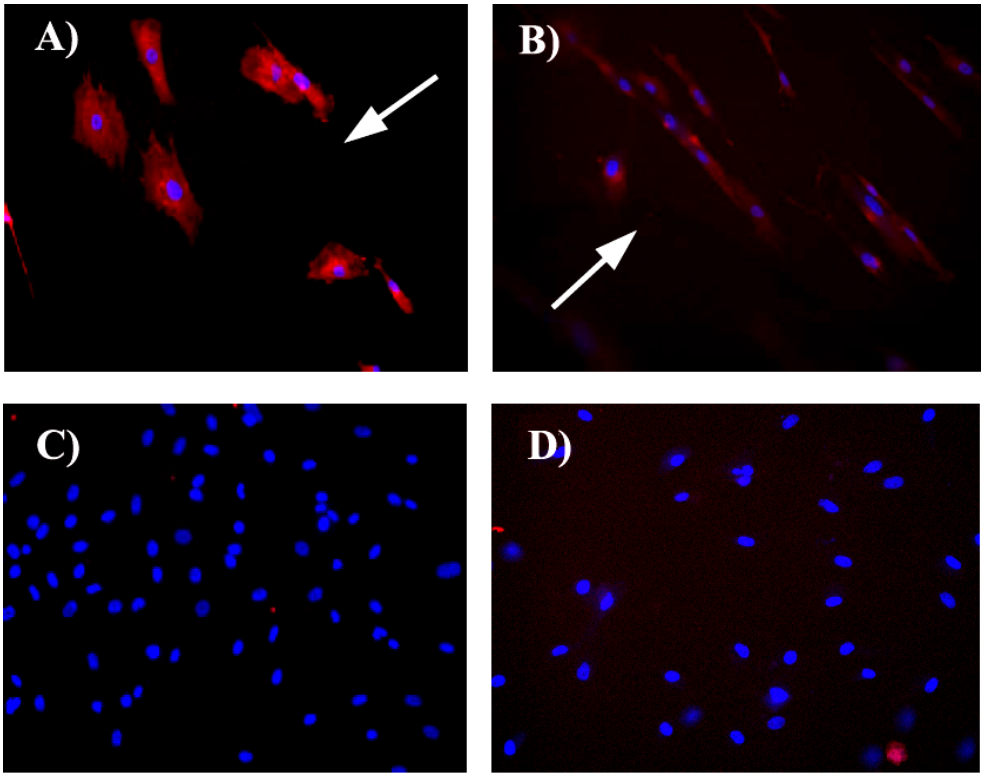

Figure 1.8: The application of cyclic uniaxial stretch to BMMSCs leads to the production of smooth muscle proteins (A) SMA and (B) h1-calponin. Control cultures (C-D) were negative for (C) SMA and (D) h1-calponin. Figure adapted from [526].

There have also been several studies investigating the influence of stretch on BMMSC differentiation to other cell types [507, 560-565]. Altman et al. [507] demonstrated that appropriately applied mechanical forces (stretch and torsion), without biochemical stimulation, induced BMMSC differentiation to a ligament cell lineage. The results of this study, particularly the increase in ECM production as a result of cyclic stretch, are consistent with others [561, 566] that have shown BMMSCs exposed to cyclic stretch increased collagen I and III synthesis in similar manner to valve interstitial cells.

Thomas and El-Haj [560] determined the dose-response of a cyclic stretch applied to 10-day-old cultures in osteo-inductive culture medium, with an emphasis in understanding

osteoblast differentiation. They demonstrated that increasing stretch magnitude resulted in elevated alkaline phosphatase levels, characteristic of early osteoblast differentiation. Similarly, BMMSCs treated with osteo-inductive media and exposed to intermittent (30 minutes-2 hours per day) cyclic stretching at both 1 Hz and 0.5 Hz have demonstrated osteoblast differentiation through increases in alkaline phosphatase, Runx2, and osteocalcin, collagen I, and collagen III production [562-565]. In the short-term, this intermittent cyclic stretching with media containing dexamethasone was found to be more osteo-inductive than dexamethasone alone [564]. In addition to the rise in osteoblast proteins expression, adipogenic proteins such as PPAR-γ were decreased by intermittent stretch, leading to the conclusion that cyclic stretching modulates adipogenesis in favor of osteoblastogenesis [562].

1.4.2.2.2 Shear

Although shear stress is another important biomechanical force in the cardiovascular system (see Sections 1.2.3.3 and 1.3.3.3), there have only been a few reports on the effects of shear stress on BMMSC as well as embryonic stem cell (ESC) differentiation. Kobayashi et al. [530] determined that pressure-dominated shear stress (120/60 mmHg, 1 dyne/cm^2) as well as combined pressure and pulsatile shear forces (120/60 mmHg, 7-14 dyne/scm^2, 90^o phase shifted) were responsible for increasing SM-MHC (SM-1 isoform) and SMA protein expression in BMMSCs. This was the first study suggesting that BMMSCs are capable of moving towards SMC lineages as a result of fluid flow. Yamamoto et al. [567] and Wang et al. [568] each demonstrated that flk-1$^+$ ESCs exposed to physiologic levels of shear stress` will express the EC proteins CD31, flk-1, flt-1, vWF, and VE-cadherin at both the protein and mRNA levels. Huang et al. [569] took this a step further by demonstrating both EC and SMC organization and differentiation as a result of pulsatile flow through a compliant tube seeded with ESCs.

In addition to cardiovascular differentiation, other studies involving shear stress and stem cells have focused on osteoblast differentiation. Oscillatory fluid shear stress was found to increase the expression of bone-related genes such as osteopontin and osteocalcin as well as increase proliferation when applied to BMMSCs grown in osteo-inductive culture medium [570]. Similar effects have been demonstrated using steady shear stress, but without any increases in proliferation as reported in the oscillatory shear study [571-573]. It is important to note that the shear stresses employed in musculoskeletal studies are on the order of about 2 dynes/cm^2, which is much lower than the shear stresses employed in cardiovascular studies. Also, the differentiation of osteo-progenitors appears to be strongly dependant upon the timing of the shear stress application following osteo-induction and is related to PGI_2 and prostaglandin production [572].

1.4.2.2.3 Pressure

As for adult SMCs and ECs, pressure has also been an under-studied stimulus for stem cells. Although Kobayashi et al. [530] reported a pressure dominated vascular differentiation response by BMMSCs, their study was not able to decouple the effects of pressure from shear stress (see Section 1.4.2.2.2). This has been the only study to date that examined the relationship of pressure to cardiovascular cell differentiation in stem cells. The majority of studies on the effects of simple hydrostatic pressure (both cyclic and static) on stem cells have centered on musculoskeletal precursors, namely osteoblast-, osteoclast- and chondrocyte-precursors derived from BMMSCs. Hydrostatic pressure appears to increase differentiation potential of osteoblast-induced BMMSCs and osteo-progenitors into osteoblasts [574, 575] and inhibit the differentiation potential of osteoclast-induced BMMSCs [576, 577]. A similar effect has been demonstrated for chondrocyte-induced BMMSCs, with pressure increasing chondrocyte-specific

matrix production and driving the chondrogenic phenotype [578-582]. The frequency and magnitude of pressure stimulation in chondrocyte-precursors appears to affect differentiation [582] more than osteoblast- [574, 575] and osteoclast-precursors [576, 577]. Although these studies indicate that BMMSCs are indeed sensitive to hydrostatic pressure, they do not decouple the pressure stimulus from other stimuli such as a chemical inductor or other mechanical stimuli, and therefore may be masking the true nature of the pressure effect. Also, in a similar manner to the effects of shear stress on osteo-progenitors, pressure-induced differentiation appears to depend upon the timing of application following induction [576, 579].

1.4.2.2.4 Summary of mechanical stimulation

Although the mechanical environment is important for maintaining the phenotype and functionality of terminally differentiated cells (see Sections 1.2.3 and 1.3.3) [25, 244, 358, 402, 583-588], only recently has attention been given to the role that mechanical forces play in the differentiation of BMMSCs. The previous studies described in Section 1.4.2.2 (summarized in **Table 1.5**) demonstrate the important potential of using mechanical stimulation to guide BMMSC (and ESC) differentiation. From the table, it is readily apparent that most of the mechanical stimulation in BMMSCs has been from the musculoskeletal perspective, utilizing low magnitudes of stimulation (for both stretch and shear stress) as well as the intermittent application of these forces. Moreover, a majority of these studies have not been conducted with multipotent BMMSCs, but rather have been performed following pre-differentiation or lineage commitment of the cells using osteo-inductive media.

Although limited in scope, the cardiovascular-related studies to date have clearly demonstrated the ability of cyclic stretch and shear stress to generate SMC and EC differentiation in BMMSCs and ESCs The motivation to study the role of mechanical

stimulation towards cardiovascular cells has be generated, in part, by recent *in vivo* data suggesting that BMMSCs have the ability to home to sites of vascular injury, and in this mechanically dynamic environment generate vascular SMCs and ECs [547, 589-592]. While the data in **Table 1.5** seems to indicate that cyclic stretch predominantly guides BMMSCs towards SMCs, and shear stress guides ESCs towards ECs, pulsatile shear stress is the only stimulus demonstrating the fully contractile marker SM-MHC in BMMSCs. In addition, there is a complete lack of data utilizing cyclic pressure that is physiologically relevant to the cardiovascular system even though there is clear evidence that pressure is an important stimulus for both ECs and SMCs (see Sections 1.2.3.2 and 1.3.3.2). The few cardiovascular-related studies have also utilized a limited range of magnitudes and paid no attention to the effects of frequency despite the wide range of both that are present from early development to maturity throughout the vasculature. These factors may ultimately be important in determining the lineage to which the stem cells differentiate but without coordinated study, we can only speculate as to their role in BMMSC differentiation.

Table 1.5: Effects of mechanical stimulation of BMMSCs and ESCS. Solid arrows indicate up (↑), down (↓), or no change (↔) in each factor. Double arrows indicate signal sustainability as up (⇑), down (⇓), or returning to baseline (⇔). CS=cyclic stretch, PF=pulsatile flow; LSS=laminar shear stress; CP=cyclic pressure; OFF=oscillatory fluid flow; UN=uniaxial; EQ=equiaxial; OI=osteo-inductive media; AI=adipo-inductive media; IM=intermittent/ <0.5 Hz; Magnitudes listed in parenthesis % for CS; dynes/cm^2 for LSS, PF, and OFF; and mmHg for CP.

Factor	Change	Stimulus and magnitude	Reference
SMC			
SMA	↑	**CS(10) UN; PF (1-14)**	**[526, 530]**
	↑⇔	**CS(10) UN; LSS (1-14)**	**[527, 530, 567]**
	↓⇓	**CS (10%) EQ**	**[527, 567]**
Calponin	↑	**CS(5-10) UN**	**[526, 558]**
SM22α	↑⇔	**CS(10) UN; LSS(1-5)**	**[527, 567]**
	↓⇓	**CS(10) EQ**	**[527]**
Caldesmon	↔	**CS(10) UN**	**[526]**
SM-MMHC	↑	**PF(1-14)**	**[530]**
EC			
VE-cadherin	↔	**CS(10) UN**	**[527]**
	↑⇑	**LSS(1-5)**	**[567]**
Flk-1	↑⇑	**LSS(1-5)**	**[567]**
PECAM	↑⇑	**LSS(1-5)**	**[567]**
vWF	↑⇑	**LSS(1-5)**	**[568]**
Osteoblast			
Alkaline phosphatase	↑⇔	**CS(3) EQ,IM, OI**	**[563]**
	↑⇑	**CS(8), CP(100) IM, +/-OI**	**[564, 574]**
	↔	**CS(10) UN; LSS(1.6) IM, OI**	**[527, 572]**
	↓	**OFF(20)**	**[570]**
Osteocalcin	↑⇑	**CS(3-4) EQ; LSS(0.36-2.7); OFF(20); CP(100) +/IM, OI**	**[562, 563, 570, 571]**
	↔⇔	**CS(2-10) UN +/-IM, +/- OI**	**[527, 564]**
Runx2	↑	**CS(4) EQ IM, OI**	**[562]**
Osteopontin	↑⇑	**OFF(20); LSS(1.6); CP(1500) IM, OI**	**[570, 572]**
Chondrocyte			
Collagen II	↔	**CS (10) UN**	**[527]**
Adipocyte			
PPAR-γ	↓	**CS(4) EQ IM, AI**	**[562]**
ECM			
Collagen I	↑⇑	**CS(8-10) UN +/-IM; OFF(20), OI**	**[507, 527, 564, 570]**
	↔	**CS(10) EQ**	**[527]**
	↓	**CP(100) IM, OI**	**[574]**
Collagen III	↑⇑	**CS(2-10) +/-OI**	**[507, 564]**
	↔	**CS(10) UN**	**[527]**
Proliferation			
	↑	**CS(3-10) UN +/-IM; OFF(20), +/-OI**	**[333, 507, 559, 563]**
	↓	**CS(10) UN**	**[526]**
	↔	**LSS(0.36-2.7) IM, OI**	**[571, 572]**

1.5 SUMMARY AND LIMITATIONS OF PREVIOUS RESEARCH

BMMSCs represent a potentially useful cellular source for regenerative medicine. While some research has been performed on BMMSCs and the means by which they can be differentiated towards bone, cartilage, and fat [56, 510], research into using BMMSCs for vascular applications is still in its infancy [53, 520, 521, 528, 529, 552, 591]. Although the biological factors discussed in Sections 1.2.2 and 1.3.2 are important for SMC and EC differentiation and maintenance, the previous studies outlined in Section 1.4.2.1 have utilized concentrations, combinations, and types of biological and biochemical factors [42, 120, 493, 501, 529, 541-543, 551, 554, 593-595] to differentiate BMMSCs to vascular cells which may not be found in the *in vivo* environment. Given the documented plasticity of BMMSCs [57, 488, 520], any stimuli used to differentiate these cells *in vitro* may be required to be maintained *in vivo*. Without such signals, the BMMSCs may not maintain their phenotype. In addition, some of the biochemical factors utilized for vascular differentiation have been demonstrated to cause differentiation into other phenotypes such as bone and cartilage [56, 524, 529, 538-540].

In light of these issues, we believe that bioactive molecular stimulation alone is insufficient for the creation and maintenance of specific cell types for use in regenerative applications, but that, at a minimum, biomechanical stimulation is also required. Yet, despite the importance of mechanical stimulation in the development and maintenance of the cardiovascular system, limited attention has been given to the use of mechanical stimulation for differentiating BMMSCs. Section 1.4.2.2.4 identifies that our current understanding is lacking a systematic analysis of BMMSC differentiation under mechanical stimulation. The limited amount of data that does exist (see **Table 1.5**) does not present a unified perspective on how mechanical stimulation can be effectively utilized for regenerative medicine, particularly vascular

regenerative medicine. Broader interpretations of the data are complicated by inconsistencies in the response to various magnitudes, frequencies, and type of stimulus as well as the presence and absence of osteo- or adipo-inductive additives and cell source. Therefore, there is need for research to elucidate the magnitude, frequency, and temporal response of BMMSCs to various mechanical stimuli. A greater understanding how stem cells respond to mechanical stimuli will ultimately aide in their use for cell therapy and in bioreactor design for the *ex vivo* production of tissue engineered products.

1.6 HYPOTHESIS AND SPECIFIC AIMS

The proposed work is designed to test the following hypothesis:

Mechanical stimulation, relevant to the vascular system, will guide the differentiation of BMMSCs towards vascular SMCs and ECs.

The overall goal of this project was to systematically analyze the response of BMMSCs to the Mechanical Panel, which we define as the parallel application of the mechanical stimuli that are physiologically relevant to the vasculature – namely cyclic stretch, pressure, and shear stress – and to assess if BMMSC differentiation was sustained following removal of the stimulus. The specific aims that were executed to test this hypothesis were as follows:

Specific Aim 1: To develop and validate a compact bioreactor capable of extended application of cyclic hydrostatic pressure.

Specific Aim 2: To elucidate the dose-dependent response of BMMSCs to varying magnitudes and frequencies of each mechanical force stimulus in the Mechanical Panel.

Specific Aim 3: To elucidate the temporal response of BMMSCs to the most appropriate frequency and magnitude determined from Specific Aim 2 for each mechanical force stimulus in the Mechanical Panel.

Specific Aim 4: To determine the plasticity of BMMSCs following differentiation via cyclic stretch.

This research project was broken into two main components. The first component was the design and validation of a cyclic hydrostatic pressure system (Specific Aim 1). Computational fluid dynamics and biological analysis of cell viability and proliferation were used as benchmarks for the successful completion of Specific Aim 1. The successful design of a cyclic hydrostatic pressure system was necessary to complete the Mechanical Panel of stimuli that were to be used in Specific Aim 2 and Specific Aim 3.

The remainder of the research project centered on the response of BMMSCs to the Mechanical Panel over a range of physiologically relevant magnitudes and frequencies (Specific Aim 2) was determined through quantitative analysis of cellular morphology and proliferation, and also by assessing changes in gene and protein expression. Next, the importance of the duration of applied stimulation to BMMSC differentiation was assessed by examining quantitative changes in gene and protein expression at two different time points (Specific Aim 3). Finally, the plasticity of BMMSCs exposed to cyclic stretch was assessed by examining quantitative changes in gene and protein expression upon removal of the stimulus (Specific Aim 4). The knowledge obtained from these studies will ultimately aide in the design of bioreactor - guided differentiation of stem cells for use in regenerative medicine.

2.0 DEVELOPMENT OF A CYCLIC PRESSURE BIOREACTOR

2.1 INTRODUCTION

2.1.1 Overall goals

Cyclic hydrostatic pressure is thought to be important in the function and/or dysfunction of many different cell types, including those of cardiovascular, bone, cartilage, renal, pulmonary, urinary tract, and ocular tissues [576, 596, 597]. For example, elevated pulmonary pressure causes increased production of inflammatory mediator proteins, primarily from macrophages, which is important for understanding mechanical ventilation injury in the lungs [598]. In the vasculature, hypertension is known to be a major cause of intimal hyperplasia and atherosclerosis [115, 185, 224, 382, 383]. In fact, it has been shown that SMCs undergo morphologic changes and increase proliferation under elevated static and cyclic pressure [225].

Maintaining cell viability under defined mechanical conditions is important for studies in cellular mechanobiology, including those related to this project. While the application of stretching and shear forces has been adequately provided for extended periods of time *in vitro* with commercially available and custom-designed devices [445, 599-602], the extended application of hydrostatic pressure has proven problematic. The hurdle in conducting long-term (>2 days) *in vitro* experimentation using applied hydrostatic pressure in cell culture has been

maintaining proper humidification, and this is especially problematic for cyclic application. Because cyclic pressure generally requires constant movement of air through the culture chamber, water can evaporate from the culture media, upsetting the osmotic balance and disrupting cellular function, eventually leading to cell death. Thus, Specific Aim 1 of this research dissertation was to develop a cyclic pressure bioreactor that was capable of sustaining cellular viability for extended periods under cyclic pressure application in order to determine the response of BMMSCs to cyclic pressure. It is noted that a majority of the work described in this chapter was published in the Journal of Biomechanical Engineering and is reproduced with permission from ASME [1].

2.1.2 Prior art and limitations

While several devices have been published reporting the application of cyclic pressure for less than two days [389, 576, 578, 596, 598], only two devices have been published that reported the application of cyclic pressure for longer periods of time ($\geq$2 days) [225, 597, 603]. Hasel et al. modified a Flexcell 4000T cyclic stretch device to apply both cyclic pressure and cyclic stretch to vascular smooth muscle cells for up to 96 hours [597]. In our opinion, the humidification system employed appears to be sub-optimal since the humidification occurred at room temperature, thus yielding an maximum absolute humidity of ~20g/m^3, which is less than half the 45g/m^3 typically required for maintaining cellular function [604]. Watase et al. [225] stimulated smooth muscle cells for 9 days with computer controlled solenoid valves regulating the entrance of air into a Plexiglas® chamber containing culture plates and a water reservoir. However, preferential evaporation from the water reservoir instead of the culture chambers is not expected. Therefore, water evaporation likely occurred in both the water reservoir and the cell

culture media. Using a similar approach, Xing et al. [603] separated their system into two compartments with a rubber diaphragm. The lower compartment, which contained the cell culture plates, a water dish for humidification, was filled with 5% CO_2 air and completely sealed beneath the diaphragm. The upper compartment was connected to a compressed air supply, and ambient pressure in the lower portion of the chamber was assumed to be equal to the pressure of the compressed air in the upper portion of the chamber when the diaphragm was at equilibrium. By limiting the amount of possible air turnover, the relative humidity in the culture portion of the chamber was maintained at 95%. However, by sealing the culture chamber, experiments were essentially limited to 48 hours before a fresh supply of air would have to be exchanged, thus disrupting the equilibrium vapor pressure which was established by evaporation from both the water dish and the culture chamber (similar to the drawback of the system described by Watase et al.[225]). For the short-term cyclic pressure devices, Pugin et al. [598] created a design that in all likelihood could have been used much longer than the 32 hour experiments they published. This device applied cyclic pressure in conjunction with cyclic stretch to macrophages by using a clinical respirator, and included a heated humidification circuit. The use of a heated humidification circuit ensured that the air entering the culture chamber was fully saturated at 37°C (unlike the system described by Hasel et al.[597]), and no water loss would be expected to occur. The main drawback to this system was the use of a clinical respirator, which added significant cost and space requirements to the system.

While each of these devices have shown some ability to apply static or cyclic pressure to cell cultures for extended periods of time, they have either employed inadequate humidifiers or required costly components, computer-driven algorithms, or large volumes of space for their operation. The goal of Specific Aim 1 was to create a system for the long-term application of

fully humidified, cyclic pressure of multiple magnitudes and frequencies. The development of our cyclic pressure system (**Figure 2.1**) was centered on four key design goals: minimal size, stability of pressure and humidity, maximal accessibility, and versatility.

2.2 METHODS

2.2.1 Design considerations

2.2.1.1 Minimal size

In order to successfully perform our Mechanical Panel experiments, which require the use of all three mechanical stimulation devices at the same time, we had to minimize the volume occupied by the cyclic pressure system. First, the system was designed to occupy only ~1400 cm^3 of total space within an incubator by minimizing the number of necessary components within the controlled environment, and keeping the rest of the system outside. The pressurized culture chamber consists of a single continuous volume, into which up to 6 microscope slides, scaffolds, or other materials may be placed (**Figure 2.1e** and **Figure 2.2**). Initial observations of fluid ripples being generated by the impinging inlet air led to the placement of two stainless steel bars (**Figure 2.1f** and **Figure 2.2**) placed directly below the inlet and outlet ports. These bars, whose height was sufficient to protrude above the media, prevented the jet impingement from causing a fluid disturbance and potentially transmitting such disturbance to the cells by converting the downward vertical velocity of the incoming air to a horizontal velocity prior to the air contacting the media. The stainless steel bars also function to constrain the slides, or other materials being stimulated, to the bottom of the chamber. Stainless steel was chosen as the

material for these bars due to its inertness (chemical reactions between the cell culture media and aluminum in earlier designs resulted in widespread cellular death).

2.2.1.2 Environmental stability

In order to study the biological effects of a given stimulus, that stimulus must be applied in a constant and consistent manner throughout the duration of the experiment. For our pressure system, this required a constant magnitude of pressure to be available as well as a constant partial pressure of the gases required for normal cell culture (i.e., 21% O_2, 5% CO_2, balance N_2). The stability for the magnitude of pressure was achieved with the internal house air system (**Figure 2.1a**), which does not significantly fluctuate. Therefore, after setting the resistors that control the mean and pulse pressure (**Figure 2.1c** and **Figure 2.1j**) to reach the desired pressure waveform, the system could operate within accepted limits without the assistance of computer control. To provide a constant source of normal cell culture gas, we mixed the air from the house air system, which was 21% O_2 balanced with N_2, with a small amount of pure CO_2 to achieve ~21% O_2, 5% CO_2, and balance N_2. The ratios of air and CO_2 were controlled with two gas rotameters (FM034-39 and FM082-03, Cole Parmer, Vernon Hills, IL).

2.2.1.3 Maximum accessibility

Because the cyclic pressure system utilizes a constantly refreshed blend of air and CO_2, we needed to quickly and easily sample the culture media to monitor dissolved gas concentrations in a sterile manner without interrupting the operation of the system. In addition, future experiments may require the capability for growth factor or biochemical addition, and/or addition or removal of growth surfaces in a sterile manner. All of these requirements were satisfied by using a single continuous culture chamber (**Figure 2.1e**), a central injection port

(**Figure 2.1g**) for sampling media and adding culture supplements, and sterile filters and at both the inlet (**Figure 2.1d**) and outlet (**Figure 2.1h**) of the chamber to allow its removal from the incubator as necessary.

2.2.1.4 Versatility

In order to investigate the dose- and frequency- response of BMMSCs to cyclic pressure (Specific Aim 2), we required the ability to apply several different physiologically-relevant magnitudes and frequencies of cyclic pressure using the same system. To control the frequency of the cyclic pressure wave, we designed a simple flip-flop circuit containing three NE555 timers (Fairchild, McLean, VA) to apply 0.5, 1.0, or 2.75 Hz frequency signals to an electrically activated solenoid (98300-12, Cole Parmer). The solenoid was placed distal to the pressure chamber (**Figure 2.1i**), and pre- and post-solenoid passive resistors were used to control the pressure magnitude. Representative waveforms generated by the system were captured using a clinical pressure monitor (Spacelabs, Issaquah, WA) (**Figure 2.1m**) connected to a data acquisition board interfaced with LabView® (National Instruments, Austin, TX) data acquisition software. The 0.5 and 1.0 Hz data were collected at 30Hz, and the 2.75Hz data was collected at 100Hz. The data was smoothed using the following centrally-weighted moving average filter equation:

$$y_s(i) = \frac{\sum_{0}^{N} y(i-N) + y(i+N)}{2*N} \qquad \textbf{(2.1)}$$

where $y_s(i)$ is each point in the smoothed data set, and N is the number of data points on either side of the raw data, y(i) [605]. For the purposes of this study, N was set to be 3 to maintain 95% of the peak pressure value.

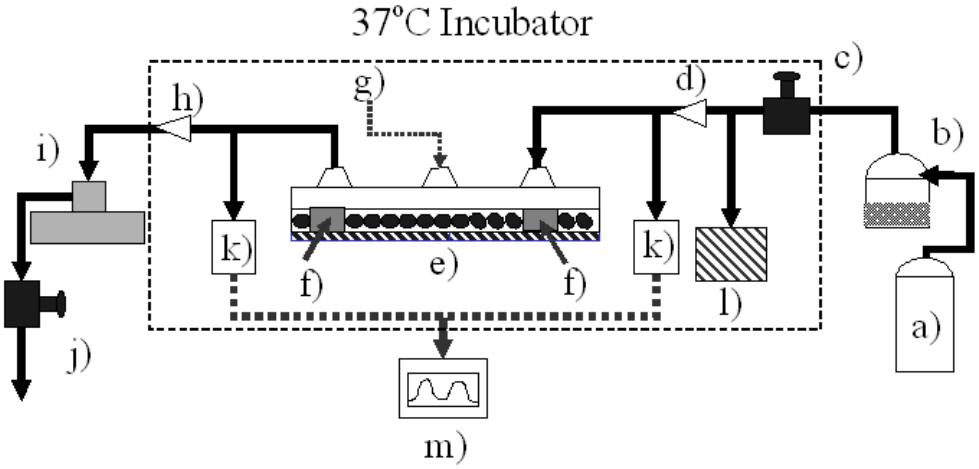

Figure 2.1: Schematic of the cyclic hydrostatic pressure system designed during the execution of Specific Aim 1. A constant pressure source (a) provides the bulk airflow that powers the cyclic pressure system, and consists of an in-house air pump and pure CO_2 blended together to achieve 5% CO_2, 20% O_2, and 75% N_2. A heated passover circuit (b) humidifies the air to ~100% before it passes through a resistor that controls the mean pressure (c). The air then passes through a sterile filter (d) before it enters the culture chamber (e) and builds a static pressure in the dead space above the culture media. Two stainless steel bars (f) deflect the incoming air and provide weight to stabilize the culture surface. An injection port (g) provides access for media sampling or chemical injection. The air then passes through a second sterile filter (h) on its way to a solenoid valve (i). When the valve is closed, pressure builds inside the system. When the valve is open, the pressure is released through a second resistor (j) that controls the diastolic pressure. Two pressure transducers (k) and their associated monitor (m) display the pressure inside the cyclic pressure chamber. A check valve (l), which has a cracking pressure of 250mmHg, allows the system to release built-up pressure in the event that one of the filters becomes obstructed. The dashed box represents the interior of the incubator. Figure reproduced with permission from ASME [1].

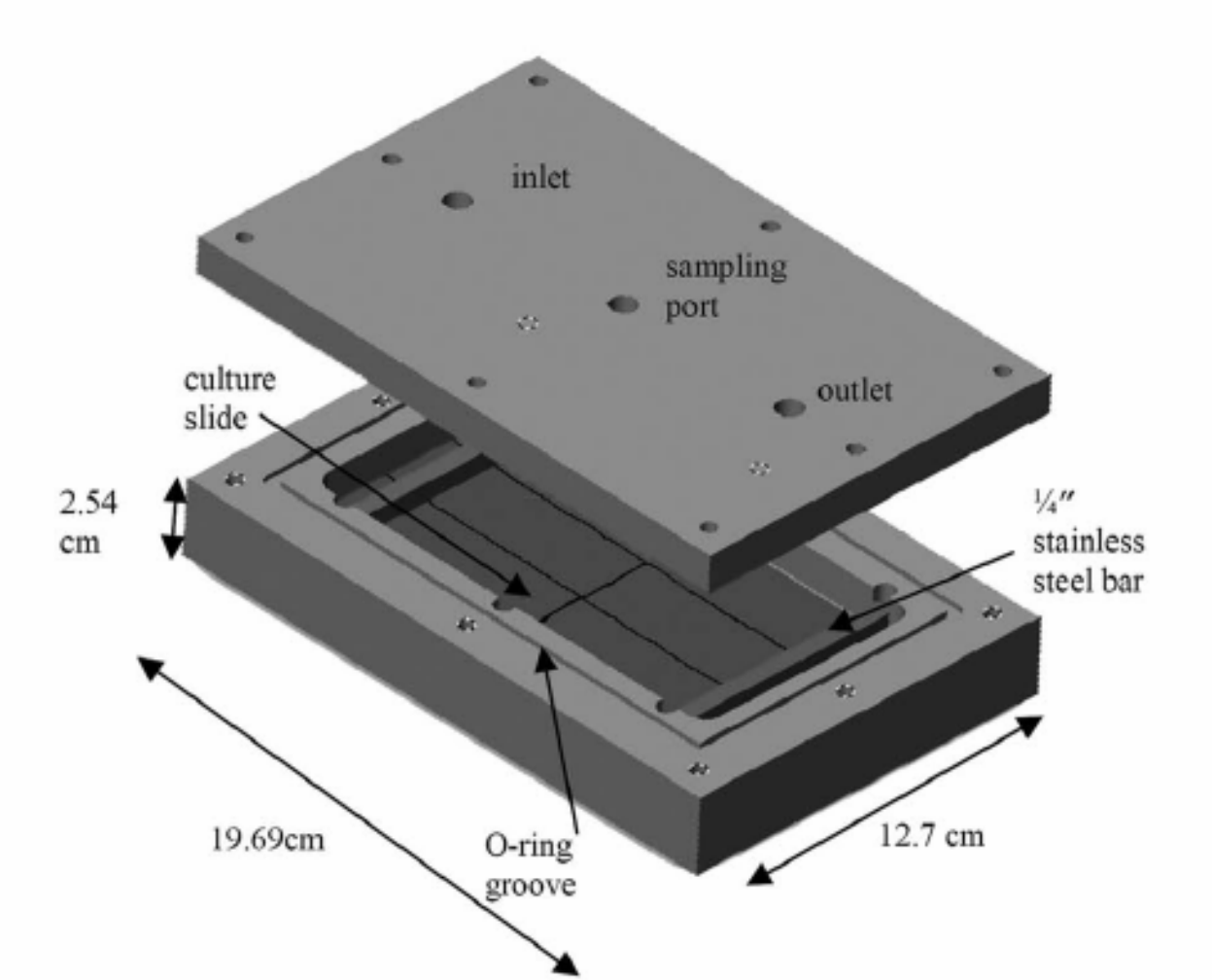

Figure 2.2: A three-dimensional exploded view (to scale) of the cyclic hydrostatic pressure chamber (see **Figure 2.1e**) depicting the lid with the inlet, outlet, and sampling ports, 6 culture slides, o-ring groove, and stainless steel bars. Figure reproduced with permission from ASME [1].

2.2.1.5 Humidifier designs

In order to achieve extended application of cyclic hydrostatic pressure, the dry air used to drive the system must be properly humidified. It has been documented that cellular dysfunction increases with time and deviation from optimal humidity ($45g/m^3$) [604]. From experience using the room temperature passover similar that used by Hasel et al.[597], we determined that the maximum humidity achieved as not sufficient to sustain viability in our system. To address this, several different options for humidifying the air were investigated (**Figure 2.3**). Each humidifier was evaluated, calculating the relative humidity following operation by measuring the amount of water and gas used during the experiment and using **Equation (2.6)**. The first humidifier used was a simple bubble humidifier. It consisted of a 250 mL side-arm flask filled with water through which the air destined to pass through the pressure chamber was bubbled (**Figure 2.3A**). This was placed in the incubator in an attempt to maintain the temperature of the water and air at 37^oC; thus raising the ability of the air to hold more water. Several experiments were attempted with this configuration, but all experiments resulted in substantial evaporation and cellular death as evident by the low relative humidity achieved (~16.8%). The next step in improving humidification was attempted by installing a heating element to heat the air prior to entering into the bubble humidifier. The heating element (2M8131 Variable Nebulizer Heater, Baxter, Deerfield, IL) was combined with copper tubing to create a small chamber to flash heat the air prior to entering the bubble humidifier (**Figure 2.3B**). This method was determined to provide only a slight improvement in the calculated humidity (~33% improvement), which was still insufficient to sustain cell viability. A bubbling stone was added to the tubing in the humidity chamber to increase the surface area-to-volume ratio of the bubbles, which increased the relative

humidity more than 3-fold, but still not to a level sufficient to sustain cell viability (**Figure 2.3C**). Finally, the humidifier volume was increased to 2 L to increase the residence time for a given molecule of air, but this did not improve humidification beyond that achieved by using the bubbling stone (**Figure 2.3D**). Although attempts were made to maximize the humidification through the bubble humidifier, a more effective method was necessary in order to sustain long-term experiments. To that end, we employed a device which is used clinically for the humidification of air for respiratory ventilators. The MR730 respiratory humidifier (**Figure 2.3E**, Fisher&Paykel, Auckland, New Zealand) employs a self-feeding, heated, domed water reservoir and heated tubing that conducts the humidified air from the reservoir into the incubator, and maintains the humidity near 100% as the air enters the culture chamber. This device has been used previously in the cyclic pressure system described by Pugin et al [598]. The MR730 was determined to adequately humidify the air entering the pressure chamber (see **Figure 2.3F**) and was used for the biological validation of the cyclic pressure system (Section 2.2.3).

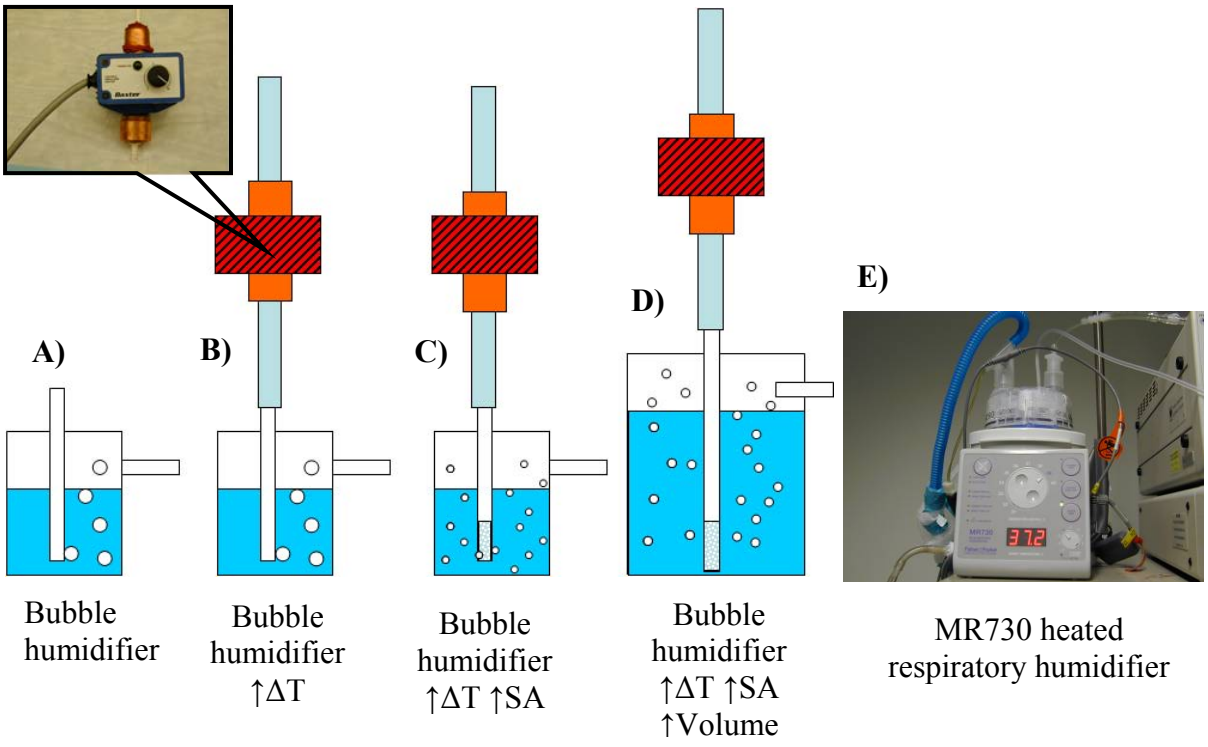

F)

Total mass used	Initial Setup	ΔT	ΔT+SA	ΔT+SA+Vol	Heated Passover
water (g)	15.0	20.9	87.0	50.0	541.0
gas (m^3)	2.1	2.2	3.0	1.7	12.7
% Humidity	16.8	22.4	67.1	66.5	98.6

Figure 2.3: Progression of humidification system design for the cyclic pressure system. (A) Simple bubble humidifier kept at 37°C. (B) The simple bubble humidifier with the added heating element (callout) to increase the air temperature prior to entry into the bubble humidifier. (C) Adding a bubbling stone increased the surface area available to pick up moisture. (D) Increasing the volume of the bubble humidifier increased the residence time for air. (E) The MR730 respiratory humidifier finally chosen as the best possible humidification system. (F) Table depicting the increased humidity achieved with each successive improvement to the humidification system. The increase in volume did not add any increase in relative humidity. The heated passover humidifier achieved the optimal humidity for the cyclic pressure system.

2.2.2 Computational fluid dynamics

Because a time-varying jet of air impacts the culture medium over the cells throughout the operational cycle, we wanted to ensure that the resulting hydrostatic pressure wave was evenly distributed along the length of the chamber, and no significant shear stress was applied to the cells. To that end, computational modeling of the cyclic pressure chamber was performed using CFD-ACE (Version 2002.2.16, CFDRC, Huntsville, AL).

2.2.2.1 Mesh development

Because of the significant computational costs associated with a three dimensional analysis in the required model, a 2-D representation of the pressure chamber with approximately 3,500 structured linear quadratic elements was generated by the plane passing through the centerlines of the inlet and outlet ports of the chamber (**Figure 2.4**). A boundary layer was created at the air/liquid interface as well as the bottom of the chamber, the region of interest vis-à-vis shear forces. An inlet flow extension with a length-to-diameter ratio of 12.5 was used to establish a fully developed flow for the air entering the chamber. The 2-D volume between the end of the chamber and the downstream solenoid was estimated by multiplying the tubing length by its diameter and modeled as a closed compliance volume attached to the outlet of the model.

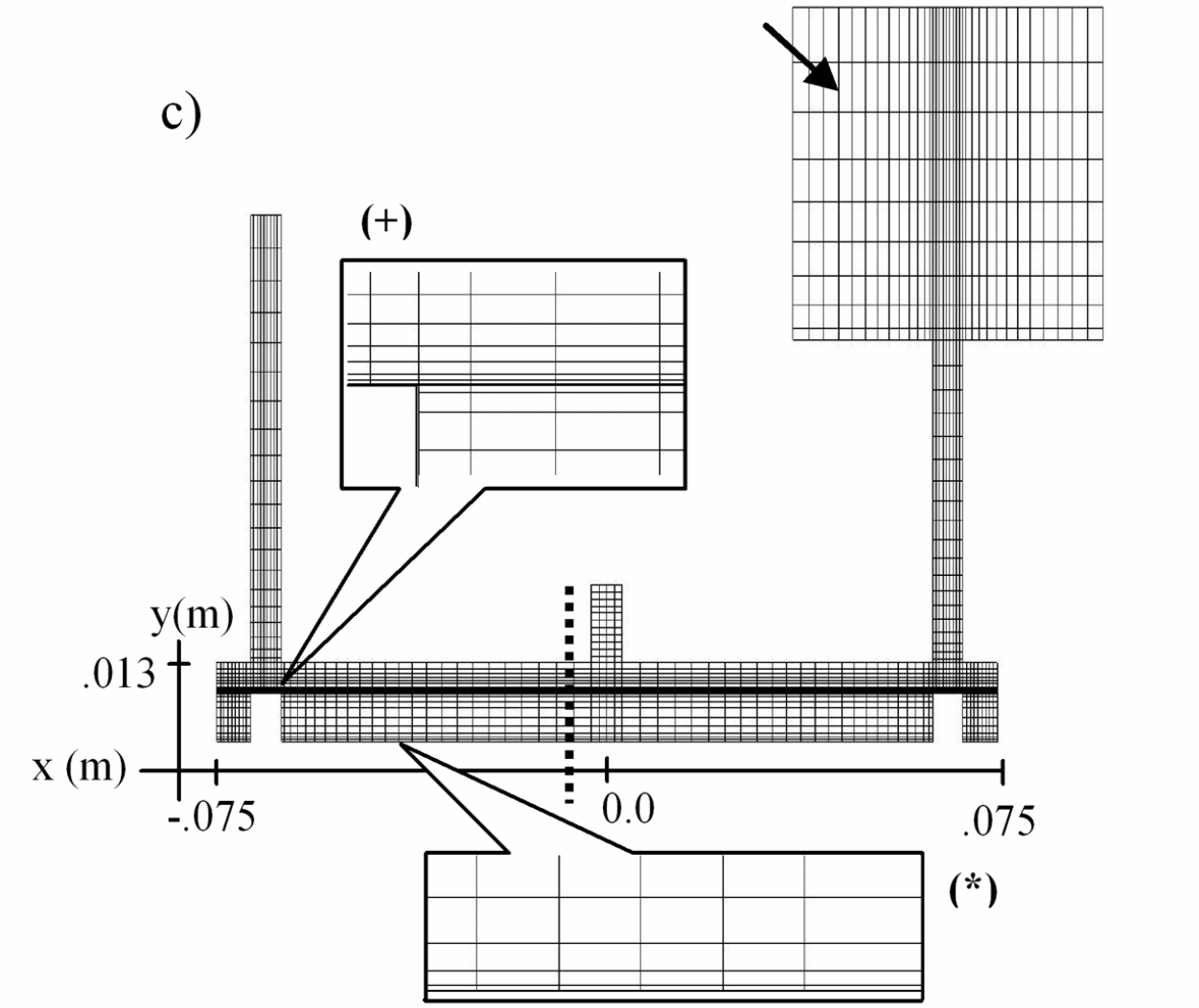

Figure 2.4: A 2-D CFD model of the pressure chamber using linear quadratic elements. Two boundary layers were created, one at the air/liquid interface (+), and the other at the base of the chamber where the cells would be located (*). A sealed box (arrow) with an equivalent 2-D volume to the volume of the circuit between the chamber and the solenoid valve was used at the outlet. The x- and y-axes depict positional information (in meters) relevant to the velocity, pressure, and shear stress plots in subsequent figures. Figure reproduced with permission from ASME [1].

2.2.2.2 Boundary conditions

The inlet boundary condition was a time-varying pressure obtained with a first-order linear regression of the first half of a duty cycle (80 to 120mmHg) from the 1 Hz data collected from the experimental system. Since the normal operation of the system occurs as an oscillation between 80 and 120 mmHg, modeling only the first half of the cycle was sufficient to determine if any shear stresses developed on the base of the chamber. The outlet boundary condition was modeled as a closed compliance chamber to simulate the air volume held between the chamber and the closed solenoid valve (removed during post-processing for scaling).

2.2.2.3 Solution Parameters

The computational model included the volume of fluid (VOF) multiphase formulation:

$$\frac{\partial F}{\partial t} + \nabla \bullet \vec{u}F = 0 \qquad \textbf{(2.2)}$$

where F is the fraction of a particular element occupied by the liquid volume, t is time, and $\vec{u}$ is the velocity vector [606]. Equation **(2.2**) was solved in conjunction with the standard mass, energy, and momentum conservation equations to solve the fluid dynamics field and the air/liquid boundary geometry at each time step using an unsteady solver with implicit first-order Euler time integration [606]. The air/liquid interface was reconstructed using a second order piecewise linear interface calculation (PLIC). Each time step was calculated via the Courant-Friedrichs-Levy (CFL) parameter (set to 0.2), which restricts the size of the time step to ensure the free surface does not cross an entire element within that time step. The air and culture media were modeled as a compressible gas and water, respectively. The fluid properties are listed in **Table 2.1**. The advection scheme was first-order upwind, and the linear equation solver was

conjugate gradient, and the pressure correction term was calculated using the SIMPLEC algorithm. The velocity and pressure under-relaxation parameters were 0.3 and 0.7, respectively and iterations were continued until the residuals were reduced by more than 4 orders of magnitude or the maximum 150 iterations were reached.

Table 2.1: Physical properties of the air and water used in the CFD model of the cyclic pressure chamber.

Air		**Water**	
Molecular weight	Kinematic viscosity (υ)	Density (ρ)	Dynamic viscosity (μ)
29g	1.589×10^{-5} m^2-s^{-1}	1,000 kg-m^{-3}	6.82×10^{-4} kg-m^{-1}-s^{-1}

Wall shear stress (τ) was calculated from the velocity vector along the long axis of the chamber according to the following equation:

$$\tau = \mu \frac{\partial V_x}{\partial y} \qquad \textbf{(2.3)}$$

where μ is the dynamic viscosity and $\frac{\partial V_x}{\partial y}$ is the gradient of the x-component of the velocity (V_x) with respect to the y-direction [607]. Post-processing line probes were used to extract the pressure, velocity, and τ from horizontal and vertical planes at various time points.

2.2.3 Biological validation

To validate the cyclic pressure system, we wished to demonstrate that bone marrow derived cells remain viable throughout their exposure to cyclic hydrostatic pressure. To that end, two different

cell types were used to validate the cyclic pressure system. In addition to biological endpoints as described below, measurements of pH, pCO_2, pO_3, and calculated HCO_3^- and relative humidity were used to determine the effective operating conditions for the cyclic pressure system.

2.2.3.1 Cell source

The two cell types employed in this study were derived from the bone marrow. The first cell type will be referred to as adherent hematopoietic cells (AHCs). To obtain AHCs, the femoral bones were obtained from freshly euthanized miniature swine (25kg). The pigs were obtained from unrelated studies, in accordance with the University of Pittsburgh's Institutional Animal Care and Use Committee. The bone marrow was harvested by flushing the femoral bone cavity with AHC media, which consisted of Media 199 (M199, Sigma, St. Louis, MO) supplemented with 10% calf serum (Invitrogen Carlsbad, CA), and 1% Penicillin/Streptomycin (Invitrogen). The isolated cells were passed through a 40μm filter (Falcon, San Jose, CA) layered on Ficoll® (Amersham, Buckinghamshire, England), and centrifuged at 330 x g and 22°C for 20 minutes. The red cell fraction at the bottom was resuspended with AHC media, and cells adherent after seven days were subcultured as AHCs. For each experiment 50,000 AHCs were plated onto glass microscope slides (Fisher, Hampton, NH) for 24 hours, and then placed into the cyclic pressure chamber or kept as static incubator controls (37°C, 5% CO_2, 95% humidity) for the duration of the experiment.

Because the proposed research was to examine the response of BMMSCs to three mechanical stimuli, BMMSCs also needed to be tested in the cyclic pressure system. BMMSCs were harvested from Sprague Dawley rats (2.5kg) using previously described methods [526]. The rats were obtained from unrelated studies, in accordance with the University of Pittsburgh's Institutional Animal Care and Use Committee. Briefly, the femurs of freshly euthanized rats

were flushed with complete bone marrow culture medium (BMCM), which consisted of Dulbecco's Modified Eagles' Media (DMEM, Sigma) supplemented with 10% calf serum (Invitrogen) and 1% penicillin/streptomycin (Invitrogen). The harvested cells were passed through a 40μm filter (Falcon) and plated in a Dexter culture fashion in BMCM [470]. Those cells remaining adherent after seven days were kept, and the non-adherent cells discarded. Cells less than passage 4 were utilized for the experiments. At the start of each experiment, 7000 cells/cm^2 were plated on collagen-coated slides (Flexcell International, Hillsborough, NC). Following a 48-hour incubation period, the slides were placed into the cyclic pressure system for the duration of the experiment while controls were kept in static incubator conditions.

2.2.3.2 BMMSC characterization

To determine the multipotentiality of BMMSCs, differentiation assays were performed. A mineralized bone matrix formation assay was performed whereby isolated BMMSCs (Section 2.2.3.1) were cultured in BMCM supplemented with ascorbic acid (100 μg/mL), β-glycerol phosphate (5 mM), and dexamethasone (1 μM) for 1 week [56, 526]. Following osteogenic induction, BMMSCs were fixed in 4% paraformaldehyde for 5 minutes and washed 3 times with phosphate buffered saline (PBS, Sigma). The presence of bone forming nodules was assessed using Alizarin Red dye (see Section 3.2.1.1.1).

An adipogenic differentiation assay was also performed by culturing isolated BMMSCs (Section 2.2.3.1) in BMCM supplemented with 3-isobutyl-1-methylxanthine (100 μg/mL), and indomethacin (60 μM) for 2 weeks [56, 526]. Following adipogenic induction, BMMSCs were washed with PBS and fixed in 4% paraformaldehyde (Sigma) for 5 minutes followed by 3

washes in tap water. Accumulation of lipid droplets in the cellular cytoplasm was determined by staining the samples with Oil Red O (see Section 3.2.1.1.2).

2.2.3.3 Pressure conditions

For initial assessment of cellular viability, AHCs were exposed to 120/80 mmHg, 0.5 Hz cyclic pressure. Control cells were kept in static incubator conditions. Each experiment lasted 5 days. For experiments investigating the effects of cyclic pressure on stem cell differentiation, proliferation, and morphology, BMMSCs were exposed to 120/80 mmHg, 1.0 Hz cyclic hydrostatic pressure. Controls were kept in static incubator conditions. Each experiment lasted 7 days.

2.2.3.4 Dissolved gas measurements

Media samples were obtained every 24 hours during both sets of experiments to measure pH, and the dissolved concentrations of CO_2 and O_2 using a dissolved gas analyzer (ABL5; Radiometer, Copenhagen, Denmark). HCO^-_3 was calculated using the Henderson-Hasselbach equation [608]:

$$pH = pK_a + \log\left(\frac{[CO_2]}{[HCO_3^-]}\right) \quad \textbf{(2.4)}$$

where $[CO_2]$ and $[HCO_3^-]$ are the concentrations of carbon dioxide and bicarbonate ion, respectively and pKa is the log of the acid dissociation constant. pK_a is calculated from [608]:

$$pK_a = 6.125 - \lg(1 + anti\log(pH - 8.7)) \quad \textbf{(2.5)}$$

The calculation of the bicarbonate content was used as a measure of proper humidification. Assuming that BMMSCs cells do not produce their own bicarbonate through carbonic anhydrase

[609], increases or decreases in the calculated HCO^-_3 can indicate a change in the concentration of media components due to water evaporation or condensation, respectively.

2.2.3.5 Relative humidity calculation

The relative percent humidity was calculated for the system after each experiment by taking the ratio of the total volume of gas used to the total volume of water used with the maximum vapor density of water in air at 37°C. The total volume of air used during an experiment (V_{air}) was calculated from flow rates recorded every 24 hours. The total volume of water used (V_{H20}) was determined by subtracting the total water left in the humidifier system from the starting volume. Relative humidity (RH) was calculated as follows:

$$RH(\%) = \frac{\sum V_{air} \Big/ \sum V_{H_20}}{\text{MVD}} * 100\% \quad \textbf{(2.6)}$$

where MVD is the maximum vapor density, which was estimated by a fourth order polynomial extrapolation of tabular data for temperature vs. maximum vapor pressure (**Figure Figure** A.1 in **Appendix A**) [610]. The average inlet air temperature was measured by a temperature probe (Fisher&Paykel) at the end of the heated conduit and used to compute the MVD.

2.2.3.6 Viability analysis

At the termination of each experiment involving AHCs, cell viability was assessed by the Live/Dead® Kit (Molecular Probes, Carlsbad, CA) according to manufacturer's protocols. Briefly, 0.1 μM ethidium bromide and 2 μM calcein were incubated on the AHCs for 1 hour followed by 3 washes in PBS. The AHCs were then fixed in 4% paraformaldehyde for 5 minute, and rinsed 3 times with PBS. Nuclei were stained with DAPI (Sigma) for 1 minute and washed

5 times with PBS before being imaged at 200x on an epifluorescent microscope (E800, Nikon). Ten random fields of view were analyzed per experiment. Overlapping DAPI and ethidium bromide staining identified dead cells. The average percent cell death was recorded for each set of 10 fields of view.

2.2.3.7 Glycosaminoglycan staining

At the termination of each experiment involving AHCs, samples were fixed in 4% paraformaldehyde for 5 minutes and washed 3 times with PBS. Glycosaminoglycan (GAG) production was assessed by Safranin O staining. Briefly, AHCs were incubated with 0.1% Safranin O (S8884, Sigma) for 5 minutes followed by alcohol dehydration and were digitally photographed (CoolPix, Nikon) at 100x on an inverted phase-contrast microscope (TS100, Nikon). Increased GAG production may indicate differentiation towards the chondrocyte phenotype, which has been previously shown for stem cells under cyclic pressure [505, 579, 611].

2.2.3.8 Morphology analysis

Morphologic analysis was performed for each experiment involving BMMSCs as described in Section 3.2.4.1. The cellular surface area and perimeter were measured for each cell in the field of view using Scion Image (Scion Corp, Frederick, MD) and used to compute the shape index (see Section 3.2.4.1 and **Equation (3.2)**).

2.2.3.9 Proliferation Analysis

Cellular proliferation was quantified using methods described in Section 3.2.4.2. Briefly, using nuclear staining, the number of cells counted in ten random fields of view was averaged,

and each averaged cell count was normalized to its corresponding control and reported as a fold change versus control.

2.2.3.10 Statistical analysis

All data is presented as mean ± standard error of the mean. Because the average cell counts were normalized to the control, a one-sample t-test was performed with $\mu=1$ and $\alpha=0.05$. For morphologic analyses, a paired Student's t-test was used to make statistical comparisons. p-values less than 0.05 were considered significant.

2.3 RESULTS

2.3.1 Pressure waveforms

Representative waveforms generated by the cyclic pressure system are shown for the oscillating frequency of the solenoid valve set to 0.5, 1.0, and 2.75Hz (**Figure 2.5**). The maximum pulse pressure possible at 2.75 Hz was 20mmHg due to inertial effects of the air. However, the waveform is consistent with neonatal blood pressure and frequency and could therefore be useful in testing the effects of such as stimulus [612].

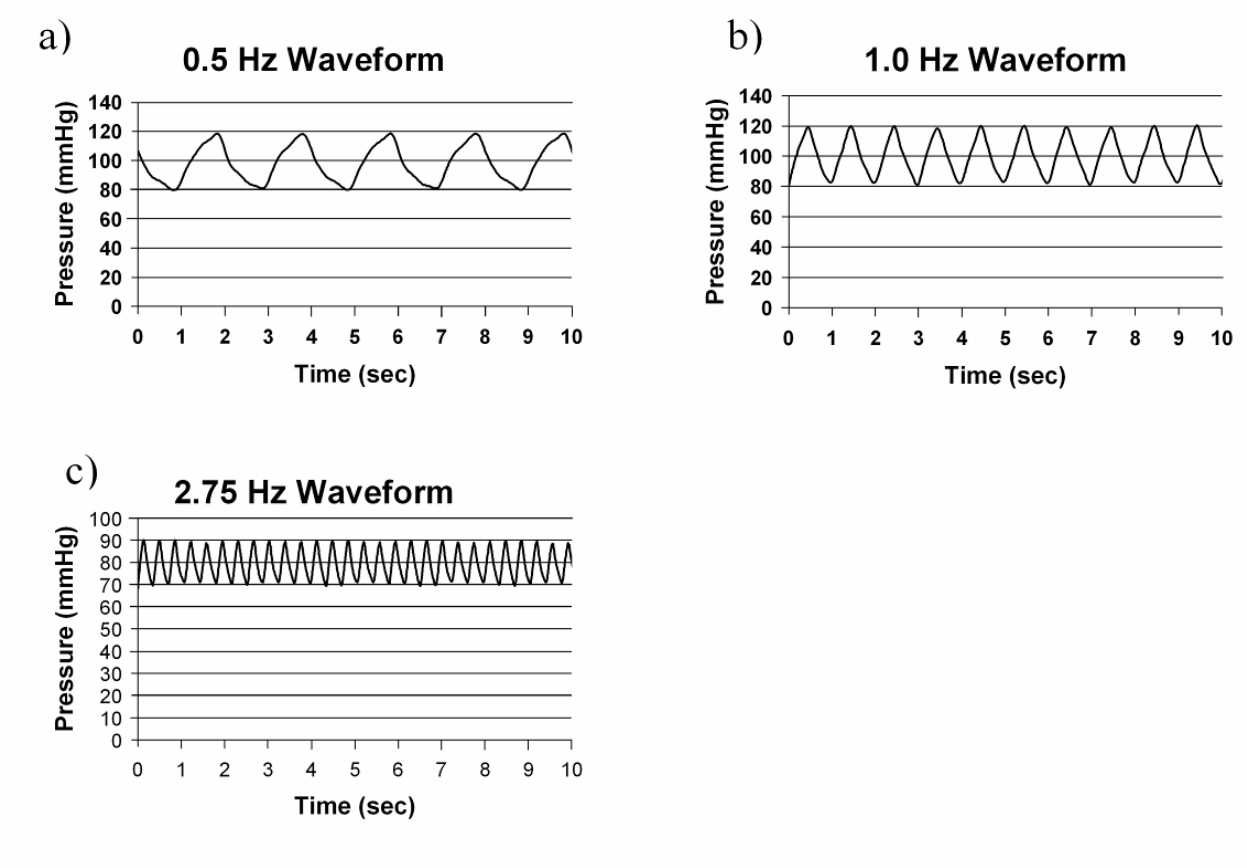

Figure 2.5: Pressure waveforms collected with the solenoid valve frequency set to (a) 0.5 Hz, (b) 1.0 Hz, and (c) 2.75 Hz. Figure reproduced with permission from ASME [1].

2.3.2 CFD results

The CFD analysis of the cyclic pressure chamber revealed a uniform pressure field established along the length of the chamber (**Figure 2.6**) and rose steadily over time (**Figure 2.7**). The pressure field did show a minor increase above the applied gas pressure due to the pressure head developed from the 6.3mm of media above the cells, but this was less than 1% and was considered negligible (**Figure 2.6**). The maximum calculated wall shear stress was ~1.2×10^{-4} Pa, which is insignificant compared to the pressure that the cells experienced (~10^4 Pa), and confirmed the assumption that cyclic pressure system is truly hydrostatic. A three-dimensional velocity profile (**Figure 2.8**) over time shows plug flow developing into the characteristic parabolic flow within the chamber as time advances. At t=0.01s, a dip in the velocity occurs, which we believe may indicate the initiation of compression and a resultant reflection of the air wave. Following this drop, the velocity profile oscillates slightly while progressing into the characteristic parabolic profile associated with laminar flow by 0.05 seconds, and remains parabolic for the rest of the simulated time (not shown). The Reynolds number (Re) was calculated to be <50, thus confirming the establishment of a laminar flow in the viscous model. The stainless steel bars, which were used as diffusers to deflect the downward impingement force of the inlet air, prevented significant disturbances in the liquid layer. However, there apparently is some liquid velocity (0.02 m-s^{-1} maximum) during the development of the air flow that was transferred ~0.8 mm into the liquid layer. However, the shear stress calculations suggest that although liquid movement was generated, no significant wall shear stress resulted.

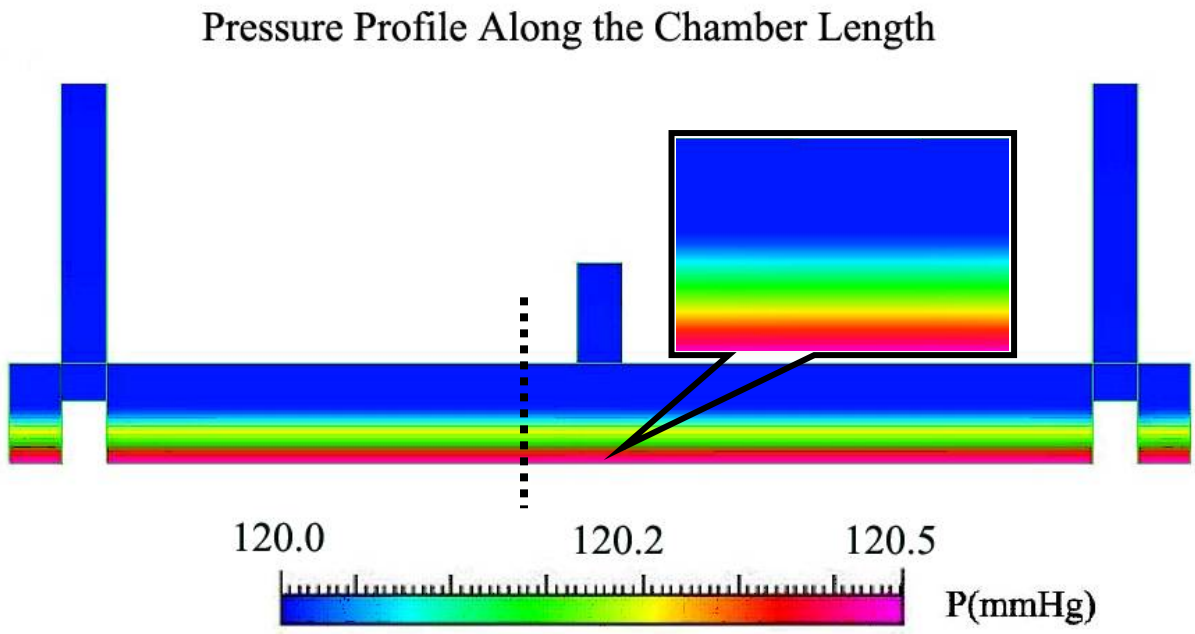

Figure 2.6: Results for CFD analysis revealing a uniform pressure distribution across the length of the chamber. There is a slidght increase in pressure in the fluid layer progressing down towards the base of the chamber (inset), which is consistent with the expected increase in pressure from the weight of the fluid. The dashed line represents the slice through which the velocity field (shown in **Figure 2.8**) along the y-axis was extracted. Figure reproduced with permission from ASME [1]**.**

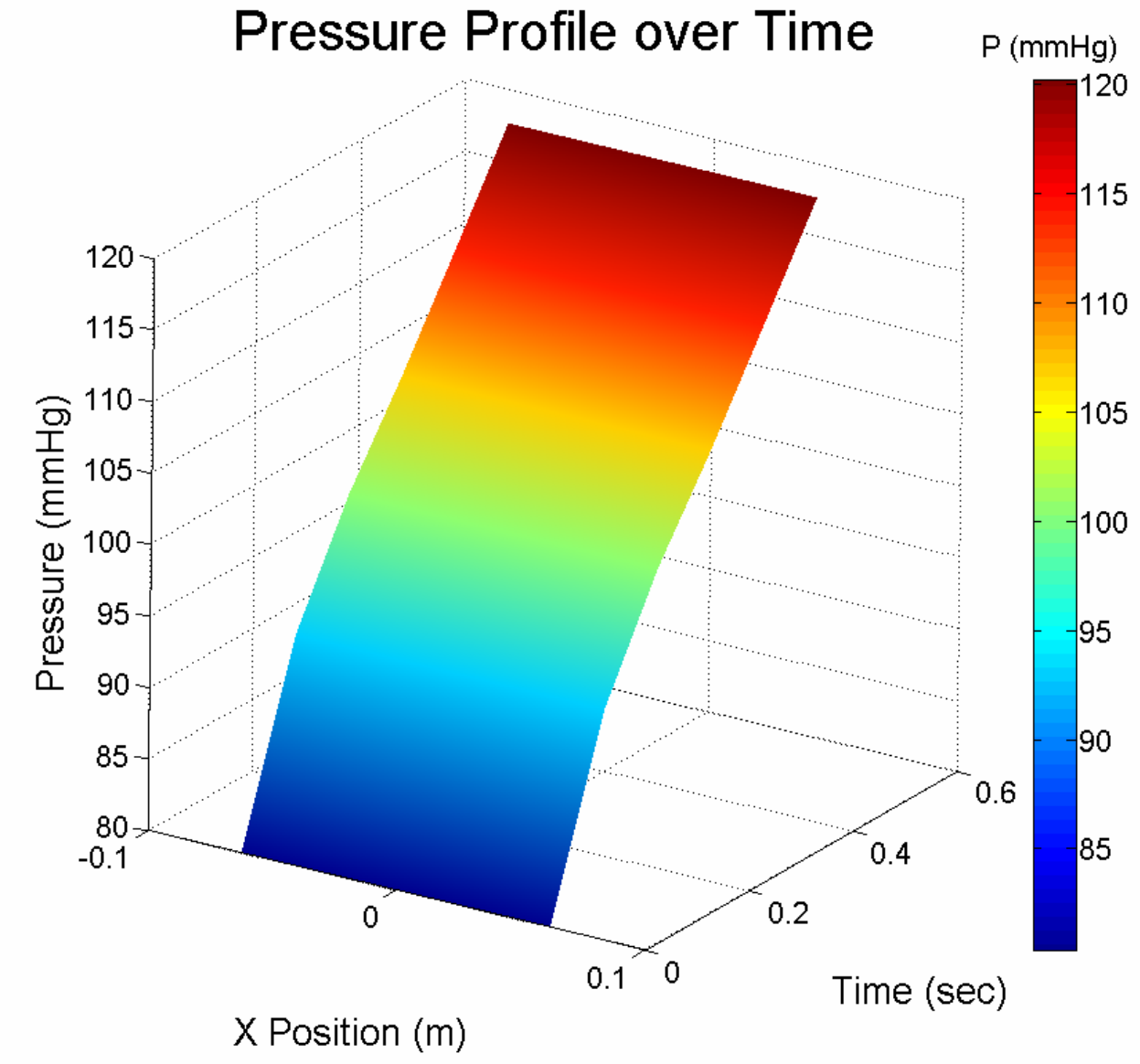

Figure 2.7: Results for the pressure vs. time vs. the X-position across the bottom of the cyclic pressure chamber indicate a smooth, continuous increase in pressure over the course of the simulation and a uniform distribution along the length of the chamber. Figure reproduced with permission from ASME [1].

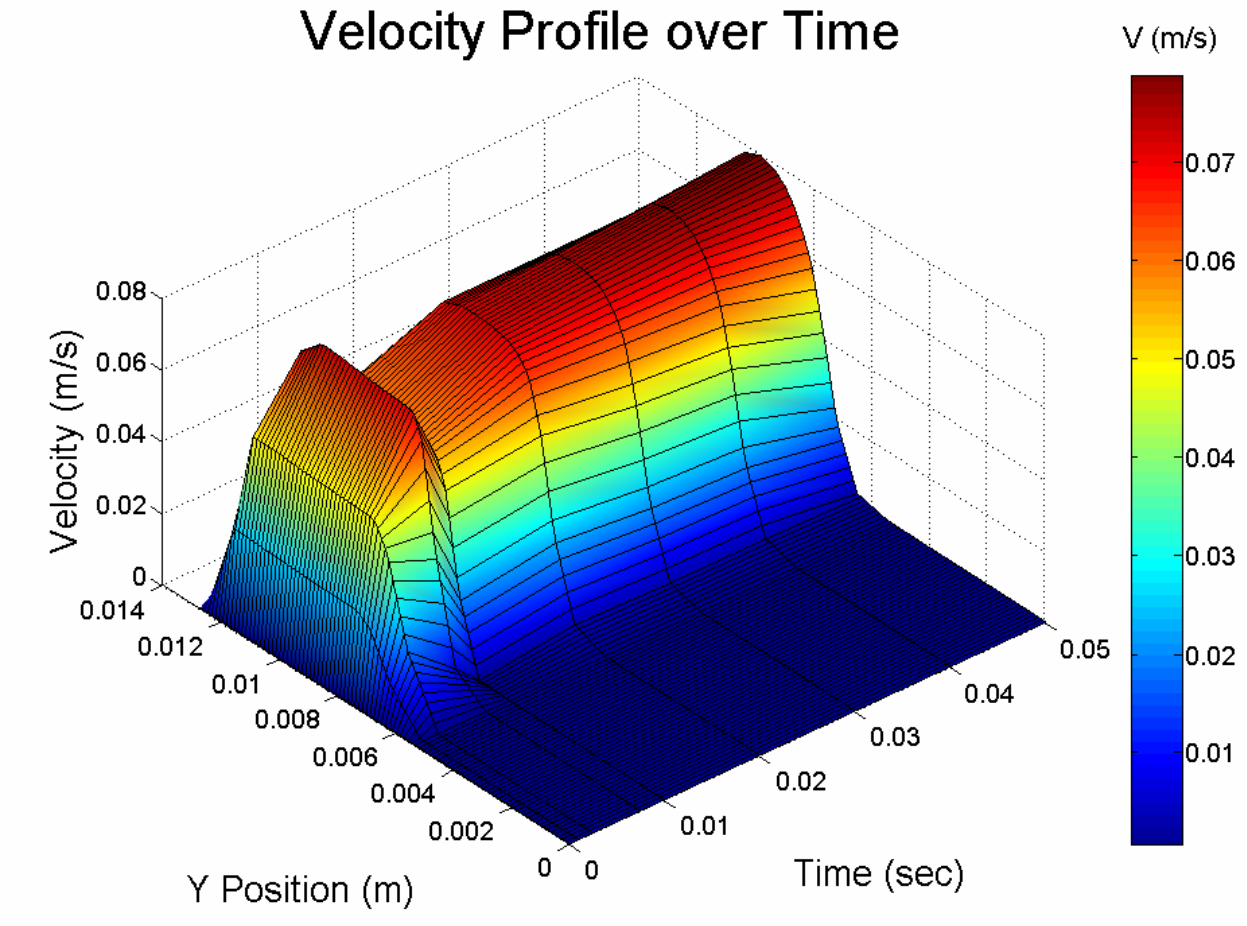

Figure 2.8: A three-dimensional spatial velocity profile over time extracted from the dashed line shown in **Figure 1.1** shows the development of parabolic flow in the air space, and that the velocity is zero in the liquid space (air-liquid interface located at y=0.063 m). Figure reproduced with permission from ASME [1].

2.3.3 Dissolved gas and relative humidity results

Dissolved gas measurements taken over the course of the experiments showed that the pH, pCO2, and HCO^-_3 values remained similar between pressure and control groups and were within acceptable limits (**Figure 2.9**). The values for pO_2 were elevated in the cyclic pressure group because of the increase in ambient pressure. However, the fractional oxygen index (FiO_2), which is the ratio of the partial pressure of dissolved oxygen to the total pressure, was nearly equivalent for the control and cyclic pressure groups (18.6 ± 0.1% vs. 18.1± 0.2%, respectively). The average relative humidity at 37^{o}C was calculated to be 99% ± 4% (absolute humidity 49.3 ± 3.4 g/m^3). These values resulted from the operation of the humidifier at 38-39^{o}C to ensure full saturation at 37^{o}C when the air crossed into the incubator section of tubing.

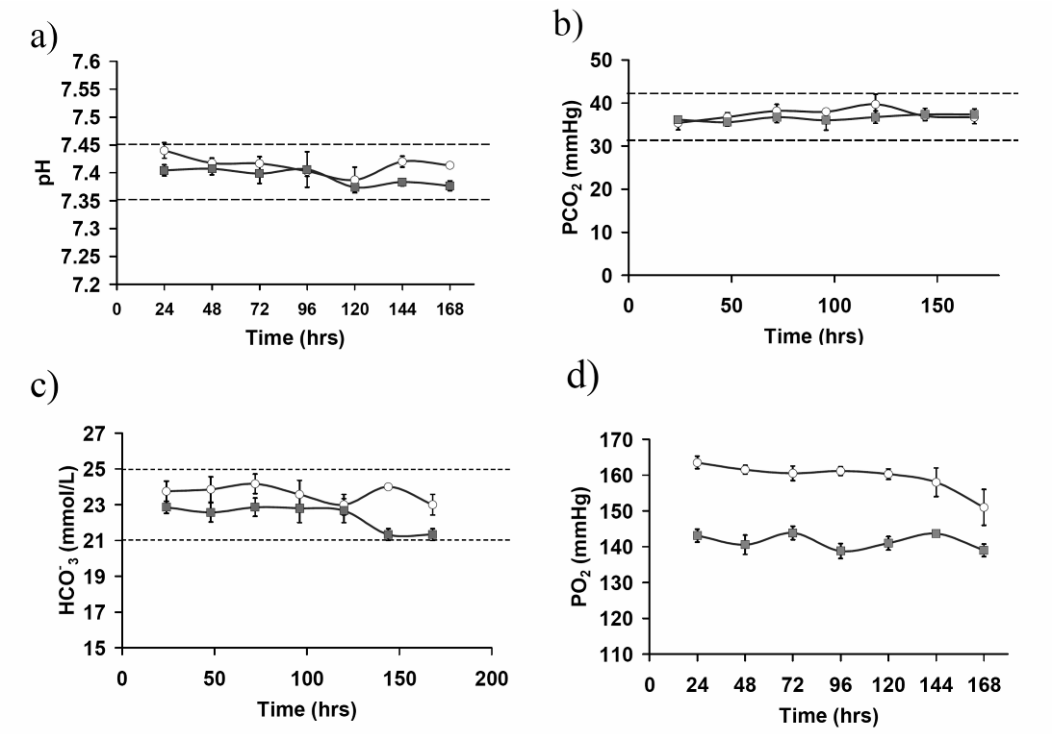

Figure 2.9: ABL readings demonstrate similar values between the cyclic pressure (○) and control experiments (■) for (a) pH, (b) pCO2, and (c) HCO-3. (n=8) Dashed lines indicate the upper and lower limits for acceptable values for each measured variable. The stability in the HCO-3 values indicates sufficient humidification. (d) pO2 values for pressure were elevated over controls throughout the experiments due to the increase in ambient pressure. These values, although statistically different ($p<0.05$), had similar FiO2 values when adjusted for ambient pressure and are not considered biologically significant. Figure reproduced with permission from ASME [1].

2.3.4 AHC viability

Analysis of the Live/Dead® staining (**Figure 2.10**) showed no difference between the cyclic pressure and control AHC groups at 5 days (p=0.16).

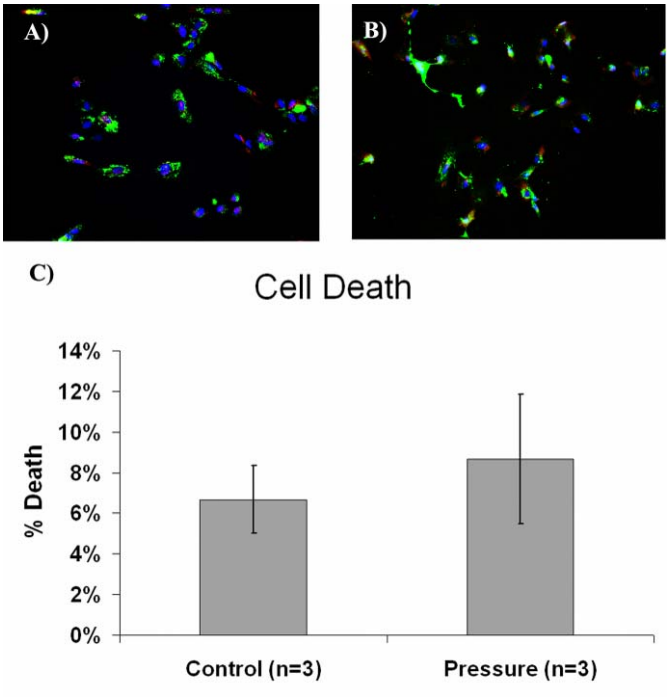

Figure 2.10: Representative Live/Dead images from AHCs exposed to (a) Control and (b) 120/80 mmHg, 0.5 Hz cyclic pressure for 5 days. (c) Averaged percentage of dead cells in 10 fields of view indicates no difference in cell death following exposure to 5 days of cyclic pressure. Bars indicate mean ± SEM.

2.3.5 GAG production in AHCs

After five days under cyclic pressure or control conditions, control cultures appear to produce more GAGs as indicated by Safranin O staining, while the cyclic pressure cultures did not stain strongly for Safranin O (**Figure 2.11**). This may indicate that early progression into

chondrogenesis (detected by GAG staining), which may be followed by subsequent osteogenesis, is prevented by the application of cyclic pressure in AHCs.

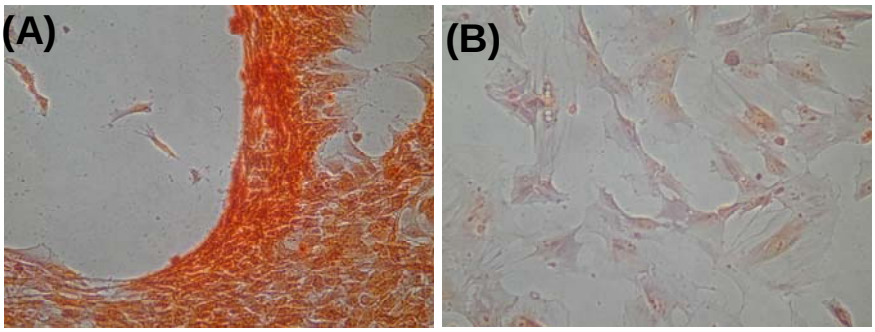

Figure 2.11: GAG production is evident in controls (A) but inhibited under cyclic pressure (B) as evidenced by Safranin O staining (n=3).

2.3.6 BMMSC morphology and proliferation, and differentiation

BMMSCs showed a significant increase in proliferation (**Figure 2.12a**) and a decrease in cell size (**Figure 2.12b**) when exposed to cyclic pressure. BMMSCs exposed to cyclic pressure also showed a significant increase in shape index (**Figure 2.12c**), which indicates a more rounded morphology.

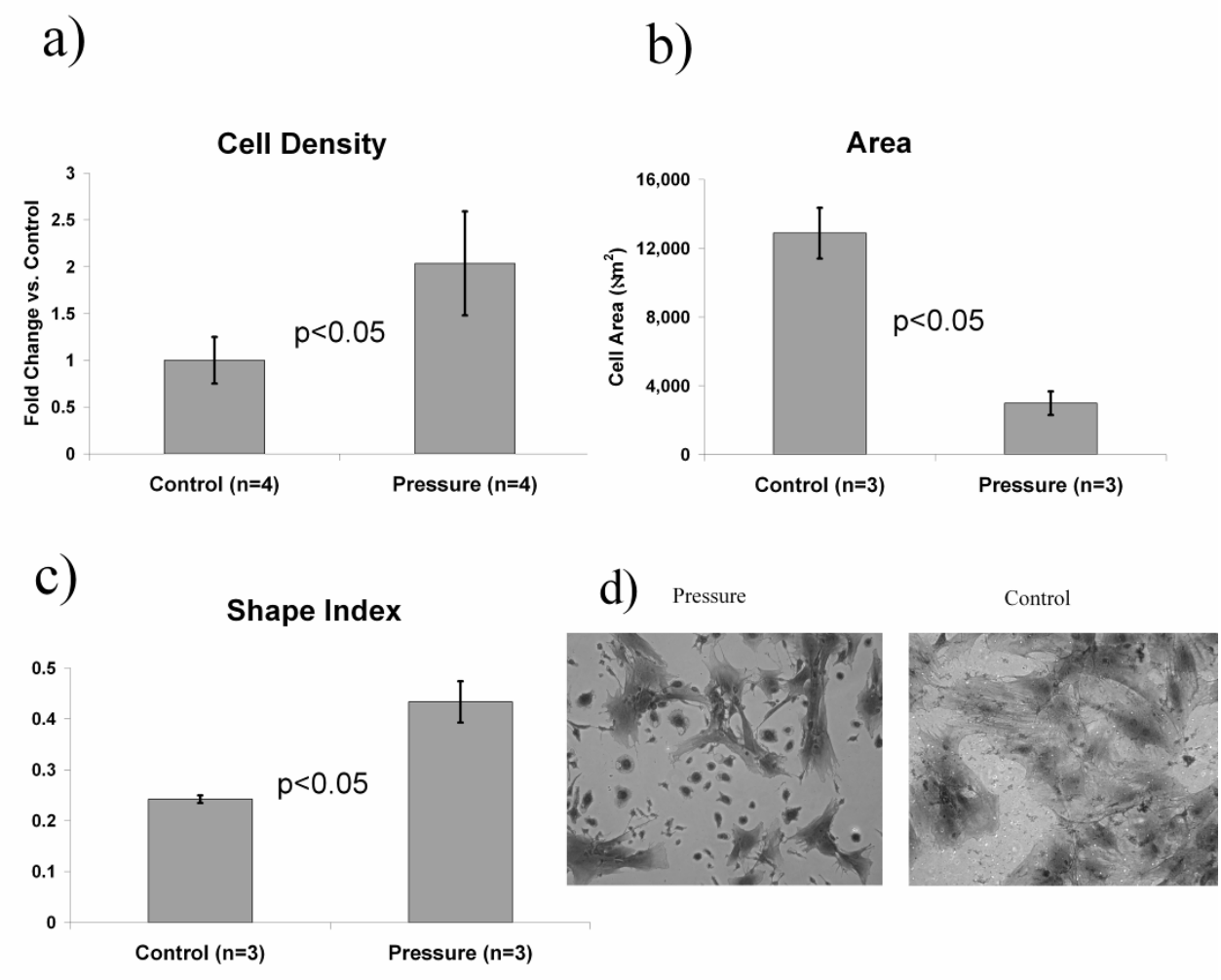

Figure 2.12: (a) Quantification of BMMSC proliferation via cell counts revealed a 1.8 fold increase in cells exposed to cyclic pressure for 7 days compared to controls. (b) BMMSCs exposed to cyclic pressure demonstrated a significant reduction in their total area. (c) Shape index measurements indicated a more rounded morphology for BMMSCs under cyclic pressure. (d) Coomassie blue stained images of pressure (left) and control (right) reflect the measured differences in morphology and proliferation that occurred upon stimulation with cyclic pressure. Images taken at 10x magnification**.** Figure reproduced with permission from ASME [1].

2.4 DISCUSSION

These results demonstrate the development of a new experimental system capable of extended application of cyclic hydrostatic pressure to cell culture. CFD simulations demonstrated the uniformity of the pressure distribution and the lack of other forces translating to the base of the chamber where cells would be cultured. The use of a heated passover humidifier provided sufficient vapor saturation to ensure minimal to no media loss in the culture chamber. This was evident in the stability of the HCO_3^- measurements (**Figure 2.9d**). Such results were not achieved with other humidifier designs assessed, including a room temperature passover system [597] and several modified bubble humidifiers (**Figure 2.3**). There is also some evidence, both in our own experimentation as well as in the literature [604], that media changes every 24 - 48 hours can mask the cell damage resulting from inadequate humidification. Importantly, our data demonstrated that there was no effect on cellular viability due to exposure to cyclic hydrostatic pressure through 7 days.

In addition to maintaining cellular viability, our experiments have also shown that cyclic pressure alters the GAG production of AHCs and the cellular morphology and proliferative rates in BMMSCs, indicating that these cells can respond to cyclic pressure (**Figure 2.11** and **Figure 2.12**). To our knowledge, this was the first evidence that bone marrow derived cells are responsive to cyclic pressure alone; i.e., without other stimulation such as D_3 [576], or chondrogenic medium [578]. The ability of the BMMSCs to respond to other physical stimuli (i.e., cyclic stretching) was recently reported by our laboratory [526]. Of particular interest is the finding that cyclic pressure enhances the proliferation of BMMSCs (**Figure 2.12a**). These

results are consistent with Rubin et al.[577], who reported a trend towards increased proliferation when D_3-stimulated BMMSCs were exposed to an increase in static pressure and other work involving cyclic pressure on ECs [386, 388, 394, 395]. However, during cyclic stretch we have previously shown that BMMSC proliferation is inhibited [526]. Cyclic hydrostatic pressure, therefore, may provide means to stimulate BMMSC proliferation without the addition of biochemicals and may prove to be useful for the *ex vivo* expansion of these cells for use in cell therapy. For example, the use of cyclic pressure could potentially decrease the expansion time required for adequate numbers of cells for use in these therapies, and the be followed other forces, such as cyclic stretch, that could halt proliferation and guide differentiation of the BMMSCs [526].

2.4.1 Limitations

While the cyclic pressure system developed here has been demonstrated to be versatile and space- and cost-efficient, it does have some limitations. If one wished to test the potential synergistic effects of different chemical stimuli acting under pressure, separate culture chambers with independent solenoids and resistors may have to be used, increasing the cost, complexity, and space requirements for such a system. However, the same humidifier and gas source could be used for several systems in a similar manner to the system described by Hasel et al [597]. Enlarging the device slightly to fit a six well dish or the development of a small barrier system to isolate the individual glass slides used in the current system are two other methods that may be used to address this issue. Additionally, the cyclic pressure waveform is a saw-tooth wave with a 50% duty cycle. More complicated waveforms can be generated but would require the use of an external controller to regulate the inlet and outlet resistors independently and reduce the cost-

efficiency of the system. Though the number of experiments performed in the validation of the cyclic pressure system was relatively small, quantification of morphology and proliferation did show statistical differences between stimulated and non-stimulated BMMSCs. Furthermore, it did not show any statistical different in AHC cellular viability, and the increased proliferation of BMMSCs indirectly confirms this.

2.5 CONCLUSIONS

In conclusion, the newly developed cyclic pressure system is versatile, compact, and does not require complex control algorithms to operate in its current configuration. The cyclic pressure system was shown to allow the culture of bone marrow derived cells under cyclic hydrostatic pressure for up to 7 days with no noticeable effects on cellular viability. In addition, the exposure of BMMSCs to cyclic hydrostatic pressure for 7 days demonstrated their ability to alter their morphology and proliferation as well as demonstrate an altered differentiation capacity as a result of cyclic pressure stimulation.

3.0 THE MECHANICAL PANEL

3.1 INTRODUCTION

3.1.1 Definition and advantages of the Mechanical Panel

The major experimental portion of this project, as outlined in Specific Aim 2 and Specific Aim 3, involves the systematic analysis of three different mechanical stimuli over a range of magnitudes, frequencies, and time points. In order to efficiently accomplish this, a unique experimental setup was developed, which was termed the Mechanical Panel (**Figure 3.1**). The Mechanical Panel permits the simultaneous exposure of a single population of cells (e.g., one T175 flask of BMMSCs) to cyclic stretch (CS), cyclic hydrostatic pressure (CP), and laminar shear stress (LSS) in a parallel manner. This experimental setup reduces the biologic variability by using the same population of cells in each of the experimental systems and permits the paired comparison between each of the stimuli as well as the control. As a result, the total number of experiments required to analyze the cellular response to the three proposed mechanical stimuli are reduced by a factor of three. Furthermore, it allows careful examination of the differential response of cells to the variety of biomechanical forces that are present within blood vessels. This is a distinct advantage over the previous studies outlined in Sections 1.2.3, 1.3.3, and 1.4.2.2, which analyzed only one type of force while ignoring others. By analyzing the

differential response to the mechanical stimuli, we can quickly identify areas for possible synergism or antagonism when combining these stimuli together. This may ultimately aide in the development of new bioreactors for the stem-cell based development of complex tissues *in vitro*.

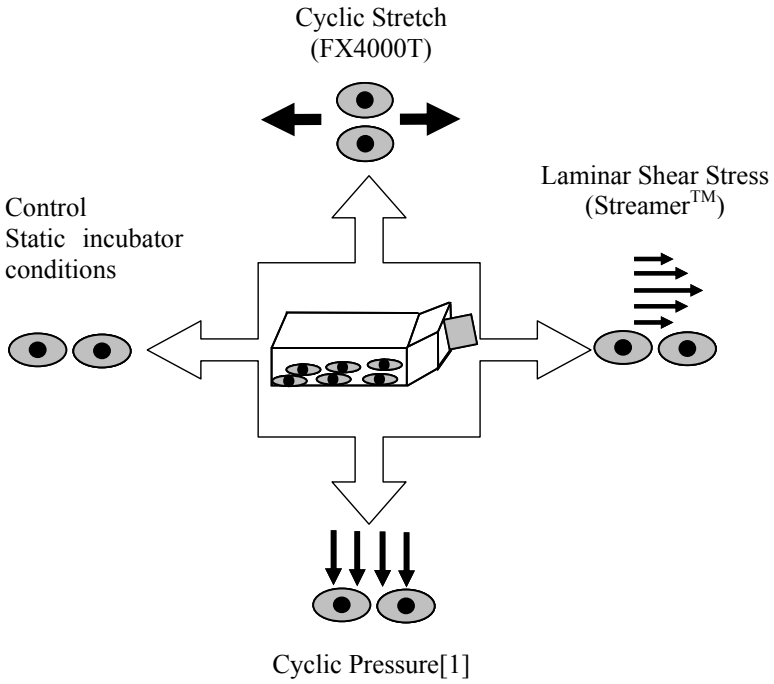

Figure 3.1: The Mechanical Panel applies mechanical stimulation in parallel from a single population of cells to determine a differential response to each of the stimuli.

3.2 METHODS

3.2.1 Cell source

The BMMSCs utilized for the experiments in Specific Aims 2-4 were obtained from the Tulane Center for Gene Therapy (TCGT) under an existing material transfer agreement and will be hereafter referred to as tBMMSCs. The TCGT is funded by the NIH to provide well-characterized BMMSCs to researchers in an effort to reduce the variability within the results of different researchers from different cell sourcing techniques. The tBMMSCs were harvested from the femurs of adolescent Lewis rats and have been characterized as $CD90^+$ and $CD59^+$ stem cells [613]. The tBMMSCs were expanded in alpha modified Eagle's media (α-MEM, Invitrogen) supplemented with 20% fetal bovine serum (FBS, Atlanta Biologicals, Atlanta, GA), 1% antibiotic/antimicotic (Invitrogen), and 10 mM L-glutamine (Invitrogen). The FBS used for the Mechanical Panel experiments was lot-selected for optimal growth (see **Figure Figure** B.1 in **Appendix B.1**). The tBMMSCs were expanded using the seed-lot method (see **Appendix B.2**) to provide cells within a few passages of each other throughout the study [614].

3.2.1.1 Assessment of the multipotentiality of tBMMSCs

Because the goal of this work was to assess the effects of mechanical forces on the differentiation of BMMSCs, it was necessary to confirm the multipotentiality of the tBMMSCs obtained from the TCGT. The ability of tBMMSCs to differentiate into osteoblasts and adipocytes confirmed their multipotentiality.

3.2.1.1.1 Osteogenic culture

To perform osteogenic differentiation assays, tBMMSCs were seeded at 200 cells/cm^2 in 6-well plates (Corning, Lowell, MA) and cultured with complete αMEM until 80% confluent. Thereafter, the complete αMEM was supplemented with ascorbic acid (100 μg/mL), β-glycerol phosphate (5 mM), and dexamethasone (1 μM) for 2 weeks [56, 526]. Following 2 weeks of osteogenic culture, tBMMSCs were fixed in 4% paraformaldehyde (Sigma) for 5 minutes and washed 3 times in PBS (Sigma).

The presence of bone forming nodules was assessed using Alizarin Red dye (A5533, Sigma), which stains calcium phosphate deposits. Fixed tBMMSCs were stained with Alizarin Red (40 mM, pH 4.2) for 10 minutes with gentle swirling. Excess dye was removed by gently swirling the dish with PBS for 15 minutes. The samples were then digitally photographed (CoolPix, Nikon, Melville, NY) at 100x on an inverted phase-contrast microscope (TS100, Nikon).

3.2.1.1.2 Adipogenic culture

To perform adipogenic differentiation assays, tBMMSCs were seeded at 200 cells/cm^2 in 6-well plates (Corning) and cultured with complete αMEM supplemented with 3-isobutyl-1-methylxanthine (100 μg/mL), and indomethacin (60 μM) for 2 weeks [56, 526]. Following adipogenic induction, tBMMSCs were washed with PBS (Sigma) and fixed in 4% paraformaldehyde (Sigma) for 5 minutes followed by 3 washes in tap water.

Accumulation of lipid droplets was determined by Oil Red O (O0625, Sigma) staining. Fixed tBMMSCs were incubated with 60% isopropanol for 5 minutes. Fresh Oil Red O solution (0.3% in isopropanol mixed 3:2 with deionized water) was added for 5 minutes with gentle swirling followed by a brief rinse with tap water. The cells were counterstained with Harris-

Hematoxylin (HS80, Sigma) for 1 minute followed by a tap water rinse. The samples were then digitally photographed (CoolPix, Nikon) at 100x on an inverted phase-contrast microscope (TS100, Nikon).

3.2.2 Device descriptions

3.2.2.1 Cyclic stretch apparatus

The cyclic stretch for these experiments was provided via the FX4000T cyclic tension system (Flexcell International, Hillsborough, NC). The FX4000T has been well established as a means to impose cyclic stretch on cell monolayers [526, 599, 615-618]. In brief, the system works by applying a vacuum to the underside of the culture plates, deforming the membrane with negligible shear stress and hydrostatic pressure variation (**Figure 3.2**). Computer control over the valves regulating the vacuum allows user-specific stretch regimens to be used. Rigid posts positioned under the membrane provide a defined stretch direction to the membranes. In the experiments described here an arctangle loading post was used to impart uniaxial stretch. The FX4000T unit is designed such that up to 4 plates (24 total wells) can be stretched at a desired level during each use.

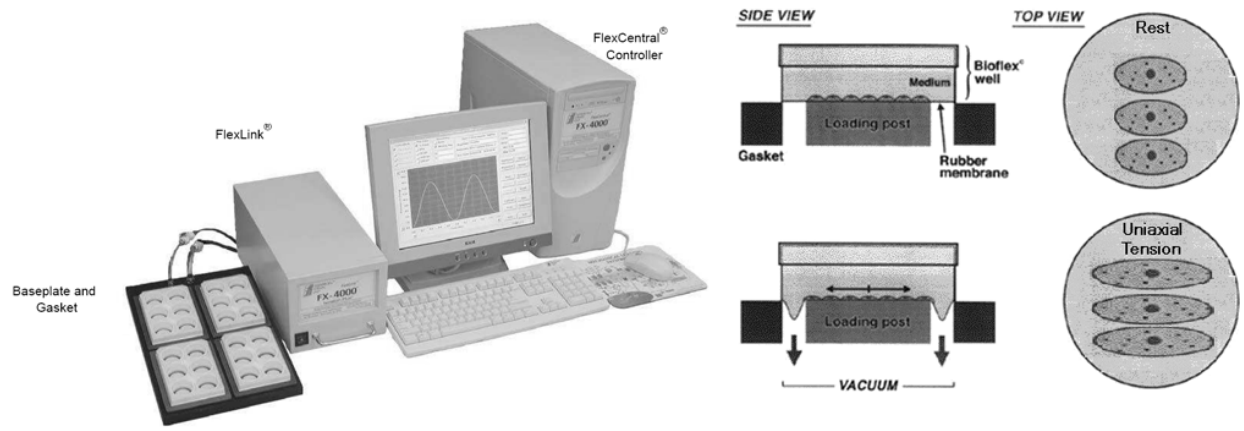

Figure 3.2: Cyclic stretch in the FX4000T is controlled by the FlexCentral® computer, which opens valves in the FlexLink® controller that shuttle vacuum in and out of the Baseplate (far left). The applied vacuum from below pulls the deformable culture surface downward. Rigid pots constrain the deformation to achieve uniaxial tension (far right). Figure adapted from www.flexcellint.com.

3.2.2.2 Shear stress apparatus

Laminar shear stress for these experiments was provided by the Streamer® (Flexcell) system (**Figure 3.3**). This system has been previously established as a means to impose shear stress on a cellular monolayer [602, 619, 620]. Briefly, culture medium is pumped from a central reservoir via a computer-controlled peristaltic pump (MasterFlex® L/S® 7550-30, Cole Parmer) through two pulse dampeners (MasterFlex® L/S® 7596-20, Cole Parmer) that eliminate high frequency noise and establish a steady flow rate. The culture medium then enters into a stainless steel parallel plate chamber (**Figure 3.3 inset**) that holds 6 microscope slides upon which the cells are grown before returning to the reservoir. Gas exchange occurs through the platinum-cured silicone tubing (MasterFlex® L/S® 17, Cole Parmer) that connects each component. The applied shear stress (τ) is controlled by the flow rate of the culture media, which is given by

$$\tau = \frac{6\mu Q}{wh^2} \qquad \textbf{(3.1)}$$

where Q is the flow rate in each channel, and w and h are the width and height of each channel, respectively.

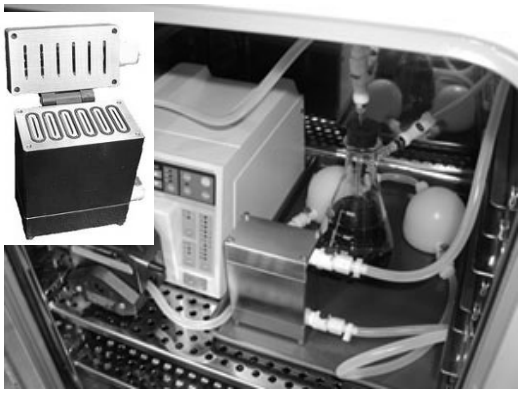

Figure 3.3: The Streamer® consists of six identical parallel plate chambers (inset). Fluid flow is imparted by a computer-controlled roller pump, and two serial pulse dampeners that ensures a steady laminar flow is delivered to the shear stress chamber. The entire setup can be contained in a standard CO_2 incubator, as shown. Figure adapted from www.flexcellint.com.

3.2.2.3 Cyclic pressure apparatus

The cyclic pressure apparatus employed in these studies (**Figure 2.1** and **Figure 3.4**) was developed in our laboratory and is fully described in Chapter 2.0 and in Maul et al.[1]. This apparatus holds 6 microscope slides that are identical to those used in the Streamer® shear stress system (see Section 3.2.2.2) and is housed in the same incubator as the Streamer®.

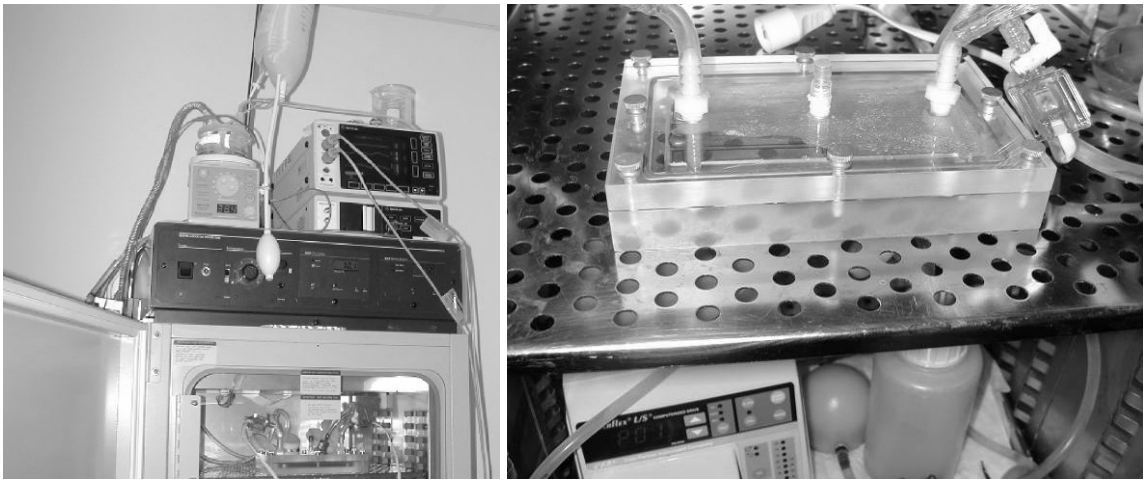

Figure 3.4: Images of the cyclic pressure system (left) and cyclic pressure chamber (right) during an experiment. As detailed in Chapter 2.0, the respiratory humidifier is fed with a pressurized sterile IV water source, and a clinical pressure monitor displays the pressure of both the cyclic pressure chamber and the humidifier. The cyclic pressure system was designed to take up minimal space in the incubator to allow the Streamer® to fit into the same incubator (seen in lower part of the right image) for the Mechanical Panel experiments.

3.2.3 Experimental Design

3.2.3.1 Substrate

The goal of this research was to determine what role mechanical forces play in the differentiation of BMMSCs towards SMCs and ECs for use in vascular regenerative medicine. In addition to the mechanical environment, stem cell differentiation is modulated by numerous other stimuli, including exogenous growth factors (discussed in Section 1.4.2.1), oxygen tension [621-623], and ECM [545, 556, 624, 625]. Therefore, the potential ECM molecules upon which to culture the tBMMSCs during experimentation included collagen I, fibronectin, laminin, and collagen IV since these are predominantly found within the vasculature [625]. Because the focus of this study is on the mechanical stimulation of BMMSCs, the choice of substrate must be motivated first by the ability of the substrate to maintain cellular adhesion. Salasznyk et al. [624] determined that, of the above choices, BMMSCs adhere best to fibronectin, followed by collagen

I. Furthermore, both fibronectin and collagen I are known to facilitate angiogenesis and are found in abundance in areas of vascular remodeling and injury, whereas laminin I is known to arrest cell growth and migration *in vivo* [625]. Fibronectin has been previously shown to have no effect on differentiation of BMMSCs [624], but has also been used in research inducing EC and SMC differentiation from BMMSCs [42, 262]. Collagen I has been shown to facilitate osteogenic differentiation in BMMSCs [624, 626, 627], but has also been used by our laboratory [628] and others [527] in generating SMC precursors from BMMSCs under cyclic stretch. Based on previous experience, collagen I was chosen as the substrate for our experiments, but fibronectin would have been a viable alternative and may be considered for future work.

3.2.3.2 Dose-response of tBMMSCs to mechanical stimulation

Experiments performed to address Specific Aim 2 were designed to determine dose-dependent response of tBMMSCs to varying magnitudes and frequencies of each separate mechanical force stimulus; i.e., laminar shear stress, cyclic stretch, and cyclic hydrostatic pressure. Because the ultimate goal of this research is to determine how to appropriately utilize mechanical stimulation to create a tissue engineered blood vessel, the magnitudes and frequencies utilized for these experiments were chosen to be consistent with the magnitudes and frequencies found in the vasculature [192, 612].

For each experiment, tBMMSCs were obtained as described in Section 3.2.1 and seeded at 200 cells/cm^2 on collagen I coated BioFlex™ (Flexcell) deformable substrates for CS and control conditions, or Culture Slips™ (Flexcell) for LSS and CP conditions. Forty-eight hours after seeding, the tBMMSCs were loaded into each of the systems described in Sections 3.2.2 while control samples were placed in static incubator conditions. For some experiments, a T0 sample was also obtained immediately following the 48 hours culture but prior to stimulation in

the event that the particular subset of cells for that given experiment were needed to determine the baseline values for the endpoints listed in Section 0.

The mechanical stimulation regimens used for these experiments can be found in **Table 3.1**. Neonatal stimuli for CS and CP are consistent with magnitudes and frequencies associated with vital signs shortly after birth [612]. Hypotensive, normotensive, and hypertensive magnitudes and frequencies were chosen to be consistent with those values reported for adults [192]. For the neonatal/sub-physiologic and hypotensive CS and CP stimuli, the magnitudes were chosen to not only be consistent with physiologic ranges of magnitude, but also to be identical in magnitude so as to provide a pure frequency response. Shear stress values for hypotensive, normotensive, and hypertensive stimuli are consistent with those found throughout adult circulation [192]. Each of the stimuli was applied in parallel to provide the benefits of Mechanical Panel stimulation as described in Section 3.1.1. Because the shear stress system used for these studies was not capable of applying cyclic shear stress, no frequency response could be determined for LSS. The shear stress found under the heading of neonatal/sub-physiologic stimulus was set as the lowest shear stress capable of being generated by the Streamer® to determine the effects of minimal flow. Although it may not be necessarily reflective of neonatal physiology, it was grouped with the neonatal/sub-physiologic stimuli (see **Table 3.1**).

Each of the dose-response experiments lasted for 5 days. Dissolved gas measurements (see Section 2.2.3.4) were made in the systems to track dissolved gas and pH changes throughout the experiments. The endpoints for these experiments included morphology (see Section 3.2.4.1), proliferation (see Section 3.2.4.2), histology (see Section 3.2.4.3), antibody staining (see Section 3.2.4.4), and gene expression (see Section 3.2.4.5).

Table 3.1: Applied stimuli for Mechanical Panel experiments to determine the dose-response of tBMMSCs to different magnitudes and frequencies of mechanical stimulation. See text for further detail about stimulus headings. Parenthetical terms denote abbreviations for each of the stimuli. For example, CS-1 denotes 1% 1 Hz cyclic stretch, and LSS-1 denotes 1 dyne/cm^2 laminar shear stress. CS-1HF denotes cyclic stretch at 1% at 2.75 Hz stimulation (high frequency).

Stimulus	Neonatal/ Sub-physiologic Stimulus	Hypotensive Stimulus	Normotensive Stimulus	Hypertensive Stimulus
Cyclic Stretch	1%, 2.75 Hz (CS-1HF)	1%, 1 Hz (CS-1)	5%, 1 Hz (CS-5)	10%, 1 Hz (CS-10)
Cyclic Pressure	90/70 mmHg, 2.75 Hz (CP-90HF)	90/70 mmHg, 1 Hz (CP-90)	120/80 mmHg, 1 Hz (CP-120)	180/140 mmHg, 1 Hz (CP-180)
Shear Stress	1 dyne/cm^2 (LSS-1)	5 dynes/cm^2 (LSS-5)	10 dynes/cm^2 (LSS-10)	20 dynes/cm^2 (LSS-20)
Control	Static incubator conditions (37^{o}C, 5% CO_2, 95% humidity)			

3.2.4 Endpoint assessment

3.2.4.1 Morphology

At the termination of each experiment described in Section 3.2.3.2, designated samples were fixed with 4% paraformaldehyde for 5 minutes and washed 3 times with PBS. Next, the samples were incubated with Coomassie Brilliant Blue R-250 (Pierce, Rockford, IL) total protein stain (to enhance contrast) for 5 minutes followed by 5 washes with PBS. Ten random fields of view were digitally photographed (CoolPix, Nikon) under 100x magnification on an inverted phase-contrast microscope (TS100, Nikon). Artificial borders were drawn as necessary to separate the cells for the edge-detection function in Scion Image [526, 629, 630]. Area, perimeter, major axis, minor axis, and angle of orientation were measured automatically within Scion for each cell. A photograph of a hemocytometer with Neubauer rulings was used for measurement calibration and was input into a custom-built Excel macro (see Appendix D) that

handled all data exported from Scion Image (Version 4.0.3.2, Scion Corporation, Frederick, MD). In addition, the macro used these measurements to calculate the shape index (SI) for each cell in the field of view, which is defined as:

$$\mathrm{SI} = \frac{4\pi A}{P^2} \tag{3.2}$$

where P and A are the perimeter and area of the cell, respectively, measured by Scion Image. The value of SI is 1 for cells that are perfect circles and approaches 0 for cells that are spindle shaped [631]. The perimeter, major axis, and minor axis measurements were also used to calculate the tortuosity index, which is defined as:

$$\mathrm{TI} = \frac{P}{2 * \pi * \sqrt{\frac{\left(a/2\right)^2 + \left(b/2\right)^2}{2}}} \tag{3.3}$$

where a and b are the major and minor axes, respectively, of the cell. The tortuosity index indicates the cell's smoothness, by comparing the measured perimeter to the computed perimeter of a perfect ellipse constructed with the cell's measured major and minor axes. Therefore a value for TI of 1 represents a cell whose perimeter is identical to a perfectly smooth ellipse and rises as the cell shape becomes more tortuous [188, 396, 632].

3.2.4.2 Proliferation

At the termination of each experiment described in Section 3.2.3.2, designated samples were fixed with 4% paraformaldehyde for 5 minutes and washed 3 times with PBS. A 0.1% solution of Triton-X 100 (Sigma) in PBS was added for 30 minutes followed by 3 washes in PBS to permeabilize the cell membranes. To stain the nuclei, DAPI (5mg/mL, Sigma) was added for 1 minute followed by 5 washed in PBS. The samples were photographed with a SPOT RT

digital CCD camera (Diagnostic Instruments) at 200x on an epifluorescent microscope (E800, Nikon). Total nuclear counts from ten random fields of view were used to quantify proliferation. The size of each field of view was determined with a 1 mm stage micrometer ruled to 0.01 mm (12-561-SM1, Fisher Scientific, Pittsburgh, PA). This value and the averaged number of cells per field of view were used to compute the cell density reported as cells/cm^2.

3.2.4.3 Histology

At the termination of each experiment described in Section 3.2.3.2, designated samples were fixed with 4% paraformaldehyde for 5 minutes and washed 3 times with PBS. To determine possible osteogenic differentiation and adipogenic differentiation, selected samples were stained with Alizarin Red (3.2.1.1.1) or Oil Red O (3.2.1.1.2), respectively.

3.2.4.4 Immunohistochemistry (IHC)

3.2.4.4.1 General methods

At the termination of each experiment described in Section 3.2.3.2, designated samples were fixed with 4% paraformaldehyde for 5 minutes and washed 3 times with PBS. The samples were then incubated for 30 min with 0.1% solution of Triton-X 100 in PBS to permeabilize the cell membranes. Non-specific binding of antibodies (listed in Section 3.2.4.4.2) was blocked by incubation for 45 minutes with 5% BSA (Fraction V, Sigma) in PBS followed by 5 washes with a solution of 0.5% BSA, 0.15% glycine (Sigma) in PBS (PBS/BSA/Gly). Next, the samples were incubated with the primary antibody diluted in PBS/BSA/Gly for 60 min in a moist chamber to prevent drying of the samples. Unbound primary antibody was removed by 5 washes with PBS/BSA/Gly. The samples were incubated with the secondary antibody (1:500) diluted in

PBS/BSA/Gly for 1 hour at room temperature in a moist chamber and then rinsed 3 times with PBS. For nuclear visualization, cells were counterstained with DAPI (Invitrogen) for 1 minutes followed by 5 washes with PBS. A negative control (primary delete) was prepared each time antibody staining occurred. This sample was prepared in an identical manner to all other samples, but the primary antibody was left out of the 1 hour incubation in PBS/BSA/Gly. All steps described for IHC staining occurred at room temperature (RT).

3.2.4.4.2 Antibodies for IHC

For all experiments, the samples were labeled with monoclonal antibodies against SMC, and EC markers (**Table 3.2**). For markers of SMCs, SMA was used for a synthetic phenotype, and h1-calponin and SM-MHC were used for a full contractile phenotype. For markers of ECs, flk-1 was used to denote EC potential, and vWF and PECAM were used as mature phenotypic markers. All secondary antibodies for the antibodies listed in **Table 3.2** were donkey anti-mouse conjugated with Alexa 488 fluorophore (Sigma). All primary and secondary antibodies were provided by the University of Pittsburgh Center for Biological Imaging.

Table 3.2: Antibodies and dilutions for IHC

Classification	Antibody	Dilution	Catalog Number	Manufacturer
SMC	SMA	1:500	MAB1522	Chemicon, Temecula, CA
SMC	h1-calponin	1:400	M3556	Dako, Carpinteria, CA
SMC	SM-MHC	1:400	M3558	Dako
EC	Flk-1	1:200	Sc-6251	Santa Cruz Biotechnology, Santa Cruz, CA
EC	vWF	1:100	V1180	Biomeda, Foster City, CA
EC	PECAM	1:100	Mab1393	Santa Cruz

3.2.4.4.3 Fluorescent microscopy

Following antibody staining, the samples were mounted on glass microscope slides (Fisher) in gelvatol (10% polyvinyl-alcohol (Sigma), 21% glycerol (Sigma), and 0.1 M Tris (pH 8.5, Sigma) in deionized water). The samples were placed overnight at 4^{o}C to cure the gelvatol before microscopy. Fluorescent microscopy was performed at 200x on an epifluorescent microscope (E800, Nikon). The primary delete sample was placed under the microscope under the FITC filter set to determine the background signal from the secondary antibody. The exposure time on the camera (SPOT RT, National Diagnostics) was increased until non-specific staining from the secondary antibody was visible. This exposure time was recorded and all subsequent images from the samples containing primary and secondary antibody was set below this level. Three to five images were taken from different areas of the culture for each antibody. Representative images for each antibody are shown in Section 3.3.5.

3.2.4.5 RNA isolation and PCR

3.2.4.5.1 RNA isolation

At the termination of experiments outlined in Section 3.2.3.2, Section 4.2.1, and Section 5.2.1, samples were processed for RNA isolation and purification (see **Figure C.1** in **Appendix C**). Protein was also extracted from experiments outlined in Section 3.2.3.2 using techniques outlined in Section 4.2.2.3, but was not of sufficient quantity to perform Western blotting.

All steps outlined in the following subsections were carried out in RNAse-free conditions at RT unless otherwise noted. As soon as each experiment was completed, samples were removed from the Mechanical Panel and rinsed in RNAse-free 4^{o}C PBS. The PBS was aspirated and followed by the addition of 1 mL of Trizol® (Invitrogen) for each BioFlex® well or 2mL of Trizol® for each CultureSlip®. Trizol® is a proprietary cell lysis buffer containing monophasic solutions of phenol and guanidine isothiocyanate suitable for isolating total RNA, DNA, and proteins [633]. Isolation procedures described here are based upon the single-step RNA isolation method developed by Chomczynski and Sacchi [634]. After 2 minutes, each sample within a given mechanical stimulus was scraped with a fresh, sterile cell scraper (Greiner Bio-one, Monroe, NC). Each sample was rinsed 3 times with its Trizol® and then serially transferred, ending in a sterile RNAse-free polypropylene conical tube (Falcon) and frozen at -80^{o}C for further processing to extract the intracellular components.

3.2.4.5.2 RNA Purification

After 24 total samples were collected in Trizol® (approximately 5-6 Mechanical Panel experiments), RNA purification was performed under RNAse-free conditions at RT unless otherwise noted. First, the samples were defrosted at 30^{o}C for 20 minutes in a heat block (Heat

Block 2 Model #049302, VWR, West Chester, PA) and vortexed (Vortex Genie 2, Model #6-650, Scientific Industries, Bohemia, NY) every 5 minutes to ensure that the entire cell lysate was well-mixed. Next, 0.2mL of chloroform (9180-33, J.T. Baker, Phillipsburg, NJ) was added to each tube using a sterile 5 mL glass pipette (Falcon). Each tube was shaken by hand for 15 seconds, vortexed, and placed at 30^{o}C in the heat block for 10 minutes with vortex agitation every 5 minutes. After the incubation, the samples were centrifuged (Legend RT, Sorvall, Newtown, CT) at 3500 x g for 30 minutes at 4^{o}C. The chloroform caused the separation of the aqueous and organic phases of the Trizol®-cell lysate mixture, with the RNA being held in the aqueous layer. The aqueous layer was removed by transfer with a sterile polystyrene pipette (Falcon) for each sample and placed in a fresh, sterile, 50 mL conical polypropylene tube (Falcon). The remaining organic layer was placed back at -80^{o}C for subsequent processing of the DNA and protein content (see Section 4.2.2.3).

The aqueous layer containing the RNA was then processed using a protocol modified from the Qiagen RNeasy Clean-up Kit (Qiagen, Valencia, CA) [635]. For each 100 µL of aqueous layer, 350 µL of RLT buffer (Qiagen) containing 0.1% β-mercaptoethanol (M-6250, Sigma) was added and mixed thoroughly by shaking. Next 250 µL of 100% ethanol (111ACS200, Pharmco-AAper, Brookfield, CT) was added and mixed thoroughly by vortexing. Each RNA/RLT/ethanol mixture was loaded into an RNeasy column (Qiagen) arranged on a manifold (QiaVac 24 Plus, Qiagen) and pulled through under standard house vacuum. These columns contain a proprietary packed-bed that selectively binds RNA under reducing conditions. Once the samples have been run into the columns, the vacuum was removed and 350 µL of buffer RW1 (Qiagen) was added to each column and drawn through with vacuum. Following this wash, 80 µL of DNAse I solution (79254, Qiagen) was pipetted directly on top of the

column and allowed to penetrate for 20 minutes at RT. Following another 350 µL wash of buffer RW1 pulled through the column by vacuum, 750 µL of buffer RPE (Qiagen) was added to the column and pulled through under vacuum.

The columns were removed from the manifold and placed into RNAse-free 2.0 mL round-bottomed collection tubes. Another 250 µL of buffer RPE was added and the columns were centrifuged at 16,000 x g at RT (5415R, Eppendorf, New York City, NY) for 1 minute. The flow-through and collection tube were discarded, replaced with a fresh collection tube, and the columns re-centrifuged for 1 minute. Again, the collection tube was discarded, and the columns placed in fresh 1.5 mL conical collection tubes (Qiagen). The RNA bound to the columns was extracted in 30 µL of RNAse-free water (Qiagen) added directly to the top of each column. The columns were centrifuged at 16,000 x g at RT for 1 minute, and the extracted RNA solution was pipetted back onto the top of the columns and then re-centrifuged for 1 minute to ensure that all available RNA was extracted from the column. The final 30 µL RNA solution was transferred from the 1.5 mL conical collection tube to an RNAse-free 1.5 mL microcentrifuge tube (Ambion, Austin, TX) and stored at -80^{o}C for analysis of RNA quantity and quality (Section 3.2.4.5.3) followed by conversion to cDNA by reverse transcriptase (Section 3.2.4.5.4) and polymerase chain reaction (PCR) analysis of gene expression (Section 3.2.4.5.5).

3.2.4.5.3 Analysis of RNA quality

All collected RNA was analyzed for quality and quantity at the core genomics facilities of the University of Pittsburgh or the Gene Expression and Genotyping Facility (GEGF) at Case Western Reserve University. Briefly, 1 µL of purified RNA (described in Section 3.2.4.5.2) was placed into a capillary electrophoresis chip (RNA 6000 Nano, Agilent, Santa Clara, CA) prepared according to manufacturer's protocols and loaded into the Bioanalyzer (Model 2100,

Agilent). The assay results were analyzed with the 2100 Expert software (v1.5, Agilent) to determine the concentration and RNA integrity number (RIN), which is a measure of RNA quality. The concentration and RIN results were used to determine if the samples were viable for PCR analysis. Concentrations greater than 10 ng/μL and RIN values greater than 8 were considered of high enough quality to perform PCR analysis.

3.2.4.5.4 Reverse transcriptase reaction

RNA samples determined to have high quality and sufficient concentration to perform PCR analysis were selected for reverse transcriptase (RT) conversion of the RNA to cDNA with the High-Capacity cDNA Reverse Transcription Kit (4374967, Applied Biosystems, Foster City, CA). These techniques were also performed according to the manufacturer's instructions by the core genomics facilities of the University of Pittsburgh or Case Western Reserve University. Briefly, 10 μL of 2X RT Master Mix (10x RT buffer, 10x random primers, 25x dNTP, MultiScribe™ reverse transcriptase, and RNAse inhibitor) was combined with 10 μL of purified RNA (as described in Section 3.2.4.5.2) and centrifuged briefly to remove any air bubbles and to bring all reactants together. The combined RT Master Mix and RNA was placed on a thermal cycler (9700, Applied Biosystems) with settings according to **Table 3.3**. The resulting cDNA was stored at -80^{o}C prior to downstream analysis.

Table 3.3: Thermal cycler protcol used for RT reaction.

	Step 1	**Step 2**	**Step 3**	**Step 4**
Temperature (^{o}C)	25	37	85	4
Time	10 minutes	120 minutes	5 seconds	∞

3.2.4.5.5 Real-time PCR analysis

Real-time PCR (RT-PCR) analysis of the RT product described in Section 3.2.4.5.4 was performed using a custom-designed TaqMan® low density PCR array (TLDA, Applied Biosystems). The gene names, phenotypic classifications, and Applied Biosystems catalog numbers for the custom-designed TLDA card are listed in **Table 3.4**. The TLDA is a custom-configured 384 well microfluidics microplate that contains pre-loaded TaqMan® gene expression assays. It offers the ability to quickly assay 32 genes by quantitative PCR from 4 experimental samples in triplicate. TaqMan® gene expression assays are built on 5' nuclease chemistry, with each assay containing two unlabeled PCR primers and a FAM™-dye labeled minor groove binding TaqMan® PCR primer. The TaqMan® primers for the TLDA are subject to the availability of the primer in stock; therefore no custom or low-demand primers were available. Working within these limits, primers were chosen to represent almost all possible phenotypic outcomes that could be associated with BMMSCs following stimulation via the Mechanical Panel.

Table 3.4: List of TaqMan® PCR primers, their classifications and catalog numbers for the first custom-designed TLDA

Classification	Gene Name	Applied Biosystems Catalog #
Adipocyte	PPAR gamma	Rn00440945_m1
Anti-Apoptosis	BCL-2	Rn99999125_m1
Apoptosis	Caspase 3	Rn00563902_m1
BMMSC	CD59	Rn00563929_m1
BMMSC	CD90	Rn00562048_m1
Cardiomyocyte	Troponin	Rn00437164_m1
Chondrocyte	Aggrecan I	Rn00573424_m1
Chondrocyte	Collagen II	Rn00563954_m1
EC	CD133/Prominin I	Rn00572720_m1
EC	Endoglin	Rn00568869_m1
EC	Flk-1	Rn00564986_m1
EC	iNOS	Rn00561646_m1
EC	vWF	Rn00788354_m1
EC	Endothelial cell adhesion molecule (ESAM)	Rn-1531509_g1
Fibroblast	Vimentin	Rn00579738_m1
Housekeeping	Ribosomal protein 18 (18s)	Rn02133666_u1
ECM	Collagen I	Rn00584426_m1
ECM	Collagen III	Rn01437683_m1
ECM	Collagen IV	Rn01401018_m1
ECM	Elastin	Rn01499782_m1
Myocyte	Desmin	Rn00574732_m1
Osteoblast	Alkaline Phosphatase	Rn00564931_m1
Osteoblast	Osteocalcin	Rn00566386_g1
Osteoblast	RUNX2	Rn01512296_m1
Secreted Peptides	BMP2	Rn00567818_m1
Secreted Peptides	FGF2	Rn00570809_m1
Secreted Peptides	TGF-β	Rn00572010_m1
Secreted Peptides	VEGF	Rn00582935_m1
Secreted Peptides	TNFα	Rn00562055_m1
SMC	Caldesmon	Rn00565719_m1
SMC	SM22α	Rn00580659_m1
SMC	Calponin	Rn00582058_m1

3.2.4.5.5.1 PCR amplification and detection

The PCR reaction was performed according to the manufacturer's specifications by the core genomics facilities at the University of Pittsburgh and Case Western Reserve University. For the TLDAs, 50 µL of 2X PCR Master Mix (4304437, Applied Biosystems) and approximately 400ng of cDNA (from Section 3.2.4.5.4) diluted to a volume of 50 µL in RNAse-free water were combined in a 1.5 mL microcentrifuge tube, mixed well, and centrifuged. The PCR Master Mix/cDNA mixture was pipetted into two loading ports on the TLDA and centrifuged at 330 x g twice for 1 minute. The individual reactions in the TLDA plate were then sealed using the Applied Biosystems sealing device which uses precision stylus assembly to seal the main fluid distribution channels in the TLDA. The TLDA was then loaded into the 7900HT Fast Real-Time PCR System (Applied Biosystems) and run for 40 cycles.

3.2.4.5.5.2 PCR data analysis

All data generated by either the TLDA RT-PCR run was analyzed by the $\Delta\Delta C_T$ method with SDS Software (Version 2.0, Applied Biosystems) [636]. The built-in automatic thresholding and outlier removal algorithms were used to determine the threshold cycle (C_T) for each gene. A relative quantitation (RQ) analysis was then performed using the C_T of the endogenous to normalize each sample followed by normalization to the control sample for each gene assayed. The resulting fold-changes in gene expression compared to controls were exported to Microsoft Excel, where a custom-built macro was used to arrange the data for export to the Experimental Database (see Section 3.2.5.1). The RQ values for each experiment were averaged to provide the average change in gene expression compared to controls.

3.2.4.5.5.3 RT negative control

Wherever possible, the primers chosen for the custom-designed TLDA spanned an exon, and were thus only capable of non-genomic amplification (designated by "m1" in the catalog number). Inevitably, there were some primers which did not span an exon, and could potentially amplify genomic DNA. Thus four RT-negative samples, derived from one Mechanical Panel experiment were handled as described in Section 3.2.4.5.4 but lacking the MultiScribe™ reverse transcriptase enzyme in the 2X RT Master Mix. These samples were analyzed on a TLDA card to determine what genomic amplification, if any, was occurring in the primers chosen. Regardless of the outcome of the RT negative sample, no genomic amplification was anticipated in any of the experimental samples as a result of the DNAse treatment in the RNA purification protocol (Section 3.2.4.5.2).

3.2.4.5.5.4 Determination of the dynamic range

In order to determine the optimal RNA mass for efficient RT and detection of a majority of the genes in the TLDA, the following experiment was performed using the TLDA configuration in **Table 3.4**. The dynamic range was determined by performing the RT reaction (see Section 3.2.4.5.4) on a starting mass of RNA that spans at least 4 logs. The RNA used for this purpose was Universal Rat RNA (636658, Clontech, Mountain View, CA) to ensure that all genes queried would show detectable amplification within 40 cycles. The RT reaction was initialized with 1, 10, 100, and 1000 ng of universal RNA, and analyzed (see Appendix H). The results helped to determine the range for the loading amount of RNA (assuming 100% conversion to cDNA) for the TLDA and single reaction assays.

3.2.5 Data storage and statistical analysis

3.2.5.1 Database design and utilization

All data (including images, spreadsheets, PDFs, SDS files, etc.) were stored in a custom-built Access (v2003, Microsoft Corporation, Redmond, WA) database for easy retrieval and export to statistical analysis software. The database was designed as fourth normal form to eliminate redundant fields and provide a modular framework that has utility outside of this particular research project [637]. A detailed description and framework of the database is found in Appendix E.

3.2.5.2 Statistical analysis from database contents

All quantifiable data (e.g., morphologic measurements, PCR, etc.) stored in the experimental database (Section 3.2.5.1 and **Appendix E**) were exported to the statistical package (SPSS v.13, SPSS Inc., Chicago, IL) for subsequent analysis.

3.2.5.2.1 Proliferation, morphology, and gene expression statistics

The data exported from the experimental database were categorized along each stimulus (control, CS, CP, or LSS). Paired t-tests were then used to make all comparisons between each stimulus and the control values with α=0.05. Next the data was filtered to compare differences within the stimulus (CS, CP, or LSS) at each of the four different magnitudes and/or frequencies of stimulation. The data were also explored using the Komolgorov-Smirnov test for normality as well as box plots for outlier and extreme value analyses. Outliers were defined as points falling between 1.5 and 3 times the interquartile range from either the upper or lower quartile in the box plot. Extreme values were defined as points falling greater than 3 times the interquartile range

from either the upper or lower quartile in the box plot [638]. Data points identified as outliers and extreme values were excluded from further analysis. The Levene statistic was first used to test the homogeneity of variance. For data with non-homogeneous variance, the Brown-Forsythe test was used to calculate the F-statistic for ANOVA. Data with a homogenous variance was assessed with the standard F-statistic. For post-hoc testing, assuming homogenous variance, the Fisher's least significant difference (LSD) was used to compare between groups since all comparisons were proposed a priori. Data with unequal variance was compared using the Games-Howell test because of its utility with small sample sizes ($n<6$) [639]. In addition to comparisons of means between magnitudes and frequencies of stimulation, the Spearman rank-correlation was calculated to determine possible relationships between the measured values and the frequency and magnitudes of stimulation. For comparisons between stimuli, the data were re-categorized along lines of similar magnitude (see **Table 3.1**), and analyzed with one-way ANOVA as described above.

3.2.5.2.2 Analysis of Cellular Alignment

Because the data from the measurement of cellular orientation was in degrees, circular statistics were determined to be the most appropriate measure of the distribution of the cellular orientation. For such data, a uniform distribution around the circumference of a circle was assumed to be the true population distribution. The probability density function described by this distribution is:

$$f(\theta) = 1/2\pi, \quad 0 \le \theta \le 2\pi \tag{3.4}$$

and implies that the probability of being at any given angle is equal. Thus, there is no preferred direction to the orientation of the cells, which is the expected outcome for cells growing randomly on any given surface.

For each experiment, the measured angle for each cell was given by the unit polar coordinates (α_i, r), where r equals 1. These were converted into rectangular coordinates (x_i, y_i), where x_i is given by:

$$x_i = r\cos(2\alpha_i) \tag{3.5}$$

and y_i is given by:

$$y_i = r\sin(2\alpha_i) \tag{3.6}$$

Because the measured angle for each cell was only on the 0-180^o plane, $2\alpha_i$ was used to normalize the data on a 360^o circle [640].

Next, the average x-coordinate for each experiment was calculated by a simple arithmetic mean:

$$X = \frac{\sum_{i=1}^{n}\cos(2*\alpha_i)}{n} \tag{3.7}$$

where *n* is the total number of cells for which the angle α_i was measured. Likewise, the average y-coordinate for each experiment was calculated by:

$$Y = \frac{\sum_{i=1}^{n}\sin(2*\alpha_i)}{n} \tag{3.8}$$

The results of **Equation (3.7)** and **Equation (3.8)** were used to give the length of the resultant vector **R** for the coordinates (X, Y):

$$R = \sqrt{X^2 + Y^2} \tag{3.9}$$

The polar direction of **R** was assumed to be the circular mean direction for that experiment and was calculated as the common angle in the 0-180^o quadrant satisfying both parts of the following:

$$\bar{a} = 0.5 * \cos^{-1}\left(\frac{X}{R}\right) = 0.5 * \sin^{-1}\left(\frac{Y}{R}\right) \quad \textbf{(3.10)}$$

Next, the average angle from each the experiment was used to compute the ranked second order (average of the average) $\overline{X}$-coordinate:

$$\overline{X} = \sum_{k=1}^{n} k * \cos(2 * \bar{a}_k) \quad \textbf{(3.11)}$$

where k is the rank of each average angle, $\bar{a}_k$, for each of the n experiments. Likewise, the ranked second order $\overline{Y}$-coordinate was computed from:

$$\overline{Y} = \sum_{k=1}^{n} k * \sin(2 * \bar{a}_k) \quad \textbf{(3.12)}$$

The results of **(3.11)** and **(3.12)** were used to compute the non-parametric Rayleigh's R*:

$$R^* = \frac{\sqrt{(\overline{X}^2 + \overline{Y}^2)}}{n^{3/2}} \quad \textbf{(3.13)}$$

The probability that R*≥r is given by:

$$p = e^{\left(-6R^{*2}n^2(n+1)^{-1}(2n+1)^{-1}\right)} \quad \textbf{(3.14)}$$

which tests the null hypothesis of uniform distribution on the ranked second order vectors [640].

For graphical purposes, a linear histogram was used, with the measured angle for each cell being placed in one of eighteen bins between 0^o and 180^o with a binwidth of 10^o. For data

that appeared to be bimodal at 0^o and 180^o, measured angles were transformed by 90^o to bring potential peaks together as a unimodal distribution. This was the case for tBMMSCs exposed to LSS where the measured angles were initiated along the direction of flow, resulting in potential bimodal peaks at 0^o and 180^o.

3.3 RESULTS

3.3.1 Multipotentiality of tBMMSC

Positive Alizarin Red staining of tBMMSCs exposed to osteogenic media (recall Section 3.2.1.1.1) and positive Oil Red O staining of tBMMSCs exposed to adipogenic media (recall Section 3.2.1.1.2) indicated a successful differentiation of the tBMMSCs into these two cellular phenotypes (**Figure 3.5**) and confirmed the multipotentiality of the cells in our hands.

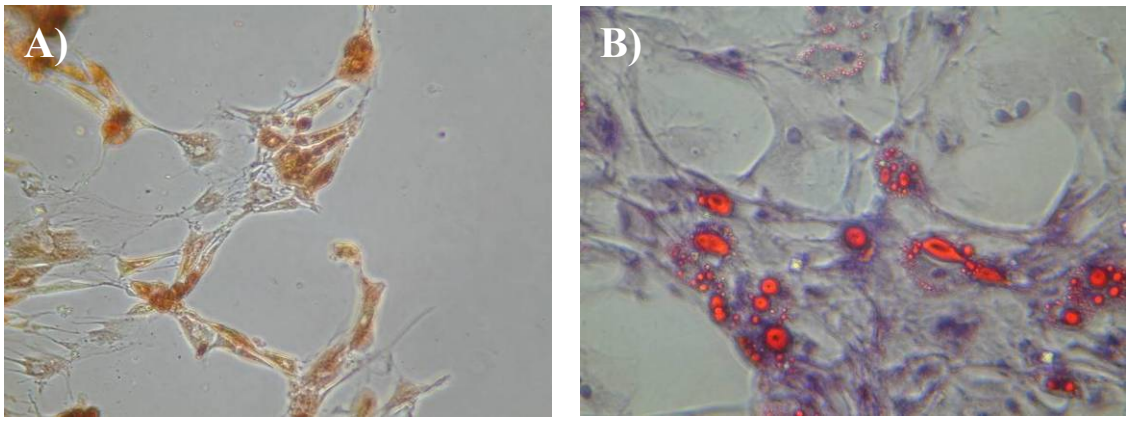

Figure 3.5: (A) Alizarin Red staining of tBMMSCs following osteogenic induction under defined media conditions confirms matrix mineralization. (B) Oil Red O staining of tBMMSCs following adipogenic induction under defined media conditions confirms lipid formation within the cells. Taken together, these images demonstrate that the tBMMSCs are multipotent. Represenative images taken at 100x.

3.3.2 Morphology

Representative images of each stimulus (**Figure 3.6**) showing gross changes in cell size, shape, and alignment demonstrate that mechanical stimulation differentially altered the morphology of tBMMSCs. These observations were confirmed through morphometric analysis of the area, major axis, perimeter, and angle data (see Section 3.2.4.1), which is detailed below.

3.3.2.1 Area changes

The mean cellular area and normalized cellular area (calculated by division of the area measurement by the control values) are presented as the average ± SEM in **Figure 3.7**. Area measurements for tBMMSCs exposed to LSS-1 ($9.6 \pm 1.2 \times 10^3$ μm^2, n=4), LSS-5 ($15.8 \pm 1.3 \times 10^3$ μm^2, n=6), LSS-10 ($10.3 \pm 1.4 \times 10^3$ μm^2, n=6), and LSS-20 ($10.3 \pm 1.1 \times 10^3$ μm^2, n=5) were all significantly elevated ($p<0.05$) when compared to control. Within LSS, the normalized area measurements for LSS-1 were significantly larger ($p<0.05$) than LSS-5, LSS-10, and LSS-20. Correlation statistics demonstrate a dose-response to LSS, with increasing LSS leading to decreasing cellular area ($\rho= -0.547$, $p<0.05$).

Under the cyclic pressure stimulus, there was a significant ($p<0.05$) decrease in cellular area for tBMMSCs exposed to CP-90HF ($2.0 \pm 0.5 \times 10^3$ μm^2, n=4), CP-90 ($2.2 \pm 7.6 \times 10^3$ μm^2, n=5), CP-120 ($2.8 \pm 3.5 \times 10^3$ μm^2, n=6), and CP-180 ($1.9 \pm 2.7 \times 10^3$ μm^2, n=6) when compared to controls. Within CP, the normalized area measurements for CP-90HF were significantly larger ($p<0.05$) than CP-90 and CP-120, and nearly significantly larger ($p=0.06$) than CP-180. Correlative statistics did not indicate there was any type of dose-response to the magnitude or frequency of stimulation for tBMMSCs exposed to CP, but there was a statistically significant difference in area for tBMMSCs exposed to CS-1 vs. CS-1HF ($p<0.05$).

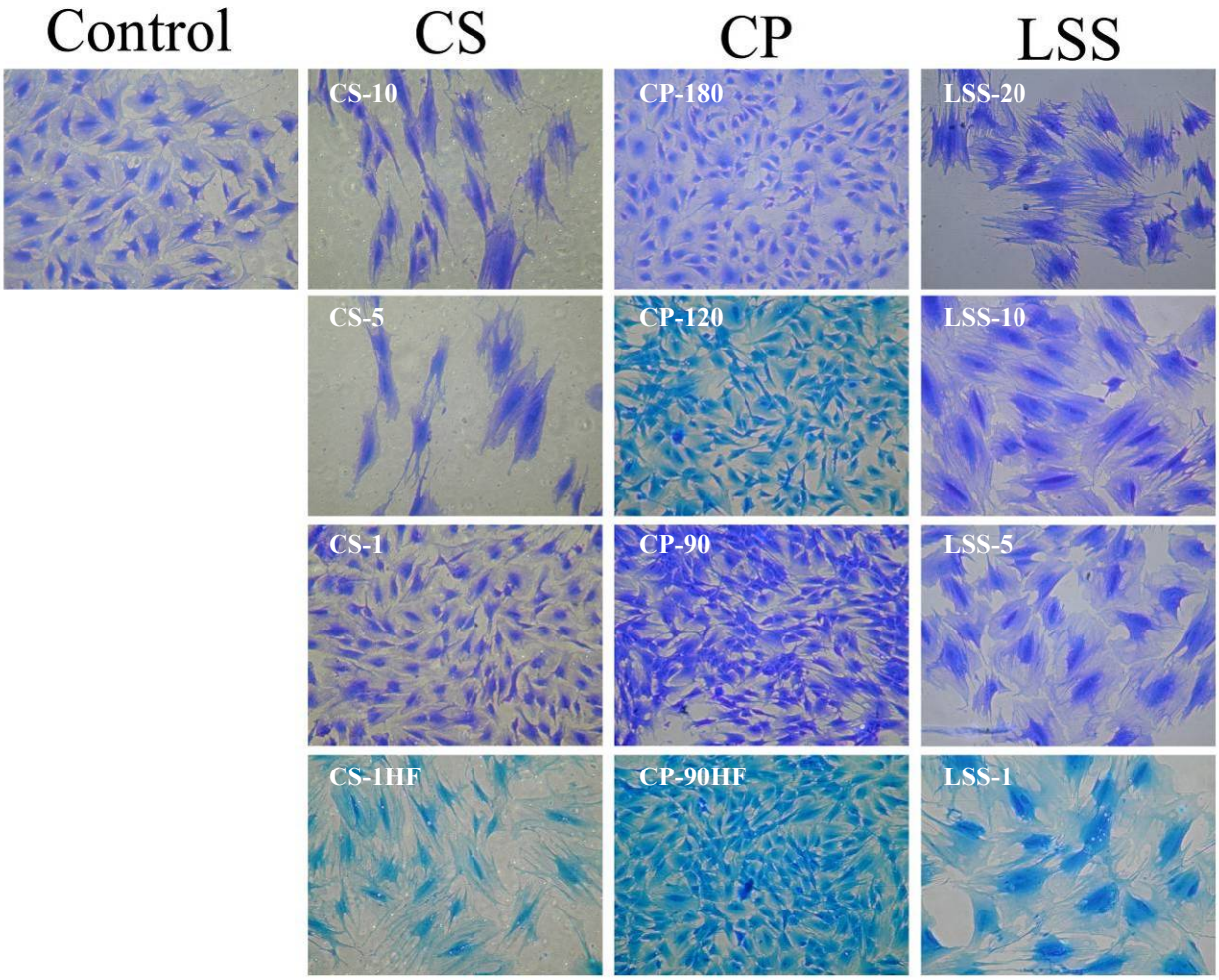

Figure 3.6: Representative images of coomassie brilliant blue stained tBMMSCs following 5 days of exposure to the Mechanical Panel. All images taken at 100X.

No significant change in area was detected for tBMMSCs exposed to CS-1HF (4.3 ± 0.9 $x10^3$ μm^2, n=4), CS-5 (3.9 ± 0.6 $x10^3$ μm^2, n=6), and CS-10 (5.9 ± 0.8 $x10^3$ μm^2, n=6) compared to controls. However, tBMMSCs did show a significant ($p<0.05$) decrease in cellular area compared to controls when exposed to CS-1 (2.5 ± 0.2 $x10^3$ μm^2, n=4). In fact, the measured cellular area for tBMMSCs exposed to CS-1 was very similar to those measured at all levels of CP. Within CS, CS-1 was significantly ($p<0.05$) smaller than CS-1HF and CS-5. When comparing CS across the same frequency, there was a threshold effect but no significant correlation as a dose-response.

Comparisons across stimuli indicate that tBMMSCs exposed to CS or CP were significantly ($p<0.05$) smaller in size than LSS. In addition CP-120 was significantly ($p<0.05$) smaller than CS-5. The relationships within and across components of the Mechanical Panel are depicted in **Figure 3.7B**.

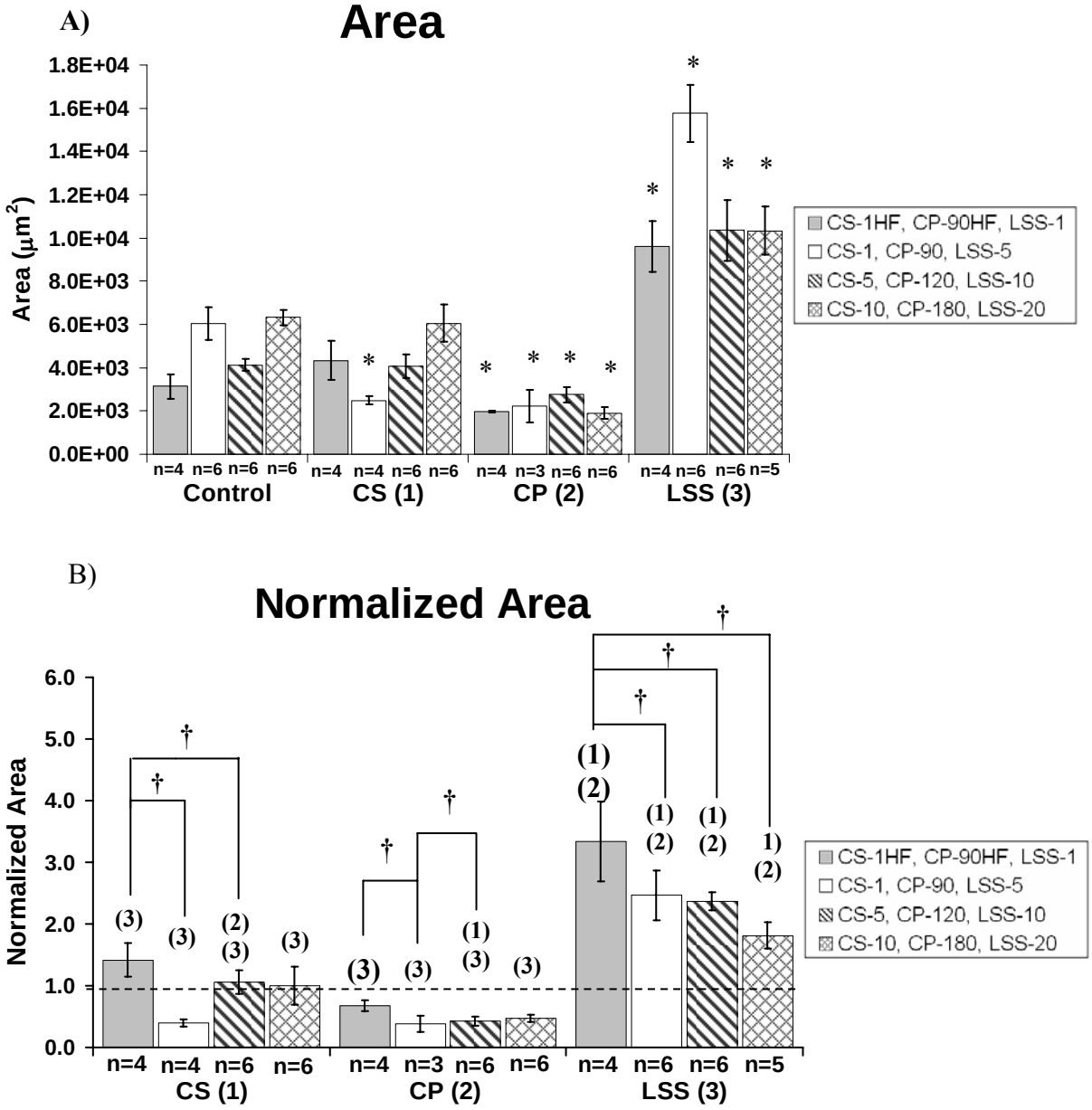

Figure 3.7 Surface area measurements for tBMMSCs exposed to 5 days of mechanical stimulation. (A) Raw measurements for all experiments. (B) Area measurements for each component of the Mechanical Panel normalized by division by the experimental control. The dashed line represents control values. All data presented as the average ± standard error of the mean (SEM). * denotes $p<0.05$ compared to controls. + denotes $p<0.1$ compared to controls. † denotes $p<0.01$ for means within each stimulus. (1), (2), (3) denote $p<0.05$ for means between stimuli of corresponding bar color where (1)=CS, (2)=CP, and (3)=LSS.

3.3.2.2 Major axis changes

The measurement of changes in the major axis has previously been interpreted as a measure of cellular elongation [526, 641, 642]. The measured major axes and normalized major axes (calculated by division of the major axis measurement by the control values) are presented as the average ± SEM in **Figure 3.8**. Similar to area measurements, major axis measurements were significantly ($p<0.05$) elevated for tBMMSCs exposed to LSS-1 (142.7 ± 5.4 μm, n=4), LSS-5 (187.0 ± 6.5 μm, n=6), LSS-10 (147.8 ± 10.7 μm, n=6), and LSS-20 (148.8 ± 8.4 μm, n=5) when compared to controls. Within LSS, the normalized major axis for LSS-1 was significantly ($p<0.05$) more elongated than LSS-5 and LSS-10. In addition, a moderate negative correlation was determined to a dose-response for tBMMSCs exposed to LSS ($\rho= -0.641$, $p<0.05$). The data indicates that as the magnitude of shear increased, the length of the major axis decreased.

For tBMMSCs exposed to CP, major axis measurements demonstrated significant ($p<0.05$) decreases at CP-90HF (67.0 ± 1.3 μm, n=4), CP-90 (72.4 ± 12.8 μm, n=5), CP-120 (79.6 ± 4.9 μm, n=6), and CP-180 (65.0 ± 3.3 μm, n=6) when compared to controls. Within CP experiments, there was a significant ($p<0.05$) decrease in the normalized major axis from CP-90HF to CP-90, CP-120, and CP-180. There was no dose-response correlation for the magnitude or frequency of CP stimulation.

Major axis measurements in tBMMSCs exposed to CS showed only significant changes at the 1% stretch magnitude compared to controls. The major axis was significantly ($p<0.05$) reduced for CS-1 (77.7 ± 3.5 μm, n=4) compared to controls in a similar fashion to the reduction found with CP exposure. However, by increasing the frequency of the applied stretch, CS-1HF (97.5 ± 8.0 μm, n=4) demonstrated a significant ($p<0.05$) increase in major axis length compared

to controls. Although CS-5 (111.3 ± 5.9 μm, n=6) and CS-10 (128.8 ± 8.8 μm, n=6) demonstrated increases in the major axis length, only CS-5 was significantly ($p<0.05$) increased compared to controls. Within CS, normalized major axis measurements for CS-1 were significantly ($p<0.05$) shorter than CS-1HF, CS-5 and CS-10. The major axis measurement was weakly correlated for a dose-response for CS ($\rho= -0.488$, $p=0.055$), and strongly correlated ($\rho= -0.873$, $p<0.01$) to a frequency-response.

Comparisons of the major axis lengths across stimuli yielded similar results to the comparisons for area across stimuli. CS-1HF, CP-90HF, and LSS-1 were each significantly ($p<0.05$) different. CS-1 and CP-90 were significantly ($p<0.05$) smaller than LSS-5, but were not different from each other. CS-5, CP-120, and LSS-10 were each significantly ($p<0.05$) different and CP-180 was significantly ($p<0.05$) smaller than CS-10 and LSS-20. The relationships within and across components of the Mechanical Panel are depicted in **Figure 3.8B**.

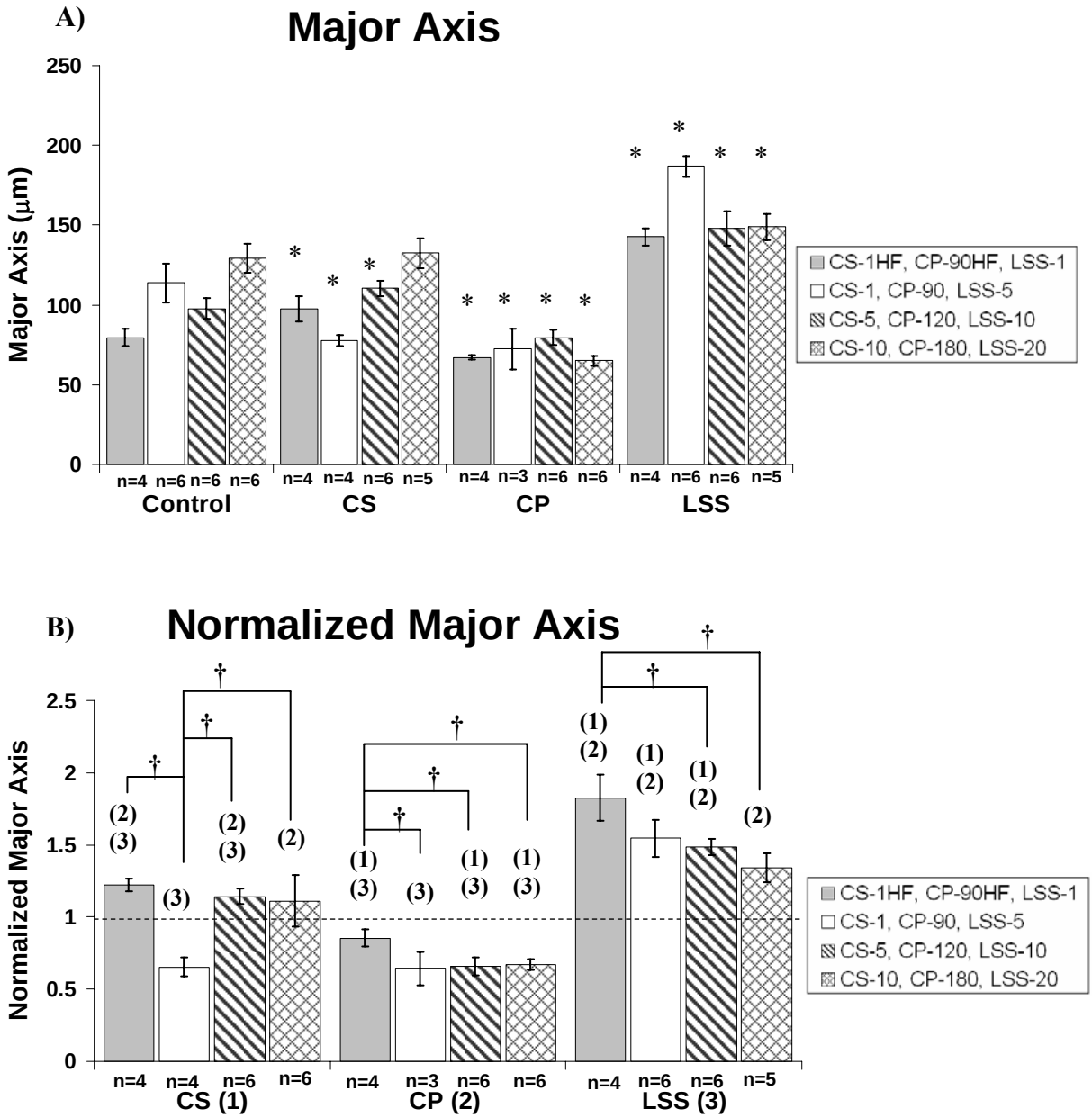

Figure 3.8: Major axis measurements for tBMMSCs exposed to 5 days of mechanical stimulation. (A) Raw measurements for all experiments. (B) Major axis measurements normalized by division by the experimental control for each of the components of the Mechanical Panel. The dashed line represents control values. All data presented as the average ± standard error of the mean (SEM). * denotes $p<0.05$ compared to controls. + denotes $p<0.1$ compared to controls. † denotes $p<0.01$ for means within each stimulus. (1), (2), (3) denote $p<0.05$ for means between stimuli of corresponding bar color where (1)=CS, (2)=CP, and (3)=LSS.

3.3.2.3 Shape index changes

The calculated shape indices and normalized shape indices (calculated by subtraction of the control shape index from each calculated shape index) are presented as the average ± SEM in **Figure 3.9**. With this normalization, negative differences relate to cells that are more spindle-shaped than the controls, while positive differences relate to cells that are more round than the controls. For tBMMSCs exposed to mechanical stimulation show significant changes depending on the type, magnitude, and frequency of applied stimulation. Shape indices for LSS-1 (0.26 ± 0.04, n=4) and LSS-5 (0.27 ± 03, n=6), and 10 dynes/cm^2 (0.24 ± 0.02, n=6) were not significantly different from controls. However, the shape index of LSS-20 dynes/cm^2 (0.18 ± 0.02) was significantly ($p<0.05$) smaller than the control, indicating that the tBMMSCs were becoming more spindle shaped at this higher shear stress. Within the LSS stimulus, LSS-20 was significantly ($p<0.05$) more spindle-shaped than LSS-10, LSS-5, and LSS-1. LSS demonstrated a strong dose-response ($\rho= -0.792$, $p<0.001$) with increasing shear stress leading to a decreased shape index, indicating a more spindle-shaped cell.

The shape indices for CP-90HF (0.37 ± .02; n=4), CP-90 (0.37 ± 0.02, n=3), CP-120 (0.33 ± 0.03, n=6), and CP-180 (0.36 ± 0.01, n=6) were significantly ($p<0.05$) greater compared to the controls, indicating that the application of CP leads to a more rounded phenotype. Within CP there was no difference at the various magnitudes or frequencies, and thus no correlation between the shape index and either the magnitude or frequency was detected.

The shape indices for CS-5 (0.23 ± 0.02, n=5), and CS-10 (0.21 ± 0.01, n=7) were significantly ($p<0.05$) smaller compared to controls, indicating a more spindle shape. However, the shape index for CS-1 (0.35 ± 0.01, n=4) was significantly ($p<0.05$) higher than controls, indicating that the tBMMSCs were more rounded. In fact, the shape index for CS-1 was very

similar to all values calculated for CP. The shape index for CS-1HF (0.25 ± 0.01, n=4) was not significantly different compared to controls. Within CS, all values were significantly ($p<0.05$) different from each other, with the exception of CS-5 and CS-10, whose shape indices were nearly identical. The normalized values for shape index for CS, which changed from a more rounded phenotype at CS-1 to a more spindle shaped phenotype for CS-5 and CS-10, had a fairly strong correlation ($\rho= -0.639$, $p<0.01$) to the magnitude of CS. A strong frequency correlation ($\rho= -0.873$, $p<0.01$) also existed for CS, with increasing frequency leading to a more spindle shape.

Comparisons across the stimuli demonstrate the strong changes in shape index between each stimulus. With the exception of CS-1 and CP-90, which had similar changes in shape index, all comparisons between CP and the other stimuli demonstrated significant ($p<0.05$) changes in shape index. The relationships within and across components of the Mechanical Panel are depicted in **Figure 3.9B**.

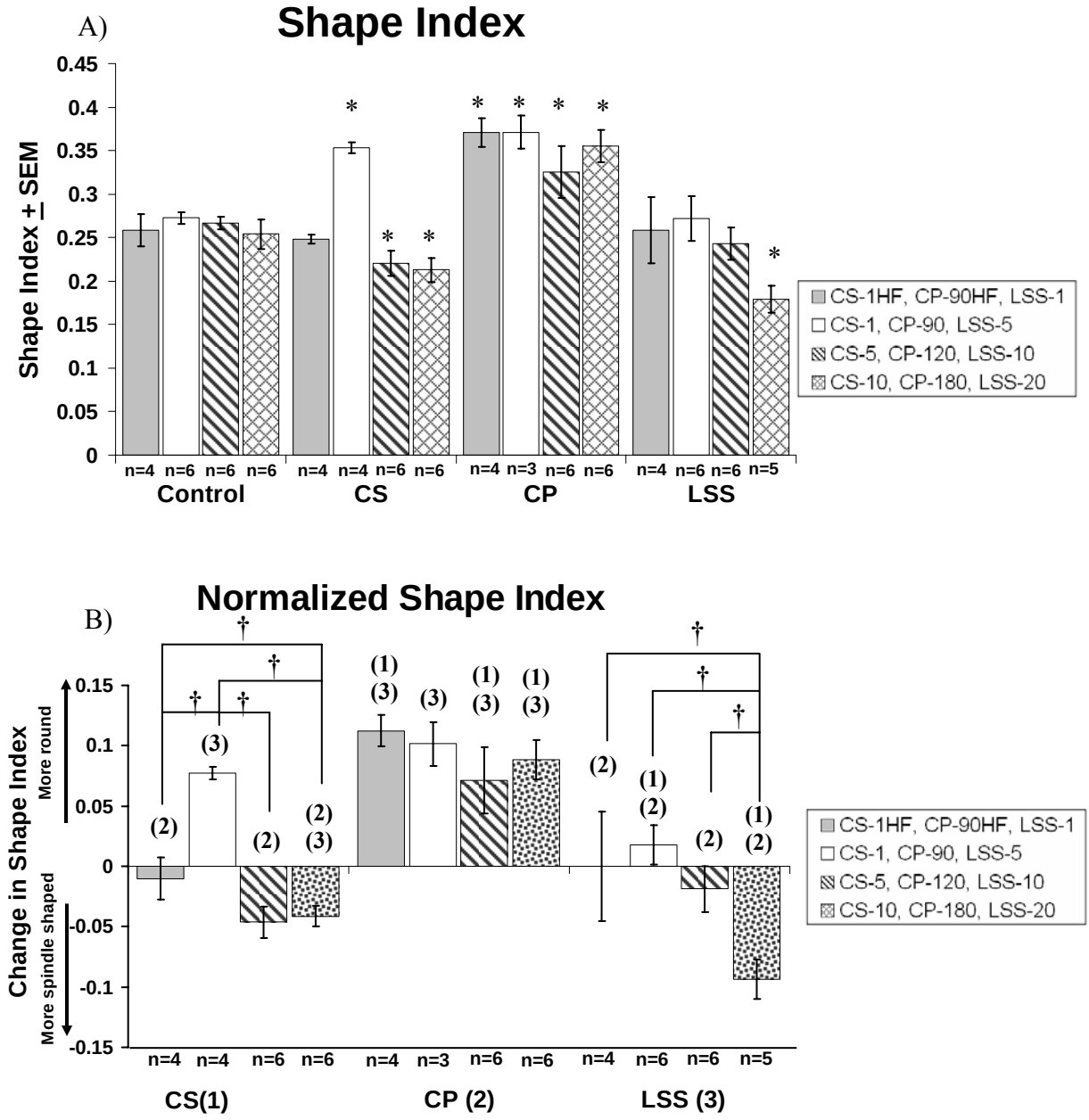

Figure 3.9: Shape Index measurements based upon the area perimeter measurements for tBMMSCs exposed to 5 days of mechanical stimulation. (A) Raw shape index calculations. (B) Shaped indices normalized by subtraction of the experimental control for each of the components of the Mechanical Panel. All data presented as the average ± SEM. * denotes $p<0.05$ compared to controls. + denotes $p<0.1$ compared to controls. † denotes $p<0.01$ for means within each stimulus. (1), (2), (3) denote $p<0.05$ for means between stimuli of corresponding bar color where (1)=CS, (2)=CP, and (3)=LSS.

3.3.2.4 Tortuosity index changes

The calculated tortuosity indices and normalized tortuosity indices (calculated by subtraction of the control tortuosity index from each calculated tortuosity index) are presented as the average ± SEM in **Figure 3.10**. With this normalization, negative differences relate to cells that are less tortuous than the controls, while positive differences relate to cells that are more tortuous than the controls. tBMMSCs exposed to LSS-1 (1.5 ± 0.09, n=4), and LSS-5 (1.43 ± 0.06, n=6) were not significantly different from the controls, but LSS-10 (1.53 ± 0.07, n=6) and LSS-20 (1.8 ± 0.08, n=5) were significantly ($p<0.05$) more tortuous compared to the controls. Within LSS, only LSS-20 was significantly ($p<0.05$) more tortuous than LSS-5. LSS demonstrated a strong correlation ($\rho=0.787$, $p<0.01$) to the magnitude of applied LSS, with increasing shear stress leading to increased tortuosity.

tBMMSCs exposed to CP-90HF (1.15 ± 0.02, n=4), CP-90 (1.13 ± 0.03, n=3), CP-120 (1.23 ± 05.06, n=6) and CP-180 (1.18 ± 0.04, n=6) were significantly ($p<0.05$) less tortuous than the controls. However, within CP, there were no differences amongst the magnitudes or frequencies. There were no statistically significant correlations for magnitude or frequency dependent changes in tortuosity following exposure to CP.

Similar to the tortuosity indices for CP, CS-1 (1.15 ± 0.03, n=4) was significantly ($p<0.05$) less tortuous than controls. However, all other calculated tortuosity indices for CS-1HF (1.39 ± 0.09, n=4), CS-5 (1.32 ± 0.12, n=5), and CS-10 (1.45 ± 0.05, n=6) were not significantly different than the controls. Within CS, only CS-1 was significantly ($p<0.05$) less tortuous than CS-10. tBMMSCs exposed to CS demonstrated a slight correlation ($\rho= -0.655$, $p=0.07$) to increases in the frequency of stretch, but not to increases in the magnitude of stretch.

Comparisons across the stimuli demonstrated significant ($p<0.05$) differences between the change in tortuosity index for CS-1 and CP-90 when compared to LSS-5. Additionally, there were significant ($p<0.05$) increases in the change in tortuosity indices from CS-10 to CP-180 and to LSS-20, and for CP-120 compared to LSS-10. The relationships within and across components of the Mechanical Panel are depicted in **Figure 3.10**.

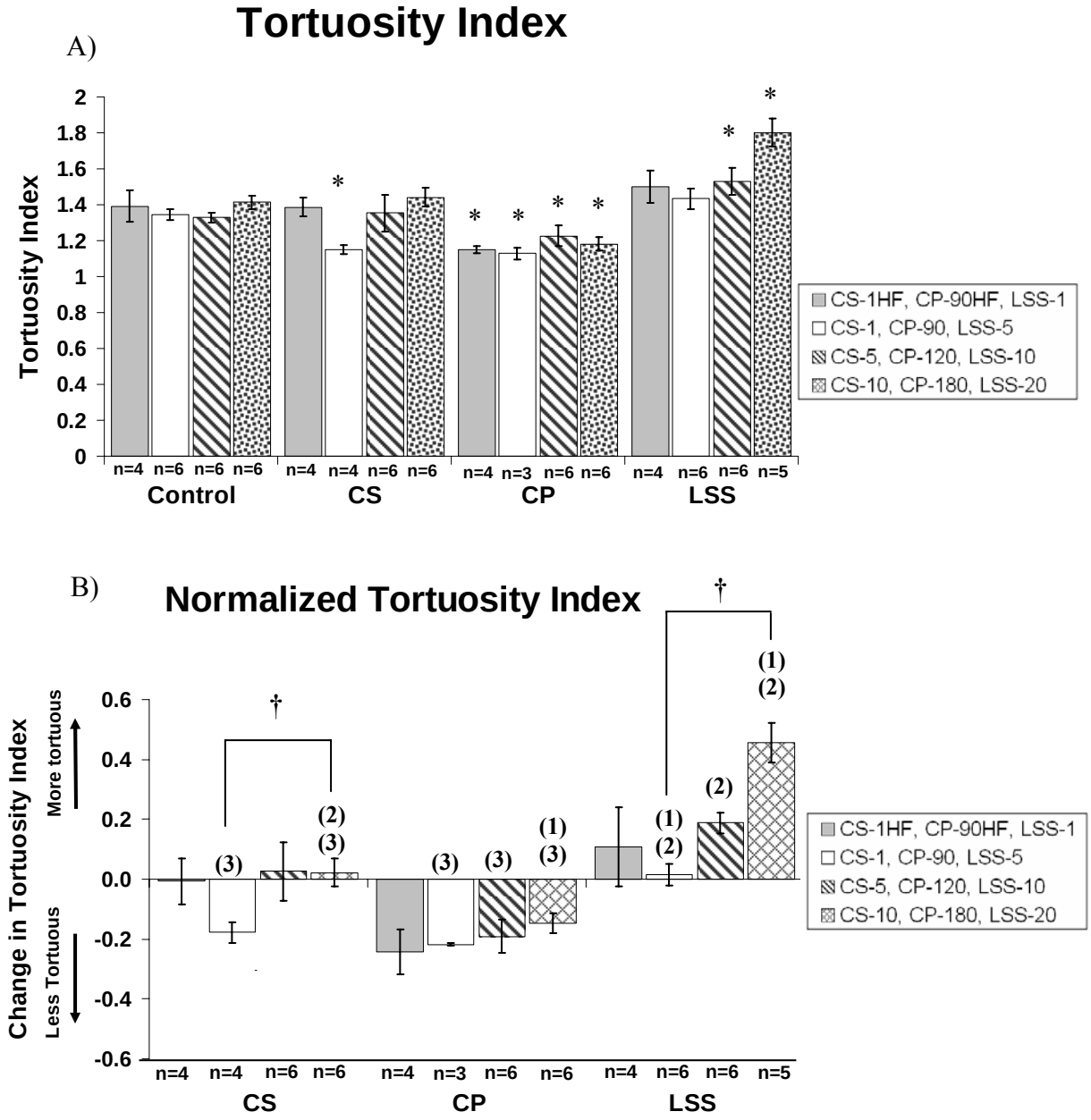

Figure 3.10: Tortuosity Index calculated from the perimeter and major axis measurement of tBMMSCs exposed to 5 days of mechanical stimulation. (A) Raw tortuosity index calculations. (B) Tortuosity indices normalized by subtraction of each component of the Mechanical Panel by their respective experimental control. All data presented as the average ± SEM. * denotes $p<0.05$ compared to controls. + denotes $p<0.1$ compared to controls. † denotes $p<0.01$ for means within each stimulus. (1), (2), (3) denote $p<0.05$ for means between stimuli of corresponding bar color where (1)=CS, (2)=CP, and (3)=LSS.

3.3.2.5 Changes in angle of alignment

Cellular alignment quantified with Scion Image is presented as average normalized incidence histograms in **Figure 3.11**, **Figure 3.12**, and **Figure 3.13**. Statistical analysis against a uniform distribution was carried out according to **Equations (3.11)**, **(3.12)**, **(3.13)**, and **(3.14)**. For tBMMSCs exposed to CP, the orientation of the cells was found to be random for CP-90HF ($R^*=0.952$, $p>0.10$, $n=4$), CP-90 ($R^*=0.816$, $p>0.10$, $n=3$), CP-120 ($R^*=0.965$, $p>0.10$, $n=5$), and CP-180 ($R^*=0.619$, $p>0.10$, $n=5$). Exposure to LSS-1 ($R^*=0.954$, $p>0.10$, $n=4$) and LSS-5 ($R^*=0.722$, $p>0.10$, $n=5$) demonstrated random orientation. However, LSS-10 ($R^*=1.23$, $p<0.05$, $n=4$) showed statistically significant orientation around the 90^o (parallel to flow) and trended towards an orientation near 90^o at LSS-20 ($R^*=1.039$, $p<0.10$, $n=5$). Application of CS-1HF ($R^*=0.176$, $p>0.10$, $n=4$) and CS-1 ($R^*=0.567$, $p>0.10$, $n=5$), did not show any preferred orientation, but CS-5 ($R^*=1.30$, $p<0.05$, $n=5$) and CS-10 ($R^*=1.29$, $p<0.05$, $n=5$) resulted in statistically significant orientation at 90^o (perpendicular to the direction of applied stretch).

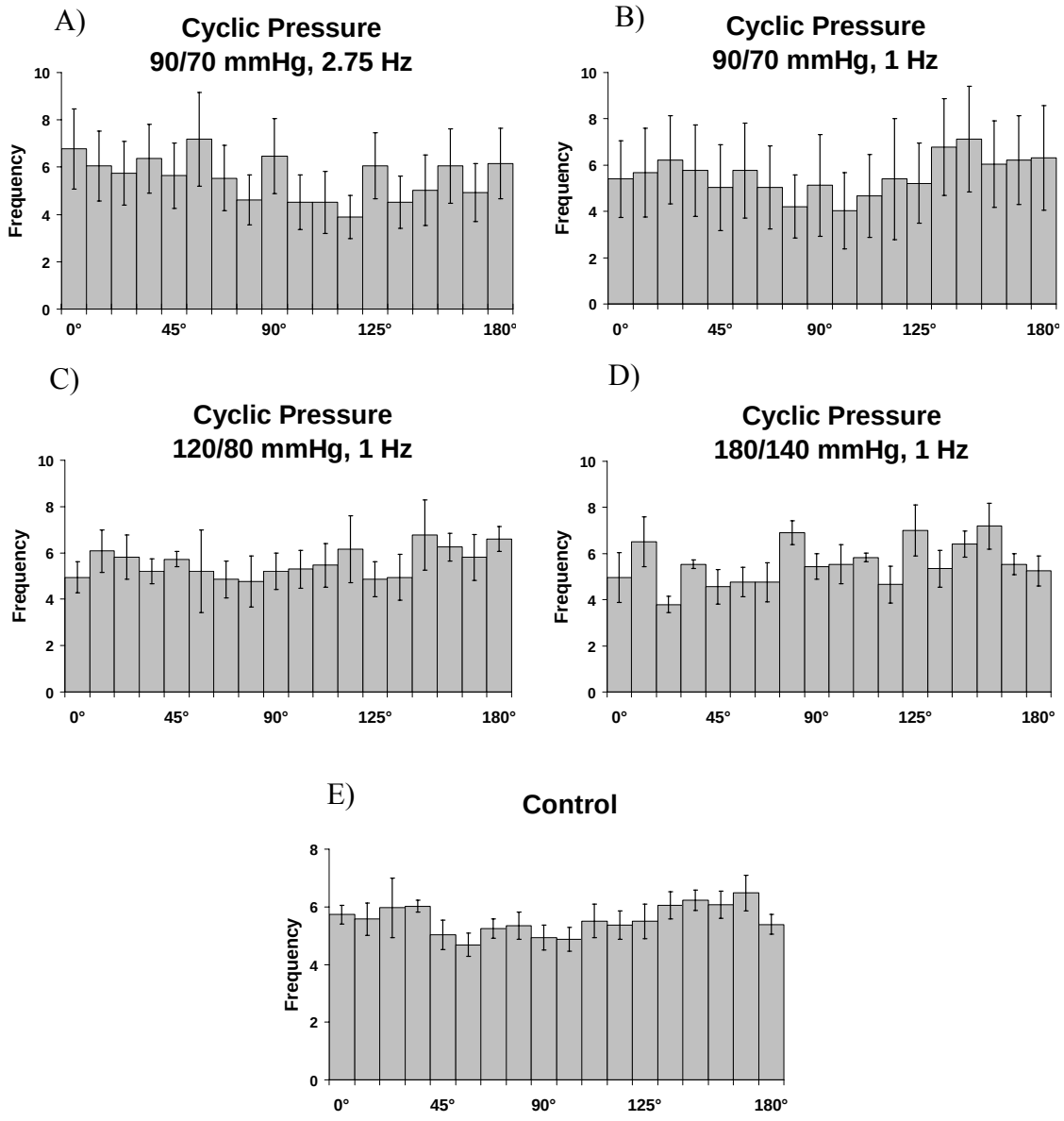

Figure 3.11: Normalized histograms for cellular of orientation in CP experiments. The error bars represent the standard error of the mean for the averaged normalized frequencies. Non-parametric analysis against a uniform distribution resulted in no statistical significant differences with any of the cyclic pressure regimens, which is in agreement with the normalized histogram for the control.

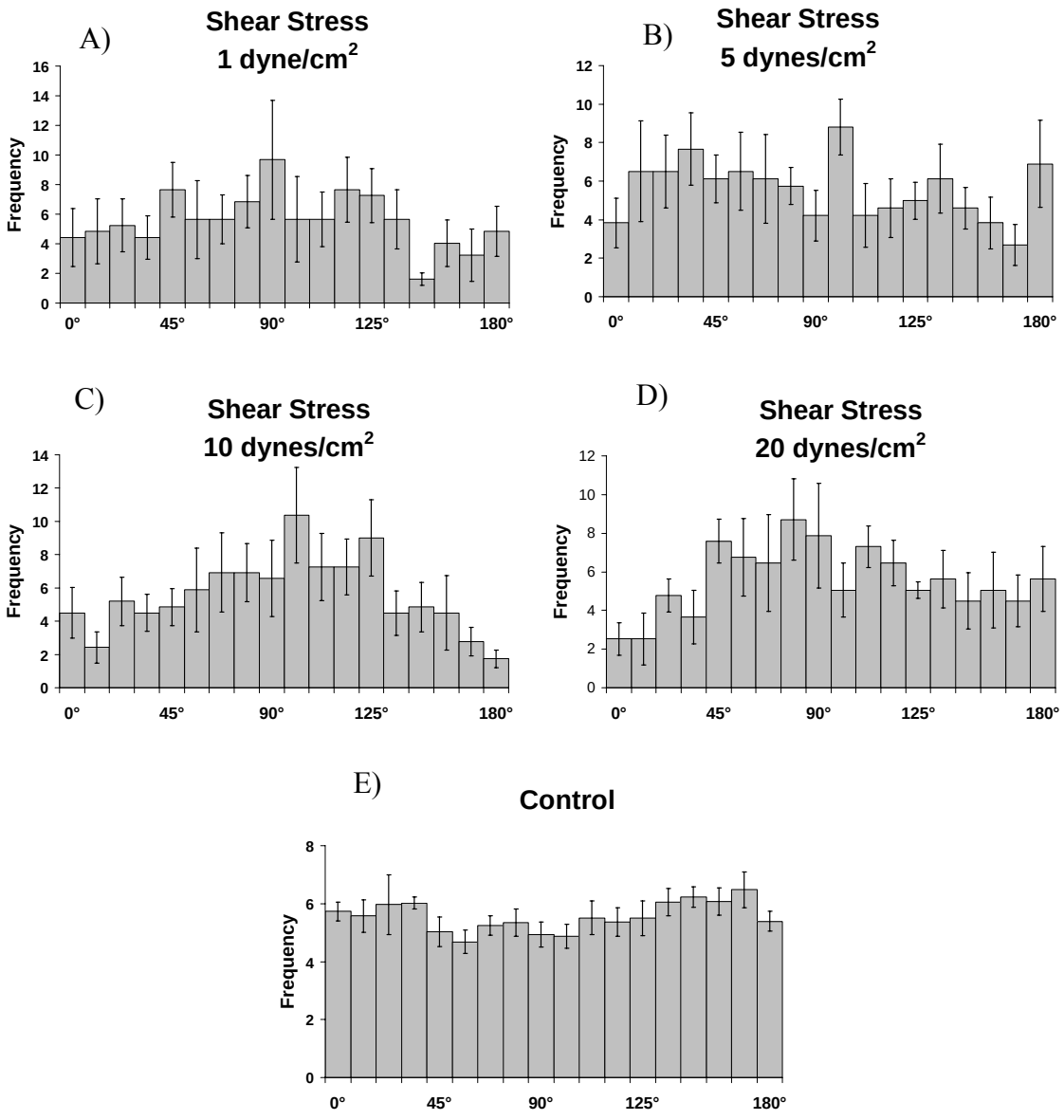

Figure 3.12: Normalized histograms for cellular orientation in tBMMSCs exposed to LSS. The error bars represent the standard error of the mean for the averaged normalized frequencies. Non-parametric analysis against a uniform distribution resulted in no statistical difference for 1 dyne/cm^2 and 5 dynes/cm^2. However, at 10 dynes/cm^2 and 20 dynes/cm^2, a preferred orientation begins to develop around 90^o, which is in the direction of flow. The histogram from control samples is provided to represent random orientation.

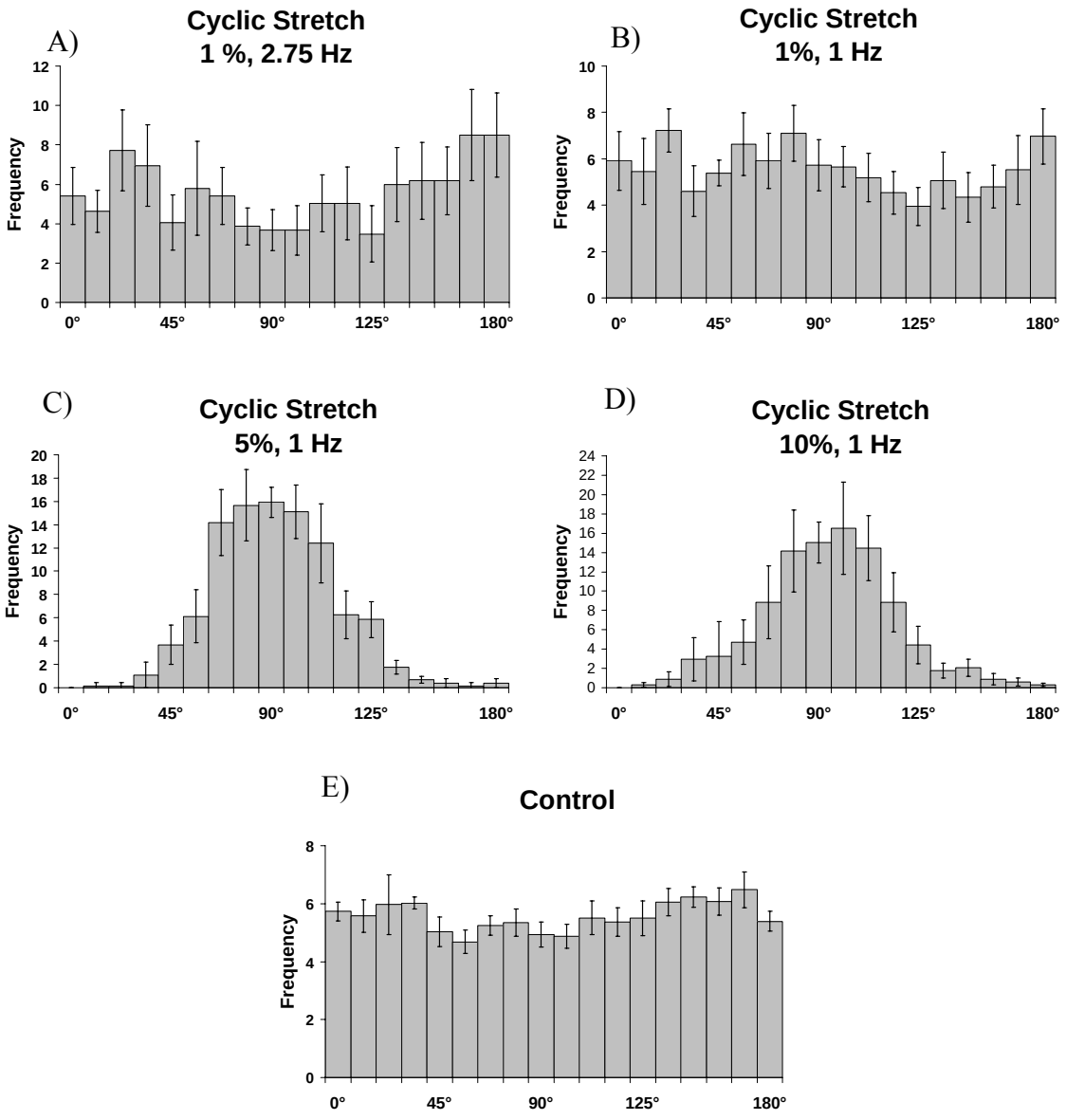

Figure 3.13: Normalized histograms for cellular orientation in tBMMSCs exposed to CS. The error bars represent the standard error of the mean for the averaged normalized frequencies. Non-parametric analysis against a uniform distribution did not demonstrate any significant changes for 1% 2.75 Hz and 1% 1 Hz cyclic stretch. However, higher magnitudes of stretch (5% 1 Hz and 10% 1 Hz) demonstrate a significant change from a uniform distribution centered on 90^{o}, which is perpendicular to the direction of stretch.

3.3.3 Proliferation

Changes in cellular proliferation following 5 days of stimulation for the Mechanical Panel settings outlined in Section 3.2.3.2 are depicted in **Figure 3.14**. The cell density of tBMMSCs exposed to CS-1HF (7.24 ± 3.73 $x10^3$ cells/cm^2, n=4), CS-5 (12.21 ± 3.36 $x10^3$ cells/cm^2, n=7) and CS-10 (4.95 ± 1.04 $x10^3$ cells/cm^2, n=7) was unchanged when compared to the controls. However, the cell density for CS-1 (16.57 ± 2.30 $x10^3$ cells/cm^2) was significantly ($p<0.05$) increased from controls. Although there appears to be possible dose- and frequency-responses for tBMMSCs exposed to CS, the Spearman correlations for magnitude and frequency were non-significant.

Similarly to CS-1, the cell density for tBMMSCs exposed to CP-90 (41.21 ± 12.53 $x10^3$ cells/cm^2, n=5), CPO-120 (21.10 ± 2.71 $x10^3$ cells/cm^2, n=7), and CP-180 (26.78 ± 4.40 $x10^3$ cells/cm^2, n=7) was significantly ($p<0.05$) increased compared to the controls. The cell density for CP-90HF (28.17 ± 6.74 $x10^3$ cells/cm^2, n=4) was elevated over controls, but not statistically significant ($p=0.07$). There was also a weak, but statistically significant correlation ($\rho= -0.483$, $p<0.05$) for a dose-dependent decrease in cell density with increasing magnitudes of CP stimulation. There was no correlation between cell density and the frequency of CP.

Conversely, the cell density for tBMMSCs exposed to LSS at 5 dyens/cm^2 (3.12 ± 1.69 $x10^3$ cells/cm^2, n=7), 10 dynes/cm^2 (2.54 ± 0.50 $x10^3$ cells/cm^2, n=6), and 20 dynes/cm^2 (2.08 ± 0.53 $x10^3$ cells/cm^2, n=6) were significantly ($p<0.05$) decreased when compared to controls. Only cell density for LSS at 1 dyne/cm^2 (2.87 ± 0.93 $x10^3$ cells/cm^2, n=4) was not significantly different from the controls. A weak, but statistically significant decrease ($\rho= -0.469$, $p<0.05$) in cell density was found for increasing magnitudes of LSS.

Comparisons made within as well as across each stimuli displayed an inconsistent homogeneity of variance. As a result, most post-hoc comparisons were made with the Games-Howell test. The few statistically significant differences detected were for an increase in cell density for CS-1 compared to CS-5 ($p<0.05$), and for increases in cell density for CP-90HF compared to CS-1HF and LSS-1 ($p<0.05$), for CS-1 compared to LSS-5 ($p<0.05$), for CP-120 compared to CS-5 and LSS-10 ($p<0.05$), as well as for CP-180 compared to LSS-20 ($p<0.05$).

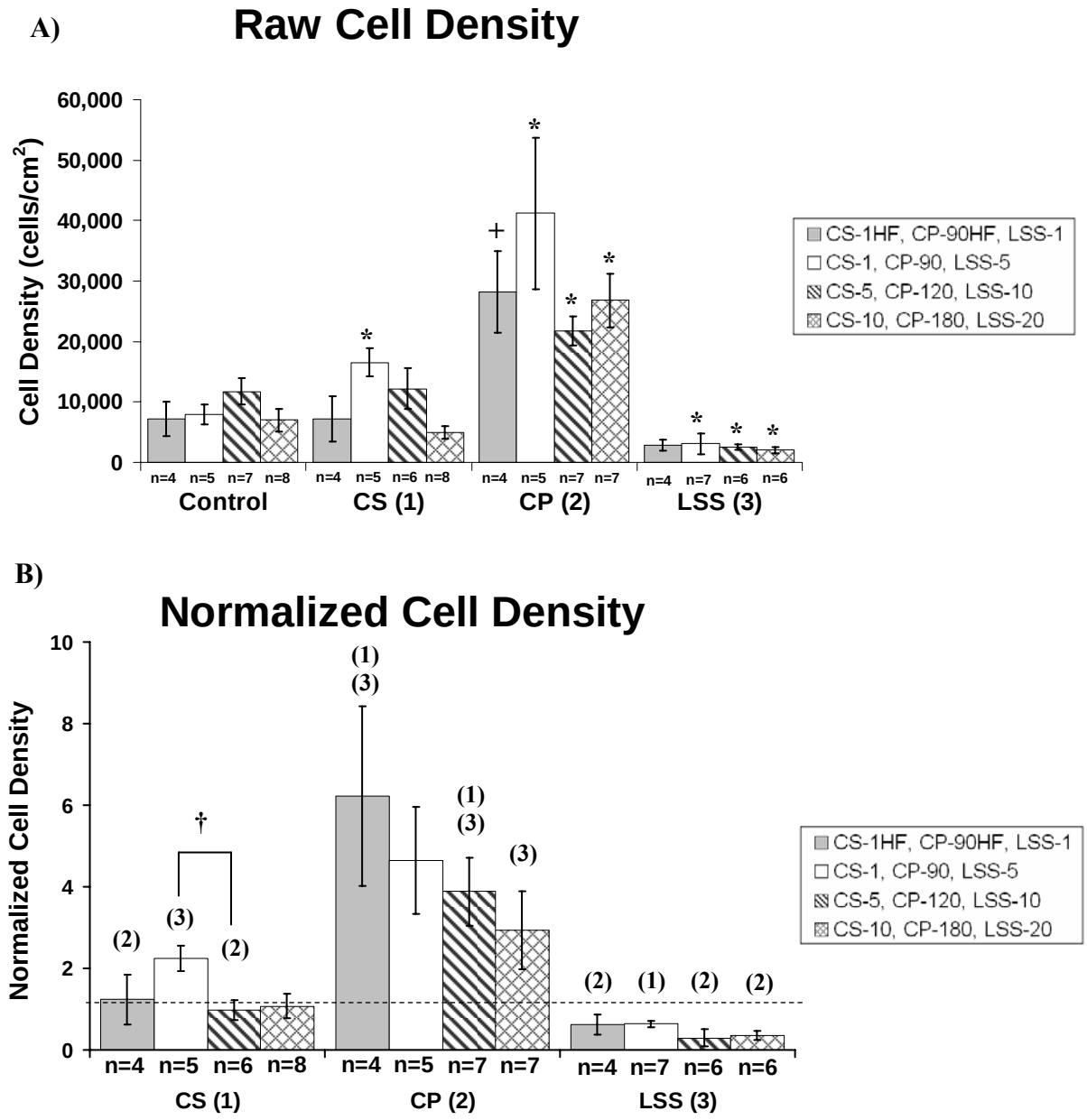

Figure 3.14: Cell density of tBMMSCs following 5 days of mechanical stimulation. (A) Raw cell density measurements for each component of the Mechanical Panel (B) Cell density for each component of the Mechanical Panel normalized by division by the experimental control. The dashed line represents control values. All data presented as the average ± SEM. * denotes $p<0.05$ compared to controls. + denotes $p<0.1$ compared to controls. † denotes $p<0.01$ for means within each stimulus. (1), (2), (3) denote $p<0.05$ for means between stimuli of corresponding bar color where (1)=CS, (2)=CP, and (3)=LSS.

3.3.4 Histology

The assessment of osteoblast or adipocyte differentiation by histological staining in tBMMSCs exposed to the Mechanical Panel at the magnitudes and frequencies listed in **Table 3.1** yielded no apparent differentiation towards osteoblast or adipocytes. No staining was detected for Alizarin Red and Oil Red O, which stain mineralized calcium (osteoblast) and lipid accumulation (adipocytes), respectively. Representative images from one 5 day Mechanical Panel experiment are presented in **Figure 3.15**. These results were consistent regardless of the magnitude, frequency, or type of applied mechanical stimulation. **Figure 3.15** shows a few very small lipid pockets in the LSS-20 sample, but these can be contrasted with the positive staining for Oil Red O in **Figure 3.5B** to see that they are insignificant compared to the differentiation towards adipocytes using adipogenic medium. The red hue in the CS-10 sample depicted in **Figure 3.15** results from the Oil Red O staining the silicone grease that coats the bottom of the membrane for samples exposed to CS, not the cells themselves.

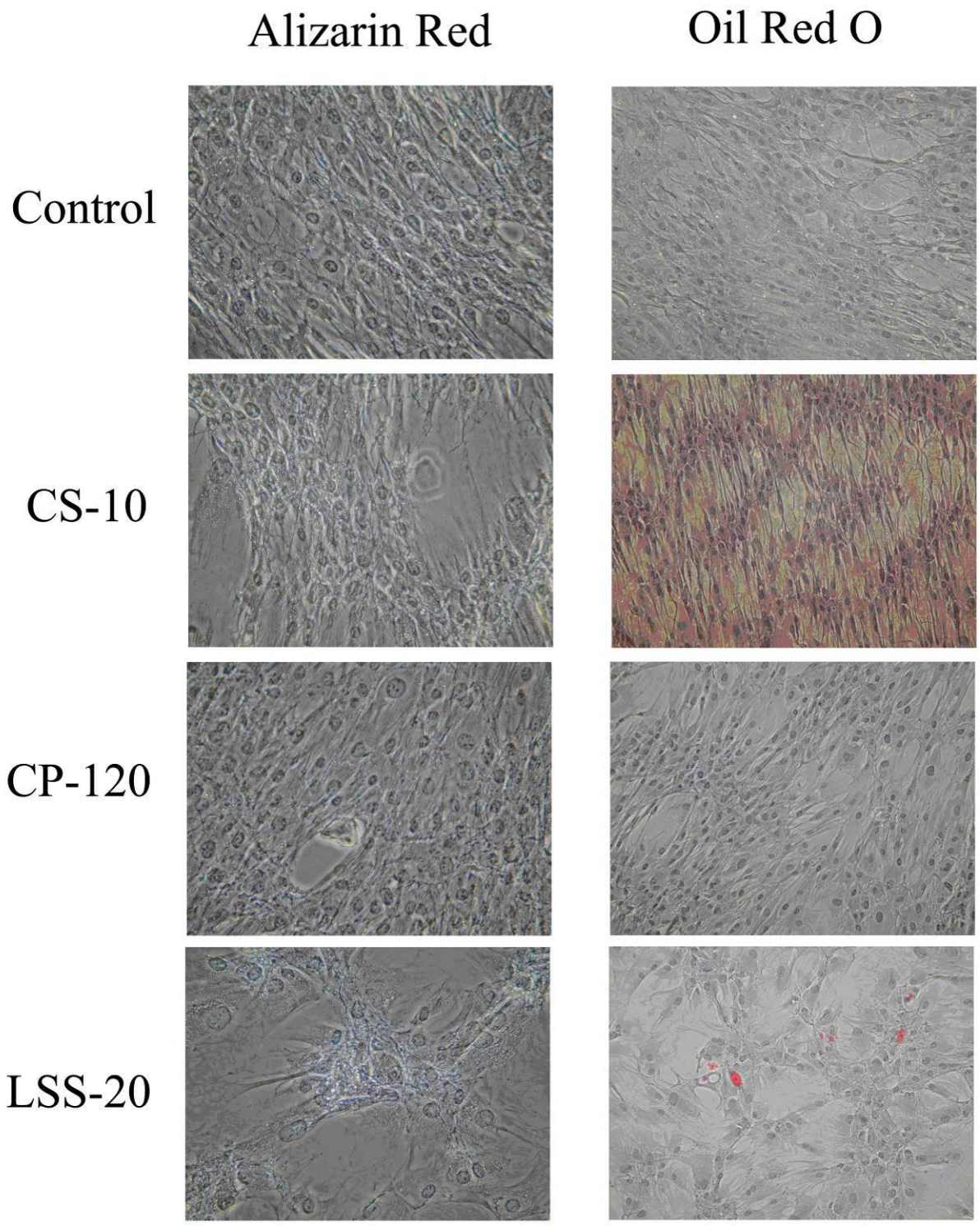

Figure 3.15: Representative histology images from a 5 day Mechanical Panel experiment stained for Alizarin Red and Oil Red O All images taken at 100x.

3.3.5 Immunohistochemistry

Representative images of each protein endpoint described in Section 3.2.4.4 are shown in **Figure 3.16**, **Figure 3.17**, **Figure 3.18**, **Figure 3.19**, **Figure 3.20**, and **Figure 3.21**.

tBMMSCs exposed to CS, regardless of the magnitude or frequency, induced the expression of SMA (**Figure 3.16**). The expression of SMA at CS-1 did appear to be weaker than that induced by CS-10 and CS-5, but this cannot be conclusively determined by IHC. CS-1HF demonstrated what appeared to be a stronger intensity signal for SMA, but the expression was restricted to smaller pockets within the field of view, as opposed to the general staining found for the other CS samples at 1 Hz. No SMA expression was detected for tBMMSCs exposed to any level of CP or LSS. In addition, SMA expression was not detected in control samples, and the IgG negative control was also negative, demonstrating a lack of non-specific binding of the secondary antibody.

Calponin expression, shown in **Figure 3.17**, demonstrated a dose-dependent threshold of staining for tBMMSCs exposed to cyclic stretch. CS-1 did not show positive staining, whereas CS-10 and CS-5 demonstrated positive staining for calponin. Positive calponin staining for CS-1HF may be indicative of a frequency response. Similar to the SMA staining at CS-1HF, only pockets of positive staining were visible within each field of view, which contrasts with the general staining shown for CS-10 and CS-5. This suggests that the higher frequency produces effects in a sub-population of the tBMMSCs. Control, CP, and LSS samples showed little or no staining for calponin, and IgG control samples were also negative.

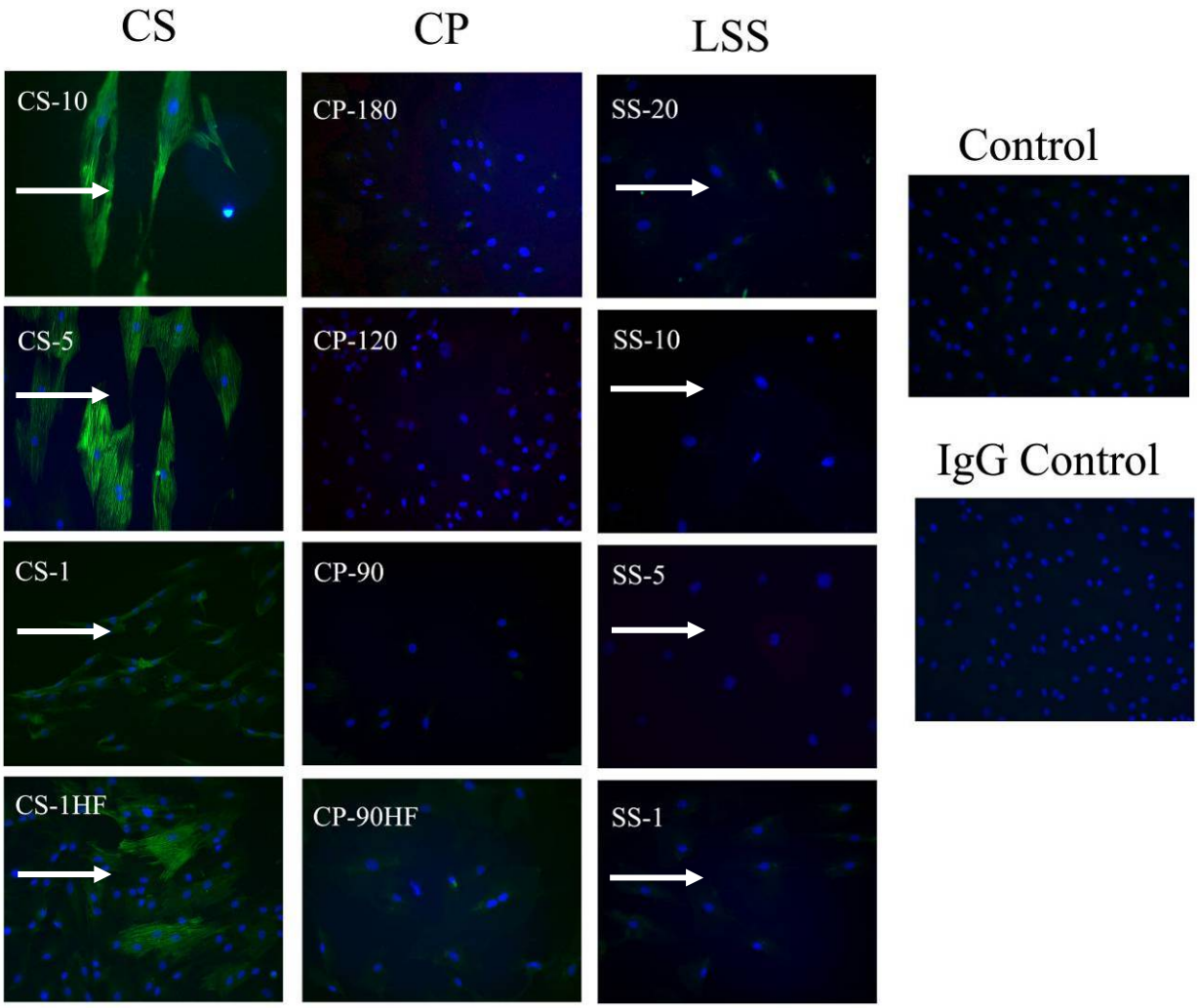

Figure 3.16: Representative immunohistochemistry images for smooth muscle α-actin. Arrows indicate the direction of applied stimulation, if applicable. All images taken at 200x.

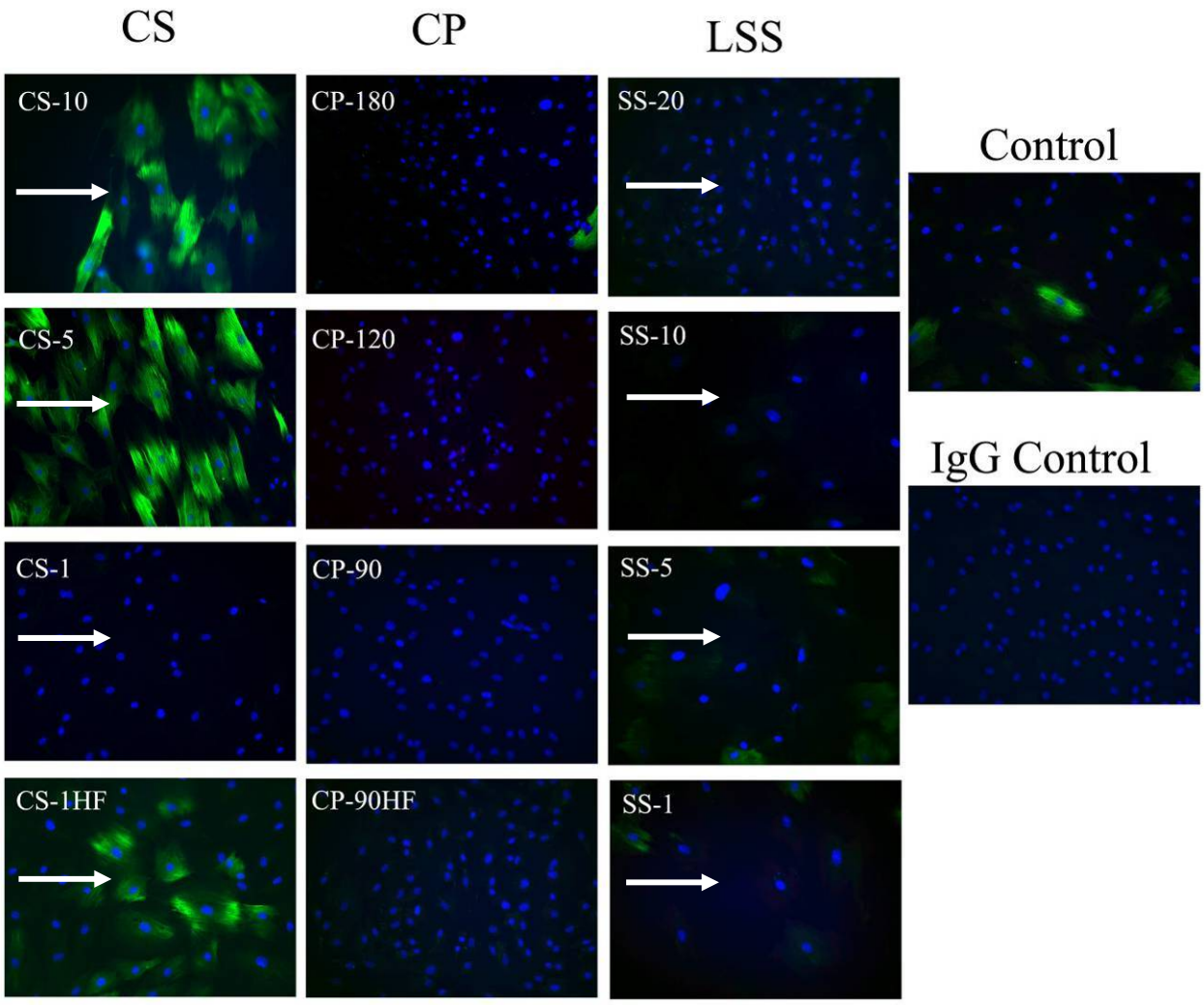

Figure 3.17: Representative immunohistochemistry images for calponin. Arrows indicate the direction of applied stimulation, if applicable. All images taken at 200x.

Myosin heavy chain expression, shown in **Figure 3.18**, also demonstrated a threshold of expression based upon the magnitude of cyclic stretch. CS-10 was weakly positive for myosin heavy chain in three out of four experiments, while CS-5 and CS-1 was negative for myosin heavy chain. The staining pattern was fairly diffuse, unlike the expected filamentous pattern which was evident in the calponin staining (recall **Figure 3.17**). Like SMA and calponin, CS-1HF did demonstrate localized staining in all experiments, again suggesting that higher frequency stimulation was similar to the higher magnitude stimulation. CP and LSS stimulation did not induce the expression of myosin heavy chain. Control and IgG negative samples were also negative for myosin heavy chain.

Flk-1 (VEGFRII) expression, shown in **Figure 3.19**, was constitutively expressed in tBMMSCs as evidenced by positive staining control samples. Flk-1 expression was maintained under all levels of CS. Like SMA, calponin, and MHC, flk-1 expression in the CS-1HF cyclic stretch samples appears to be heterogeneous in intensity. The higher intensity staining was centered on the similar core, swirl pattern seen in the SMA, calponin, and MHC samples. In addition, although not quantitative, the staining intensity for the 1 Hz CS stimuli did not appear to vary in any manner similar to the variance in intensity seen with SMA. Flk-1 expression was also maintained under cyclic pressure at CP-180, but was lost at CP-120, CP-90 and CP-90HF. A similar response to that found with CP was noted for tBMMSCs exposed to LSS. The higher magnitudes of shear, including LSS-20 and LSS-10 maintained expression of flk-1. Lower magnitudes, including LSS-5 and LSS-1 lost the expression of flk-1. It should be noted that the staining intensity for the positive samples was much lower in the tBMMSCs exposed to cyclic pressure and laminar shear stress relative to control and cyclic stretch samples from the same group. Although IHC is not quantitative, this may indicate that despite the presence of positive

staining there was likely a modulation of the expression to levels lower than that seen in the control and cyclic stretch.

The more mature marker for ECs, PECAM (shown in **Figure 3.20**) was negative for the controls as well as all levels of CS, CP, and LSS. The other mature EC marker tested, vWF (shown in **Figure 3.21**), was also negative for the controls as well as all levels of CS, CP, and LSS.

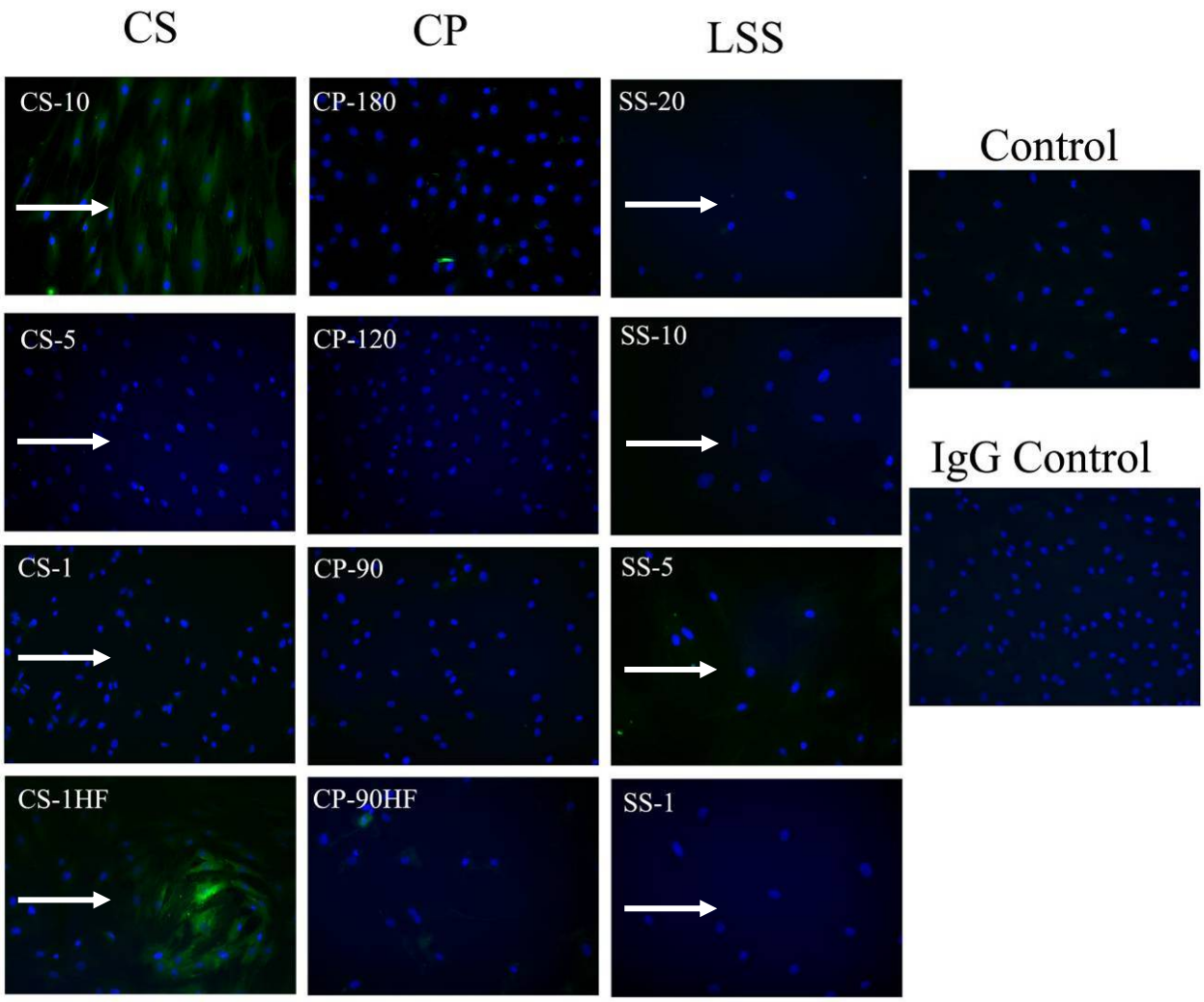

Figure 3.18: Representative immunohistochemistry images for myosin heavy chain. Arrows indicate the direction of applied stimulation, if applicable. All images taken at 200x.

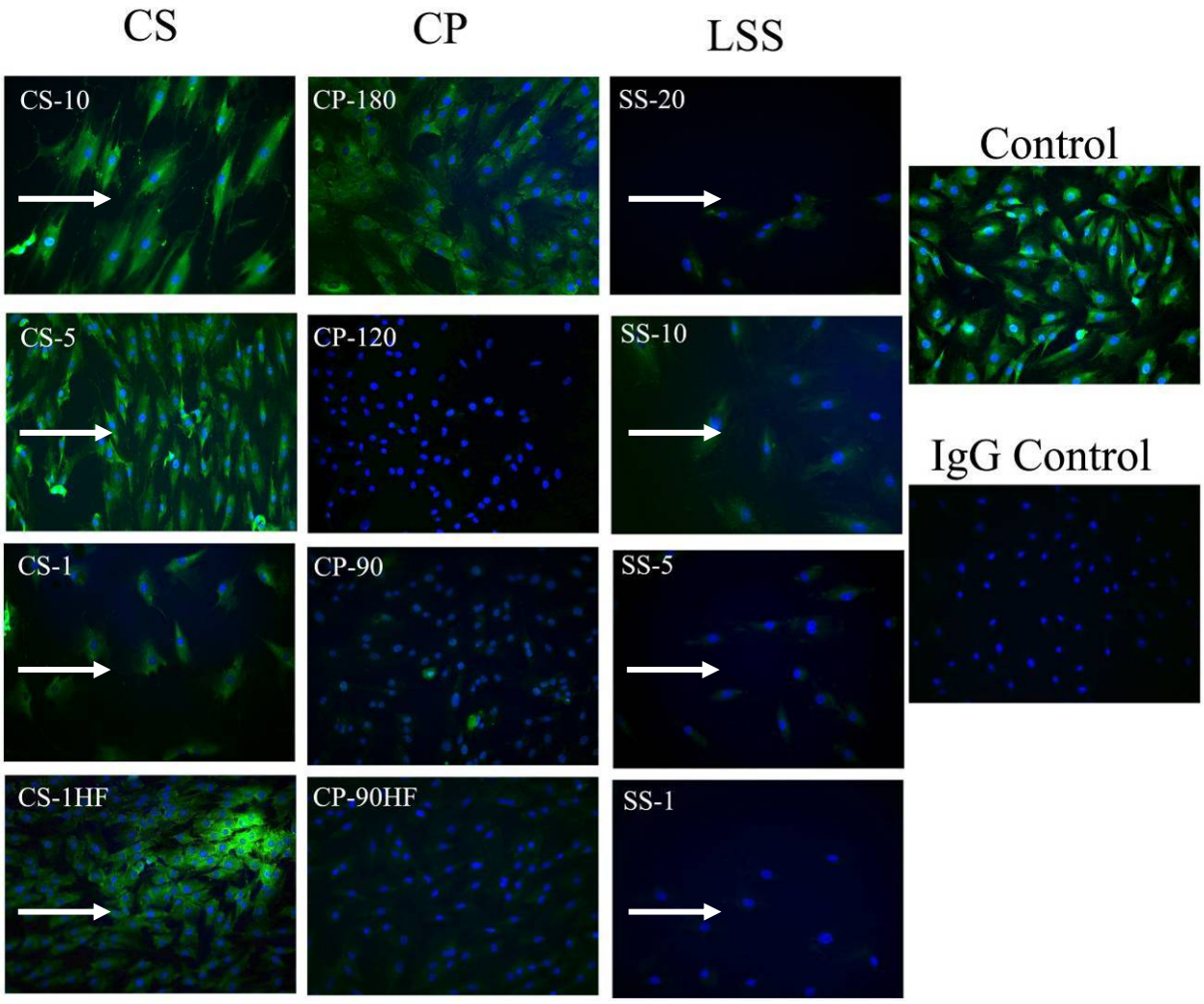

Figure 3.19: Representative immunohistochemistry images for flk-1. Arrows indicate the direction of applied stimulation, if applicable. All images taken at 200x.

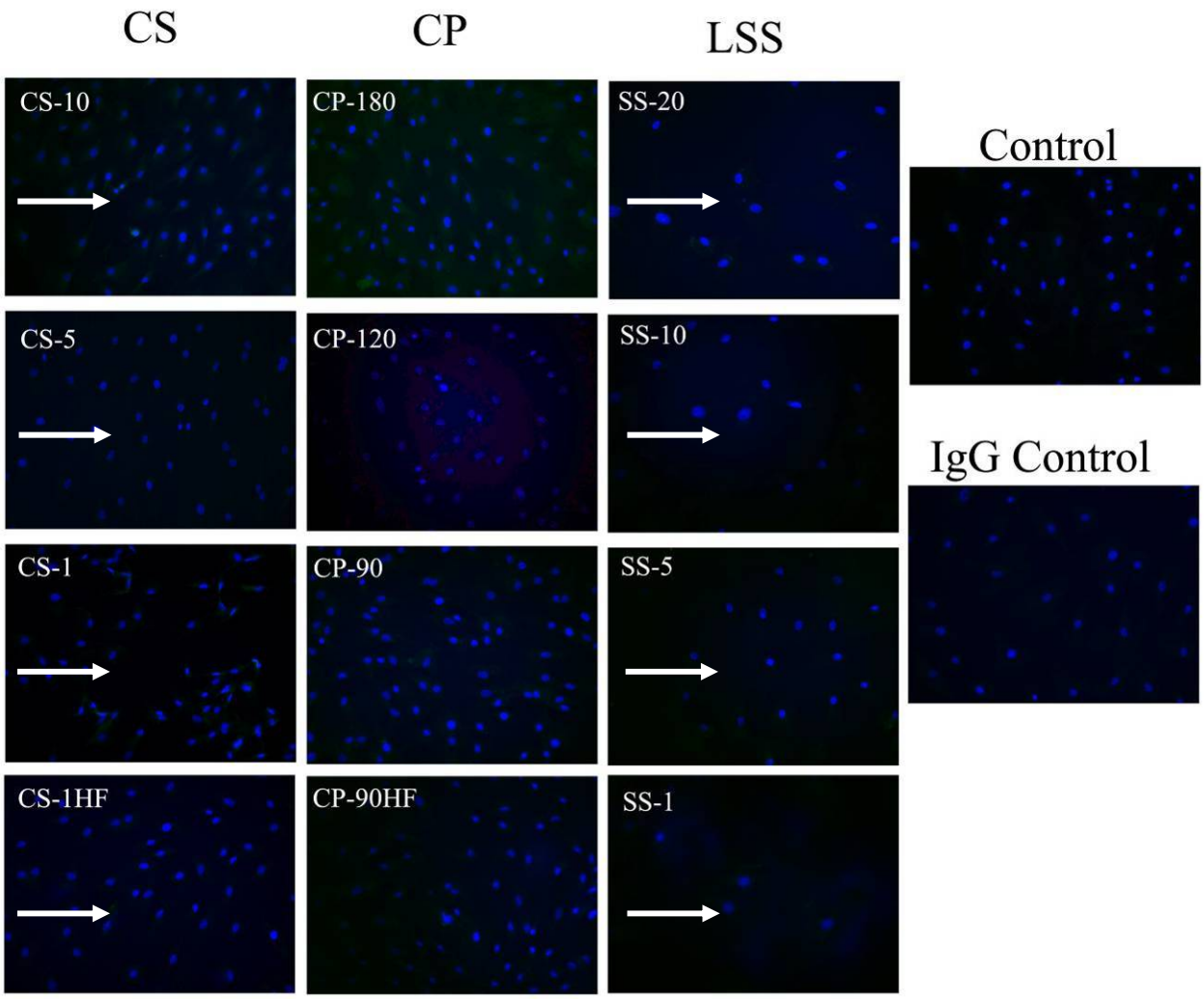

Figure 3.20: Representative immunohistochemistry images for PECAM. Arrows indicate the direction of applied stimulation, if applicable. All images taken at 200x.

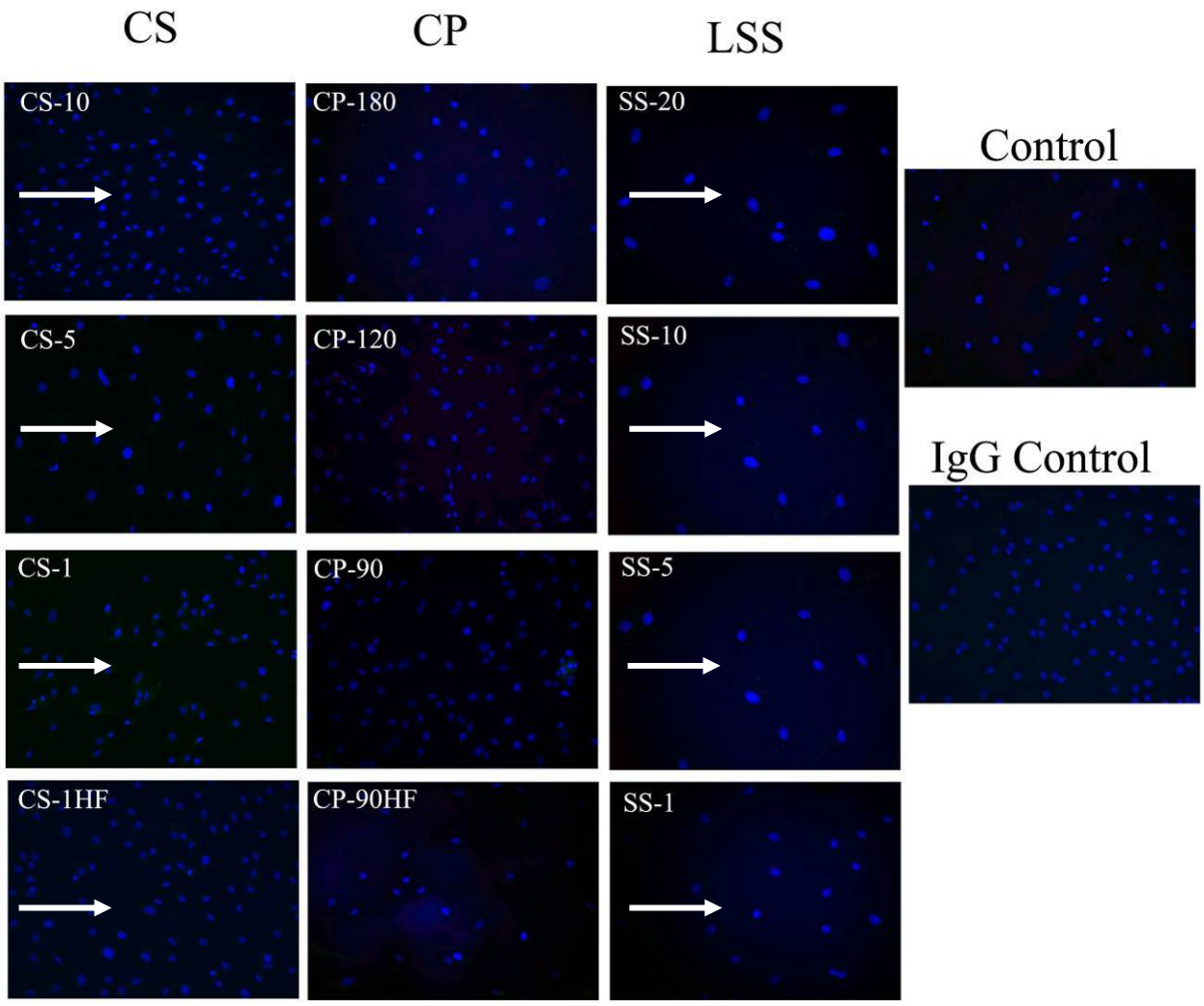

Figure 3.21: Representative immunohistochemistry images for vWF. Arrows indicate the direction of applied stimulation, if applicable. All images taken at 200x.

3.3.6 Gene expression

All gene targets (see **Table 3.4**) analyzed in the RT-negative experiments failed to produce sufficient signal to determine a C_T value, demonstrating that no genomic amplification occurred. The amplification plot for an RT-negative sample, shown in **Figure 3.22A**, is contrasted with a normal RT-PCR run, shown in **Figure 3.22B.**

For all PCR endpoints, the results are presented as the average fold-change from control values ± standard deviation (SD) with associated sample numbers achieving a positive interrogation. Samples failing to register any detectable transcripts were not used to tabulate the average gene expression for that endpoint. Because the sample numbers reaching positive interrogation were relatively low for many of the genes in question (limiting our ability to perform statistical analysis), results with potential biological significance (i.e., greater than ± 1.3 fold changes in gene expression) are highlighted in green and red to indicate potential up- and down-regulation, respectively. This value has previously been used in the literature as a guide for further investigation when analysis is limited by sample size [643, 644]. Genes were grouped according to their classifications found in **Table 3.4** to help detect trends in related endpoints.

A)

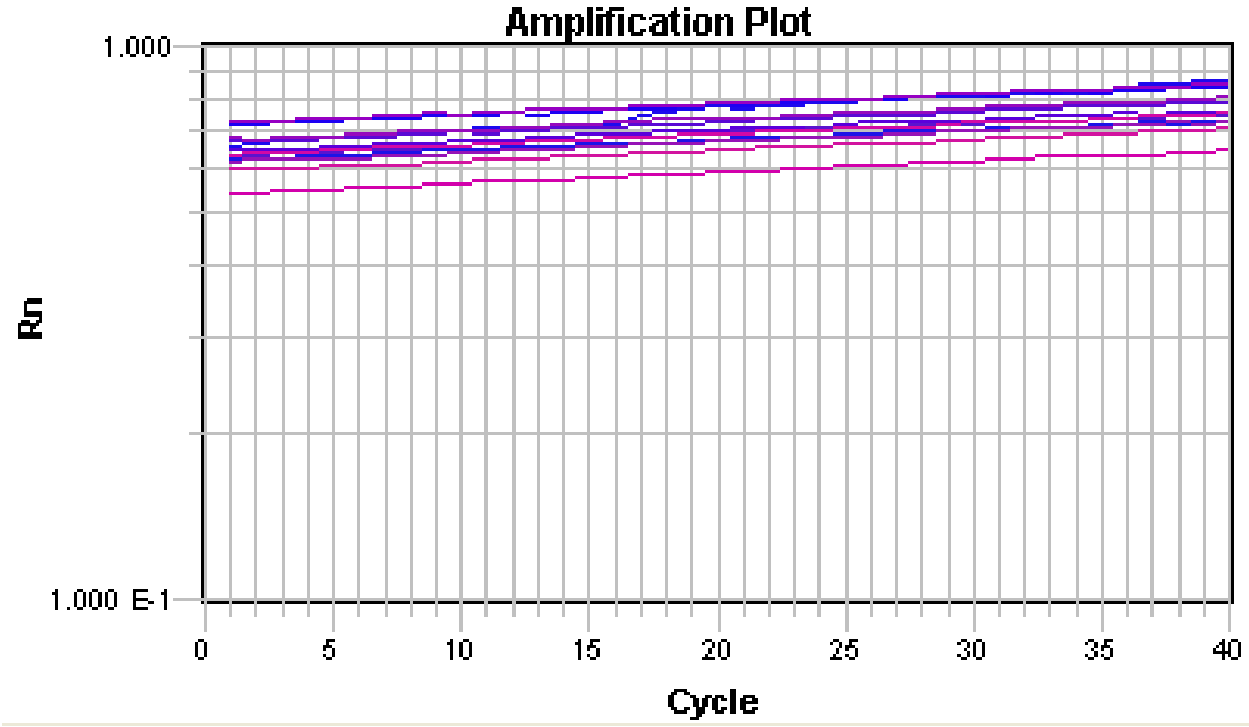

B)

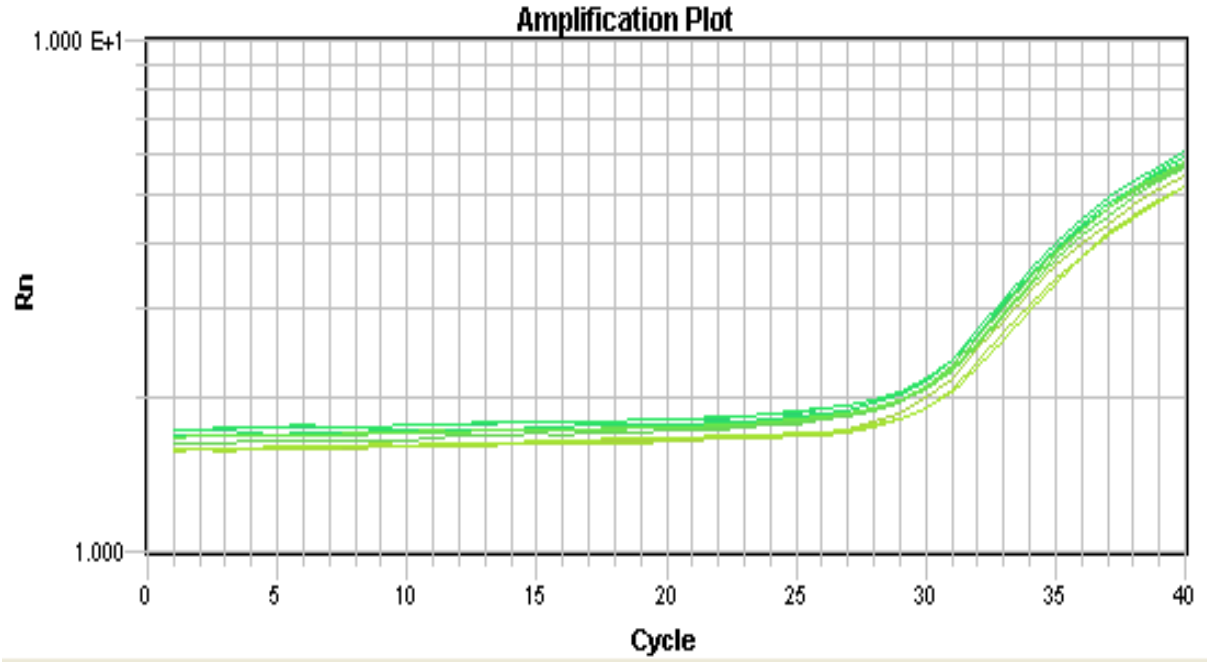

Figure 3.22: RT-PCR reaction products curves. (A) Osteocalcin reaction products for RT-negative samples do not show an exponential increase, demonstrating no genomic amplification. (B) Osteocalcin reaction products for experimental samples show the appropriate exponential increase indicating proper amplification.

3.3.6.1 Muscle-related genes

The average RQ values ± SD for muscle-related genes are depicted in **Table 3.5**. Although relatively few endpoints reached biological and statistical significance because of a failure to interrogate, enough samples were detected at greater than ± 1.3 fold changes in gene expression to postulate that some effect is being produced by mechanical stimulation. SMC genes, which include caldesmon, calponin, and SM22α, tended to be upregulated by mechanical stimulation in general, regardless of type, magnitude or frequency. However, for caldesmon expression, CS did not appear to have the same effect as CP and LSS, failing to create much of any change in gene expression over the range of magnitudes and frequencies tested. Other muscle-related genes more specific to cardiac muscle (cardiac troponin) tended to be strongly downregulated by LSS ($p<0.05$ for all magnitudes), and were highly variable under CS and CP. Desmin, another muscle-related gene more often associated with skeletal muscle, also was highly variable but on average tended to be upregulated by mechanical stimulation, regardless of the type, magnitude, frequency.

Table 3.5: Fold changes in muscle-related gene expression relative to control for each component of the Mechanical Panel as analyzed by the low density qPCR. Green and red highlights indicate an average fold change greater than 1.3 or less than 0.7 (considered biologically relevant), respectively. Data are presented as the mean ± SD with sample numbers. + p<0.10, *p<0.05, and ND=No detectable transcripts.

	Muscle		
Stimulus	**Caldesmon**	**Calponin**	**Cardiac Troponin**
CP-90HF	1.41 +/- 0.78, n=4	0.96 +/- 0.57, n=4	7.89 +/- 14.13, n=4
CP-90	1.14 +/- 0.31, n=3	2.93 +/- 2.45, n=2	0.32 +/- 0.32, n=2
CP-120	**1.71 +/- 0.4, n=3 +**	1.62 +/- 0.55, n=3	4.8 +/- 6.57, n=3
CP-180	1.59 +/- 0.85, n=4	0.74 +/- 0.66, n=4	1.18 +/- 1.06, n=3
CS-1HF	1.21 +/- 0.39, n=4	2.17 +/- 1.27, n=4	3.78 +/- 5.3, n=4
CS-1	1.11 +/- 0.32, n=5	9.03 +/- 9.68, n=2	1.68 +/- 2.04, n=5
CS-5	1.09 +/- 0.26, n=4	2.34 +/- 1.18, n=4	6.31 +/- 11.42, n=4
CS-10	0.8 +/- 0.29, n=3	1.28 +/- 0.73, n=3	0.3 +/- 0.22, n=2
LSS-1	**1.39 +/- 0.13, n=4 ***	**3.93 +/- 1.72, n=4 ***	**0.06 +/- 0.09, n=3 ***
LSS-5	0.81 +/- 0.45, n=3	0.93 +/- 0.73, n=3	**0.01 +/- 0.01, n=2 ***
LSS-10	1.85 +/- 0.87, n=4	2.38 +/- 2.39, n=4	**0.07 +/- 0.1, n=3 ***
LSS-20	1.2 +/- 0.23, n=5	16.6 +/- 23.44, n=2	**0.19 +/- 0.16, n=4 ***

	Muscle	
Stimulus	**Desmin**	**SM22α**
CP-90HF	4.18 +/- 6.77, n=4	1.62 +/- 0.84, n=4
CP-90	0.2 +/- 0, n=1	0.92 +/- 0.36, n=3
CP-120	1.18 +/- 0.58, n=2	**1.96 +/- 0.06, n=3 ***
CP-180	1.9 +/- 1.1, n=3	1.91 +/- 0.93, n=4
CS-1HF	4.21 +/- 6.26, n=4	1.88 +/- 1.07, n=4
CS-1	1.43 +/- 0.94, n=3	1.05 +/- 0.16, n=5
CS-5	2.75 +/- 1.68, n=3	**2.08 +/- 0.74, n=4 +**
CS-10	9.6 +/- 14.02, n=3	1.17 +/- 0.46, n=3
LSS-1	4.48 +/- 6.7, n=4	**5.95 +/- 0.96, n=4 ***
LSS-5	**0.37 +/- 0.04, n=2 ***	**2.29 +/- 0.7, n=3 +**
LSS-10	1.54 +/- 0.56, n=3	**6.49 +/- 2.85, n=4 ***
LSS-20	3.29 +/- 5.31, n=4	**2.92 +/- 1.95, n=5 +**

3.3.6.2 Endothelial-related genes

The average RQ values ± SD for endothelial-related genes are depicted in **Table 3.6**. Like the muscle-related genes, most endothelial-related genes failed to show any statistically significant changes from control levels. LSS had the most profound affect, statistically downregulating most of the interrogated endothelial-related genes, particularly flk-1 and vWF. vWF was significantly downregulated for LSS-1 ($p<0.10$) and LSS-5 ($p<0.05$), but LSS-10 and LSS-20 showed no change in the expression of vWF. CP tended to increase several of the endothelial related-genes including endoglin, CD133 and vWF, although none were statistically significant. The effect of CP on flk-1 appears to have a threshold around CP-120, with steady to increased expression at CP-120 and CP-180, respectively, but undetectable expression and downregulated expression at CP-90 and CP-90HF. Conversely, CS demonstrated some ability to increase the expression of flk-1, which the exception at CS-10, which may downregulate flk-1 expression. Looking across CS-10, it would appear that this high level of stretch strongly inhibited any endothelial gene expression, with downregulation or non-detection at all other endothelial-genes. iNOS failed to show detectable expression in most samples.

Table 3.6: Fold changes in endothelial-related gene expression relative to control for each component of the Mechanical Panel as analyzed by the low density qPCR. Green and red highlights indicate an average fold change greater than 1.3 or less than 0.7 (considered biologically relevant), respectively. Data are presented as the mean ± SD with sample numbers. + $p<0.10$, *$p<0.05$, compared to controls, and ND=No detectable transcripts.

	Endothelial		
Stimulus	**CD133**	**Endoglin**	**ESAM**
CP-90HF	18.08 +/- 21.79, n=2	1.45 +/- 0.61, n=3	0.07 +/- 0, n=1
CP-90	2.16 +/- 0, n=1	18.09 +/- 19.08, n=3	ND
CP-120	40.88 +/- 0, n=1	20.91 +/- 28.13, n=3	ND
CP-180	137.47 +/- 0, n=1	1.68 +/- 1.25, n=4	0.04 +/- 0, n=1
CS-1HF	2.92 +/- 0, n=1	7.16 +/- 13.52, n=4	18.02 +/- 20.43, n=3
CS-1	1.51 +/- 0.52, n=3	**0.85 +/- 0.05, n=3 ***	ND
CS-5	ND	0.72 +/- 0.6, n=4	15.34 +/- 0, n=1
CS-10	ND	**0.17 +/- 0, n=2 ***	ND
LSS-1	0.06 +/- 0, n=1	0.54 +/- 0.28, n=3	7.75 +/- 8.28, n=3
LSS-5	ND	5.26 +/- 9.11, n=3	ND
LSS-10	48.28 +/- 0, n=1	0.58 +/- 0.69, n=4	7.83 +/- 11.04, n=2
LSS-20	**0.12 +/- 0.03, n=3 ***	**0.15 +/- 0.15, n=3 ***	ND

	Endothelial		
Stimulus	**iNOS**	**Flk-1**	**vWF**
CP-90HF	ND	0.46 +/- 0.76, n=3	1.48 +/- 0.93, n=4
CP-90	0.05 +/- 0, n=1	0.21 +/- 0, n=1	1.23 +/- 0.43, n=3
CP-120	ND	1.03 +/- 1.43, n=2	1.57 +/- 0.57, n=3
CP-180	ND	2.91 +/- 3.02, n=3	1.73 +/- 1.04, n=4
CS-1HF	ND	1.78 +/- 1.62, n=3	1.13 +/- 0.41, n=4
CS-1	0.56 +/- 0.55, n=2	11.31 +/- 19.08, n=4	1.2 +/- 0.41, n=5
CS-5	ND	10.46 +/- 18.35, n=4	0.86 +/- 0.14, n=4
CS-10	ND	0.45 +/- 0.19, n=2	0.59 +/- 0.26, n=3
LSS-1	ND	**0.02 +/- 0.03, n=3 ***	**0.62 +/- 0.32, n=4 +**
LSS-5	ND	**0.01 +/- 0, n=2 ***	**0.39 +/- 0.11, n=3 ***
LSS-10	ND	**0.06 +/- 0.09, n=3 ***	0.95 +/- 0.53, n=4
LSS-20	0.75 +/- 0.81, n=2	**0.11 +/- 0.13, n=3 ***	0.89 +/- 0.5, n=5

3.3.6.3 Soluble factor- and apoptosis-related gene expression

The average RQ values ± SD for soluble factor and apoptosis-related genes are depicted in **Table 3.7**. The most striking trend was the general increase in expression for FGF2 and TGF-β exposed to LSS, much of it with some statistical significance. FGF-2 was also generally increased by CS, although none to any statistical levels. VEGF-A expression was seemingly unaffected by mechanical stimulation, maintaining near-baseline levels for almost all conditions except LSS-20, which was significantly increased ($p<0.05$) and LSS-5, which was significantly decreased ($p<0.05$). On average, soluble factor expression was increased for all three for the higher magnitudes of LSS.

Gene expression for Bcl-2 (anti-apoptotic) and caspase 3 (pro-apoptotic) did not appear to definitively show any propensity for or against apoptosis. In general, both genes followed each other in terms of up- or down-regulation. TNFα did not demonstrate any detectable expression for any condition.

Table 3.7: Fold changes in soluble factor and apoptosis-related gene expression relative to control for each component of the Mechanical Panel as analyzed by the low density qPCR. Green and red highlights indicate an average fold change greater than 1.3 or less than 0.7 (considered biologically relevant), respectively. Data are presented as the mean ± SD with sample numbers. + $p<0.10$, *$p<0.05$ compared to controls, and ND=No detectable transcripts.

	Soluble Factor		
Stimulus	**FGF2**	**TGF-β**	**VEGF-A**
CP-90HF	0.85 +/- 0.48, n=4	1.09 +/- 0.37, n=4	0.89 +/- 0.37, n=4
CP-90	0.8 +/- 0.48, n=3	1.09 +/- 0.37, n=3	0.81 +/- 0.15, n=3
CP-120	1.28 +/- 0.57, n=3	1.45 +/- 0.54, n=3	1.04 +/- 0.42, n=3
CP-180	1.57 +/- 1.79, n=4	1.74 +/- 1.17, n=4	1.41 +/- 1.27, n=4
CS-1HF	1.53 +/- 0.79, n=4	1.32 +/- 0.53, n=4	1.17 +/- 0.37, n=4
CS-1	0.89 +/- 0.13, n=5	0.98 +/- 0.19, n=5	1.07 +/- 0.13, n=5
CS-5	1.38 +/- 0.63, n=4	1.2 +/- 0.4, n=4	0.89 +/- 0.3, n=4
CS-10	1.31 +/- 0.72, n=3	0.83 +/- 0.35, n=3	0.73 +/- 0.27, n=3
LSS-1	**4.06 +/- 0.68, n=4 ***	**2.46 +/- 0.5, n=4 ***	1.18 +/- 0.31, n=4
LSS-5	1.84 +/- 1.02, n=3	1.62 +/- 0.84, n=3	**0.64 +/- 0.12, n=3 ***
LSS-10	**6.51 +/- 3.8, n=4 +**	**4.69 +/- 2.26, n=4 ***	1.92 +/- 1.2, n=4
LSS-20	**4.38 +/- 0.91, n=5 ***	**3.56 +/- 0.69, n=5 ***	**1.9 +/- 0.63, n=5 ***

	Apoptosis		
Stimulus	**Bcl2**	**Caspase 3**	**TNF-α**
CP-90HF	6.9 +/- 6.27, n=4	1.21 +/- 0.76, n=4	ND
CP-90	ND	1.14 +/- 0.18, n=2	ND
CP-120	4.34 +/- 4.47, n=3	1.33 +/- 0.48, n=3	ND
CP-180	1.39 +/- 1.15, n=4	1.55 +/- 0.92, n=4	ND
CS-1HF	2.18 +/- 1.67, n=3	1.25 +/- 0.28, n=4	ND
CS-1	10.87 +/- 0, n=1	1.34 +/- 0.28, n=2	ND
CS-5	1.1 +/- 0.8, n=4	0.99 +/- 0.25, n=4	ND
CS-10	6.56 +/- 10.6, n=3	0.76 +/- 0.36, n=3	ND
LSS-1	3.38 +/- 3.28, n=3	1.4 +/- 0.56, n=4	ND
LSS-5	**0.53 +/- 0.08, n=2 +**	0.79 +/- 0.42, n=3	ND
LSS-10	0.75 +/- 0.53, n=4	1.97 +/- 0.99, n=4	ND
LSS-20	ND	1.75 +/- 0.55, n=2	ND

3.3.6.4 Extracellular matrix-related gene expression

The average RQ values ± SD for matrix-related genes are depicted in **Table 3.8**. The most striking effects on matrix gene expression came from LSS, which had some statistical significance to upregulating collagen I, while downregulating elastin gene expression. Other

potentially strong changes occurred under CP, which seems to upregulate collagen I and III as well as elastin gene expression. CS did not seem to affect matrix gene expression except for increasing elastin gene expression at CS-1 and CS-5 before downregulating it at CS-10. Collagen IV gene expression was inconsistent, often failing to detect any transcripts.

Table 3.8: Fold changes in extracellular matrix-related gene expression relative to control for each component of the Mechanical Panel as analyzed by the low density qPCR. Green and red highlights indicate an average fold change greater than 1.3 or less than 0.7 (considered biologically relevant), respectively. Data are presented as the mean ± SD with sample numbers. + $p<0.10$, *$p<0.05$, compared to controls, and ND=No detectable transcripts.

	Matrix			
Stimulus	**Collagen I**	**Collagen III**	**Collagen IV**	**Elastin**
CP-90HF	1.38 +/- 0.66, n=4	1.76 +/- 1.01, n=4	14.84 +/- 0, n=1	5.4 +/- 6.21, n=4
CP-90	1.11 +/- 0.42, n=3	**1.37 +/- 0.18, n=3 +**	0.03 +/- 0, n=1	11.88 +/- 14.7, n=3
CP-120	**1.51 +/- 0.27, n=3 +**	2.53 +/- 1.61, n=3	0.04 +/- 0, n=1	**3.79 +/- 0.95, n=3 ***
CP-180	1.58 +/- 0.8, n=4	**2.29 +/- 0.91, n=4 +**	0.15 +/- 0, n=1	**4.56 +/- 2.36, n=4 +**
CS-1HF	1.32 +/- 0.44, n=4	1.07 +/- 0.37, n=4	ND	1.05 +/- 0.97, n=4
CS-1	1.12 +/- 0.35, n=5	1.04 +/- 0.11, n=5	2.6 +/- 1.19, n=3	3.11 +/- 4.39, n=5
CS-5	1.26 +/- 0.27, n=4	1.07 +/- 0.2, n=4	1.01 +/- 0, n=1	1.56 +/- 1.22, n=4
CS-10	0.74 +/- 0.34, n=3	0.76 +/- 0.41, n=3	1.24 +/- 0, n=1	0.33 +/- 0.41, n=3
LSS-1	2.95 +/- 1.94, n=4	1.18 +/- 0.58, n=4	ND	0.73 +/- 0.85, n=4
LSS-5	**2.41 +/- 0.63, n=3 +**	0.94 +/- 0.67, n=3	0.04 +/- 0, n=1	**0.18 +/- 0.17, n=3 ***
LSS-10	**4 +/- 2.06, n=4 +**	**1.38 +/- 0.06, n=4 ***	0.1 +/- 0, n=1	0.53 +/- 0.52, n=4
LSS-20	**6.49 +/- 3.04, n=5 ***	1.21 +/- 0.39, n=5	**0.24 +/- 0.35, n=3 +**	**0.23 +/- 0.21, n=4 ***

3.3.6.5 Stem-cell related gene expression

The average RQ values ± SD for stem cell-related genes are depicted in **Table 3.9**. CD59 and CD90, which are reported to be expressed in tBMMSCs were most affected by LSS, which significantly downregulated CD90, and showed some moderate increases in CD59. CP tended to behave in an almost opposing fashion, with borderline downregulation of CD59, and some upregulation of CD90, although none were statistically significant. Vimentin expression was

relatively unchanged with some increases under higher CP (CP-120 and CP-180) and some decreases under CS-10 and LSS-5. However, no particular patterns seemed to develop.

Table 3.9: Fold changes in stem cell-related gene expression relative to control for each component of the Mechanical Panel as analyzed by the low density qPCR. Green and red highlights indicate an average fold change greater than 1.3 or less than 0.7 (considered biologically relevant), respectively. Data are presented as the mean ± SD with sample numbers. + p<0.10, *p<0.05, compared to controls.

	Stem Cell		
Stimulus	**CD59**	**CD90**	**Vimentin**
CP-90HF	0.76 +/- 0.3, n=4	1.28 +/- 0.74, n=4	1.08 +/- 0.52, n=4
CP-90	**0.51 +/- 0.25, n=3 +**	1 +/- 0.2, n=3	0.84 +/- 0.34, n=3
CP-120	0.76 +/- 0.47, n=3	1.39 +/- 0.29, n=3	1.26 +/- 0.41, n=3
CP-180	1.03 +/- 0.48, n=4	1.51 +/- 0.77, n=4	1.62 +/- 0.97, n=4
CS-1HF	1.71 +/- 1.02, n=4	1.22 +/- 0.43, n=4	1.12 +/- 0.25, n=4
CS-1	0.91 +/- 0.17, n=5	1.11 +/- 0.13, n=5	1.13 +/- 0.22, n=5
CS-5	1.77 +/- 0.67, n=4	0.98 +/- 0.07, n=4	1.03 +/- 0.21, n=4
CS-10	0.98 +/- 0.27, n=3	**0.56 +/- 0.24, n=3 +**	0.62 +/- 0.27, n=3
LSS-1	**3.45 +/- 1.55, n=4 +**	**0.37 +/- 0.18, n=4 ***	0.94 +/- 0.2, n=4
LSS-5	0.83 +/- 0.27, n=3	**0.19 +/- 0.08, n=3 ***	**0.47 +/- 0.16, n=3 ***
LSS-10	4.99 +/- 4.73, n=4	**0.46 +/- 0.17, n=4 ***	1.27 +/- 0.65, n=4
LSS-20	**1.94 +/- 1.12, n=5**	**0.33 +/- 0.05, n=5 ***	0.95 +/- 0.1, n=5

3.3.6.6 Osteoblast-related gene expression

The average RQ values ± SD for osteoblast-related genes are depicted in **Table 3.10**. The most consistent result from this gene subset was either non-expression or downregulation, especially with respect to Runx2 and osteocalcin. Alkaline phosphatase expression was inconsistent, and BMP2 expression was relatively unchanged.

Table 3.10: Fold changes in osteoblast-related gene expression relative to control for each component of the Mechanical Panel as analyzed by the low density qPCR. Green and red highlights indicate an average fold change greater than 1.3 or less than 0.7 (considered biologically relevant), respectively. Data are presented as the mean ± SD with sample numbers. + $p<0.10$, *$p<0.05$ compared to controls, and ND=No detectable transcripts.

	Osteoblast			
Stimulus	**Alkaline Phosphatase**	**BMP2**	**Osteocalcin**	**Runx2**
CP-90HF	19.93 +/- 22.47, n=3	0.83 +/- 0.58, n=4	0.36 +/- 0.48, n=2	ND
CP-90	0.92 +/- 0, n=1	**0.52 +/- 0.25, n=3 +**	0.85 +/- 0, n=1	ND
CP-120	ND	0.94 +/- 0.39, n=3	35.69 +/- 50.39, n=2	ND
CP-180	25.96 +/- 0, n=1	1.44 +/- 1.23, n=4	0.83 +/- 0, n=1	0.02 +/- 0, n=1
CS-1HF	0.02 +/- 0, n=1	1.31 +/- 0.43, n=4	0.89 +/- 0.41, n=2	ND
CS-1	1.19 +/- 0.41, n=3	1.13 +/- 0.55, n=5	0.81 +/- 0.24, n=3	ND
CS-5	23.57 +/- 9.89, n=2	1.26 +/- 0.46, n=4	0.52 +/- 0.68, n=2	0.02 +/- 0, n=1
CS-10	ND	0.98 +/- 0.47, n=3	ND	ND
LSS-1	31.59 +/- 31.4, n=3	0.75 +/- 0.23, n=4	**0.03 +/- 0.02, n=2 ***	ND
LSS-5	25.52 +/- 0, n=1	**0.4 +/- 0.03, n=3 ***	ND	ND
LSS-10	16.68 +/- 0, n=1	1.96 +/- 1.34, n=4	0 +/- 0, n=1	0.01 +/- 0, n=1
LSS-20	2.4 +/- 1.2, n=3	**1.87 +/- 0.54, n=5 ***	0.64 +/- 0.41, n=3	ND

3.3.6.7 Chondrocyte- and adipocyte-related gene expression

The average RQ values ± SD for chondrocyte- and adipocyte-related genes are depicted in **Table 3.11**. With respect to chondrocyte-related genes, only aggrecan demonstrated consistently detectable expression. Aggrecan expression was strongly downregulated with statistical power for LSS-5, LSS-10, and LSS-20. Conversely, CS-1HF, CS-1, and CS-5 and CP in general tended to upregulate aggrecan expression. Collagen II expression was detected only occasionally under LSS. However, when it was detected, it was strongly upregulated, usually greater than 20-fold. With respect to adipocyte-related gene expression, PPAR-γ expression was strongly downregulated by LSS, and only moderately increased under CP.

Table 3.11: Fold changes in chondrocyte and adipocyte-related gene expression relative to control for each component of the Mechanical Panel as analyzed by the low density qPCR. Green and red highlights indicate an average fold change greater than 1.3 or less than 0.7 (considered biologically relevant), respectively. Data are presented as the mean ± SD with sample numbers. + $p<0.10$, *$p<0.05$ compared to controls, and ND=No detectable transcripts.

	Chondrocyte		Adipocyte
Stimulus	**Aggrecan**	**Collagen II**	**PPAR-γ**
CP-90HF	3.53 +/- 5.39, n=4	ND	1.23 +/- 0.59, n=4
CP-90	1 +/- 0.64, n=3	17.77 +/- 0, n=1	0.9 +/- 0.29, n=3
CP-120	1.4 +/- 0.62, n=3	ND	**1.48 +/- 0.26, n=3 +**
CP-180	1.22 +/- 0.24, n=4	ND	1.54 +/- 0.94, n=4
CS-1HF	1.7 +/- 0.69, n=4	ND	0.97 +/- 0.4, n=4
CS-1	1.18 +/- 0.39, n=5	ND	1.03 +/- 0.14, n=5
CS-5	**1.55 +/- 0.36, n=4 +**	ND	0.98 +/- 0.24, n=4
CS-10	0.81 +/- 0.31, n=3	ND	**0.72 +/- 0.16, n=3 +**
LSS-1	0.98 +/- 0.33, n=4	34.94 +/- 24.13, n=3	**0.18 +/- 0.01, n=4 ***
LSS-5	**0.38 +/- 0.29, n=3 +**	ND	**0.1 +/- 0.04, n=3 ***
LSS-10	**0.56 +/- 0.2, n=4 ***	22.07 +/- 0, n=1	**0.18 +/- 0.06, n=4 ***
LSS-20	**0.33 +/- 0.09, n=5 ***	194.33 +/- 0, n=1	**0.17 +/- 0.04, n=5 ***

3.4 DISCUSSION

3.4.1 Differential morphology and proliferation changes

The use of our novel Mechanical Panel experimental design allowed for the differential analysis of how mechanical stimulation impacts stem cell morphology, growth, and differentiation. Our morphology and proliferation results, summarized in **Table 3.12**, demonstrate that after 5 days of mechanical stimulation – including cyclic stretch, cyclic hydrostatic pressure, and laminar shear stress – we detected significant changes in the morphology, alignment, and proliferation of tBMMSCs. In many cases, these changes were dependent upon the type, magnitude, and frequency of stimulation as evidenced by statistically significant correlation coefficients.

Table 3.12: Summary of the morphology and proliferation results for the 5 day Mechanical Panel experiments. Double arrows indicate a significant increase or decrease ($p<0.05$) in the measured parameter from control values. Single arrows denote a moderate ($p<0.10$) change in the measured parameter. $\perp$ and $\|$ indicate significant perpendicular and parallel alignment ($p<0.05$), respectively.

Stimulus	Area	Length	Shape Index	Tortuosity Index	Alignment	Proliferation
CP-90HF	↓↓	↓↓	↑↑	↓↓	-	↑
CP-90	↓↓	↓↓	↑↑	↓↓	-	↑↑
CP-120	↓↓	↓↓	↑↑	↓↓	-	↑↑
CP-180	↓↓	↓↓	↑↑	↓↓	-	↑↑
CS-1HF	-	↑↑	-	-	-	-
CS-1	↓↓	↓↓	↑↑	↓↓	-	↑↑
CS-5	-	↑↑	↓↓	-	$\perp$	-
CS-10	-	-	↓↓	-	$\perp$	-
LSS-1	↑↑	↑↑	-	-	-	-
LSS-5	↑↑	↑↑	-	-	-	↓↓
LSS-10	↑↑	↑↑	↓	↑↑	$\|$	↓↓
LSS-20	↑↑	↑↑	↓↓	↑↑	$\|$	↓↓

Overall, our results demonstrate that cyclic pressure leads to a significantly smaller, and more rounded cell with fewer pseudopods (as measured by the tortuosity index). Previous reports on ECs under pressure have demonstrated an increase in tortuosity concurrent with cellular elongation [396]. It is unclear, however, whether BMMSCs should behave in manner similar to aortic ECs. Cyclic pressure not only affected BMMSC size and shape, but it also caused a dramatic increase in proliferation that had statistically significant negative correlation ($\rho= -0.483$, $p<0.05$) to the magnitude of stimulation. This increase in proliferation as a result of cyclic pressure has been demonstrated in other cell types including SMCs [225, 228, 645] and ECs [386, 646] as well as in Dexter cultured BMMSCS [1].

Cyclic stretch had varying effects on tBMMSCs depending upon the magnitude and frequency of stimulation. Higher frequency stretching at low magnitude (CS-1HF) caused the cells to behave more similarly to the higher magnitudes of stimulation at 1 Hz. However, low

magnitude 1 Hz (CS-1) stimulation caused the cells to behave similar to the tBMMSCs exposed to cyclic pressure, leading to a smaller, more rounded morphology, and increased proliferation. The higher magnitudes of cyclic stretch (5% and 10% stretch) caused a more elongated, spindle shaped cell and resulted in a perpendicular alignment to the direction of stretch. These changes are in agreement with previously published data in other stem cells [526, 647]. The changes in alignment are characteristic of stress-shielding and occur in any cell type that is free to move in two dimensions [199, 527, 647, 648]. Unlike previously published research [526], CS did not seem to have a negative impact on proliferation despite the increase in staining for SMC-related proteins. This observation contradicts earlier theories of mutually exclusive proliferation and differentiation. One potential reason for this may have been the high serum content (20% FBS) used for the culture of these cells which was maintained throughout the Mechanical Panel experiments. We maintained the same serum content during the experiments to prevent any changes in cell behavior as a result of chemical changes not associated with mechanical stimulation.

Laminar shear stress induced a dramatic increase in cell size that diminished slightly with increasing shear stress. Cellular alignment and elongation began to occur at 10 dynes/cm^2. In addition, increasing shear stress was associated with a decrease in cell number. It is uncertain whether this decrease in cell number was related to an inhibition of proliferation, or positive selection of non-proliferating cells caused by washing away cells attempting to divide. We do have some evidence (**Appendix F**) based upon preliminary Ki67 staining that shows a diminished proliferation index following exposure to LSS-5, which supports either a global inhibition of proliferation or the positive selection of non-proliferating cells. There is also evidence in the literature that supports a decrease in proliferation by shear stresses greater than 5

dynes/cm^2 in mature ECs [193, 405, 649]. Perhaps this is a conserved mechanism regardless of cell phenotype.

When looking at the overall trends in the morphology and proliferation data, a pattern begins to appear. Based upon our data, there appears to be a correlation between cell size and shape, and proliferation. This is most apparent when comparing the cyclic pressure and CS-1 samples with the shear stress samples. The larger, more elongated cells tend to proliferate much less than the smaller, more rounded cells. This is confirmed by correlation testing that shows a strong, positive correlation for shape and proliferation (ρ=0.729, $p<0.001$) and a weaker, negative correlation between area and proliferation (ρ= -0.435, $p<0.001$). This positive correlation between shape and proliferation indicates that as shape index increases (i.e., the cells become more rounded), proliferation increases. Likewise, as the cells size (area) increases, proliferation tends to decrease, albeit in a weaker fashion. Additionally, shape index has a weak negative correlation (ρ= -0.367, $p<0.001$) with area, meaning that as the cell shape index increases (becomes more rounded), the area tends to decrease. A linear regression model (**Table 3.13**) of proliferation with area and shape index (SI) as independent variables is given by:

$$Density\,(cells/cm^2) = -1.13\left(\frac{cells/cm^2}{\mu m^2}\right)Area + 9.03x10^4\left(cells/cm^2\right)SI - 6.94x10^3\left(cells/cm^2\right) \quad \textbf{(3.15)}$$

and had an R^2 of 0.665 (p=0.00), which indicates that area and shape index can account for more than 66% of the variance in the data (**Figure 3.23**).

Table 3.13: Linear regression output from SPSS for proliferation regressed against area and shape index. Despite the weak correlation between shape index and area, they do not exhibit colinearity, and are therefore suitably compatible in the linear regression model.

Coefficients[a]

	Unstandardized Coefficients		Standardized Coefficients			Collinearity Statistics	
	B	Std. Error	Beta	t	Sig.	Tolerance	VIF
(Constant)	-6.94E+003	3.56E+003		-1.952	.055		
Area	-1.13E+000	1.89E-001	-.417	-5.977	.000	.894	1.119
Shape	9.03E+004	1.09E+004	.578	8.296	.000	.894	1.119

a. Dependent Variable: Cell Density

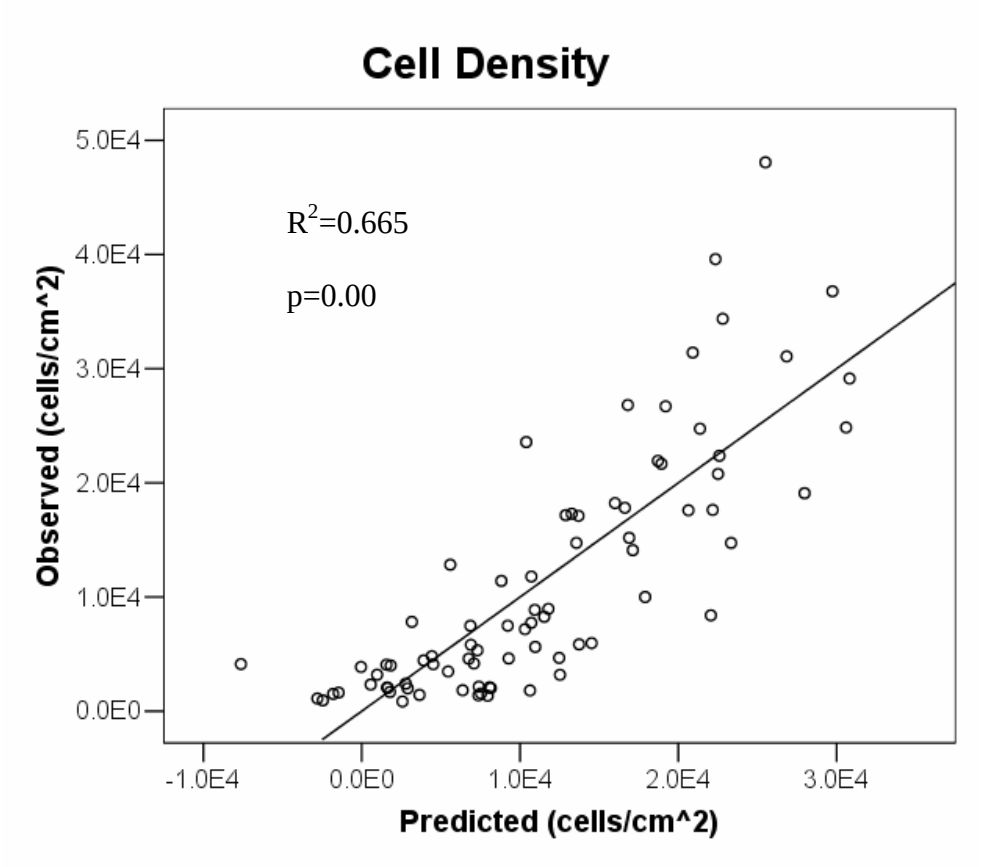

Figure 3.23: Non-normalized regression model fit for cell density with cellular area and shape index as independent variables. Observed values for cell density (cell/cm^2) are plotted against values predicted by the model in **Equation (3.15).**

3.4.2 Differential protein expression

One of the main objectives of the work presented in this chapter was to determine what role, if any, each of the three mechanical stimuli that comprise the Mechanical Panel have on the differentiation of stem cells. Our results are summarized in **Table 3.14**.

Table 3.14: Summary of IHC results for Mechanical Panel experiments. ++ indicates strong homogenous staining intensity. + indicates a moderate to weak homogeneous staining intensity. +/- indicates heterogenous staining. – indicates no staining was evident.

Stimulus	SMA	Calponin	MHC	Flk-1	PECAM	vWF
CP-90HF	-	-	-	-	-	-
CP-90	-	-	-	-	-	-
CP-120	-	-	-	-	-	-
CP-180	-	-	-	+	-	-
CS-1HF	+/-	+/-	+/-	++	-	-
CS-1	+	-	-	++	-	-
CS-5	++	++	-	++	-	-
CS-10	++	++	+	++	-	-
LSS-1	-	-	-	-	-	-
LSS-5	-	-	-	-	-	-
LSS-10	-	-	-	+	-	-
LSS-20	-	-	-	+	-	-
Control	-	-	-	++	-	-

We have found an apparent CS-dose-dependent expression of SMC protein markers. CS-1 caused the tBMMSCs to express SMA (**Figure 3.16**); CS-5 led to the expression of both SMA and calponin (**Figure 3.17**); and CS-10 stimulated expression of both of these, in addition to the highly selective contractile protein, SMMHC (**Figure 3.18**). CS-1HF also resulted in expression of all three markers, but not to the extent seen for CS-5 and CS-10 in terms of the relative

numbers of positive cells within a field of view. Exposure of BMMSCs to CP, LSS, or control conditions did not induce the expression of any of these SMC-related proteins. These stretch-dependent changes in SMC protein expression are consistent with previously published data on stem cells obtained from different sources, but only exposed to a single loading regimen [526, 527, 650]. However, to our knowledge, these are the first studies to comprehensively study the magnitude and frequency effects of cyclic stretch in BMMSCs.

In addition to the SMC protein expression changes that result from cyclic stretch, we have also discovered that these cells constitutively express flk-1 (see **Figure 3.19**), or VEGFRII, the active signaling receptor for VEGF (see Section 1.3.1.1). Although we did not see any other markers of EC differentiation, the presence of flk-1 still allows the potential for these cells to differentiate to ECs since flk-1 expression is necessary for any EC differentiation during development and has been used as a sorting marker for ESCs with EC potential [567, 651, 652]. The expression of flk-1 was maintained by the cells under all levels of CS (**Figure 3.19**), regardless of the expression of SMC markers. Although it would appear contradictory for stem cells to express EC-related markers as well as SMC-related markers that have traditionally been viewed as terminal differentiation, this type of phenomenon has also been reported in SMC-precursors derived from the blood [262]. The expression of flk-1 was also maintained under CP-180 and LSS-10 and LSS-20, but CP and LSS magnitudes below these resulted in a loss of flk-1 expression. No expression of EC-related proteins (PECAM and vWF), or positive staining for alizarin red (osteoblasts) or oil red (adipocytes) was detected, thus strongly suggesting a specificity of differentiation for this particular set of stimuli.

3.4.3 Differential gene expression

In addition to the immunohistochemistry data, we have some evidence, although as yet inconclusive, that mechanical stimulation modulates gene expression for targets associated with SMCs, cardiomyocytes, ECs, adipocytes, osteoblasts, and chondrocytes (**Table 3.5-Table 3.10**). The increases in SMC gene expression are in agreement with other published gene expression data on BMMSCs from another source [527l, 653]. Unlike the protein expression, the increase in several SMC genes was not restricted to cyclic stretch, as our results suggest that LSS and CP may increase SMC-related gene expression. This is in accordance with other published studies of stem cells exposed to pressure with shear stress [530, 569]. However, we did not detect concomitant protein expression under the regimens tested. This may be a result of post-translational modification or knock-down of the transcribed genes through other mechanisms that we have not yet investigated. One such possibility might be a potential increase in PDGF expression. Decreases in SMA protein levels as a result of PDGF-BB stimulation have previously been shown to derive from post-translational destabilization of the SMA mRNA [129] even though SMA transcription may still occur at high levels [128]. PDGF has a similar effect on myosin production in SMCs, causing more than a 35% decrease in SM-1 protein but doubling non-muscle myosin protein [130]. In addition to the potential post-transcriptional modifications, there is evidence for transcriptional regulation of SMC genes by PDGF-BB through several mechanisms, including increases in the myocardin-related transcription repressors kruppel-like factor 4 (KLF4) [654] and megakaryoblastic leukemia-1 (MKL-1) [655] as well as the displacement of myocardin from serum response factor (SRF) through phosphorylation of Elk-1 [656]. These molecules are all potential targets for future studies into the mechanisms of how mechanical stimulation modulates gene expression in stem cells.

Concurrent with our analysis of SMC-related genes, we have obtained some evidence that EC-related genes can be modulated in stem cells by mechanical stimulation. Flk-1 gene expression was downregulated under LSS and in the lower magnitudes of CP, which is consistent with our observations of flk-1 protein expression by immunohistochemistry. Although we did not detect any vWF expression in our tBMMSCs exposed to mechanical stimulation, our gene expression results indicate that vWF may be expressed under CP. This again raises the question of post-translational modification. Additionally, this apparent disconnect between gene and protein expression may be a result of timing and/or concentration. It is possible that these genes are just being turned on by the fifth day of stimulation, and no detectable protein has been produced yet. Future studies centered on these specific endpoints may help to identify the appropriate processes driving this phenomenon. The downregulation of other EC-related genes by LSS seems to contradict the literature for other stem cell types, particularly embryonic stem cells [567, 568, 651]. However, we do have evidence that LSS downregulates flk-1, which was found to be necessary for EC gene expression in embryonic stem cells exposed to shear stress [567].

The lack of gene expression for osteoblast, chondrocyte, and adipocyte-related genes seems to fit our data demonstrating a no late-stage osteoblast and adipocyte differentiation using Alizarin Red and Oil Red O assays. The increase in soluble factor expression, particularly FGF-2 and TGβ, by LSS may be related to the convection of the large volume of media required to operate the Streamer® apparatus. The shear stress device contained over 400 mL of cell culture media, which was over an order of magnitude greater than the cyclic pressure, control, and cyclic stretch cultures. The constant movement of this media over the cells in the shear stress system could potentially eliminate local microenvironments driving autocrine and paracrine signaling by

washing away secreted factors, leading the cells to continually secrete these biomolecules. This potentially constant production of growth factors and the lack of signaling may drive the increase in cell size and decreased proliferation seen under LSS. Although a linear regression demonstrates that cell size and shape were able to account for more than 66% of the variability in proliferation (**Table 3.13** and **Figure 3.23**), this does not imply a causal relationship.

3.4.4 Limitations

As with any *in vitro* study, there are experimental limitations that may have an impact on the results obtained. As a primary isolation, the tBMMSCs were invariably heterogenous. Although the Mechanical Panel was designed to minimize the effects of heterogeneity between stimuli, our interpretation of the data must include the potential that the applied mechanical stimuli were selecting for a subpopulation of cells within the original heterogenous mix. Selection need not occur through apoptotic mechanisms, but may be a result of a selective increase or inhibition of proliferation in a particular sub population.

Another important limitation to the current study was the use of profoundly subconfluent cultures (200 cells/cm^2 starting density) to initiate the Mechanical Panel. In addition to being the standard culture conditions published for the tBMMSCs [613], subconfluent cultures were used to potentially identify the individual response of the cells to each of the Mechanical Panel components through morphologic and proliferation changes that were relatively unaffected by neighboring cells. While this aided in the ease of analysis and may allow for a heterogeneous cell population to be interrogated with relative certainty that each cell is behaving independently, cells do not exist in a subconfluent state *in vivo*. At no time during their development and subsequent life are cells without some form of cell-cell contact. This isolation may have a

profound effect on the way the cells responded to the mechanical stimulation, and confluent cultures, which would be required to generate enough cellular material for tissue engineering applications, may have a completely different outcome. Nonetheless, having subconfluent cultures did allow for us to identify potentially useful stimulations regimens, such as cyclic pressure, that may be used to expand cells quickly for tissue engineering applications as well as further determine the role of cyclic stretch on differentiation of these BMMSCs towards SMCs.

In addition to the potential implications for altering cell behavior, subconfluent cultures imposed a serious limitation on the available biologic material for assays such as RT-PCR and Western blotting. As a result of low protein yields, no Western blotting could be performed to corroborate the IHC or RT-PCR data that was generated. Even the RT-PCR analysis was somewhat limited in that only one TLDA could be run with the available RNA and we believe that several TLDAs were under loaded as a result of low RNA yields. This resulted in the failure to successfully interrogate several genes and resulted in empty data sets with essentially no reserve materials to repeat the assay, further hampering our statistical analysis of the gene expression results.

Another limitation which may have had a significant impact on the RT-PCR results was the use of 18s as the endogenous control gene. The use of 18s has recently been reported to be insufficient as an endogenous control gene because of its extremely high abundance relative to target mRNA transcripts [657]. This can result inadequate normalization for vastly different transcriptomes. We have evidence, found in **Appendix G**, which demonstrates that not only is 18s expressed at significantly higher levels than target mRNA, but it has a variance in expression that is not related to the target mRNA. In retrospect, an investigation of all of the potential endogenous control genes should have been performed to identify a gene or set of genes (as is

currently suggested in the literature [657, 658]) that would achieve their C_T near the threshold of the genes of interest as well as remain stable under the various mechanical stimuli used in this study. This test of endogenous controls was performed for subsequent experiments on the temporal change in gene expression as a result of mechanical stimulation (see Chapter 4.0).

Although we have demonstrated that cyclic stretch induces differentiation towards an SMC phenotype, including the highly differentiated contractile protein SMMHC, we have not provided evidence that these differentiated cells are functionally equivalent to adult SMCs. The use of contractile agents, such as carbachol, to initiate and visualize cellular contraction [659] has been impeded by our ability to image the BioFlex® culture plates at the end of a CS experiment. In order to ensure that the membrane experiences uniform stretch, silicone grease is applied to the underside to help it glide over the loading post. This effectively prevents an inverted microscope from being able to view the cells following an experiment without cutting the membrane out and cleaning it with harsh scraping techniques that disturb unfixed cells. Furthermore, the membrane itself was permanently deformed by the cyclic stretching process and did not present a uniform focal plane on which to image the cells following an experiment.

Another limitation, which was mentioned previously, was the high volume of media needed to operate the shear stress system. This essentially presented the cells with an infinitely fresh media supply relative to their counterparts in the other apparatuses in the Mechanical Panel. To mitigate this effect over time, no media changes were performed during the 5 day experiments for shear stress, while media changes were performed every 48 hours in accordance with the standard culture protocol for the tBMMSCs in the control, cyclic stretch, and cyclic pressure systems. In addition, the shear stress system operated in the absence of any form of

pulsatile flow, unlike the other components of the Mechanical Panel, which is not physiologic for the vascular system that was being modeled for our studies.

3.5 CONCLUSION

We have demonstrated that mechanical stimulation has differential effects on the morphology, proliferation, protein, and gene expression in BMMSCs. Our results have confirmed previous observations that cyclic stretch can drive stem cell differentiation towards an SMC phenotype and have extended our understanding of the role cyclic stretch plays in differentiation by the use of multiple magnitudes and frequencies of stimulation. We have demonstrated that cyclic pressure accelerates proliferation, and that a correlation exists between cell size, shape, and proliferation. To our knowledge, this work is the first comprehensive study examining multiple types of mechanical stimulation in parallel across a broad range of magnitudes and multiple frequencies and has future applications in bioreactor design and tissue engineering research.

4.0 TEMPORAL RESPONSE TO MECHANICAL STIMULATION

4.1 INTRODUCTION

Based upon the successful identification of the differential response of BMMSCs to three mechanical stimuli using our Mechanical Panel, the next step was to investigate the time-dependent evolution of this response. Previous work using both embryonic stem cells and bone marrow derived stem cells has demonstrated temporal changes in gene expression in response to mechanical stimuli. Park et al. [527] demonstrated that SM22α and SMA gene transcription were both transiently increased in BMMSCs exposed to 10% cyclic uniaxial stretch for 1-3 days. Similarly, Yamamoto et al. [567] found that flk-1^+ embryonic stem cells exposed to shear stress had increased RNA levels for SM22α and SMA within 24 hours, but that these genes fell back towards control levels at 48 and 72 hours. However, EC-related genes including flk-1 and PECAM experienced sustained increases in RNA levels with shear stress. Similar sustained, shear-induced increases in EC markers have also been demonstrated in C3H10T1/2 embryonic stem cells [568]. To further characterize the mechanobiology of tBMMSCs, we investigated their response to 1 and 3 days of stimulation in the Mechanical Panel. In addition, we attempted to address some of the limitations identified in Section 3.4.4. In these experiments, we used confluent cultures to model more physiologic microenvironments as well as improve our yield of

biological material for PCR and Western blotting. Furthermore, we performed the necessary tests to determine a more suitable gene to be used as an endogenous control for PCR endpoints.

4.2 METHODS

4.2.1 Experimental design

4.2.1.1 Time points

Experiments performed to address Specific Aim 3 were designed to determine the time-dependent response of tBMMSCs to a specific magnitude and frequency of each mechanical force stimulus from the Mechanical Panel (see Section 3.1.1). Because the overall goal of this study is to determine how gene and protein expression changes in tBMMSCs, time points of 24 hours and 3 days were chosen to potentially capture the maximal gene and protein changes associated with the Mechanical Panel based upon other research conducted in stem cell differentiation [527, 558, 567]. Each of these studies has shown significant changes in gene expression for some of the endpoints listed in **Table 4.2** within 24 hours of mechanical stimulation. Furthermore, 3 days of continued stimulation was sufficient time to determine whether the changes in gene expression were transient, and whether there was an associated change in protein expression.

4.2.1.2 Cell source

For each experiment, tBMMSCs were obtained as described in Section 3.2.1 and seeded at confluence (21,000 cells/cm^2) on collagen I coated BioFlex™ (Flexcell) deformable substrates

for stretch and control conditions, or Culture Slips™ (Flexcell) for shear and pressure conditions. Forty-eight hours after seeding, the tBMMSCs were loaded into each of the systems described in Section 3.2.2 while control samples were placed in static incubator conditions.

4.2.1.3 Mechanical panel parameters

The regimens employed in these experiments are listed in **Table 4.1**. These regimens were chosen based upon the response of the tBMMSCs during the 5 day experiments. CS-10 was chosen because it exhibited the maximal changes in phenotype, namely SMMHC, calponin, and SMA expression determined by IHC (see **Figure 3.16**, **Figure 3.17**, and **Figure 3.18**), and also displayed an elongated, spindle shaped morphology (see **Figure 3.8** and **Figure 3.9**) which is characteristic of SMCs [59, 213]. Because the tBMMSC response to cyclic pressure did not appear to be affected by the magnitude or frequency of stimulation, we chose to use CP-120 because it was the most physiologically relevant as a vascular pressure. In addition, research using other cell types, including ECs and SMCs, has shown higher magnitudes of pressure (>150 mmHg) to be deleterious to the cells, leading to abnormal phenotypes and increased rates of apoptosis [229, 384-390]. Furthermore, although CP-120 demonstrated a decrease in flk-1 staining from the constitutive expression (**Figure 3.19**), the flk-1 gene expression was not different than the control (**Table 3.6**). LSS-20 was chosen because it was the maximum magnitude tested at the 5 day time point and exhibited the greatest changes in cell morphology; namely, elongation and markedly spindle shaped (see **Figure 3.8**and **Figure 3.9**) and decreased proliferation (**Figure 3.14**). These changes in morphology are consistent with ECs under shear stress [188]. Furthermore, EC differentiation in an embryonic mesenchymal progenitor cell line (10T1/2 cells) has been demonstrated using 15 dynes/cm^2 shear stress [568].

Table 4.1: Stimulation regimens used for Mechanical Panel experiments to determine the temporal response of tBMMSCs to mechanical stimulation. tBMMSCs were exposed to these conditions for 24 hours or 3 days.

	Control	Cyclic Stretch	Cyclic Pressure	Shear Stress
Regimen	Static incubator conditions	10%, 1 Hz (CS-10)	120/80 mmHg, 1 Hz (CP-120)	20 dynes/cm^2 (LSS-20)

4.2.2 Endpoints

After 24 hours or 3 days of stimulation in the Mechanical Panel, the samples were removed and processed for RNA extraction and purification (see Section 3.2.4.5) followed by RT-PCR (see Section 4.2.2.1). In addition, protein extraction and Western blotting (see Section 4.2.2.3) were performed to identify changes in the protein targets of some of the RT-PCR endpoints.

4.2.2.1 RNA isolation and qualitative assessment

Cell lysis and RNA isolation was performed with Trizol™ immediately following the withdrawal of each stimulus using techniques described in Section 3.2.4.5.1. The isolated RNA was purified using the RNeasy Kit (Qiagen) according to protocols described in Section 3.2.4.5.2. Following purification, RNA quality and quantity were assessed by the GEGF at Case Western Reserve University. RNA concentration was assayed using a NanoDrop Spectrophotometer (ND-1000, NanoDrop Technologies, Wilmington, DE), and RNA quality was assessed with a BioAnalyzer (Model 2100, Agilent Technologies) using techniques described in Section 3.2.4.5.3. RNA samples attaining an RIN value of greater than 8 were selected for RT-PCR.

4.2.2.2 TaqMan® RT-PCR Low Density Array

RNA samples suitable for RT-PCR analysis were converted to cDNA through reverse transcriptase reactions (see Section 3.2.4.5.4). The converted cDNA was then loaded into a custom TaqMan® Low Density Array (TLDA, Applied Biosystems). The gene names, catalog numbers, and classifications for the primers loaded into the TLDAs used for these experiments are listed in **Table 4.2**. Because new primers are continually added to the available inventory for TLDA design, we chose to eliminate several gene targets whose expression was extremely low or never detected (e.g., Runx2 and TNFα) in favor of other gene targets, (e.g., PECAM and cyclin B1) that had recently become available for use on the custom TLDAs. In addition, testing was performed to identify a more appropriate endogenous control gene for use on the TLDAs which was also used in the new custom TLDAs (see Section 4.2.2.2.1). RT-PCR was performed by the technicians at the GEGF according to protocols described in Section 3.2.4.5.5.1.

Table 4.2: List of TaqMan® PCR primers, classifications, and catalog numbers for the second custom-designed TLDA card. Many of the genes listed in the first card (see **Table 3.4**) that are not found on the second card were removed because of their lack of expression, or were moved to single assays because we wished to examine the primer in conjunction with a non-inventoried primer that could not be placed on a TLDA.

Classification	Gene Name	Applied Biosystems Catalog #
Adipocyte	PPAR γ	Rn00440945_m1
BMMSC	CD59	Rn00563929_m1
BMMSC	CD90	Rn00562048_m1
Cardiomyocyte	Troponin	Rn00437164_m1
Chondrocyte	Aggrecan I	Rn00573424_m1
Chondrocyte	Collagen II	Rn00563954_m1
EC	CD133/Prominin I	Rn00572720_m1
EC	Endoglin	Rn00568869_m1
EC	Flk-1	Rn00564986_m1
EC	iNOS	Rn00561646_m1
EC	vWF	Rn00788354_m1
EC	CD31	Rn01467262_m1
EC	E-Selectin	Rn00594072_m1
Fibroblast	Vimentin	Rn00579738_m1
Housekeeping	Gusb	Rn00566655_m1
ECM	Collagen I	Rn00584426_m1
ECM	Collagen III	Rn01437683_m1
ECM	Collagen IV	Rn01401018_m1
ECM	Elastin	Rn01499782_m1
Myocyte	Desmin	Rn00574732_m1
Osteoblast	Alkaline Phosphatase	Rn00564931_m1
Osteoblast	Osteocalcin	Rn00566386_g1
Osteoblast	Osteopontin/SPP1	Rn01449972_m1
Proliferation	Cyclin B1	Rn00596848_m1
Secreted Peptides	BMP2	Rn00567818_m1
Secreted Peptides	FGF2	Rn00570809_m1
Secreted Peptides	TGF-α	Rn00572010_m1
Secreted Peptides	VEGF	Rn00582935_m1
SMC	Caldesmon	Rn00565719_m1
SMC	SM22α	Rn00580659_m1
SMC	Myocardin	Rn01786178_m1

4.2.2.2.1 Determination of endogenous control gene

Following the initial results with the first custom-designed TLDA (**Table 3.4**), it became apparent that the endogenous control supplied by Applied Biosystems in the TLDA card may not have been appropriate for our cell type and/or experimental conditions (see **Appendix F**). Therefore, alternative endogenous control genes were investigated. Equal masses (200ng) of 16 cDNA samples encompassing a wide range of magnitudes, stimuli, frequencies, time points, and states of confluence (see **Table 4.3**) were chosen for analysis in 2 Endogenous Control TLDAs (Applied Biosystems) which contained TaqMan® gene expression assays for 16 common endogenous control genes (**Table 4.4**) in quadruplicate. The Endogenous Control TLDAs were analyzed by RT-PCR according to techniques outlined in Section 3.2.4.5.5.

The output from the RT-PCR reaction was processed using SDS software to determine the raw C_T values for each of the 16 endogenous control genes for the 16 experimental samples. These raw C_T values were imported into GeNorm, an Excel-based applet created by Vandesompele et al.[657] that calculates an expression stability parameter *M* for each gene as the average pair-wise variation *V* for that gene compared to all other genes in the data set. The software computes the stability parameter for each gene, then removes the gene with the largest *M* value, and recalculates the stability parameter for each of the remaining genes. The process is repeated until two genes remain, at which point no further ranking can be determined. To make the choice between the two most stable genes from the GeNorm output, the variance in the C_T was compared and the gene with the lower variance was chosen as the endogenous control gene for the second set of custom-designed TLDAs (**Table 4.2**). As per Applied Biosystems' quality control policy, the 18S gene was still required to be on the TLDA although it would no longer be used to normalize the RT-PCR results.

Table 4.3: Sample list analyzed by the endogenous control TLDA. The samples were chosen to represent each component of the Mechanical Panel at different magnitudes, frequencies, times of exposure, and confluence.

Stimulus	Magnitude	Frequency	Exposure Time	Starting Density
Control	0	0	5 days	200 cells/cm^2
CS	1%	2.75 Hz	5 days	200 cells/cm^2
LSS	1 dyne/cm^2	N/A	5 days	200 cells/cm^2
CP	90/70 mmHg	2.75 Hz	5 days	200 cells/cm^2
Control	0	0	5 days	200 cells/cm^2
CS	5%	1 Hz	5 days	200 cells/cm^2
LSS	10 dynes/cm^2	N/A	5 days	200 cells/cm^2
CP	180/140 mmHg	1 Hz	5 days	200 cells/cm^2
Control	0	0	24 hours	21,000 cells/cm^2
CS	10%	1 Hz	24 hours	21,000 cells/cm^2
LSS	20 dynes/cm^2	N/A	24 hours	21,000 cells/cm^2
CP	120/80 mmHg	1 Hz	24 hours	21,000 cells/cm^2
Control	0	0	3 days	21,000 cells/cm^2
CS	10%	1 Hz	3 days	21,000 cells/cm^2
LSS	20 dynes/cm^2	N/A	3 days	21,000 cells/cm^2
CP	120/80 mmHg	1 Hz	3 days	21,000 cells/cm^2

Table 4.4: List of the endogenous control genes used in the Endogenous Control TLDA. Each of these endogenous control genes have been commonly employed in research involving gene expression.

Gene Name	Protein
18s	18s Ribosomal RNA
Actb	β-actin
Arbp	Acidic ribosomal phosphoprotein P0
B2m	β2 microglobulin
GAPDH	Glyceraldehyde-3-phosphate dehydrogenase
Gusb	Glucuronidase, β
Hmbs	Hydroxymethylbilane synthase
Hprt	Hypoxanthine guanine phosphoribosyl transferase
Pgk1	Phosphoglycerate kinase 1
Ppia	Peptidylprolyl isomerase A
Ppib	Peptidylprolyl isomerase B
Rplp2	Ribosomal protein, large P2
Tbp	TATA box binding protein
Tfrc	Transferrin receptor
Ubc	Ubiquitin C
Ywhaz	Tyrosine 3-monooxygenase/tryptophan 5-monooxygenase activation protein, zeta polypeptide

4.2.2.3 Protein isolation and quantification

The remaining organic phase from the Trizol™ preparation (see Section 3.2.4.5.1) was processed further to obtain the total cellular protein (see **Figure C.1** in **Appendix C**) for application in Western blotting (Section 4.2.2.4). The general methods for protein extraction, purification, and quantification are described in the following sections.

4.2.2.3.1 Protein extraction

For each milliliter of Trizol™ in the original extraction, 0.3 mL of 100% ethanol (Pharmco-AACP) was added and mixed by gentle inversion to precipitate the DNA remaining in

the organic layer. The Trizol™/chloroform/ethanol mixture was incubated for 3 minutes at RT before centrifugation at 2000 x g for 5 minutes at 4°C. The supernatant was removed with a glass pipette and held on ice for protein extraction while the DNA pellet was frozen at -80°C for possible future analysis of total DNA content.

To precipitate the protein from the remaining Trizol™/chloroform/ethanol mixture, 1.5 mL of 100% isopropanol (PX1835-14, EMD, San Diego, CA) per milliliter of original Trizol™ volume was added and vortexed to ensure proper mixing. The Trizol™/chloroform/ethanol/isopropanol mixture was incubated at RT for 10 minutes before centrifugation at 11,500 x g for 30 minutes at 4°C to pellet the dissolved protein. The supernatant was discarded, and the remaining protein pellet was further processed to eliminate potential organic contaminants.

4.2.2.3.2 Protein Purification

To purify the extracted protein, the initial pellet was washed with 2mL of wash solution (2.9% guanidine hydrochloride (5010, EMD) in 95% ethanol (Pharmco-AACP)) per milliliter of original Trizol™ volume. The wash solution was mixed thoroughly with the protein pellet by vortexing, and incubated for 20 minutes at RT. The sample was then centrifuged at 11,500 x g for 5 minutes at 4°C. The supernatant was discarded, and the process repeated 3 times to eliminate organic contaminants from the protein pellet. After the final wash, the protein pellet was mixed with 2mL of 100% ethanol (Pharmco-AACP) and incubated for 20 minutes at RT. The sample was then centrifuged at 11,500 x g for 5 minutes at 4°C. After centrifugation, the supernatant was discarded and the sample placed in a desiccating jar under vacuum for 5 minutes to remove any further traces of ethanol. The dehydrated protein was then resuspended in 50 mM Tris HCl (pH 8.0, T-3038, Sigma) and 0.1% sodium dodecyl sulfate (SDS, BP166, Fisher

Scientific) containing HALT® anti-proteinase (Pierce) by tituration and incubation at 50°C. The resuspended protein was centrifuged at 16,000 x g to pellet any insoluble material and transferred to a fresh 1.5mL tube and stored at -80°C.

4.2.2.3.3 Total protein quantification

The amount of total resuspended protein from Section 4.2.2.3.2 was quantified using a Bradford colorimetric assay (BCA, Pierce) according to the manufacturer's specifications. Briefly, 196 µL of Reagent A, 4 µL of Reagent B, and a 10 µL dilution of the protein sample were mixed in a 96-well plate and incubated for 30 minutes at 37°C. The optical density of the final reaction was measured at 570 nm using a microplate reader (Model 680, Bio-Rad, Hercules, CA). A standard curve using known concentrations of BSA was generated in triplicate and used calculate the concentration of the unknown protein samples. The protein concentration and total yield of sample were recorded in the experimental database (see Section 3.2.5.1).

4.2.2.4 Western blotting

Relative changes in protein expression for the experiments outlined in Section 4.2.1 were quantified by Western blotting. The general methods for the Western blotting are described in the following sections.

4.2.2.4.1 Protein electrophoresis and transfer

Purified protein (as described in Section 4.2.2.3.2) was separated by electrophoresis under reducing conditions. Approximately 20-40 µg of protein (as determined from the BCA assay described in Section 4.2.2.3.3) was mixed 1:5 (v/v) with 6X sample buffer (50 mM Tris (pH 6.8, Sigma), 26% glycerol (G5516, Sigma), 6.5mmol DTT (43815, Sigma), 0.06%

Bromphenol Blue (161-0404, Bio-Rad), 0.4% SDS) and heated to 95°C for 3 minutes before being loaded in a 4-15% Tris-HCL gradient gel (161-1158, Bio-Rad). The gel was run at 200 V for 30 minutes in Tris-SDS-Glycine buffer (161-0772, Bio-Rad) prior to being transferred to a nitrocellulose (Immobilon-NC, Millipore, Billerica, MA) or PVDF (Bio-Rad) membrane. Separate transfer protocols and solutions were used depending on the protein of interest and are outlined in **Table 4.5**.

Table 4.5: Transfer solutions and settings for each protein endpoint interrogated by Western blotting.

Endpoint	Transfer Solution	Transfer Settings	Membrane
SMA	25 mM Tris HCl pH 8.0, 190 mM Glycine, 20% methanol	40 V for 90 minutes	PVDF
Calponin	25 mM Tris, 190 mM Glycine, 20% methanol	100 V, 2 hours	Nitrocellulose
SM-MHC	50 mM Tris, 380 mM Glycine, 0.1% SDS, 20% methanol	30 V, 16 hours followed by 100 V, 1 hour	Nitrocellulose
Flk-1	50 mM Tris, 380 mM Glycine, 0.1% SDS, 20% methanol	30 V, 16 hours followed by 100 V, 1 hour	Nitrocellulose
PECAM	50 mM Tris, 380 mM Glycine, 0.1% SDS, 20% methanol	30 V, 16 hours followed by 100 V, 3 hours	Nitrocellulose

4.2.2.4.2 Immunoblotting

Following protein transfer, the nitrocellulose membrane was blocked for 1 hour and incubated with the primary antibody diluted in the blocking agent for 1 hour at RT. A list of the blocking solutions and primary antibody dilutions is found in **Table 4.6**. The membrane was washed four times for 5 minutes to remove any unbound primary antibody, and incubated with the horseradish peroxidase (HRP) conjugated secondary antibody (Pierce) in the blocking agent

for 1 hour at RT. After four 5 minutes washes in buffer, the membrane was developed with enhanced chemiluminescence (SuperSignal West Femto, Pierce) according to the manufacturer's instructions. The developed membrane was imaged on a Kodak Image Station (Model 2100, Eastman Kodak, Rochester, NY). For endpoints whose molecular weight was less than 60 kDa, the membrane was stripped using Blot Rejuvenate® (Chemicon) and reprobed with GAPDH. For endpoints greater than 60 kDa, the membrane was cut and GAPDH staining performed separately.

Table 4.6: Reagent details for each of the endpoints interrogated by Western blotting.

Endpoint (molecular weight)	Positive Control (µg/lane)	Blocking Buffers	Primary Dilution	Secondary Ab (Source)
SMA (42 kDa)	A-10 (25µg)	Superblock	1:180,000 (45°C)	1:20,000 Goat anti-mouse (Pierce)
Calponin (32 kDa)	A-10 (50µg)	50mM Tris, pH 7.5; 200mM NaCl; 0.1% Tween 20; 1% dry milk	1:500	1:20,000 Goat anti-mouse (Pierce)
MHC (200 kDa)	A-10 (50µg)	50mM Tris, pH 7.5; 200mM NaCl; 0.1% Tween 20; 1% dry milk	1:500	1:20,000 Goat anti-mouse (Pierce)
Flk-1 (150-200 kDa)	ECV304 (50µg)	TBS; 0.5% Tween 20; 5% non-fat dry milk	1:1000	1:20,000 Goat anti-mouse (Pierce)
PECAM (130-140 kDa)	Jurkat (50µg)	15mM Tris buffer, pH 8.0; 140mM NaCl; 0.05% Tween 20; 5% non-fat dry milk	1:5000	1:20,000 Goat anti-mouse (Pierce)
GAPDH (37 kDa)	N/A	PBS, 0.1% Tween, 5% non-fat dry milk	1:1000	1:2,000 Mouse anti-goat (Pierce)

4.2.2.4.3 Antibodies

For SMC protein detection, SMA (MAB1522, Chemicon), calponin (M3556, Dako) and MHC (M3558, Dako) were used. A-10 (a rat aortic SMC line) cell lysates (sc-3806, Santa Cruz) were used as a positive control for all SMC proteins. For EC protein detection, flk-1 (cs-6251, Santa Cruz) and PECAM (MAB1393, Chemicon) were used. ECV304 (a transformed EC cell line) cell lysate (sc-2269, Santa Cruz) was used as a positive control for flk-1, and Jurkat cell lysate (sc-2204, Santa Cruz) was used as a positive control for PECAM. GAPDH (sc-20357, Santa Cruz) was used as an internal loading control.

4.2.2.4.4 Image analysis

Images of the Western blots were imported into Scion Image (Scion Corp) for densitometry analysis. Each protein band at the correct molecular weight for each antibody was highlighted and the integrated optical density was measured. The integrated optical density for each lane was normalized to its respective GAPDH loading control, and then divided by the normalized control sample for each experiment to provide a fold-change in protein expression.

4.2.3 Statistical analysis

The RQ values for each RT-PCR run and fold-changes in protein expression as determined from the Western blots were stored in the Experimental Database (see Section 3.2.5) and exported to SPSS software for statistical analysis. For comparisons to the control, a one-sample t-test was performed against $\mu=1$ with $\alpha=0.05$. For comparisons between stimuli and time points, one-way ANOVA with post-hoc LSD testing at $\alpha=0.05$ was used to detect significant differences.

4.3 RESULTS

4.3.1 Determination of endogenous control gene

In light of the earlier RT-PCR results (see Section 3.3.6 and **Appendix F**), 16 endogenous control genes were evaluated using samples found in **Table 4.3**. The resulting expression levels were evaluated using the stability index calculated by GeNorm software [657]. The results are displayed in **Figure 4.1** and demonstrate that the two most stable genes for our experimental conditions are GAPDH and Gusb. The calculated stability index for these genes was 0.10, which is below the recommended value of 0.15 [657]. By this stability index, either gene would therefore be suitable as the endogenous control for our experimental system. To help make a definitive decision between these two genes, we also examined the average C_T and C_T variance for the endogenous control genes (**Table 4.7**). Gusb had the lowest computed variance (0.0953 cycles) and had an average C_T (25.96 cycles), which was most similar to the C_T values for the target genes in our TLDAs. Based upon the independent confirmation by GeNorm analysis and our computed variance of Gusb as the most stable gene, we chose Gusb as the endogenous control gene for all of our subsequent RT-PCR.

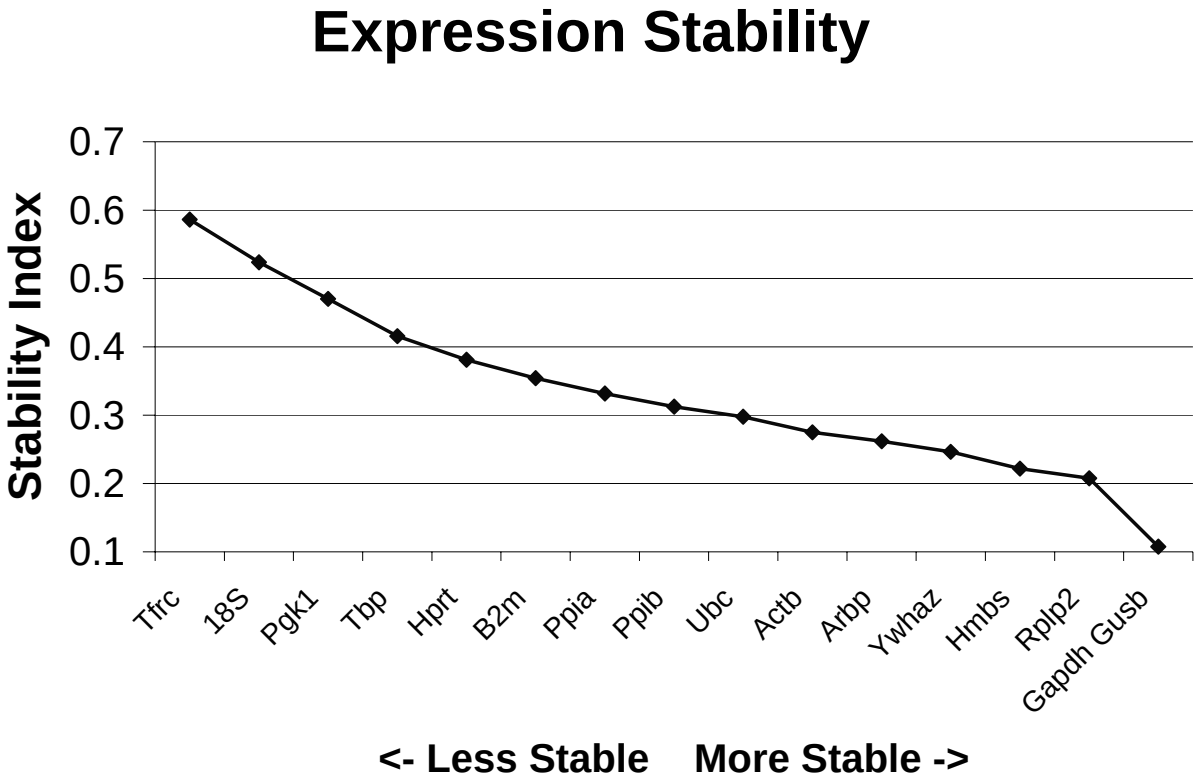

Figure 4.1: Plot of the stability index calculated from the variance in gene expression as a function of the stepwise removal of each of the genes listed on the X-axis.

Table 4.7: Table depicting the average and variance of the C_T for each of the potential endogenous control genes.

Detector	Detector Average	Detector Variance
18S	12.21	13.3260
Ppia	22.47	8.1199
Tbp	29.74	6.4745
Tfrc	27.86	4.0181
Rplp2	22.42	3.4542
Ppib	22.32	3.0567
Ywhaz	23.33	2.3627
Pgk1	22.10	0.8304
B2m	19.96	0.5312
Gapdh	19.57	0.5005
Arbp	21.32	0.4463
Hprt	23.01	0.3862
Actb	17.18	0.2729
Hmbs	25.44	0.1546
Ubc	21.81	0.1341
Gusb	**25.96**	**0.0953**

4.3.2 Gene Expression

4.3.2.1 Muscle related genes

The average RQ values ± SD for muscle-related genes are depicted in **Table 4.8**. Similar to the previous 5 day data, caldesmon did not seem to be affected by mechanical stimulation, maintaining expression levels near controls. The lone exception was a statistically significant ($p<0.05$, but not biologically relevant) decrease in caldesmon under LSS at 3 days, which was also significantly lower than the 24 hour expression ($p<0.05$). The expression of cardiac troponin significantly decreased ($p<0.05$) for CP and LSS at both 24 hours and 3 days. However, under CS, the expression is unchanged at 24 hours and 3 days. Desmin expression was significantly decreased ($p<0.05$) for LSS at both 24 hours and 3 days, and unchanged for CP. Desmin expression was not affected by CS at 24 hours, but increased nearly 2-fold ($p<0.05$)

at 3 days. SM22α expression changes under CS were not statistically significant, but the data seems to trend towards a transient downregulation at 24 hours followed by a return towards control values at 3 days. On average, there appears to be some biologically relevant increase in expression in SM22α for CP and LSS at 3 days, but the expression patterns were highly variable as demonstrated by the high standard deviation. Myocardin (recently available on the TLDA), which has been reported as a selectively expressed master transcription factor for SMC genes [62, 103-106, 656], was significantly downregulated ($p<0.05$) at 24 hours by CP and LSS, and remained downregulated for LSS (although not statistically significant). No change was evident for CS at 24 hours, but a trend towards upregulation ($p<0.05$) was developing by 3 days.

Table 4.8: Fold changes in muscle-related gene expression relative to control for each component of the Mechanical Panel. Green and red highlights indicate an average fold change greater than 1.3 or less than 0.7 (considered biologically relevant), respectively. Data are presented as the mean ± SD with sample numbers. + $p<0.10$, *$p<0.05$, vs. controls.

		Muscle		
Time	**Stimulus**	**Caldesmon**	**Cardiac Troponin**	**Desmin**
24 Hours	CP-120	1.04 +/- 0.27, n=6	**0.29 +/- 0.06, n=6 ***	**0.78 +/- 0.14, n=6 ***
	CS-10	1.01 +/- 0.17, n=6	0.87 +/- 0.29, n=6	1.21 +/- 0.95, n=6
	LSS-20	**1.4 +/- 0.26, n=6 ***	**0.18 +/- 0.07, n=6 ***	**0.41 +/- 0.12, n=6 ***
3 Days	CP-120	1.04 +/- 0.21, n=5	**0.47 +/- 0.12, n=5 ***	**0.76 +/- 0.22, n=5 +**
	CS-10	0.93 +/- 0.11, n=8	**1.33 +/- 0.33, n=8 ***	**1.82 +/- 0.51, n=8 ***
	LSS-20	**0.84 +/- 0.06, n=6 ***	**0.27 +/- 0.18, n=6 ***	**0.34 +/- 0.17, n=6 ***

		Muscle	
Time	**Stimulus**	**Myocardin**	**SM22α**
24 Hours	CP-120	**0.71 +/- 0.13, n=6 ***	**1.63 +/- 0.61, n=6 +**
	CS-10	0.99 +/- 0.1, n=6	**0.47 +/- 0.4, n=6 ***
	LSS-20	**0.69 +/- 0.15, n=6 ***	1.34 +/- 0.56, n=6
3 Days	CP-120	0.96 +/- 0.25, n=5	1.5 +/- 0.97, n=5
	CS-10	**1.24 +/- 0.17, n=8 ***	0.9 +/- 0.15, n=8
	LSS-20	0.78 +/- 0.38, n=6	1.18 +/- 0.76, n=6

4.3.2.2 Endothelial Related Genes

The average RQ values ± SD for endothelial-related genes are depicted in **Table 4.9**. CD133 was downregulated by all three mechanical stimuli at 24 hours, and had variable expression at 3 days, showing some an average trend towards upregulation in CP and LSS. Endoglin, which is the TGF-β receptor reported to be highly expressed in ECs [321, 660], was significantly downregulated ($p<0.05$) by both CS and LSS at 24 hours and 3 days. Conversely, endoglin expression was unchanged at 24 hours and trending towards and increase in expression for CP at 3 days. E-selectin, which was another new addition to the TLDAs, appears to be highly variable. However, this is a result of the failure of the control sample to register a C_T value for one experiment, which caused the C_T for the remaining samples to be calculated against an assumed C_T of 40 cycles, resulting in extremely large RQ values. The individual fold-changes for E-selectin under LSS were always more than two-fold (range 2.4 - 54 fold) greater than controls and can therefore be considered a biologically relevant increase in expression. Similarly, vWF gene expression was significantly increased for LSS at 24 hours ($p<0.05$) and 3 days ($p<0.05$). iNOS expression, which had never registered any transcripts in any sample at 5 days (see **Table 3.6**), was significantly elevated ($p<0.10$) under LSS at both 24 hours and 3 days. Similarly to E-selectin, the relative changes in iNOS to control samples were highly variable because of the failure to register transcript values under several control samples. For LSS, changes in iNOS expression ranged from 1 to 84-fold over controls. PECAM (CD31) was another new assay to the TLDA, and exhibited biologically and statistically relevant ($p<0.10$) increases under CP and LSS at 24 hours and 3 days. No changes were found for CS from the controls at either time point. Flk-1 expression was significantly downregulated under LSS at 24

hours ($p<0.05$) and 3 days ($p<0.05$) as well as CP at 3 days ($p<0.05$). Conversely, flk-1 was significantly upregulated ($p<0.05$) under CS-10 at 3 days.

Table 4.9: Fold changes in endothelial-related gene expression relative to control for each component of the Mechanical Panel. Green and red highlights indicate an average fold change greater than 1.3 or less than 0.7 (considered biologically relevant), respectively. Data are presented as the mean ± SD with sample numbers. + $p<0.10$, *$p<0.05$ vs. controls.

		Endothelial			
Time	Stimulus	CD133	Endoglin	E-Selectin	vWF
24 Hours	CP-120	1.28 +/- 0.98, n=6	1.29 +/- 0.74, n=6	4.16 +/- 7.74, n=5	1.06 +/- 0.33, n=6
	CS-10	0.84 +/- 0.64, n=6	**0.38 +/- 0.14, n=6 ***	6.48 +/- 8.72, n=6	1.09 +/- 0.17, n=6
	LSS-20	0.83 +/- 0.55, n=6	**0.19 +/- 0.1, n=6 ***	**25.87 +/- 27.98, n=6 +**	**1.76 +/- 0.34, n=6 ***
3 Days	CP-120	**2.5 +/- 1.52, n=5 +**	1.17 +/- 0.54, n=5	18.5 +/- 30.25, n=3	0.93 +/- 0.16, n=5
	CS-10	0.88 +/- 0.77, n=8	**0.56 +/- 0.13, n=8 ***	10.86 +/- 16.1, n=6	**1.09 +/- 0.1, n=8 ***
	LSS-20	1.78 +/- 2.12, n=6	**0.29 +/- 0.16, n=6 ***	55.43 +/- 72.11, n=6	**1.3 +/- 0.14, n=6 ***

		Endothelial		
Time	Stimulus	iNOS	PECAM	Flk-1
24 Hours	CP-120	**81.91 +/- 64.8, n=5 ***	12.32 +/- 25.03, n=6	0.86 +/- 0.53, n=6
	CS-10	9.19 +/- 7.88, n=3	1.22 +/- 1.26, n=5	1.27 +/- 1.09, n=6
	LSS-20	**27.4 +/- 21.47, n=5 +**	**4.8 +/- 3.96, n=5 +**	**0.28 +/- 0.16, n=6 ***
3 Days	CP-120	78.45 +/- 47.31, n=2	**1.8 +/- 0.7, n=5 +**	**0.44 +/- 0.24, n=4 ***
	CS-10	19.77 +/- 21.97, n=3	0.98 +/- 0.86, n=8	**1.84 +/- 0.5, n=7 ***
	LSS-20	**82.19 +/- 64.54, n=4 +**	**2.81 +/- 1.84, n=6 +**	**0.32 +/- 0.3, n=5 ***

4.3.2.3 Soluble factor-related genes

The average RQ values ± SD for soluble factor-related genes are depicted in **Table 4.10**. In a similar fashion to the 5 day data (see **Table 3.7**), LSS significantly upregulated FGF2, TGF-β, and VEGF-A at 24 hours ($p<0.05$) and 3 days ($p<0.05$). CP at 24 hours and CS-10 at 3 days

were the only other stimuli showing statistically significant ($p<0.05$), but not quite biologically relevant, changes in VEGF-A.

Table 4.10: Fold changes in soluble factor-related gene expression relative to control for each component of the Mechanical Panel. Green highlights indicate an average fold change greater than 1.3 (considered biologically relevant), respectively. Data are presented as the mean ± SD with sample numbers. + $p<0.10$, *$p<0.05$ vs. controls.

		Soluble Factor		
Time	**Stimulus**	**FGF2**	**TGF-β**	**VEGF-A**
24 Hours	CP-120	**1.3 +/- 0.36, n=6 +**	1.11 +/- 0.16, n=6	**1.28 +/- 0.22, n=6 ***
	CS-10	0.9 +/- 0.72, n=6	0.72 +/- 0.57, n=6	0.96 +/- 0.16, n=6
	LSS-20	**4.84 +/- 1.81, n=6 ***	**4.35 +/- 1.51, n=6 ***	**3.43 +/- 1, n=6 ***
3 Days	CP-120	1.42 +/- 0.51, n=5	1.07 +/- 0.28, n=5	1.13 +/- 0.34, n=5
	CS-10	**1.22 +/- 0.27, n=8 +**	0.95 +/- 0.1, n=8	**0.83 +/- 0.2, n=8 ***
	LSS-20	**3.51 +/- 1.82, n=6 ***	**3 +/- 0.73, n=6 ***	**2.76 +/- 0.95, n=6 ***

4.3.2.4 Extracellular matrix-related gene expression

The average RQ values ± SD for matrix-related genes are depicted in **Table 4.11**. In general, LSS demonstrated increased expression for all ECM genes with the exception of collagen IV, there was no detectable signal at 24 hours and 3 days. Collagen I showed similar increases in expression under LSS at 24 hours ($p<0.05$) and 3 days ($p<0.05$) compared with the 5 days data (**Table 3.8**). Elastin and collagen III expression were also increased under LSS, which is contrary to the previous data at 5 days. CS showed a significant upregulation of collagen III at 24 hours and 3 days, while significantly downregulating elastin at 24 hours and returning to baseline values at 3 days. CS also showed a statistically significant ($p<0.05$, but not biologically relevant) transient decrease in collagen I expression at 24 hours, followed by a return to baseline

values at 3 days. Collagen IV expression in general was highly variable across the samples, with a greater tendency towards strong downregulation ($p<0.05$) under CS and LSS at 24 hours.

Table 4.11: Fold changes in ECM-related gene expression relative to the control for each component of the Mechanical Panel. Green and red highlights indicate an average fold change greater than 1.3 or less than 0.7 (considered biologically relevant), respectively. Data are presented as the mean ± SD with sample numbers. + $p<0.10$, *$p<0.05$ vs. controls.

		Matrix			
Time	Stimulus	Collagen I	Collagen III	Collagen IV	Elastin
24 Hours	CP-120	**1.43 +/- 0.5, n=6 +**	1.09 +/- 0.34, n=6	3.1 +/- 3.25, n=6	3.03 +/- 2.49, n=6
	CS-10	**0.82 +/- 0.13, n=6 ***	**1.38 +/- 0.08, n=6 ***	**0.35 +/- 0.19, n=6 ***	**0.5 +/- 0.12, n=6 ***
	LSS-20	**3.96 +/- 1.7, n=6 ***	**2.4 +/- 0.97, n=6 ***	**0.25 +/- 0.29, n=6 ***	**5.71 +/- 3.78, n=6 ***
3 Days	CP-120	1.08 +/- 0.55, n=5	1.03 +/- 0.28, n=5	0.42 +/- 0.49, n=2	**3.25 +/- 1.76, n=5 ***
	CS-10	0.93 +/- 0.21, n=8	**1.26 +/- 0.15, n=8 ***	12.28 +/- 23.49, n=4	0.76 +/- 0.59, n=8
	LSS-20	**3.18 +/- 0.75, n=6 ***	1.46 +/- 0.32, n=6 *	**0.12 +/- 0.13, n=2 +**	**26.79 +/- 20.16, n=6 ***

4.3.2.5 Stem cell-related gene expression

The average RQ values ± SD for stem cell-related genes are depicted in **Table 4.12**. CP showed statistically significant ($p<0.05$), transient decreases in CD90 and vimentin staining at 24 hour followed by a return to baseline at 3 days. CD90 was also significantly downregulated by LSS at 24 hours and 3 days ($p<0.05$), while vimentin levels (which is highly expressed in immature cells and fibroblasts [661]) were significantly elevated at 24 hours ($p<0.1$) before returning to baseline at 3 days. CS showed a statistically significant ($p<0.05$, but not biologically significant) decrease in CD59 followed by a return to baseline levels. Only LSS at 24 hours appears to have upregulated CD59 ($p<0.05$) and on average retained this increase (although not statistically significant).

Table 4.12: Fold changes in stem cell-related gene expression relative to control for each component of the Mechanical Panel. Green and red highlights indicate an average fold change greater than 1.3 or less than 0.7 (considered biologically relevant), respectively. Data are presented as the mean ± SD with sample numbers. + $p<0.10$, *$p<0.05$ vs. controls.

		Stem Cell		
Time	**Stimulus**	**CD59**	**CD90**	**Vimentin**
24 Hours	CP-120	1.04 +/- 0.29, n=6	**0.79 +/- 0.09, n=6 ***	**0.75 +/- 0.08, n=6 ***
	CS-10	**0.82 +/- 0.15, n=6 ***	1 +/- 0.14, n=6	**1.33 +/- 0.22, n=6 ***
	LSS-20	**1.7 +/- 0.6, n=6 ***	**0.6 +/- 0.16, n=6 ***	**1.76 +/- 0.35, n=6 ***
3 Days	CP-120	1.19 +/- 0.54, n=5	0.9 +/- 0.17, n=5	0.9 +/- 0.13, n=5
	CS-10	0.92 +/- 0.2, n=8	1.05 +/- 0.15, n=8	**1.22 +/- 0.15, n=8 ***
	LSS-20	1.32 +/- 0.39, n=6	**0.38 +/- 0.03, n=6 ***	1.02 +/- 0.19, n=6

4.3.2.6 Osteoblast-related gene expression

The average RQ values ± SD for osteoblast-related genes are depicted in **Table 4.13**. Alkaline phosphatase expression tended to be increased by mechanical stimulation, with the exception of CS at 24 hours, which has a significant downregulation ($p<0.05$). The osteo-inductor BMP2 was significantly upregulated for CS at 24 hours ($p<0.05$) and 3 days ($p<0.05$). LSS showed some increased expression ($p<0.10$) early on at 24 hours for all osteoblast-related genes except osteocalcin, which was significantly downregulated ($p<0.05$) at 24 hours and 3 days. Alkaline phosphatase and osteopontin were increased ($p<0.10$) and decreased ($p<0.10$), respectively, by CP at 24 hours. Although osteopontin expression was increased for CS at 24 hours ($p<0.05$) and 3 days (biologically, but not statistically), the late osteoblast marker, osteocalcin showed no change at either time point.

Table 4.13: Fold changes in osteoblast-related gene expression relative to control for each component of the Mechanical Panel. Green and red highlights indicate an average fold change greater than 1.3 or less than 0.7 (considered biologically relevant), respectively. Data are presented as the mean ± SD with sample numbers. + p<0.10, *p<0.05 vs. controls.

		Osteoblast			
Time	Stimulus	Alkaline Phosphatase	BMP2	Osteocalcin	Osteopontin
24 Hours	CP-120	**2.45 +/- 1.51, n=6 +**	1.06 +/- 0.26, n=6	0.88 +/- 0.29, n=6	**0.68 +/- 0.39, n=6 +**
	CS-10	**0.63 +/- 0.11, n=6 ***	**2.16 +/- 0.79, n=6 ***	0.87 +/- 0.33, n=6	**1.68 +/- 0.53, n=6 ***
	LSS-20	**2.73 +/- 1.05, n=6 ***	**2.19 +/- 1, n=6 ***	**0.49 +/- 0.35, n=6 ***	**2.21 +/- 1.36, n=6 +**
3 Days	CP-120	3.28 +/- 3.1, n=5	1.26 +/- 0.57, n=5	**0.87 +/- 0.12, n=5 +**	1.51 +/- 0.65, n=5
	CS-10	1.39 +/- 0.7, n=8	**1.56 +/- 0.63, n=8 ***	0.95 +/- 0.26, n=8	1.36 +/- 0.8, n=8
	LSS-20	7.58 +/- 8.78, n=6	1.43 +/- 0.86, n=6	**0.31 +/- 0.14, n=6 ***	1.06 +/- 0.99, n=6

4.3.2.7 Chondrocyte-related gene expression

The average RQ values ± SD for chondrocyte-related genes are depicted in **Table 4.14**. LSS was the only stimulus that showed statistically significant downregulation of aggrecan at both 24 hours ($p<0.10$) and 3 days ($p<0.05$). These results are consistent with the 5 days data for LSS-20 (see **Table 3.11**). The expression of collagen II, on the other hand, was extremely variable, due to the fact that no control sample ever registered a C_T value and several of the Mechanical Panel samples also failed achieve adequate signal for a C_T value (note n=1 or 2 although at least y6 experiments were interrogated). Only CP and CS at 24 hours showed statistically significant ($p<0.05$) for the 3 samples that registered transcripts.

Table 4.14: Fold changes in chondrocyte-related gene expression relative to control for each component of the Mechanical Panel. Green and red highlights indicate an average fold change greater than 1.3 or less than 0.7 (considered biologically relevant), respectively. Data are presented as the mean ± SD with sample numbers. + p<0.10, *p<0.05 vs. controls.

		Chondrocyte	
Time	**Stimulus**	**Aggrecan**	**Collagen II**
24 Hours	CP-120	1.04 +/- 0.14, n=6	**7.7 +/- 0.51, n=3 ***
	CS-10	0.67 +/- 0.54, n=6	**14.91 +/- 4, n=3 ***
	LSS-20	**0.8 +/- 0.18, n=6 ***	38.33 +/- 15.64, n=2
3 Days	CP-120	1.08 +/- 0.2, n=5	143.02 +/- 196.32, n=2
	CS-10	1.05 +/- 0.25, n=8	32.17 +/- 0, n=1
	LSS-20	**0.52 +/- 0.24, n=6 ***	72.5 +/- 91.86, n=3

4.3.2.8 Adipocyte-related gene expression

The average RQ values ± SD for the adipocyte-related gene PPAR-γ are depicted in **Table 4.15.** No statistically significant changes in PPAR-γ were detected, although on average, RQ values tended to increase 3 days under LSS.

Table 4.15: Fold changes in PPAR-γ expression relative to control for each component of the Mechanical Panel. Green and red highlights indicate an average fold change greater than 1.3 or less than 0.7 (considered biologically relevant), respectively. Data are presented as the mean ± SD with sample numbers. No significant differences were found compared to controls.

		Adipocyte
Time	**Stimulus**	**PPAR-γ**
24 Hours	CP-120	0.94 +/- 0.25, n=6
	CS-10	0.97 +/- 0.36, n=6
	LSS-20	0.97 +/- 0.74, n=6
3 Days	CP-120	1.18 +/- 0.44, n=5
	CS-10	1.09 +/- 0.22, n=8
	LSS-20	1.33 +/- 0.68, n=6

4.3.2.9 Proliferation-related gene expression

The average RQ values ± SD for the proliferation-related gene cyclin B1 are depicted in **Table 4.16**. Cyclin B1, which is part of the control mechanism for the G2/M transition in the cell cycle [662], was a newly added gene to the TLDA to assess cell cycle regulation changes that may have been occurring under mechanical stimulation. At 24 hours, both CP and LSS demonstrated a statistically significant ($p<0.05$) downregulation of cyclin B1. The drop was most severe under LSS ($p<0.01$ compared CP) and persisted through 3 days, while CP returned

to baseline values. CS showed no change at 24 hours, and a statistically significant ($p<0.05$) increase in cyclin B1 expression at 3 days.

Table 4.16: Fold changes in cyclin B1-related gene expression relative to control for each component of the Mechanical Panel. Green and red highlights indicate an average fold change greater than 1.3 or less than 0.7 (considered biologically relevant), respectively. Data are presented as the mean ± SD with sample numbers. + $p<0.10$, *$p<0.05$ vs. controls.

		Proliferation
Time	**Stimulus**	**CyclinB1**
24 Hours	CP-120	**0.55 +/- 0.13, n=6 ***
	CS-10	0.89 +/- 0.7, n=6
	LSS-20	**0.04 +/- 0.03, n=6 ***
3 Days	CP-120	0.94 +/- 0.4, n=5
	CS-10	**1.58 +/- 0.41, n=8 ***
	LSS-20	**0.04 +/- 0.03, n=6 ***

4.3.3 Protein expression

The following section describes our results with the calponin, which was the only antibody we were able to successfully detect by Western blot, despite several attempts and troubleshooting procedures for the other endpoints. Representative images and descriptions for our attempts at detecting SMA, SMMHC, flk-1 and PECAM are found in **Appendix J**.

4.3.3.1 Calponin

Calponin expression in the 24 hour and 3 day Mechanical Panel experiments was confirmed by Western blotting as shown in **Figure 4.2**. Following successful probing, the membrane was stripped and reprobed for GAPDH as an endogenous loading control. GAPDH was deemed suitable as a protein loading control based upon our PCR endogenous control study (see Section 4.3.1). Each band was measured by densitometry, and the integrated optical density for calponin was normalized by the integrated optical density for GAPDH in that lane followed by normalization to the control sample for that experiment. The average fold-change ± SD for calponin at 24 hours and 3 days is depicted in **Figure 4.3**. Although the high variability in the data limited our ability to detect statistical differences, there was a significant decreased ($p<0.05$) for LSS at 3 days compared to controls and CS at 3 days.

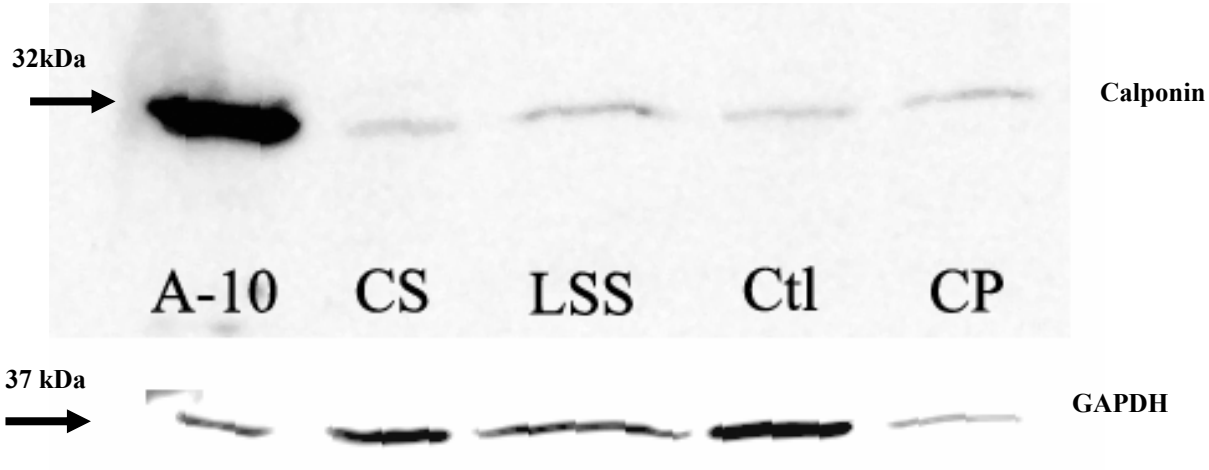

Figure 4.2: Western blot stained for calponin (upper band) with 40µg of the A-10 cell lysate serving as a positive control. The membrane was stripped and reprobed for GAPDH (lower band) to serve as an endogenous loading control.

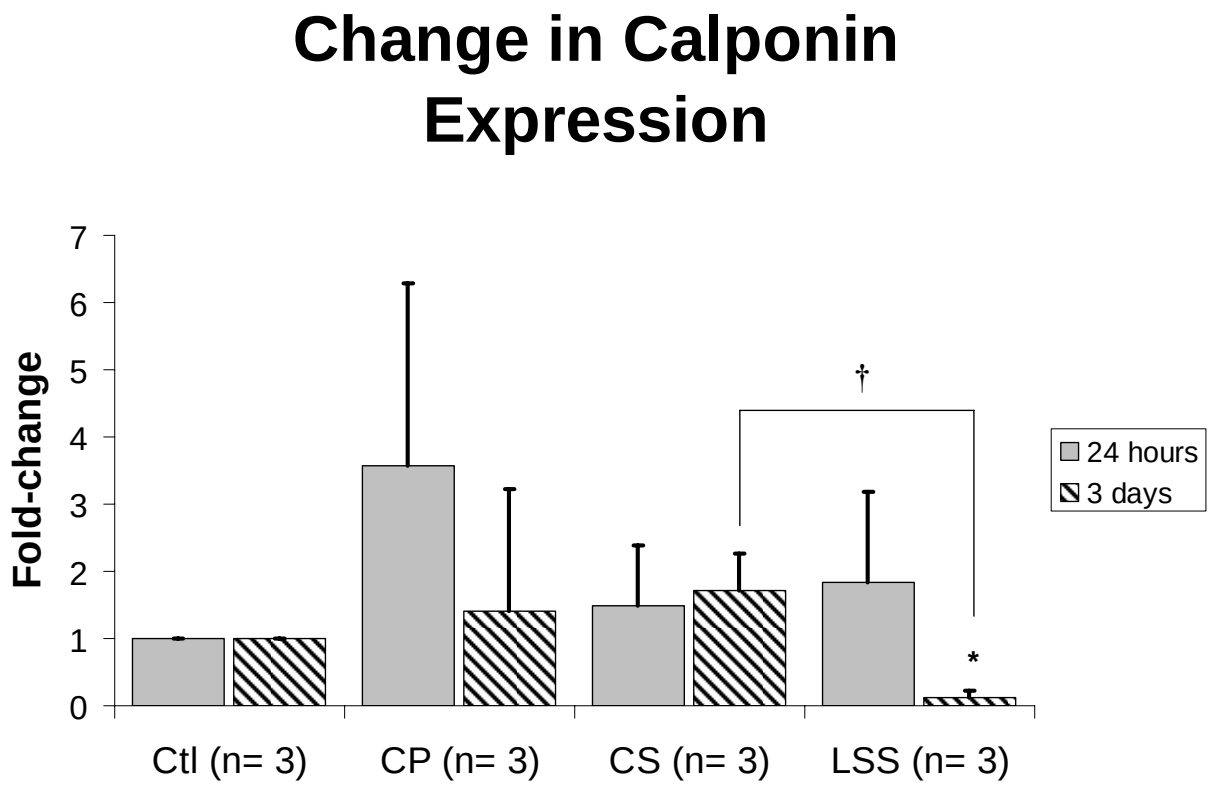

Figure 4.3: Time-dependent changes in calponin expression in tBMMSCs following mechanical stimulation. Data are presented as the mean ± SD. † $p<0.05$ compared to CS and *$p<0.05$ compared to controls.

4.4 DISCUSSION

4.4.1 The importance of choosing an appropriate endogenous control gene

The results of our endogenous control gene test using experimental samples confirmed our earlier concern over the gene expression results from our initial Mechanical Panel experiments. We were able to definitively prove that 18s, which we had previously used as the endogenous control, was the2nd least stable gene by the GeNorm analysis (**Figure 4.1**), and had the highest computed variance in addition to having an average C_T (**Table 4.7**) which was more than 10

cycles below our the C_T values for the other target genes in our TLDAs. Based upon the current opinion in the literature [657, 658, 663], our erroneous utilization of 18s as the endogenous control gene likely diminished our ability to distinguish with any certainty the relative change in expression for the 5 day experiments (see Section 3.3.6). For example, looking at one experiment using either 18s or Gusb as the endogenous control alters the RQ value between -27% and 88% (see Error! Reference source not found.), which could completely alter the interpretation of the data. In order to rectify this to provide a more meaningful representation of the gene expression changes in the 5 day experiments, individual RT-PCR reactions with 18s and Gusb on the any remaining samples of cDNA from the experiments performed in Chapter 3.0 should be performed. By performing these single reactions, we hypothesize a correction factor equivalent to average C_T value of Gusb for the previous TLDAs can be computed according to:

$$\frac{18s_{single}}{Gusb_{single}} \overset{?}{\cong} \frac{18s_{TLDA}}{Gusb^{*}_{TLDA}} \tag{4.1}$$

where $18s_{single}$ and $Gusb_{single}$ are the average C_T values from the single RT-PCR reactions, $18s_{TLDA}$ is the C_T value from the TLDA, and $Gusb^{*}_{TLDA}$ is the hypothetical C_T value for Gusb on the same TLDA as $18s_{TLDA}$.

We will validate this hypothesis by performing the calculation in **Equation (4.1)** using the current TLDA configuration, which has both 18s and Gusb as target genes, and additional single reactions with 18s and Gusb on the same cDNA loaded into the TLDA. If we can correctly reproduce the TLDA results using this technique, we should be able to more accurately re-analyze the results from our initial TLDA assays.

4.4.2 Temporal changes in gene expression

Expanding upon our 5 day data, we have demonstrated that that mechanical stimulation can alter the phenotypic gene expression of BMMSCs in a time-dependent manner. A summary of our results, broken down by gene group, is found in **Table 4.17**.

Table 4.17: Summary of the changes in gene expression for phenotypic groups by mechanical stimulation. To give some global sense to the data, a change index (CI) was calculated by averaging a score of 0 for no change, +/- 1 for a biological or statistical ($p<0.1$) trend, and +/- 2 for a biologically relevant and statistically significant change for each of the genes in that category. ↑↑ and ↓↓ indicate a majority increase or decrease ($CI>0.75$) in the overall gene expression for that group from control values. Single arrows denote a moderate change ($0.25\leq CI\leq 0.75$) in the majority of the genes for a particular phenotype, and ↔ indicates no change ($CI<0.25$).

Gene Group	Cyclic Pressure		Shear Stress		Cyclic Stretch	
	24 hours	3 days	24 hours	3 days	24 hours	3 days
Muscle	↓	↓	↓	↓↓	↓	↑↑
Endothelial	↑	↑	↑	↑	↓	↔
Bone	↔	↑	↑↑	↔	↑	↑↑
Cartilage	↑↑	↑	↔	↓	↑	↑
Fat	↔	↔	↔	↑	↔	↔
Growth Factor	↑↑	↔	↑↑	↑↑	↔	↔
ECM	↑↑	↔	↑↑	↑	↓	↑
Stem Cell	↓	↔	↑	↓	↑	↑
Proliferation	↓↓	↔	↓↓	↓↓	↔	↑↑

In general, LSS and CP seemed to downregulate muscle-related genes. These results are contrast to other results reported by Kobayashi et al.[530] who found that shear stress and pressure-dominated shear stress increased the protein expression of SMA and SMMHC. We were not able to assay for these particular genes in our TLDA format, but based upon the decreased expression of myocardin, which is necessary for nearly all SMC proteins, including SM22α, SMA, caldesmon, calponin, and SM-MHC [62, 105-107], we can hypothesize that that these

genes and/or proteins would also be diminished by LSS and CP. Furthermore, our gene results in these studies are in agreement with our 5 day stimulation data in that LSS and CP failed to demonstrate staining for SMA, calponin, or SMMHC by IHC (see **Figure 3.16**, **Figure 3.17**, and **Figure 3.18**). The expression of two muscle-related genes, myocardin and desmin, was initially unchanged by CS at 24 hours, and then upregulated ($p<0.1$ and $p<0.05$) at 3 days. Similarly, gene expression for SM22α following the application of CS also trends downward (although not statistically significant) in the first 24 hours and then returns to control levels at 3 days. These trends are somewhat in contrast to previously reported data from Park et al.[527] who reported a transient increase in SM22α for BMMSCs on collagen exposed to 10% CS at 24 hours followed by a return to baseline levels. The authors attributed this decrease in muscle gene expression to the migration of the BMMSCs to a perpendicular position, effectively shielding them from the uniaxial stretch. Subsequent studies forcing the alignment of BMMSCs in the direction of stretch showed that calponin expression could be maintained at a higher level than BMMSCs allowed to re-orient perpendicular to the direction of stretch. However, despite the re-orientation, calponin was significantly increased over the controls [558]. Our laboratory also has evidence to support this, showing that SMA and calponin expression are induced by static stress and cyclic stretch in tBMMSCs aligned parallel to the direction of stress and stretch in a 3-dimensional fibrin construct [557]. In addition we also have published data showing that despite perpendicular alignment, expression of SMA and calponin are maintained after 7 days [526] of cyclic stretch. Our current data at these early time points indicates a trend of decreased muscle-related gene expression in the 24 hour period followed by a return to baseline levels in CS. The return of SM22α to baseline levels may be a result of the increasing levels of myocardin, which should precede changes in expression of the other SMC proteins that under the same promotional

control [62]. However, caldesmon expression was not affected by mechanical stimulation in a similar manner as myocardin and SM22α, which is inconsistent with its transcriptional control by myocardin.

Overall changes in endothelial-related gene expression tended to be increased by both CP and LSS at 24 hours and 3 days. Conversely, CS stimulation started with a trend towards downregulation at 24 hours and then increased to control levels at 3 days. CP and LSS demonstrated expression of both E-selectin and iNOS, two genes which typically have had little or no detectable expression under control and CS conditions, leading us to hypothesize that the BMMSCs are becoming more endothelial-like. This is supported by our evidence that two of the most consistently upregulated genes by LSS and CP were vWF and PECAM, which are associated with more mature ECs. However, we have thus far been unable to detect either of these proteins by IHC in the 5 day experiments (see **Figure 3.20** and **Figure 3.21**), and have not been able to detect PECAM by Western blot (see **Appendix J**). Furthermore, gene expression for vWF, which was also investigated at 5 days, was upregulated under CP but strongly downregulated under LSS (see **Table 3.6**). We hypothesize that this change in the LSS from the 5 day experiments to the 24 hour and 3 day experiments may be a result of the state of confluence of the cells since CP at 5 days were confluent (see Coomassie Blue images in **Figure 3.6**), and had increased vWF gene expression (see **Table 3.6**). Likewise, for these temporal changes in gene expression, the experiments were begun at confluence, and we subsequently detected increases in vWF and PECAM gene expression under both CP and LSS. Our endothelial-related gene expression results are in agreement with other work by Yamamoto et al. [567] and Wang et al. [568] who found similar increases in endothelial gene expression for embryonic stem cells. However, flk-1 expression did not follow these trends for our BMMSCs.

Like the previous 5 day data, flk-1 gene expression was decreased for both CP and LSS at 3 days, which is in contrast to the shear stress studies for the embryonic stem cells [567, 568].

The expression of growth factors, including VEGF-A, was consistently upregulated by LSS at 24 hours and 3 days in a manner similar to our previous 5 day data. Similar results for the regulation of VEGF have been shown for embryonic stem cells [568] and vascular endothelial cells [308] exposed to shear stresses similar in magnitude to that used in our study. However, under lower shear stress (5 dynes/cm^2), Yamamoto et al. [567] found no changes in VEGF expression, which is similar to our 5 day data (see **Table 3.6**). Despite the increases in both TGF-β and VEGF-A under LSS, their receptors (endoglin and flk-1) were downregulated under shear stress. Given that a positive-feedback loops have been shown to exist between TGF-β and endoglin [664-666], the downregulation of endoglin in conjunction with the upregulation of TGF-β in our LSS studies may be indicating that although the BMMSCs are increasing their expression of the growth factor, they are not receiving any signaling from their receptors as a result of the convection and dilution of these factors away from the cells.

The expression of ECM genes under mechanical stimulation at 24 hours and 3 days provided some departure from the expression levels detected in the subconfluent cultures at 5 days. Most striking was the increase in expression of elastin under LSS, which we had previously found downregulated at 5 days (see **Table 3.8**). This too may be a function of the presence of a confluent monolayer of cells. In the developing artery, elastin mRNA expression has been spatially correlated to the presence of TGF-β [667]. The increased TGF-β gene expression also seen under LSS seems to support this type of mechanism, but the concurrent decrease in endoglin expression seems to point to a lack of TGF-β signaling in the cells. However, without evidence of localized TGF-β protein or increased downstream messengers

such as the SMAD complexes [668, 669], we can only speculate about the mechanisms involved. LSS continued to upregulate expression of other ECM genes, including collagen I and III. CS also increased collagen III expression at 24 hours and 3 days, and downregulated elastin production at 24 hours. The increase in collagen III gene expression is contrary to that reported by Park et al. [527] who found no change in collagen III expression from CS, but the decrease in elastin expression was similar to what we found for CS-10 at 5 days of stimulation. Other research examining the response of BMMSCs to mechanical loading has found increased collagen III similar to that found with mechanical stimulation of heart valve interstitial cells [561] and tissue-engineered ligaments [507].

The expression of bone- and chondrocyte-related genes by BMMSCs under mechanical stimulation was relatively inconclusive. Alkaline phosphatase gene expression seemed to be increased by mechanical stimulation in general, but there was a significant downregulation by CS at 24 hours. Alkaline phosphatase, which is expressed in high levels by BMMSCs, has been reported to diminish with differentiation [551]. Other osteoblast genes, including osteocalcin and osteopontin, have previously been reported to increase in stromal cells under extremely low levels of shear stress (0.27 – 2.5 dynes/cm^2) [572, 573], but under our 20 dyens/cm^2 shear, we found them to be significantly downregulated at 3 days, and our 5 day data seems to indicate a decrease in osteoblast gene expression at all levels of LSS tested (1-20 dynes/cm^2). Osteopontin gene expression by BMMSCs under CS was significantly elevated at 24 hours and remained elevated, but not statistically significant, at 3 days. Although previous reports on gene expression in BMMSCs have indicated that no transcripts for osteopontin should be detected in non-osteoblast differentiated BMMSCs [551], osteopontin mRNA has been detected in a variety of other cells including vascular SMCs and ECs, with implications for atherosclerosis [670-672].

The presence of osteopontin in other cell types has also been attributed to its potential role in cell adhesion because it contains the Arg-Gly-Asp-Ser adhesion molecule which is capable of binding fibronectin [673, 674].

Because our time course experiments were conducted at confluence, our previous methods of assessing proliferation were not feasible. Therefore, we added cyclin B1 to the TLDA to detect changes in proliferation as a result of mechanical stimulation. Cyclin B1 has been used for this purpose previously [662, 675], and more recently the similar study by Kurpinski et al.[558], where they demonstrated an increase in cyclin B1 expression as a result of CS. Our data also indicate a significant increase in cyclin B1 expression following exposure to CS at 3 days. In agreement with our nuclear counting data at 5 days, LSS was a strong downregulator of cyclin B1 expression, effectively arresting the cell in the G2/M phase of the cell cycle. Similar results have been shown for ECs under laminar shear stress [649, 676, 677]. Cyclin B1 was also transiently decreased at 24 hours by CP before returning to baseline levels at 3 days. This was surprising given our previous 5 day data indicating that CP induced large increases (>2.5 fold; see **Figure 3.14**) in cell number. There is other evidence in the literature that CP increases proliferation in bone marrow derived cells as well as ECs, SMCs, and chondrocytes [1, 225, 228, 386, 394, 577, 645]. More recently, mechanisms involving VEGF [394] and the PI3k/Akt pathway [645] have been proposed as potential mediators for increased proliferation. Our results may suggest that contact inhibition of the BMMSCs played a more dominant role in their cell cycle progression, which is in contrast to the effect of pressure on aortic ECs that lose their contact inhibition in the presence of pressure [396]. It is possible that the arrest at the G2/M phase of the cell cycle may be a result of other paracrine signals previously unavailable to the BMMSC, which were only just reaching confluence in the 5 day

experiments. Further studies utilizing other markers of proliferation should be undertaken to obtain a more accurate proliferation profile of these cells.

4.4.3 Temporal changes in calponin expression

Our results for the Western blotting of calponin demonstrate that calponin is expressed in confluent cultures of tBMMSCs on collagen. On average calponin expression in the controls was approximately 7.5 fold less than fully differentiated stem cells. And only LSS at 3 days showed significant decreases compared to controls and CS. The calponin expression as measured by densitometry was highly variable; sometimes being upregulated by mechanical stimulation, and other times downregulated. In one instance, the control sample measured 1.5-fold more calponin than the positive control. These results are highly perplexing given our previous IHC results (see **Figure 3.17** and previous studies [526, 557]). However, Western blot results from other cells types including platelets and fibroblasts have shown positive staining for calponin [81]. In addition, groups studying the effects of stretch have demonstrated that calponin is expressed in control cultures of stem cells [558, 647], and IHC data on BMMSCs has shown calponin staining in a diffuse pattern which does not coincide with its role as an actin binding protein [678]. It has also been well-documented that BMMSCs tend to acquire SMC-like cytoskeletal proteins in long-term culture, which typically involves growth to confluence and beyond [528, 552, 679]. Therefore, in our cultures starting at confluence on a collagen surface, it is not inconceivable that calponin expression developed in the 3-5 days of experiment time. In addition to the sometimes high level of expression of calponin in the control samples, the lack of change in calponin expression following CS was troubling in light of our previous results (see [526] and **Figure 3.17**). However, the change in SMC protein expression in response to

mechanical stimulation has been reported both as increased [526, 527, 530, 557, 558, 569, 650] and decreased [527, 647] depending upon cell source and type of stretch (uniaxial vs. equiaxial). Yet, despite occasional results that seem to contradict each other, the majority of research continues to point to the increase in SMC protein expression in stem cells as a result of cyclic stretch.

4.4.4 Limitations

Although the use of confluent cultures in our Mechanical Panel system provided a more physiologically relevant milleu for paracrine and cell-cell signaling, and generated more available RNA for our gene expression studies, our ability to detect subsequent protein expression by Western blot continued to be hampered by low yields. Several experiments could not be analyzed by Western blotting because one or more samples with high RNA content yielded less than 50μg of protein. These issues may be a result of the use of Trizol™ to extract the RNA and protein from our experiments. As part of the extraction process, proteins are precipitated by alcohol, washed several times in a high-alcohol solution, and finally dried. This dried protein pellet required extensive work at >50^{o}C with our protein resuspension buffer. Often, one or more samples within an experimental group did not fully resuspend, suggesting the possibility that we may in effect have left out many of the highly hydrophobic membrane proteins such as PECAM and flk-1, as well as other intracellular high molecular weight proteins including myosin heavy chain. Future studies may have to rely on separate extraction techniques, one for protein and one for RNA, or increase the amount of detergent to 1% or higher. Other possibilities may be that these membrane-bound proteins make up a very small fraction of the total protein, potentially requiring immunoprecipitation for successful Western

blotting, or that our transfer protocols are inefficient for the high molecular weight proteins (e.g., SMMHC; see **Appendix J.2**).

Another limitation in the interpretation of this data was the high variability in the Western blotting results for calponin. There was an inconsistent level of expression of calponin in the control cultures, despite utilizing cells from the same lot that were within a 3-4 passages of each other and culturing the cells in the same lot of FBS. Furthermore, there were no distinguishing signs throughout the culture periods leading up to the experiments that may have indicated the tBMMSCs were abnormal in any way. One possible explanation again points to the protein extraction technique, which had variable success in solubilizing the dehydrated protein from the Trizol^{TM} extraction. This could have effectively limited our ability to determine real changes in protein expression between the 4 arms of the Mechanical Panel.

4.5 CONCLUSION

We have continued our exploration of the response of BMMSCs to mechanical stimulation using our unique Mechanical Panel approach to follow the temporal changes in gene and protein expression. Using confluent cultures of BMMSCs in an attempt to create a more physiologic signaling environment as well as enable us to obtain enough biologic material for RNA and protein analysis, we have determined that LSS and CP tend to upregulate the expression of several EC-related genes at 24 hours and 3 days. This is the first indication we have that our BMMSCs are capable of EC differentiation. Unfortunately, we were unable to detect subsequent protein expression for flk-1 and PECAM by Western blotting but are encouraged enough by the gene expression data to continue these studies. Our data for CS at 24 hours seems to indicate a

decrease in muscle-related protein expression, but by 3 days, several genes including cardiac troponin, desmin, and myocardin were becoming more prominent, suggesting that the cells are potentially entering a myofibroblast phenotype. Perhaps given further cues including biochemical stimulation such as TGF-β [647, 650], BMMSCs under mechanical stimulation may continue down the path towards functional SMCs and ECs, which would provide important steps forward for vascular tissue engineering.

5.0 LINEAGE COMMITMENT FOLLOWING MECHANICAL STIMULATION

5.1 INTRODUCTION

Another important issue with stem cell research is the lineage commitment of the cells following their initial differentiation. It has been well documented that SMCs, which exist in a highly mechanically dynamic environment, alter the expression of genes and proteins associated with their mature phenotype upon static culture *in vitro* [189, 196-198]. This type of phenotypic alteration raises the question of whether stem cells, once differentiated into a particular lineage by chemical or mechanical means, can maintain their commitment to that lineage should they experience withdrawal of those stimuli. This is of particular importance in cell therapy applications where these tissue-committed cells may find their way into an unintended tissue bed. Experiments performed to address Specific Aim 4 were designed to test whether tBMMSCs exposed to cyclic stretch could maintain their differentiated state following withdrawal of the stimulus, or if they would return to their baseline levels of gene and protein expression.

5.2 METHODS

5.2.1 Experimental Design

For each experiment, tBMMSCs were obtained as described in Section 3.2.1 and seeded at confluence (21,000 cells/cm^2) onto 3 collagen I coated BioFlex™ (Flexcell) deformable substrates. After 48 hours of pre-culture, two BioFlex™ plates were exposed to 10% cyclic stretch at 1 Hz (CS-10) and one to static control conditions for 3 days. After 3 days, the control and one of the cyclically stretched BioFlex™ plates were removed and processed for RNA and protein endpoints (see Section 4.2.2). The second plate of the cyclically stretched tBMMSCs was placed back in static culture for an additional 3 days (DeDiff) before being processed for RNA and protein endpoints as described in Section 4.2.2.

5.3 RESULTS

5.3.1 Gene expression

5.3.1.1 Muscle related genes

The average RQ values ± SD for muscle-related genes are depicted in **Table 5.1**. No statistically significant differences from control values were detected, with only a trend ($p<0.1$) towards decreased expression present for caldesmon under CS-10 that may not be biologically relevant. Although the high variance, particularly with the DeDiff samples, precludes statistical significance, cardiac troponin was increased on average in both CS-10 and DeDiff samples.

Gene expression for caldesmon in the DeDiff samples was significantly ($p<0.05$) higher than CS-10 as a result of the extended static culture time. However, caldesmon expression for DeDiff samples was not different from the 3 day control values.

Table 5.1: Fold changes in muscle-related gene expression relative to control for CS or DeDiff samples. Green highlights indicate an average fold change greater than 1.3 (considered biologically relevant). Data are presented as the mean ± SD with sample numbers. +$p<0.10$, vs. controls.

	Muscle		
Stimulus	**Caldesmon**	**Cardiac Troponin**	**Desmin**
CS-10	**0.88 +/- 0.06, n=3 +**	1.37 +/- 0.27, n=3	1.82 +/- 0.61, n=3
DeDiff	1.19 +/- 0.13, n=3	1.66 +/- 1.06, n=3	1.27 +/- 0.36, n=3

	Muscle	
Stimulus	**Myocardin**	**SM22α**
CS-10	1.24 +/- 0.2, n=3	0.91 +/- 0.22, n=3
DeDiff	0.92 +/- 0.26, n=3	1.04 +/- 0.24, n=3

5.3.1.2 Endothelial Related Genes

The average RQ values ± SD for endothelial-related genes are depicted in **Table 5.2**. Compared to controls, only endoglin and flk-1 showed any statistically relevant change with downregulation of endoglin ($p<0.05$) and upregulation of flk-1 ($p<0.1$) in CS-10. Other EC-related genes showing biologically relevant changes included CD133, E-selectin, and iNOS, each appearing to be increased on average. As evident from the SD values, there was large variability in both E-selectin and iNOS, which was a result of the failure of one of the control samples to register a detectable signal. The other two samples which did have corresponding controls that

registered showed a downregulation for CS-10 (RQ=0.44 ± 0.47) and no change for DeDiff (RQ=0.89 ± 1.17) compared to the controls. Comparisons between CS-10 and DeDiff did, however, reveal a significant decrease in flk-1 ($p<0.05$) with the extended static culture time.

Table 5.2: Fold changes in endothelial-related gene expression relative to control for CS and DeDiff samples. Green and red highlights indicate an average fold change greater than 1.3 or less than 0.7 (considered biologically relevant), respectively. Data are presented as the mean ± SD with sample numbers. + $p<0.10$, *$p<0.05$ vs. controls.

	Endothelial			
Stimulus	**CD133**	**Endoglin**	**E-Selectin**	**vWF**
CS-10	1.39 +/- 0.86, n=3	**0.57 +/- 0.11, n=3 ***	12.76 +/- 21.34, n=3	1.14 +/- 0.13, n=3
DeDiff	2.03 +/- 1.7, n=3	0.87 +/- 0.76, n=3	4.8 +/- 6.82, n=3	1.07 +/- 0.2, n=3

	Endothelial		
Stimulus	**iNOS**	**PECAM**	**Flk-1**
CS-10	7.61 +/- 8.89, n=2	1.28 +/- 1.15, n=3	**2.13 +/- 0.61, n=3 +**
DeDiff	42.32 +/- 56.75, n=2	1.23 +/- 0.79, n=3	0.79 +/- 0.59, n=3

5.3.1.3 Soluble factor -related genes

The average RQ values ± SD for soluble factor-related genes are depicted in **Table 5.3**. No statistical differences were evident for any of the 3 genes interrogated compared to the controls. On average, DeDiff was slightly elevated compared to controls for FGF-2 and TGF-β, and did show statistically a significant increase in TGF-β ($p<0.05$) compared to CS-10.

Table 5.3: Fold changes in soluble factor-related gene expression relative to control for CS and DeDiff samples. Green highlights indicate an average fold change greater than 1.3 (considered biologically relevant). Data are presented as the mean ± SD with sample numbers. No statistically significant differences were found for CS-10 or DeDiff when compared to controls.

	Soluble Factor		
Stimulus	**FGF2**	**TGF-β**	**VEGF-A**
CS-10	1.05 +/- 0.07, n=3	0.94 +/- 0.06, n=3	0.89 +/- 0.13, n=3
DeDiff	1.95 +/- 1.05, n=3	1.39 +/- 0.31, n=3	1.02 +/- 0.34, n=3

5.3.1.4 Extracellular matrix-related gene expression

The average RQ values ± SD for ECM-related genes are depicted in **Table 5.4**. No statistically significant differences were detected compared to controls. As in previous samples (see **Table 3.8** and **Table 4.11**), collagen IV was highly variable as a result of only one control sample registering a detectable signal. In that single instance, collagen IV was strongly downregulated by CS-10 (RQ=0.24) and even further downregulated by DeDiff (RQ=0.02). Comparisons between CS-10 and DeDiff did not reveal any significant changes with the added static culture time.

Table 5.4: Fold changes in extracellular matrix-related gene expression relative to control for CS and DeDiff samples. Green and red highlights indicate an average fold change greater than 1.3 or less than 0.7 (considered biologically relevant), respectively. Data are presented as the mean ± SD with sample numbers. No statistically significant differences were found for CS-10 or DeDiff when compared to controls.

	Matrix			
Stimulus	**Collagen I**	**Collagen III**	**Collagen IV**	**Elastin**
CS-10	0.93 +/- 0.4, n=3	1.16 +/- 0.11, n=3	23.87 +/- 33.42, n=2	1.07 +/- 0.96, n=3
DeDiff	1.24 +/- 0.56, n=3	1.41 +/- 0.4, n=3	8.68 +/- 12.25, n=2	0.67 +/- 0.49, n=3

5.3.1.5 Stem-cell related gene expression

The average RQ values ± SD for stem cell-related genes are depicted in **Table 5.5**. CS-10 showed the only statistically significant change ($p<0.05$) in stem cell markers by slightly upregulating vimentin expression compared to controls, but vimentin expression was not statistically different between CS-10 and DeDiff.

Table 5.5: Fold changes in stem cell-related gene expression relative to control for CS and DeDiff samples. Green highlights indicate an average fold change greater than 1.3 (considered biologically relevant). Data are presented as the mean ± SD with sample numbers. *$p<0.05$ vs. controls.

	Stem Cell		
Stimulus	**CD59**	**CD90**	**Vimentin**
CS-10	0.95 +/- 0.31, n=3	1.04 +/- 0.25, n=3	**1.26 +/- 0.09, n=3 ***
DeDiff	0.93 +/- 0.4, n=3	1.01 +/- 0.25, n=3	1.37 +/- 0.22, n=3

5.3.1.6 Osteoblast-related gene expression

The average RQ values ± SD for osteoblast-related genes are depicted in **Table 5.6**. Of the genes assayed, only BMP2 showed a statistically significant increase under CS-10. There were no differences between CS-10 and DeDiff. Overall osteoblast gene expression tended to be increased for both samples compared to controls, but the variability was almost equal to or higher than the average change in most instances.

Table 5.6: Fold changes in osteoblast-related gene expression relative to control for CS and DeDiff samples. Green highlights indicate an average fold change greater than 1.3 (considered biologically relevant). Data are presented as the mean ± SD with sample numbers. *p<0.05 vs. controls.

	Osteoblast			
Stimulus	**Alkaline Phosphatase**	**BMP2**	**Osteocalcin**	**Osteopontin**
CS-10	1.55 +/- 1.23, n=3	**1.26 +/- 0.09, n=3 ***	0.93 +/- 0.24, n=3	1.83 +/- 1.19, n=3
DeDiff	2.33 +/- 3.23, n=3	1.87 +/- 1.78, n=3	1.39 +/- 0.73, n=3	4.27 +/- 3.93, n=3

5.3.1.7 Chondrocyte-related gene expression

The average RQ values ± SD for chondrocyte -related genes are depicted in **Table 5.7**. Similar to previous results, collagen II failed to interrogate in all the control samples and was only able to successfully be interrogated in separate experiments with CS-10 and DeDiff. No other statistically significant changes were evident, although a slight trend towards upregulation may be seen in aggrecan gene expression by the DeDiff sample.

Table 5.7: Fold changes in chondrocyte-related gene expression relative to control for CS and DeDiff samples. Green indicate an average fold change greater than 1.3 (considered biologically relevant). Data are presented as the mean ± SD with sample numbers. No statistically significant differences were found for CS-10 or DeDiff when compared to controls.

	Chondrocyte	
Stimulus	**Aggrecan**	**Collagen II**
CS-10	1.2 +/- 0.38, n=3	32.17 +/- 0, n=1
DeDiff	1.56 +/- 0.56, n=3	37.35 +/- 0, n=1

5.3.1.8 Adipocyte-related gene expression

The average RQ values ± SD for the adipocyte -related gene PPAR-γ are depicted in **Table 5.8**. No statistically significant changes in PPAR-γ were detected for either CS or DeDiff samples. However, there was a trend towards a downregulation of PPAR-γ by the extra time in control culture following CS ($p<0.1$).

Table 5.8: Fold changes in PPAR-γ expression relative to control for CS and DeDiff samples. Data are presented as the mean ± SD. No biologically relevant (±1.3 fold change) or statistically significant changes were found for CS-10 or DeDiff compared to controls.

	Adipocyte
Stimulus	**PPAR-γ**
CS-10	1.23 +/- 0.2, n=3
DeDiff	0.73 +/- 0.4, n=3

5.3.1.9 Proliferation-related gene expression

The average RQ values ± SD for cyclin B1 are depicted in **Table 5.9**. Similar to the previous 3 day data, there was a trend towards upregulation by CS-10, but the variability in DeDiff samples was much higher, with one DeDiff experiment showing a fairly strong upregulation (RQ=3.26) , and one experiment strongly downregulated (RQ=0.26). As a result, there was no difference between CS-10 and DeDiff samples.

Table 5.9: Fold changes in cyclin B1-related gene expression relative to control for CS and DeDiff samples. Green highlights indicate an average fold change greater than 1.3 (considered biologically relevant). Data are presented as the mean ± SD. No statistically significant differences were found for CS-10 or DeDiff when compared to controls.

	Proliferation
Stimulus	CyclinB1
CS-10	1.34 +/- 0.32, n=3
DeDiff	1.58 +/- 1.55, n=3

5.3.2 Protein expression

As a result of the previously-mentioned difficulties in performing Western blots on the higher molecular weigh proteins (PECAM, flk-1, SMMHC) and SMA (see Section 4.3.3), we were only able to obtain results for the stability of calponin expression following withdrawal of mechanical stimulation. Our results were again plagued by high variability for reasons alluded to in Section 4.4.4, and we did not find any statistically significant change in expression for any group. The average ± SD for normalized calponin expression is presented in **Figure 5.1.** Two Western blots

for calponin and GADPH blots are provided in **Figure 5.2** to highlight the general variability in calponin expression between experiments.

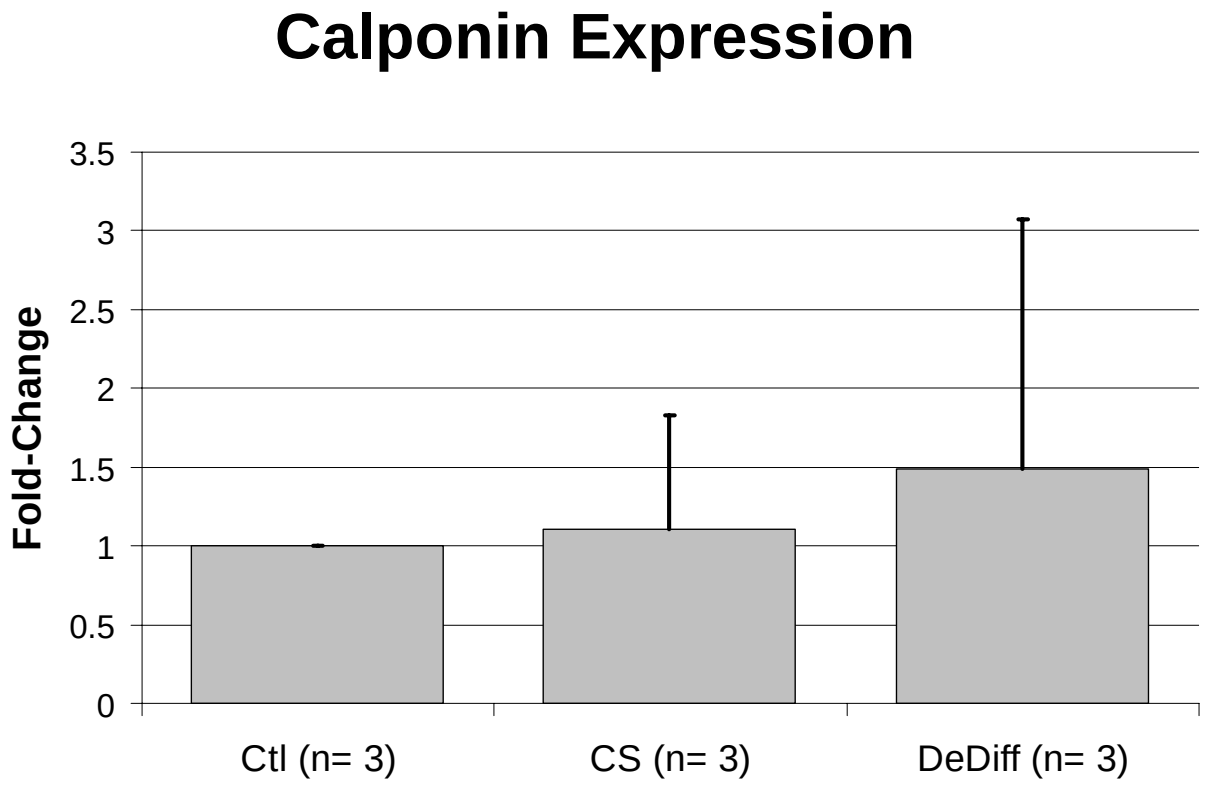

Figure 5.1: Changes in normalized calponin expression as determined by Western blot. Data are presented as the mean ± SD.

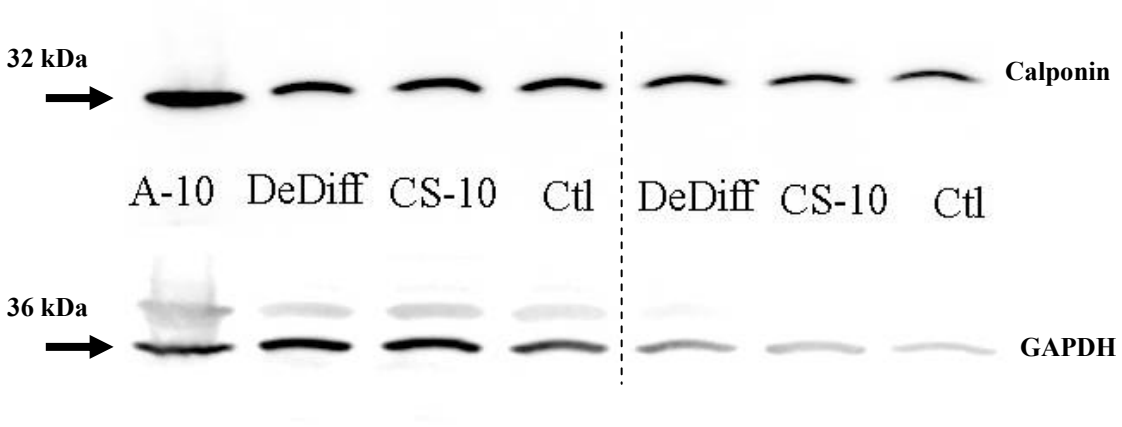

Figure 5.2: Representative Western blot for calponin (top) and GAPDH (bottom) for two experiments (separated by dashed line). A-10 cell lysates were used as a positive control.

5.4 DISCUSSION

Because one of the central questions in stem cell biology is whether these multipotential cells can maintain their phenotypic state following removal of the particular stimulus driving their differentiation, we investigated the changes in gene and protein expression that occurred from 3 days of static culture following 3 days of cyclic stretch. Using highly sensitive RT-PCR techniques that can examine multiple gene targets, we found just 3 of 30 target genes were altered by the cessation of mechanical stimulation in the tBMMSCs (summarized in **Table 5.10**). Although the removal of stretch appears to increase caldesmon gene expression compared to the cyclically stretched sample, the level of expression is in fact becoming closer control values; perhaps indicating that whatever changes were occurring in the tBMMSCs as a result of being cyclically stretched were being reversed. The reversal of increases in SMC-related protein expression following cyclic stretch has also been demonstrated in ECs [83].

The increases in caldesmon and TGF-β gene expression following mechanical stimulation may be linked together as TGF-β has consistently been linked to the increased expression of SMC proteins in other cell types including ECs [77, 78, 680] and various stem cell populations [149, 161, 647, 661]. This raises the possibility that with this potential TGF-β stimulation, caldesmon expression may continue to climb. Although our experimental variability precluded any statistical significance, this may be supported by the slight trend of increasing calponin expression starting with the control samples, and increasing through the DeDiff samples. Here, too, may be preliminary indications that TGF-β is playing a role in this post-stimulation time period to further drive the BMMSCs towards a myogenic lineage. Another possible role of TGF-β in this post-stimulation time frame may have been to modulate the flk-1 expression, which was previously elevated by CS-10. Similar to our finding of increased TGF-β and decreased flk-1 expression in the DeDiff samples, increases in TGF-β have been shown to lead to decreases in VEGF-A and flk-1 during developmental [681] and angiogenic [682, 683] processes.

Table 5.10: Summary of the statistically significant changes in gene expression following removal of the cyclic stretch stimulation in the tBMMSCs.

Gene Name (classification)	Change following removal of stimulation
Caldesmon (SMC)	↑
Flk-1 (EC)	↓
TGF-β (Growth factor)	↑

5.4.1 Limitations

Like the experiments discussed in Chapter 4.0, our investigation into the effects of stimulus withdrawal on the differentiation of tBMMSCs was impacted by our inability to completely solubilize the protein following Trizol^{TM} extraction of the RNA. As result, we were unable to investigate the higher molecular weight proteins that were of relevance to our study, namely SMMHC, PECAM, and flk-1. Furthermore, the protein data that we were able to generate was highly variable, making interpretations difficult. Concerning our experimental setup, while stopping the control and one CS sample at 3 days and placing a second CS sample back into static culture seemed like an ideal way to test the ability of the tBMMSCs to maintain their phenotype following mechanical stimulation, these experiments may have benefited from a second set samples that were in either CS or control conditions for the entire 6 days (plus 2 day pre-incubation) period of the experiment. This may have been able to shed more light on the eventual fate of the BMMSCs. Although some correlations to the 5 day data may be inferred, the starting cell density between the experiments was much too different to make any meaningful inferences. Additional methodologies which might better test the commitment of tBMMSCs would be additional subculture with the use of inductive media for adipogenic and osteogenic phenotype following the 3 days of rest after mechanical stimulation.

5.5 CONCLUSION

By examining the ability of the tBMMSC to maintain their gene and protein expression phenotype following the withdrawal of mechanical stimulation, we have attempted to provide

insight into one of the fundamental questions in stem cell biology, namely whether these cells, once guided towards a particular phenotype, will remain committed or have the ability to return towards their original stem cell state. Our results seem to indicate that removal of cyclic stretch did not alter gene expression in BMMSCs, as many of the gene endpoints did not show a significant change between CS and DeDiff cultures. However, the three genes that did show changes (see **Table 5.10**) seem to indicate progression towards myogenic differentiation in light of studies linking TGF-β expression to increases in SMC and decreases in EC gene expression, as well as the observed trend for increasing calponin protein expression (see **Figure 5.1**) in our experiments. Without statistical support, we can only hypothesize that myogenic differentiation is continuing following the removal of CS. Further tests will be necessary to confirm this observation.

6.0 DISCUSSION

6.1 SUMMARY OF RESULTS

We have developed a unique approach to investigating the role of mechanical stimulation for differentiation of stem cells through the Mechanical Panel. By utilizing simultaneous mechanical stimuli, we were able to effectively study the differential response to each stimulus while attempting to limit the effects of heterogeneity that exist in primary mesenchymal stem cells. A brief summary of each specific aim will be presented followed by comments on the general advantages and disadvantages of these studies. Finally, areas of future work will be discussed as they relate to our study findings.

6.1.1 Specific aim 1

In order for the proposed work utilizing the Mechanical Panel to move forward, we needed to develop a bioreactor capable of long-term application of cyclic hydrostatic pressure. We designed and built a versatile, compact bioreactor and used a constant pressure source with a simple oscillating valve on a variable timing circuit to create various magnitudes and frequencies of cyclic hydrostatic pressure. CFD analysis of a 2D model of our bioreactor demonstrated our system was completely hydrostatic, with no unanticipated shear stresses from the impinging air stream. A major problem limiting the use of cyclic pressure bioreactors for long-term cell

culture is caused by the need to cycle air into and out of the system, which disrupts the vapor pressure equilibrium over the culture media and drives evaporation. To address this, we utilized a heated passover humidifier to raise the water vapor content of the incoming air to the bioreactor to and limit the disruption in vapor pressure equilibrium in the bioreactor itself. The time-averaged vapor density of our system, which was calculated by measuring the mass of air and water consumed throughout the course of an experimental run, demonstrated our ability to maintain a properly humidified environment with a vapor density exceeding 45 g/L. We biologically validated our pressure bioreactor by demonstrating cell viability under cyclic hydrostatic pressure for up to 7 days with no increase in cell necrosis. In addition, we demonstrated that cyclic hydrostatic pressure can alter the morphology, proliferation, and differentiation of BMMSCs.

6.1.2 Specific Aim 2

The goal of specific aim 2 was to address our hypothesis that physiologically relevant applied mechanical stimulation can drive the differentiation of stem cells to specific phenotypes. We utilized our Mechanical Panel setup to differentially expose BMMSCs to three separate mechanical stimuli relevant to the vasculature. We varied the magnitudes and frequencies of these stimuli to determine potential dose-responses. Our results demonstrate that each stimulus differentially affects BMMSC morphology, proliferation, and gene and protein expression.

Morphologic changes in response to cyclic stretch were dependent upon the magnitude and frequency of stimulation, with higher magnitudes or frequencies generating a more elongated, spindle-shaped cell. Cyclic stretch at 1%, 1 Hz was found to increase proliferation, while higher magnitudes or frequencies did not appear to affect proliferation. Laminar shear

stress, on the other hand, caused a dramatic increase in cellular size, and decreased proliferation. As the magnitude of applied shear stress increase, both cell size and proliferation tended to decrease. Cyclic hydrostatic pressure also had a very different effect on BMMSC morphology, resulting in a smaller, more rounded phenotype that did not express proteins associated with SMCs. While cyclic pressure did not demonstrate any dose- or frequency-dependent changes in morphology or proliferation, we did find that there was a striking similarity to 1% 1 Hz cyclic stretch. The similarities in morphology and proliferation between these two types of stimuli may point to common signaling mechanisms that occur as a result of low-level mechanical stimulation.

The differentiation of BMMSCs towards a smooth muscle-like lineage, as determined by protein expression through immunohistochemistry, was most affected with either increasing magnitudes or higher frequencies of cyclic stretch. With the exception of constitutive expression of flk-1 (VEGFRII) other EC-related proteins were detected by immunohistochemistry. The expression of flk-1 protein did not appear to be affected by cyclic stretch, but did appear to be diminished by both cyclic pressure and laminar shear stress.

Changes in gene expression by RT-PCR were difficult to interpret due to high variability, which we believe was related to our choice of endogenous control genes. On average, our results indicated a general increase in most of the tested myogenic genes as a result of mechanical stimulation despite the lack of evidence in protein data for cyclic pressure and laminar shear stress. While flk-1 gene expression appeared to correlate with our protein expression results, other EC-related genes tended to be increased for cyclic pressure, but EC-related gene expression data for cyclic stretch and laminar shear stress was decreased or unchanged. All the mature osteoblast and chondrocyte genes were either undetectable or strongly downregulated by the

applied mechanical stimuli. Other trends in gene expression that were not specific to a particular lineage included the upregulation of FGF2, TGF-β, and collagen I in response to laminar shear stress. ECM proteins including collagen I, III and elastin were also increased on average by cyclic pressure, while moderate stimulation by cyclic stretch seemed to increase elastin expression.

6.1.3 Specific Aim 3

Based upon the results of our 5 day experiments, we investigated the temporal evolution of the response to a single magnitude and frequency of each of the Mechanical Panel stimuli. We also increased the cell seeding density to provide more biological materials for Western blotting and RT-PCR, which in previous experiments was limited by the low cell number in the systems. In general, cyclic pressure and laminar shear stress increased EC-related gene expression starting at 24 hours and continuing through 3 days. Muscle-related gene expression was relatively unaffected in these earlier time periods, with the exception of cardiac troponin, which was strongly downregulated by cyclic pressure and laminar shear stress. By 3 days, cyclic stretch was showing significant upregulation of desmin, and other vascular related genes including myocardin and cardiac troponin were on the rise. Growth factor gene expression was similar to our earlier findings, with laminar shear stress upregulating FGF-2, TGF-β, and VEGF-A at both 24 hour and 3 days. Similarly, extracellular matrix gene expression, including collagen I, III and elastin, was also elevated for laminar shear stress at both 24 hours and 3 days. Cyclic B1 expression was significantly decreased under laminar shear stress at both 24 hours and 3 days, which was in agreement with the findings of our 5 day experiments. Cyclic pressure also downregulated cyclin B1 in the 24 hour period, which was surprising given our previous 5 day

findings. Conversely, cyclic stretch upregulated cyclin B1 expression at the 3 day time point. Considering that the experiments started at confluence, it was not surprising to find the diminished cyclin B1 expression which may be a product of contact inhibition. However BMMSCs re-orient perpendicular to the direction of strain within 24 hours of cyclic stretch. As a consequence of this migration they may have lost their contact inhibition, resulting in the observed increased cyclin B1 expression.

In addition to changes in gene expression, we also attempted to quantify changes in protein expression with Western blotting. However, due to problems with the resuspension of the solubilized protein, we were unable to detect proteins larger than 90 kDa in any of our samples. The only protein that we were successfully able to probe for was calponin, but because of extremely large variability in expression, we were unable show any significant changes in expression for any of the applied stimuli at either 24 hours or 3 days.

6.1.4 Specific Aim 4

Similar to the study of the temporal evolution of BMMSC differentiation in response to mechanical stimuli, we designed a set of experiments to determine whether the differentiation of the BMMSCs following cyclic stretch would be reversed upon the removal of the applied stimuli. Similar to Specific Aim 3, we performed RT-PCR for a variety of genes designed to determine the differentiation state of the cell. Our results revealed that just 3 of the 30 genes in our assay - caldesmon, flk-1, and TGF-β - were significantly altered by the removal of the cyclic stretch stimulus. Caldesmon and TGF-β were increased by the withdrawal of the stretch stimulus, while flk-1 was downregulated. Our attempts to quantify protein expression were also impeded by the absence of high molecular weight proteins. Western blots for calponin continued

to show relatively high variability, but on average increased with the removal of stretch. Although we have no statistical significance for our calponin results, because of the general trends in the gene and protein expression, we hypothesize that the BMMSCs are continuing down a myogenic lineage, possibly by utilizing autocrine/paracrine TGF-β signaling.

6.2 APPLICATIONS FOR VASCULAR REGENERATIVE MEDICINE

The overall goal for this research was to improve our understanding of how mechanical stimulation can be utilized to provide appropriate cues for stem cell differentiation into the vascular SMCs and ECs for use in regenerative medicine applications. Our results have indicated that for mesenchymal cells derived from the bone marrow, mechanical stimulation tends to increase gene and protein expression for the myogenic lineage. This was particularly evident for cyclic stretch, which we found to generate an elongated, spindle-shaped cell that expressed many of the proteins associated with contractile SMCs; namely SMA, calponin, and SMMHC. Therefore, it would seem appropriate to think that stem cells impregnated into the wall of a tubular construct and exposed to the cyclic deformation resulting from pulsatile blood flow would preferentially head towards a smooth muscle lineage and not an undesired lineage such as bone, fat, or chondrocytes. Furthermore, we have found that cyclic pressure and shear stress on average increase endothelial gene expression, particularly for the more mature proteins such as PECAM and vWF when these stimuli are applied to a confluent monolayer of cells. Therefore, we believe that implanting a vascular graft that is populated throughout its thickness with bone marrow-derived stem cells could ultimately establish an endothelial monolayer and a muscular wall based upon the cellular exposure to the local mechanical environment; namely

cyclic pressure, shear and stretch in the lumen, and cyclic stretch in the wall. There is some evidence to support this recapitulation of the morphogenic processes of development. Huang et al.[569] have demonstrated that embryonic stem cells seeded into a compliant micro-porous polyurethane tube and exposed to a gentle pulsing fluid flow developed both an endothelial lumen, and a muscular neointima based solely on the applied mechanical stimulation. Our laboratory has also been able to provide some direct evidence that a single population of stem cells impregnated into porous, compliant polymer can develop both ECs and SMCs as a result of being implanted into the circulation [684]. However, although we may be able to generate cells that express genes and proteins that are considered appropriate markers of a mature phenotype, this in no way implies that the resultant cells are functionally equivalent to the native SMCs and ECs. The real test for these tissue engineered vascular grafts will be their ability to prevent thrombotic occlusion and resist the overhealing hyperplastic response that is common to synthetic vascular grafts that lack the functional abilities promised by tissue engineered vascular grafts.

6.3 ADVANTAGES OF METHODOLOGY

Mammalian tissues, even those that aren't associated with the musculoskeletal system, are under constant changes in compression, tension, and flexure as a result of movement, fluid flow, etc. The biggest advantage of our experimental setup was the concept of the Mechanical Panel and its utility in assessing the response of stem cells to one of several potential forces they may encounter *in vivo*. Primary cultures of mesenchymal stem cells from the bone marrow typically contain a mixture of committed, partially-committed, and non-differentiated cells. By applying

mechanical stimulation in parallel to unbiased population samples from a given set of stem cells, we can begin to capture the true effects of these stimuli because the heterogeneity at the start of each experiment is identical for each system. Understanding how mechanical forces differentially affects stem cell differentiation, from basic morphology to complex genomic analysis, is just one part of the complex control system that we can harness to control stem cell behavior, both *in vivo* and *in vitro*, for therapeutic purposes. Mechanical forces can potentially augment or reverse the effects of other biological signals such as growth factors, ECM composition, and pH. While such effects may not drastically alter the response of a tissue-committed cell, they may present potentially critical problems with stem cell therapies and warrant equal consideration.

6.4 LIMITATIONS OF METHODOLOGY

As stated previously, the BMMSCs utilized for these experiments were not a pure population of stem cells. As a result, our interpretation of the effects of mechanical stimulation is clouded by the potential that only a population of the cells is responding to the mechanical stimulation. Despite this, our findings still indicate mechanical stimulation is an important stimulus for the generation of vascular cells in these particular cells, and thus has utility for vascular regenerative medicine.

A major limitation with any study of gene expression is that transcriptional changes that are found (or not found for that matter) may not directly translate into changes (or lack of changes) in protein expression, which is the only true measure of biological change. Post-transcriptional and -translational modifications are known to be factors in the final protein levels

of many cell types including stem cells [685-687]. For instance, Tian et al. [685] have demonstrated through combined microarray and 2D-DIGE proteomic techniques that transcriptional changes in hematopoietic and liver cells can account for only 40% of the detected changes in protein expression. Another study by Pratt et al. [688] evaluated the turnover rate of proteins by examining the mass shifts of tryptic fragments of radiolabeled amino acid sequences. They discovered that the steady state degradation rates for 50 proteins were 2-10%/hour, which suggests that protein turnover should to be taken into account when trying to correlate changes in the proteome and transcriptome. In our studies, we found differential changes morphology, proliferation, protein expression (by IHC), and gene expression that could not always be correlated and did not fit into tidy categories of gene expression (e.g., all EC-specific genes went up, or simultaneous expression of supposedly lineage restricted genes like myocardin or osteocalcin). Furthermore, in a majority of the gene expression data, no statistically or biologically relevant changes were seen, despite the clear changes in morphology and proliferation. These types of incongruities force us to acknowledge the presence of this multidimensional state of the cell involving the transcriptome and proteome that cannot be addressed by limited proteomic techniques such as immunohistochemistry and Western blotting. The need for systems biology approaches to analyzing biologic data are becoming more and more apparent as techniques and assays improve our ability to simultaneously measure the molecular processes of the cell.

6.5 FUTURE WORK

Mechanical signals are just one of many different signaling mechanisms used by cells to respond to their environment. Growth factors, extracellular matrix composition, pH, pO_2, and other biochemicals also have an effect on cell biology. Thus, in engineering terms, a cell is a dynamic multi-input, multi-output control system. Current research is limited by a lack of understanding of the underlying cellular processes when multiple stimuli are utilized, instead relying on a "black box" approach [689]. Most established differentiation protocols for multipotent stem cells consist of a combination of multiple growth factors, exogenous chemicals, and mechanical stimuli without an understanding of potential synergies or antagonistic relationships [56, 524, 525, 536, 537, 539, 595, 690]. Advances in analysis of intracellular signaling kinetics, genomics, and proteomics coupled with statistical modeling are showing great promise for predicting the final outcome of a multi-stimulus environment [691-693].

For example, by simultaneously analyzing the kinetics for the Akt, PKC, Smad, Erk, and JNK pathways (using a high-throughput kinase assay) as well as transcriptional changes for hundreds of genes (using TLDAs or cDNA microarrays) and subsequent proteomic alterations (using antibody microarrays or 2 dimensional difference in gel electrophoresis (2D-DIGE)) under our Mechanical Panel alone or in conjunction with chemical stimulation, we can build and train statistical models that can not only predict the various biometric outcomes, but also lead us to seek other previously unrecognized synergisms [691]. The techniques for these processes and others are already being developed and utilized in neuroscience, development, and stem and cancer cell biology [691-698]. By employing these systems biology approaches that take into consideration the vast amounts of cellular information at our fingertips, the resulting transcriptional and proteomic changes in stem cells from these multiple inputs may actually be

predicted. Consequently, this has the potential to increase our ability to more precisely control stem cell behavior and tissue commitment for therapeutic applications. Similar techniques can also be envisioned for tissue engineering applications as form of predictive quality control. A given tissue engineered product could be sampled at various times throughout its incubation period for its transcriptome and proteome. The results of the analysis could help to predict whether the product is progressing towards its target and terminated, saving thousands of dollars in wasted materials, or provide a prescribed adjustment to its culture protocol to put it back on track and avoid wasting the effort already placed into its development.

APPENDIX A

A.1 ESTIMATION OF THE MAXIMUM VAPOR DENSITY

The maximum vapor density (MVD, g/m^3) at a given temperature was calculated according to:

$$MVD = 4x10^{-6}T^4 + 4x10^{-5}T^3 + 0.0143T^2 + 0.2785T + 5.1222 \quad \textbf{(A.1)}$$

where T is the temperature (^{o}C). Equation (A.1) was obtained by fitting a fourth-order polynomial function to the data in saturated vapor density tables (**Figure A.1**) [610]. The MVD was used in Equation **(2.6)** to estimate the relative humidity for all cyclic pressure experiments.

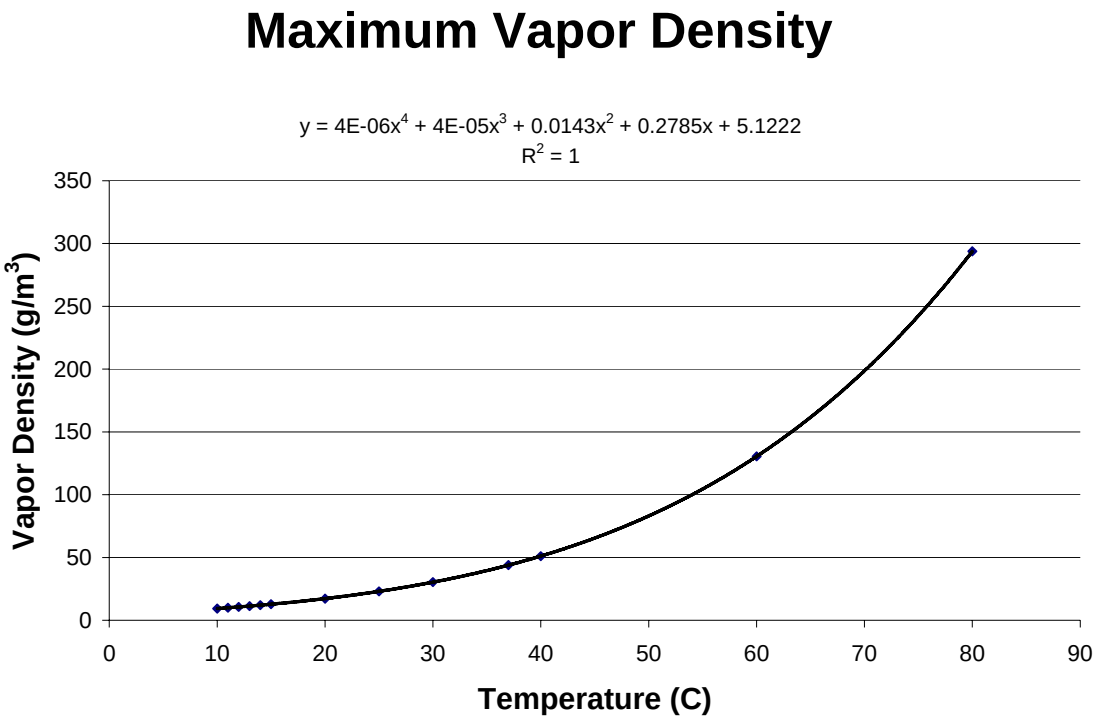

Figure A.1: Maximum vapor density curve generated from tabular data [610] and fit with a fourth order polynomial curve to extrapolate the maximum vapor density (g/cm^3) possible at a given temperature.

APPENDIX B

GROWTH OF BONE MARROW DERIVED MESENCHYMAL STEM CELLS

B.1 SERUM SELECTION

In order to maintain the tBMMSCs according to the protocols established by Javazaon et al.[613], we analyzed the growth curves of the tBMMSCs exposed to 2 different lots of fetal bovine serum that were similar to the serum lot currently in use by the TCGT. Upon arrival from the TCGT, the tBMMSCs were thawed in standard FBS (Invitrogen) and allowed to attach to 10cm Petri dish overnight. The tBMMSCs were immediately subcultured, with a portion placed at 200 cells/cm^2 into a 6 well dish (Falcon), and the remainder refrozen in α-MEM containing 30% FBS (Invitrogen) and 10% dimethyl sulfoxide (DMSO, D2650, Sigma). Those tBMMSCs subcultured into 6 well dish were treated in duplicate with two different lots of FBS (Atlanta Biologicals) as well as the standard FBS they were cultured in upon arrival. The 6 well dishes were then placed in a robotic cell culture system in the Stem Cell Research Laboratories directed by Dr. Johnny Huard [699-703]. The robotic cell culture system is a custom-built device from Automated Cell, Inc. (Harmar, PA) that combines a motorized stage (Ludl Electronic Products, Hawthorne, NY) on an inverted microscope (Eclipse TE 2000, Nikon) with a sealed

bioenvironment to maintain 37°C, 5% CO_2, and 95% humidity (Automated Cell, Inc.). The system allows live cells in many regions of interest to be imaged (ES Cool Snap CCD, Photometric) with time-lapse photography. The system is driven by CellMonitor (Automated Cell, Inc.) scanned each well to image 3 regions of interest per well every 10 minutes over 72 hours. The number of cells in each image were counted to create growth curves for each of the three sera used in this experiment (**Figure B.1**). The serum lot J0133 was identified as having the best growth curve, and all subsequent tBMMSCs were expanded in this lot of serum.

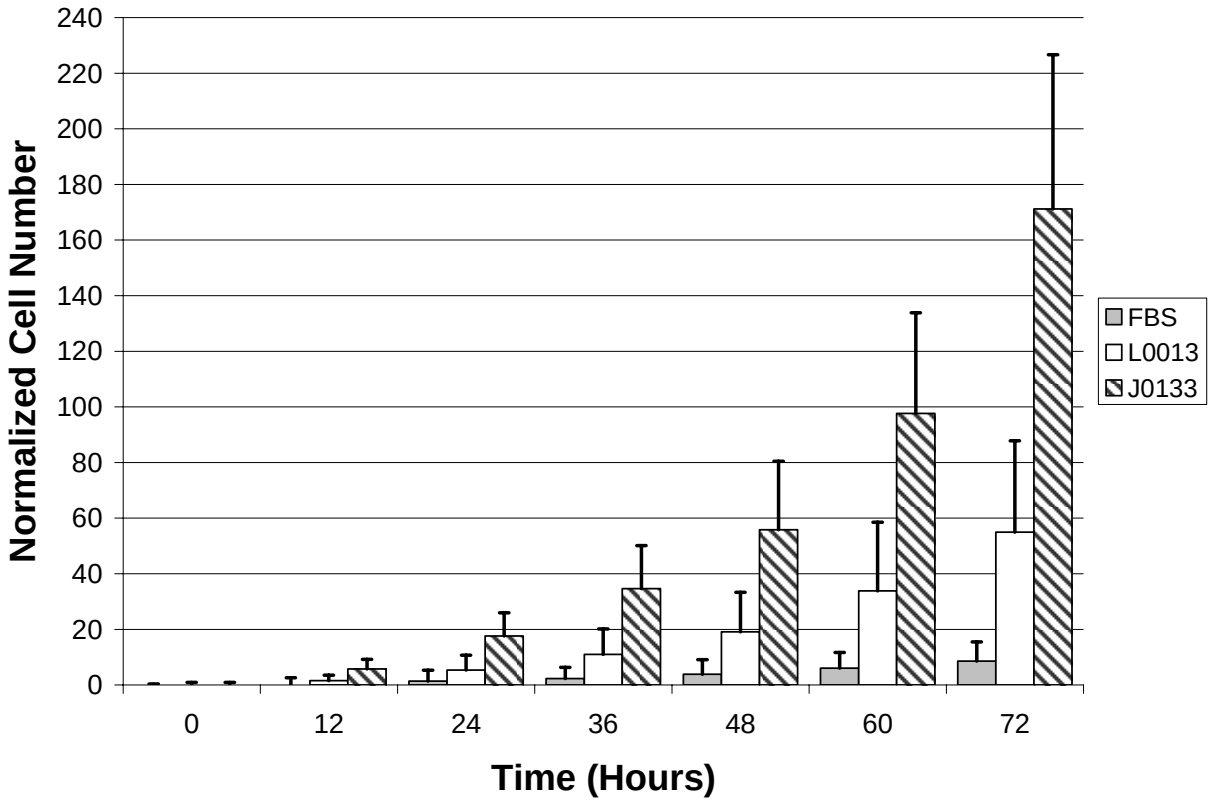

Figure B.1: Growth curves for serum selection experiment. Lot J0133 had the greatest proliferation rate and was chosen as the lot of serum for subsequent use in the Mechanical Panel experiments. The data is presented as the average and standard deviation of the replicates.

B.2 SEED LOT METHOD FOR SUBCULTURE

All subsequent culture of tBMMSCs following serum selection was performed according to the Seed Lot Method [614], whereby early passage material was always available for the creation of new stock lines of cells. The process is depicted in **Figure B.2**. Briefly, the initial culture of cells is expanded until sufficient numbers are attained to freeze 10 vials of cells at 250,000 cells/mL. The first 5 vials are used as the Working Lot 1, and the second 5 vials are the Seed Lot 1. After exhaustion of Working Lot 1, one vial of Seed Lot 1 is expanded to 5 new vials called Working Lot 2. This process is repeated throughout all of the vials of Seed Lot 1 until the last vial, which is then used to make Working Lot 6 and Seed Lot 2. For each experiment performed in Chapters 3.0, 4.0, and 5.0, one vial tBMMSCs was thawed, subcultured one to two times depending upon the number of cells needed for the experiment. This ensured that each experiment was within a few passages of all the experiments performed in this dissertation.

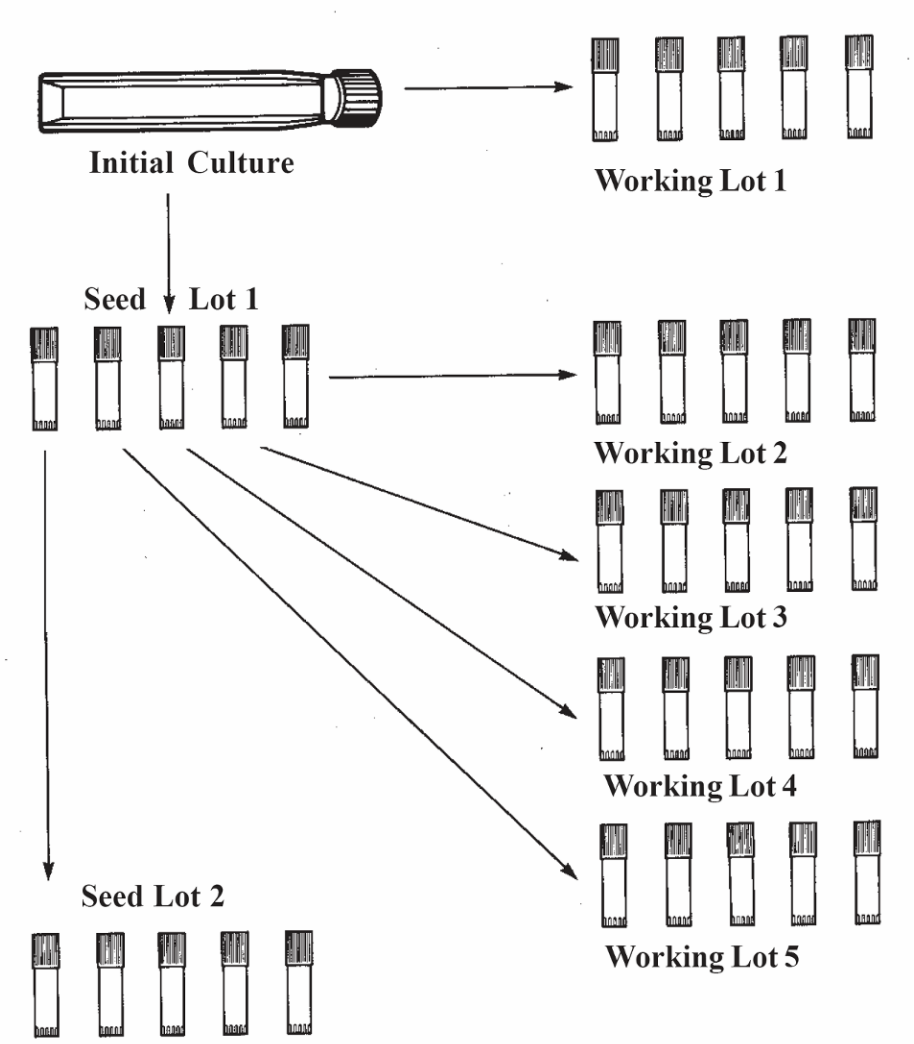

Figure B.2: Seed lot method for culture of tBMMSCs adapted from the *Cryopreservation Manual* [614]. The initial culture is expanded into a see Lot and a Working Lot. Each working lot is used for an experiment, ensuring that all experiments in a given study are within a few passages of each other.

APPENDIX C

RNA, DNA, AND PROTEIN ISOLATION WORK FLOW

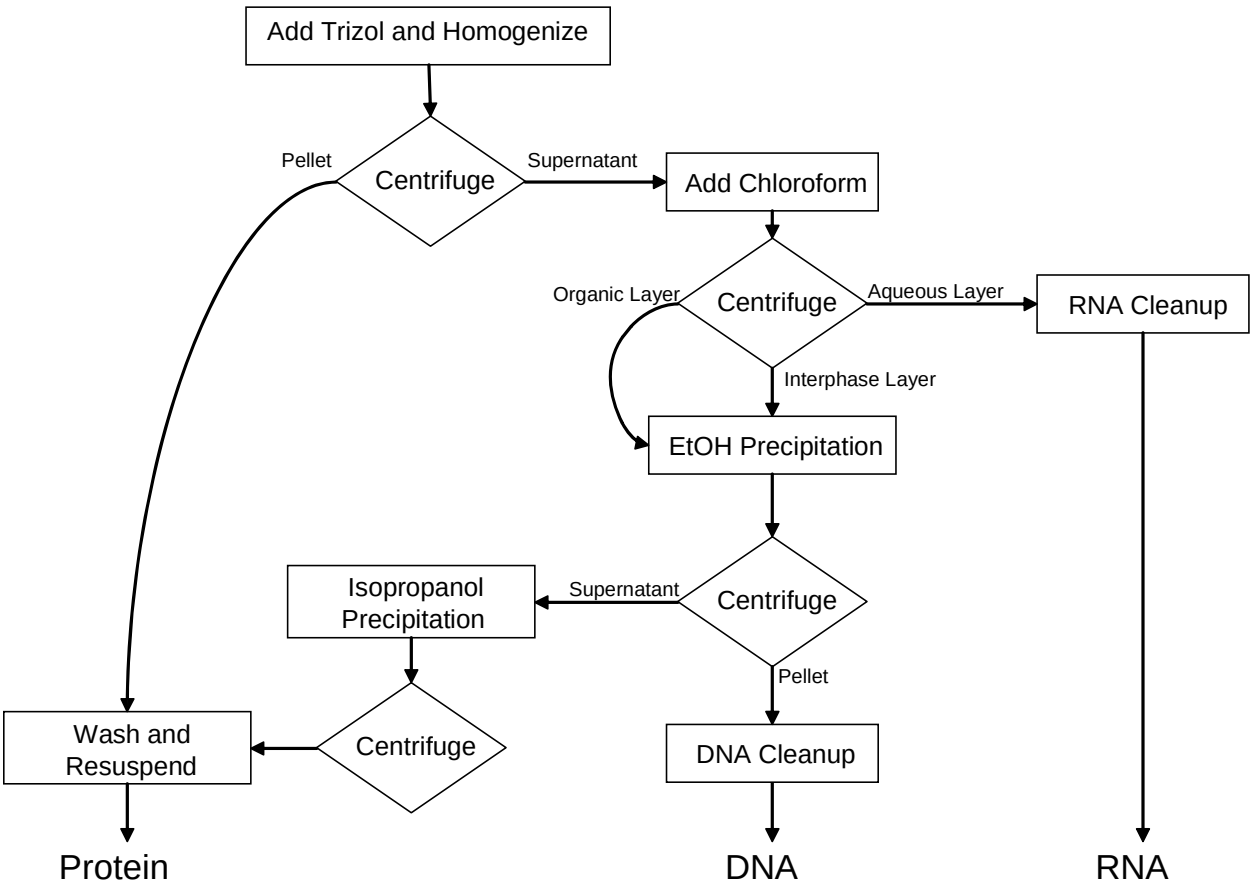

Figure C.1: Flow diagram demonstrating the sequential isolation of RNA, DNA and protein from Trizil™ for each component of the Mechanical Panel.

APPENDIX D

SCION ANALYSIS MACRO

The *Scion Analysis Macro* was written in Microsoft Visual Basic (v6.3, Microsoft Corporation) and Microsoft Excel (v2003, Microsoft Corporation) to efficiently process the measured cell parameters (area, perimeter, major axis, minor axis, and angle) from Scion Image for each of the components of the Mechanical Panel for the experiments outlined in Section 3.2.3. Through a series of user interfaces, the raw measurements from Scion Image for each Mechanical Panel stimulus were converted to the proper units, grouped according to the type of measurement, explored with basic statistics, and displayed graphically.

D.1 USER INTERFACES

The *Start Menu* (**Figure D.1**) allowed the user to start or continue an analysis. By choosing "Start Analysis" the user is prompted to either choose to work with the current workbook, or import new data (as an Excel, Scion, or a text file).

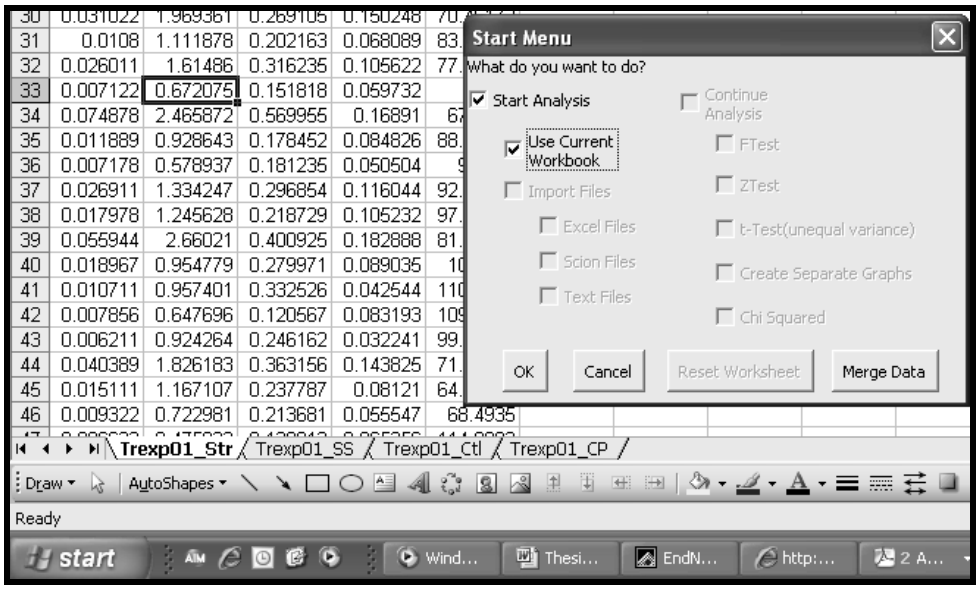

Figure D.1: Screen shot for the Scion Analysis Macro *Start Menu.* The raw data from Scion, arranged by columns in separate worksheets for each componentn of the Mechanical Panel is visible in the background.

The *Options Menu* (**Figure D.2**) then asks user to identify which of the possible measurements from Scion Image are found in the worksheets.

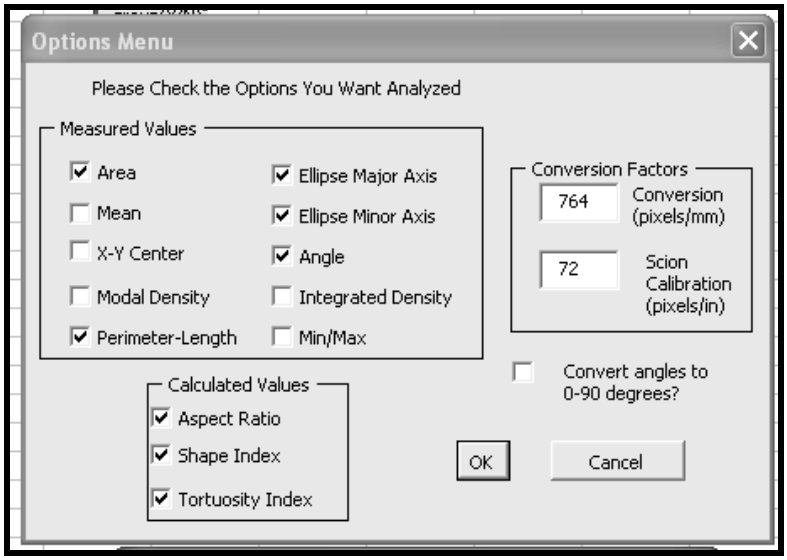

Figure D.2: Screen shot for the Scion Analysis Macro *Options Menu*. The user has selected the Measured Values, indicated which calculated values are desired, and has entered the conversion factors.

Selecting appropriate morphometric measurements enabled each of the three Calculated Values – Shape Index, Tortuosity Index, and Aspect Ratio – to be selected. The user was also prompted for the conversion factor for their Images. The Scion Calibration text box was the default calibration for Scion Image (72 pixels/inch), and the Conversion text box was the measured pixels per millimeter for the hemocytometer image for that experimental image set. The program then converted all measurements of length from inches to micrometers using the following:

$$NewValue(\mu m) = \frac{Raw\,value(inches) * Scion\,Calibration\left(\frac{pixels}{inch}\right)}{Conversion\left(\frac{pixels}{mm}\right)} * \frac{1x10^{3}\,\mu m}{mm} \qquad \textbf{(A.2)}$$

This process was repeated for the area measurements, which were in^2. The values entered by the user were stored in the Custom Document Properties of Excel and could be recalled if the data was re-analyzed. After the unit conversion, each measured parameter was placed in its own worksheet. Next, the selected Calculated Values were computed by creating arrays of measured parameters necessary for the calculation. The Shape Index and Tortuosity Index was calculated using **Equations (3.2)** and **(3.3)**, respectively. The Aspect Ratio was simply the ration between the major axis and the minor axis, and was our main measure of cell shape prior to the use of the Shape Index. Once the measured and calculated values were separated, the built-in descriptive statistics commands within Excel were called to evaluate data. Graphs of the average values ± SEM were automatically generated for each of the measured parameters. For the angle data, each measurement was copied to a temporary worksheet and placed in an appropriate 10^o bin between 0^o and 180^o. The frequency of occurrences in each bin was used to generate a histogram. Next, a *Statistics Menu* (**Figure D.3**) prompted the user to choose any desired statistics to interrogate the data. The F-test for variance, t-test, and z-test used the standard statistical functions in Excel to compare the variances or means, as appropriate, of each component of the mechanical panel. The Chi-squared test utilized the angular frequency tables for each component of the mechanical panel to create the observed and expected frequencies before calculating the chi-sum and using the built-in Excel function CHIDIST to generate a p-value for the distribution of the angular data for that experiment. The Scion Analysis Macro results in an organized analysis of the data generated from Scion Image (**Figure D.4**).

After the Scion Analysis Macro finished, the data could be saved and ready for import into the Experimental Database (see **Appendix E**). The Scion Analysis Macro was extremely useful for examining each experiment for consistency and trends within itself. However, the

greatest utility for the program was as a time-saver. The Scion Analysis Macro performed approximately 2 hours worth of data handling in 2 minutes. Other features of the Scion Analysis Macro that were not utilized for this study, but were built for future work include the ability to create separate average graph values for experiment components that have a common string in their name. For example, if a mechanical panel experiment was performed using different ECM proteins such as collagen I, elastin, and laminin, separate average value graphs could be created for each ECM protein to compare its effect on each component of the Mechanical Panel. Likewise, all similar Mechanical Panel components could be graphed together to compare differences in ECM coating.

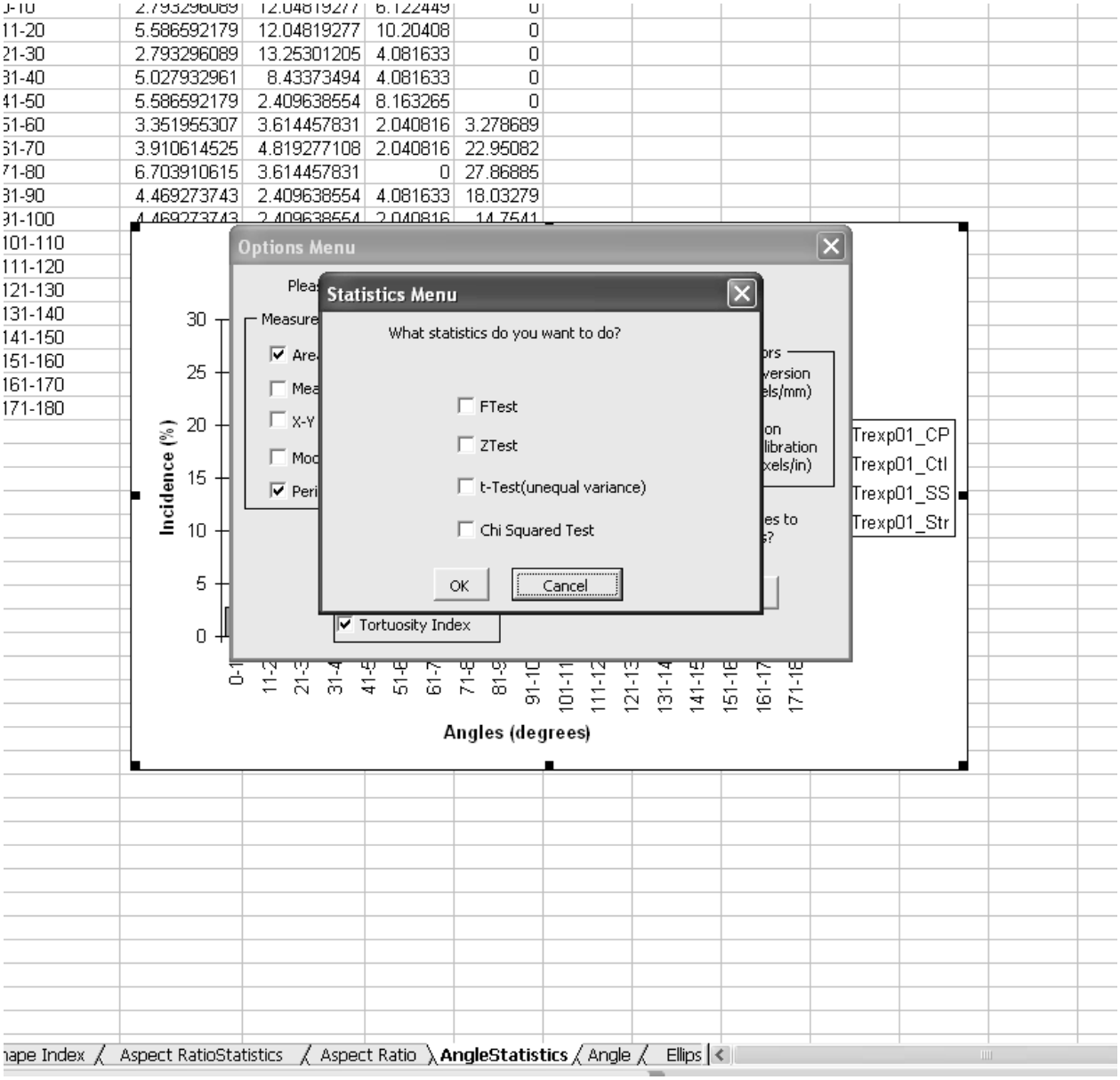

Figure D.3: The *Statistics Menu* prompts the user to choose from a variety of statistical tests to analyze the data. Each selected statistical test is peformed sequentially on each pair of the available components of the Mechanical Panel.

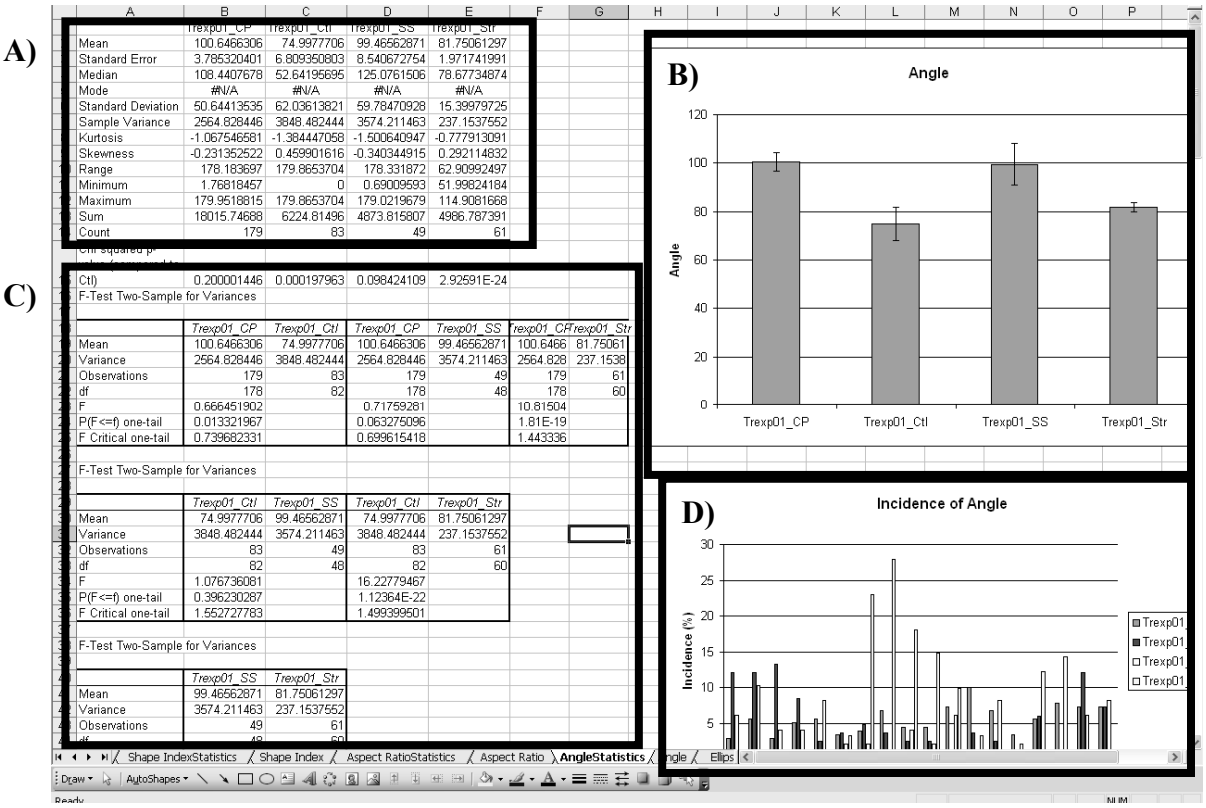

	Trexp01_CP	Trexp01_Ctl	Trexp01_SS	Trexp01_Str
Mean	100.6466306	74.9977706	99.46562871	81.75061297
Standard Error	3.785320401	6.809350803	8.540672754	1.971741991
Median	108.4407678	52.64195695	125.0761506	78.67734874
Mode	#N/A	#N/A	#N/A	#N/A
Standard Deviation	50.64413535	62.03613821	59.78470928	15.39979725
Sample Variance	2564.828446	3848.482444	3574.211463	237.1537552
Kurtosis	-1.067546581	-1.384447058	-1.500640947	-0.777913091
Skewness	-0.231352522	0.459901616	-0.340344915	0.292114832
Range	178.183697	179.8653704	178.331872	62.90992497
Minimum	1.76818457	0	0.69009593	51.99824184
Maximum	179.9518815	179.8653704	179.0219679	114.9081668
Sum	18015.74688	6224.81496	4873.815807	4986.787391
Count	179	83	49	61

Ctl)	0.200001446	0.000197963	0.098424109	2.92591E-24		
F-Test Two-Sample for Variances						
	Trexp01_CP	*Trexp01_Ctl*	*Trexp01_CP*	*Trexp01_SS*	*Trexp01_CP*	*Trexp01_Str*
Mean	100.6466306	74.9977706	100.6466306	99.46562871	100.6466	81.75061
Variance	2564.828446	3848.482444	2564.828446	3574.211463	2564.828	237.1538
Observations	179	83	179	49	179	61
df	178	82	178	48	178	60
F	0.666451902		0.71759281		10.81504	
P(F<=f) one-tail	0.013321967		0.063275096		1.81E-19	
F Critical one-tail	0.739682331		0.699615418		1.443336	
F-Test Two-Sample for Variances						
	Trexp01_Ctl	*Trexp01_SS*	*Trexp01_Ctl*	*Trexp01_Str*		
Mean	74.9977706	99.46562871	74.9977706	81.75061297		
Variance	3848.482444	3574.211463	3848.482444	237.1537552		
Observations	83	49	83	61		
df	82	48	82	60		
F	1.076736081		16.22779467			
P(F<=f) one-tail	0.396230287		1.12364E-22			
F Critical one-tail	1.552727783		1.499399501			
F-Test Two-Sample for Variances						
	Trexp01_SS	*Trexp01_Str*				
Mean	99.46562871	81.75061297				
Variance	3574.211463	237.1537552				
Observations	49	61				
df	48	60				

Figure D.4: Format of the data following the completion of the Scion Analysis Macro. Each measured morphometric parameter is listed as a separate worksheet tab as well as a Statistics tab. For example, the Angle Statistics tab contains the (A) descriptive statistics, (B) average value graph, (C) statistical analysis, and (D) histogram, and of the angle data.

APPENDIX E

EXPERIMENTAL DATABASE

In order to keep track of the large amount of information generated from each Mechanical Panel experiment, a database was created to perform the following tasks:

1. Track the cell culture identification numbers for the tBMMSCs used in each experiment.
2. Store the Mechanical Panel parameters for easy grouping of the data in queries.
3. Identify which biological assays had been performed store their results or hyperlink to the raw data.
4. Keep track of all samples generated and their storage location.
5. Provide a framework to export experimental parameters and values to SPSS statistical software.

E.1 GENERATION OF THE FOURTH NORMAL FORM

The database was designed in Microsoft Access (v2003, Microsoft Corporation) and was in fourth normal form. For a review of relational theory and the nomenclature used throughout this appendix, the reader is directed to an excellent review of the topic by Kent [637] as well as "Developing Quality Complex Database Systems: Practices, Techniques and Technologies" by Shirley Becker [704]. The database was built using 47 tables, 39 queries, 20 forms, 16 reports. Visual Basic (v6.3, Microsoft Corporation) was used to manipulate the forms and enter and retrieve data from the tables.

By definition, all normal forms are additive, so by being fourth normal, it is implied that the Experimental Database is also first, second, and third normal. First normal form indicates that repeating fields are eliminated. This is best exemplified by the Mechanical Panel, which contains up to five experimental components (**Figure E.1**). By converting (A) into (B) and (C), searching for all experiments for ones that had CP easily returns a list containing the ExpID for each experiment.

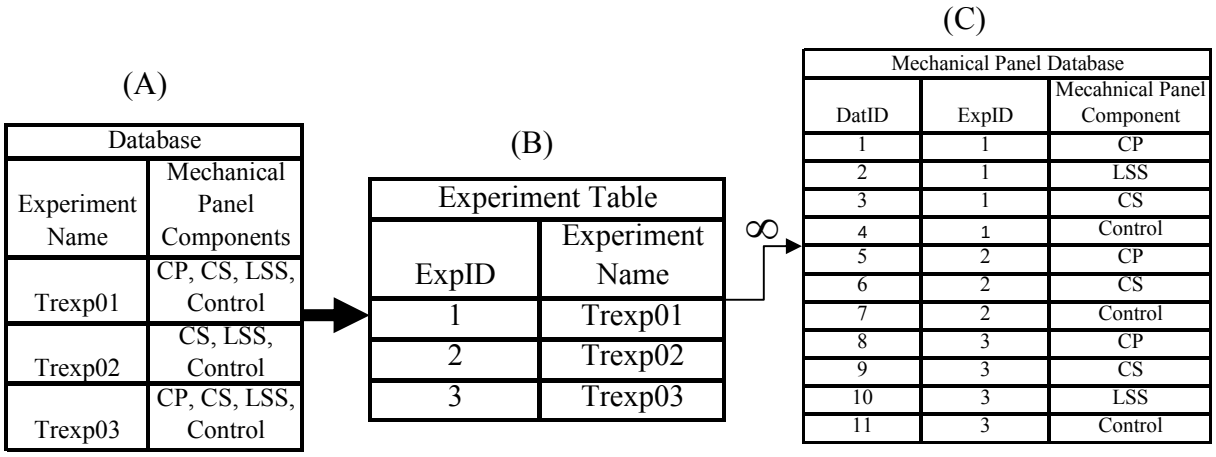

Figure E.1: Conversion of the Mechanical Panel to a first normal form Database. The infinity symbol denotes the "many" table for the one-to-many relationship.

Second normal form indicates that redundant fields are eliminated. To convert **Figure E.1** to second normal form, a new table listing CP, LSS, CS, and Control only once is created with a junction table to link it to the Experiment Table (D).

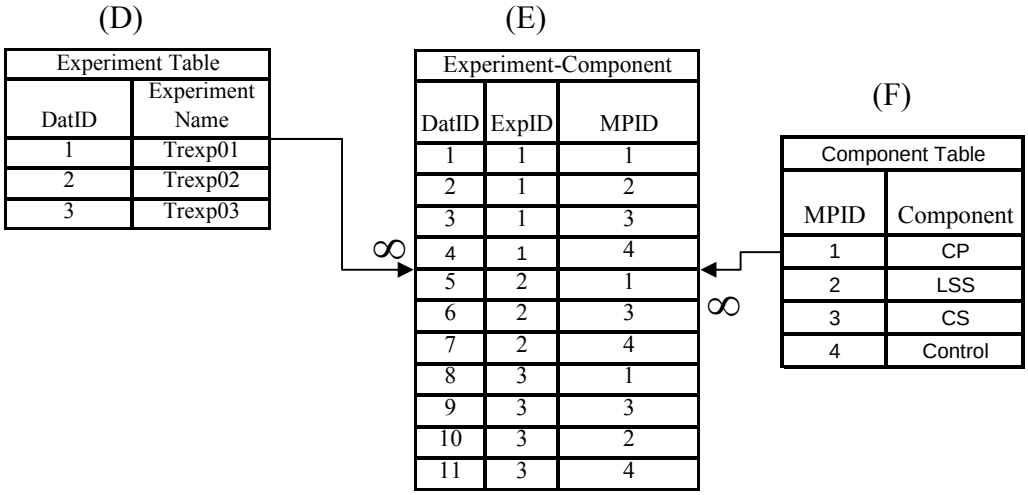

Figure E.2: The configuration in **Figure E.1** is converted to second normal form through a junction table (E) connecting (D) and (F). The infinity symbol denots the "many" table for the one-to-many relationship.

Third normal form is created by eliminating columns not dependent on a primary key. The configuration of our database in **Figure E.2** does not violate third normal form unless we begin to consider other data necessary for the database, such as the genes assayed by PCR. Each RQ value generated by RT-PCR is linked to a specific gene. However, the primary key which identifies each RQ value does not have a relationship with the gene name. Therefore, that information must be moved to a different table. This was important for the instance where we changed several genes on the second TLDA. New genes were added which did not exist before and others were removed. Without third normal form, gene available for analysis that had no current RQ value would not be listed at all. This concept is illustrated in **Figure E.1**.

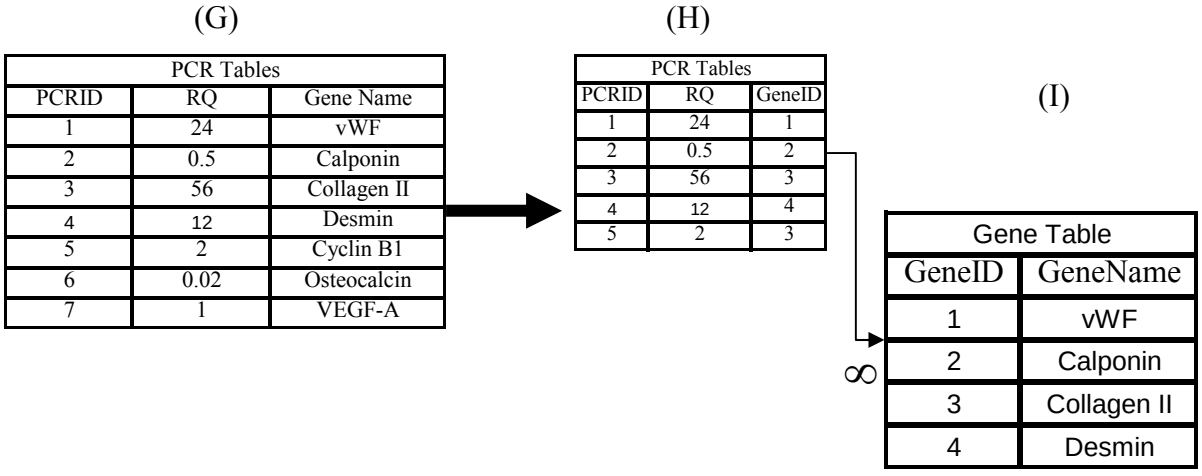

Figure E.3: Representation of third normal form. Gene names which would be non-existant in the database prior to registering an RQ value are stored independent from the PCR tale. The infinity symbol denots the "many" table for the one-to-many relationship.

The final step for the creation of the Experiment Database was to achieve fourth normal form. For a database to be in fourth normal form, no table can contain two or more one-to-many or many-to-many relationships that are not directly related. This prevents the creation of dummy

records when an expected endpoint is not generated. For example, each Mechanical Panel experiment consists of several components – CS, CP, LSS, and Control. This is a one-to-many relationship. Furthermore, each component of the Mechanical Panel can generate 3 biological samples – RNA, DNA, and protein. This creates a one-to-many relationship with a given experiment component and a many-to-many relationship between the experiment and the biological samples. To efficiently organize this data for searching, these details should be stored as separate rows in separate tables with independent primary keys. These tables are joined together by separate junction tables, which contain only the primary keys for the two tables they are joining. This configuration for three tables is indicated in **Figure E.4.** Another reason to organize the database in this fashion is to avoid update errors. If a single junction table had been used, deletion of a sample from one side would either force both samples to be deleted or force the junction table to create a dummy value in its place. Multiple junction tables containing the field ID numbers for a particular endpoint and its corresponding experiment identifier also allow for easy querying of the results for any specific set of independent conditions, such as a list of all the experiments with 5% CS, PCR results, and IHC results (see **Figure E.11** as an example).

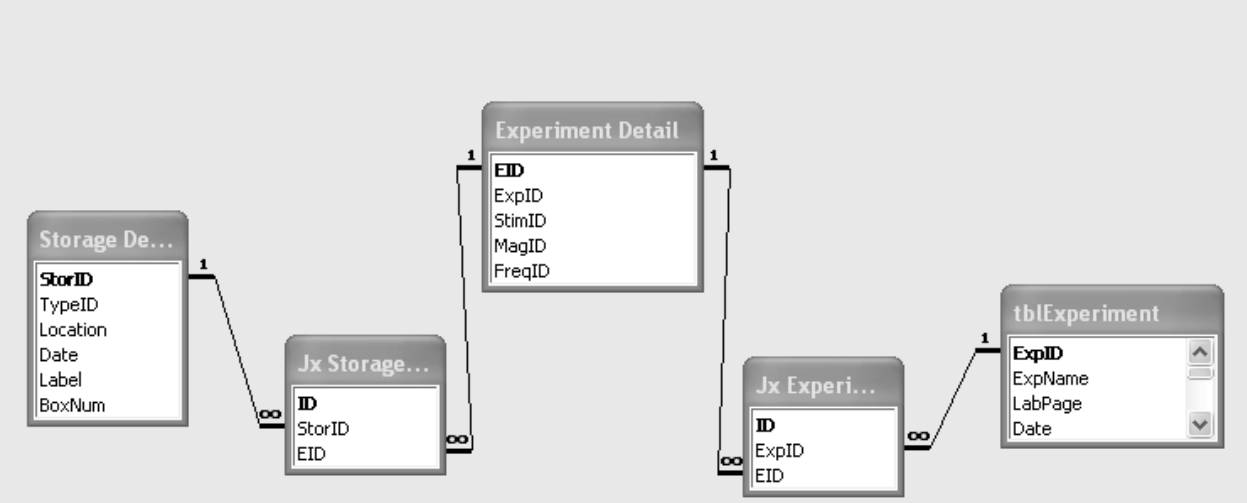

Figure E.4: Relationships view of Storage Detail and tblExperiment tables to the Experiment Detail table in the Experiment Database. The Primary Key is in bold type. Junction tables (denoted by Jx) are used to connect the one-to-many relationships that exist between the primary keys. The infinity symbol denots the "many" table for the one-to-many relationship.

E.2 USER INTERFACES

In addition to efficiently storing data for fast retrieval, the Experiment Database provided the means to extract large quantities of data from Excel spreadsheets containing the morphometric analysis for a given experiment, or the RQ values for the 32 genes on the TLDA card. User interfaces were designed to efficiently navigate through the database and enter and retrieve data. The main form (**Figure E.5**) displays all the relevant information about an experiment at a glance. It displays the types of mechanical stimulation used for an experiment as well as the magnitudes and frequencies of each stimulus. The presence of assay results or stored samples is denoted by check-boxes that are activated as soon as data is stored in the relevant tables. Several command buttons provide quick access to reports or queries. For example, The "Sample

Processing Reports" section provides tables similar to those shown in **Figure E.6**. Moving into the PCR Form demonstrates the functionality for the database to pull the RQ data for all TLDA genes and place them into the proper text boxes (**Figure E.7**). Other main data-entry forms, including those for the morphometric data, proliferation data, storage form, and experiment search form are depicted in **Figure E.8**, **Figure E.9**, **Figure E.10**, **Figure E.11**.

The PCR form represents the ideal reason for creating a fourth normal form database. The PCR data was not originally part of the experiment database, but shortly after deciding to use TLDAs to perform RT-PCR, the form depicted in **Figure E.7** was a necessity if we were going to effectively manage 570 data points per experiment generated by the PCR data. By being in fourth normal form, the Experiment Database is modular, and new assays or endpoints that become part of the experimental plan can be seamlessly incorporated with all the other information linked to main experiment detail.

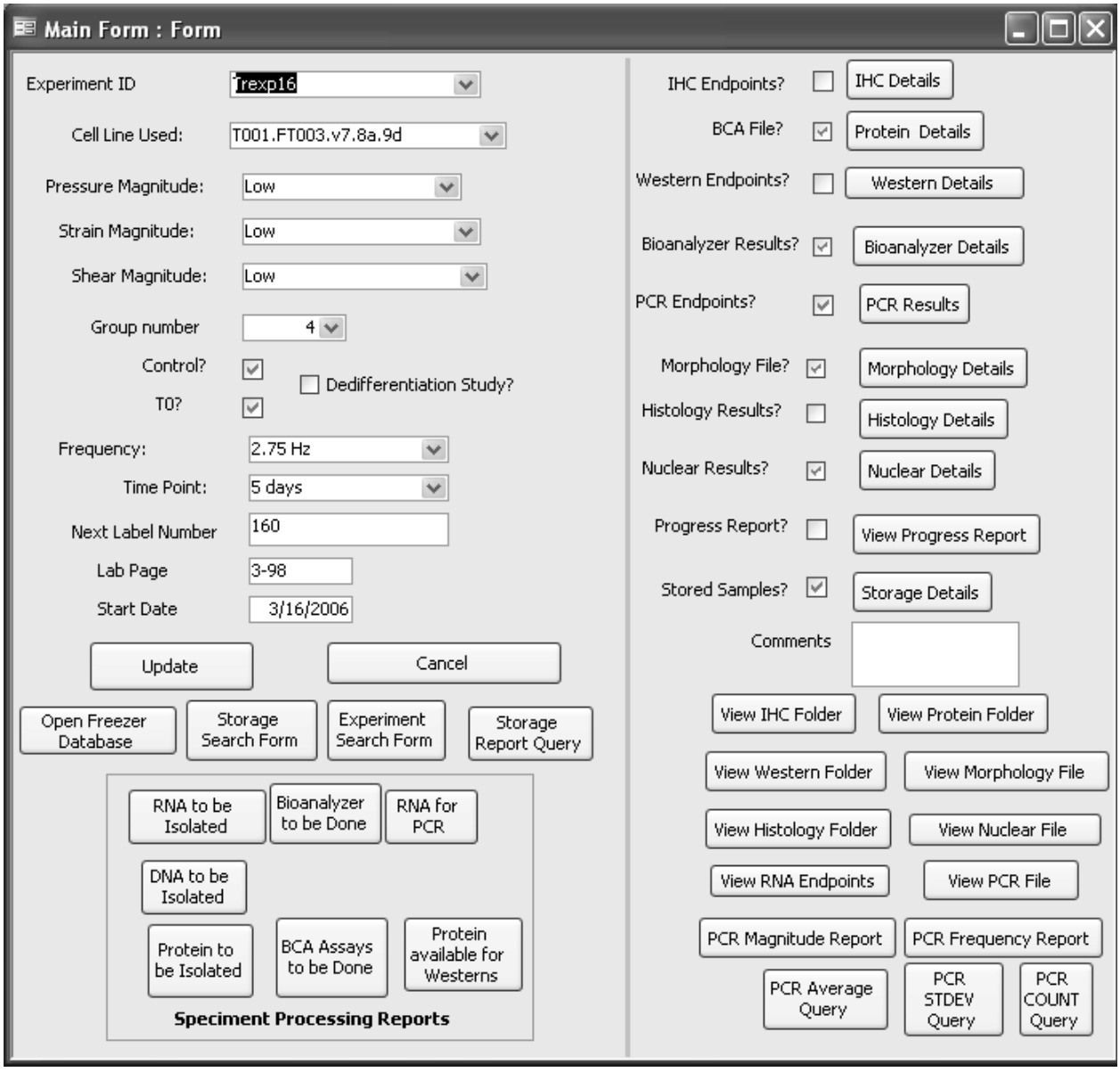

Figure E.5: The main form displaying Experiment 16. As soon as an experiment number is chosen, the remaining fields self-populate to relate the information about that experiment stored throughout the database. Quick launch buttons are also provide to show various reports or query results, and launch stored hyperlinks to files and folders.

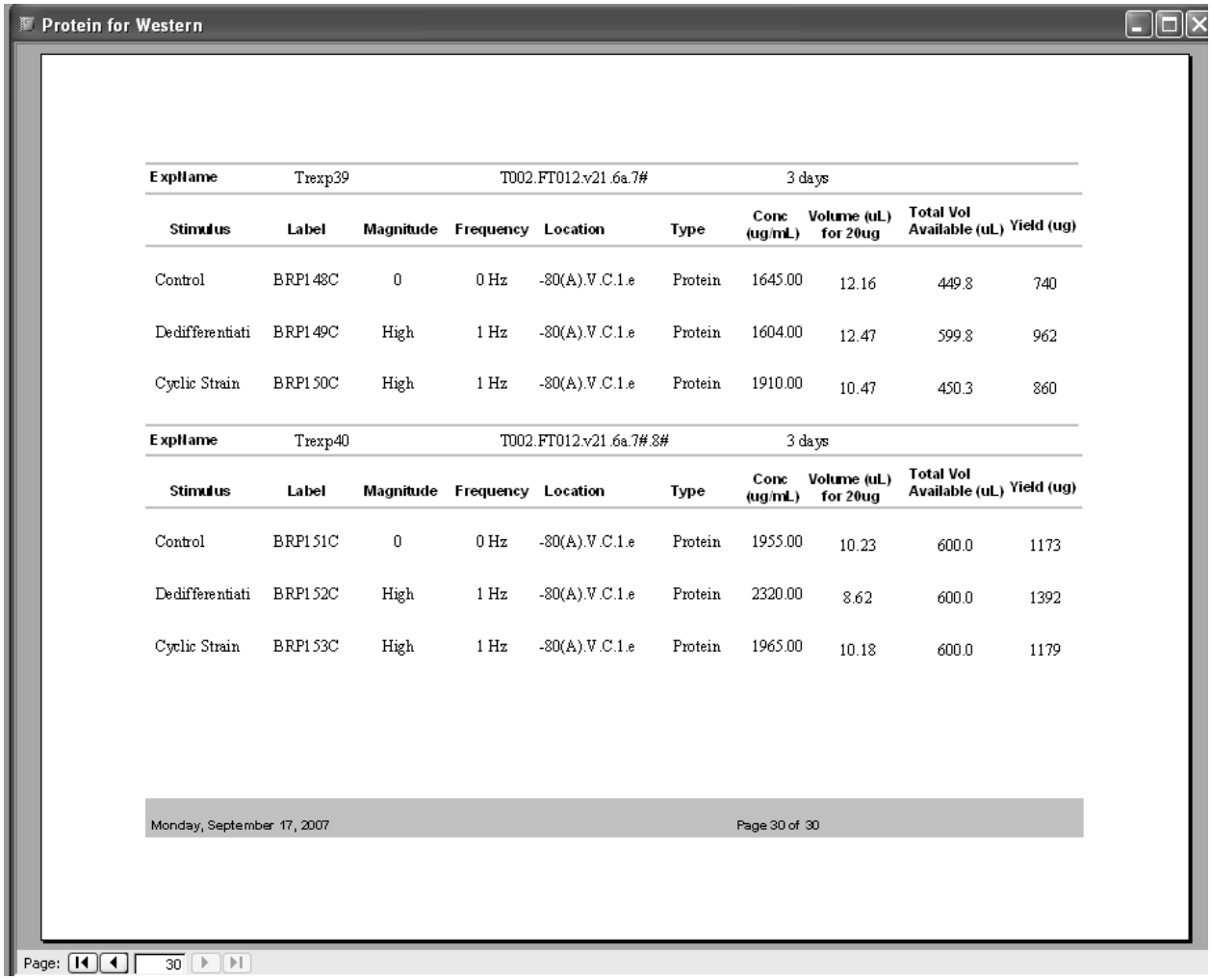

Figure E.6: Protein for Western blotting report generated by the Experiment Database from the Main Form. The report lists the experiment details as well as storage location, concentration, and yield and calculates the volume required for 20µg of protein.

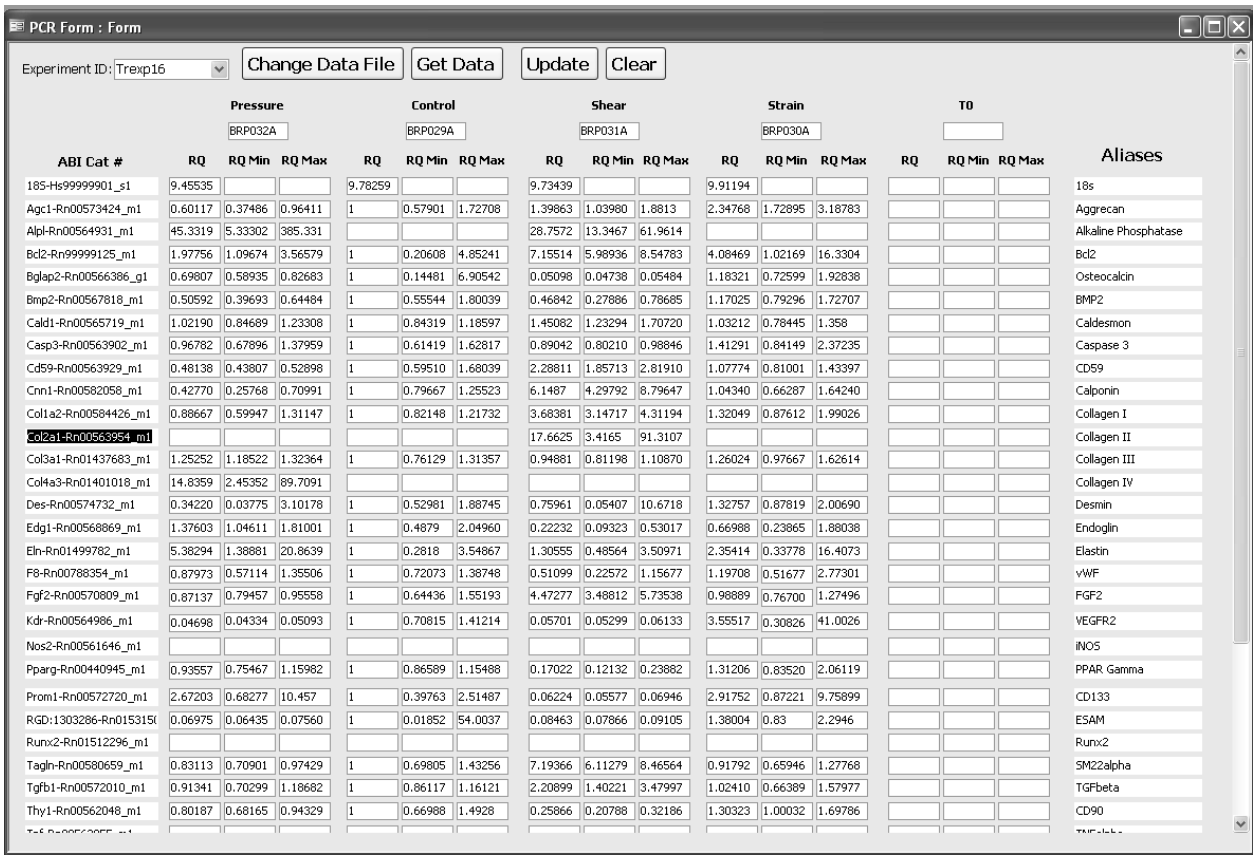

Figure E.7: The PCR Results Form is reached from the Main Form. All RQ values for each of the genes and components of the mechanical panel (570 text boxes in total) are instantly obtained from the Data File as the push of a button and stored in the PCR Results Table.

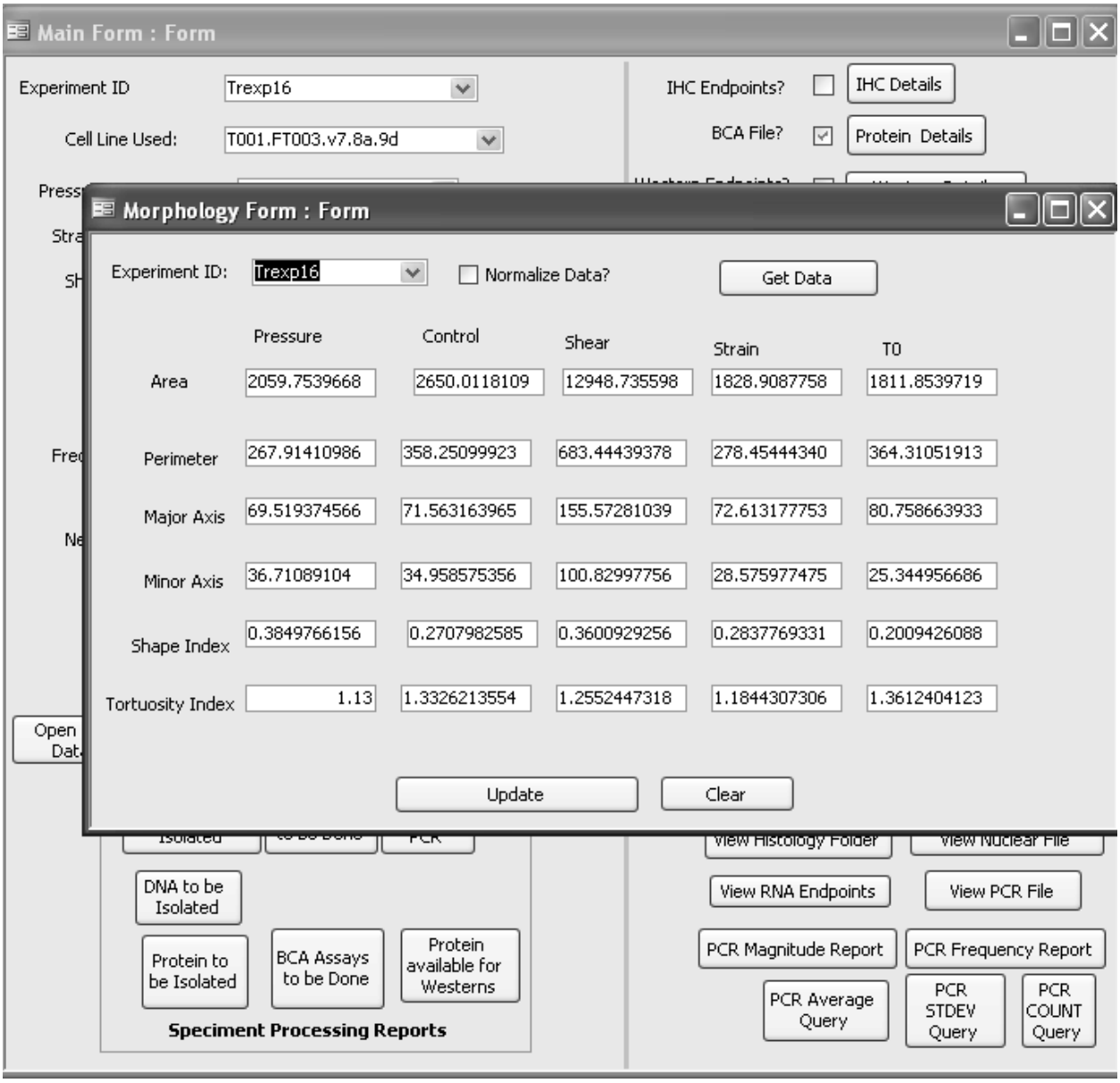

Figure E.8: Morphology Form from the Experiment Database. The "Get Data" button extracts the average values from each sheet that was created from the Scion Analysis Macro (see **Figure D.4**). The "Normalize Data" check box divides each value by the control value, and stores the normalized data in a separate table.

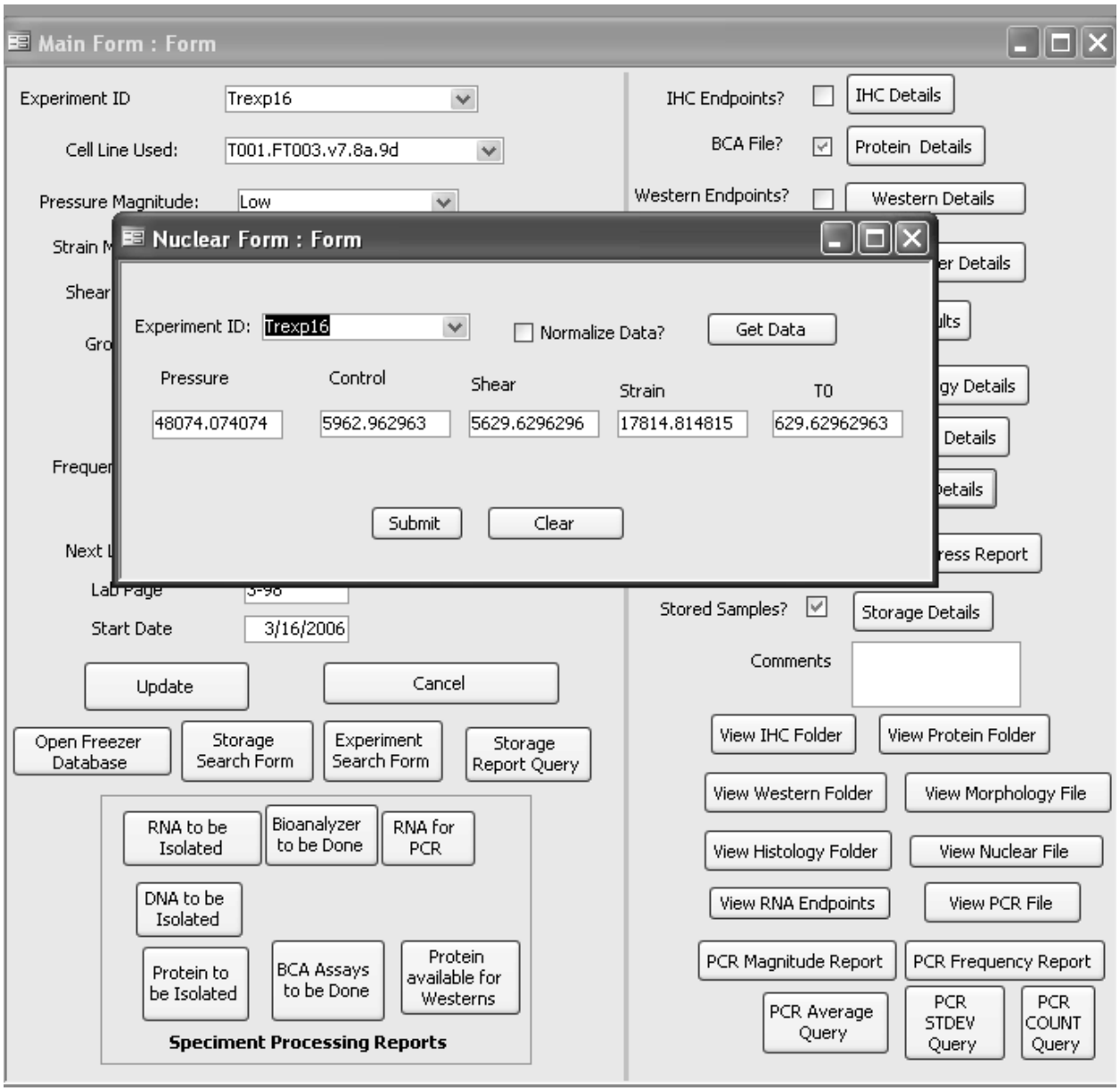

Figure E.9: The Nuclear Form imports the average cell density measurements for each component of the Mechanical Panel from an Excel spreadsheet containing the raw cell counts. The "Normalize Data" check box divides each value by the control value, and stores the normalized data in a separate table.

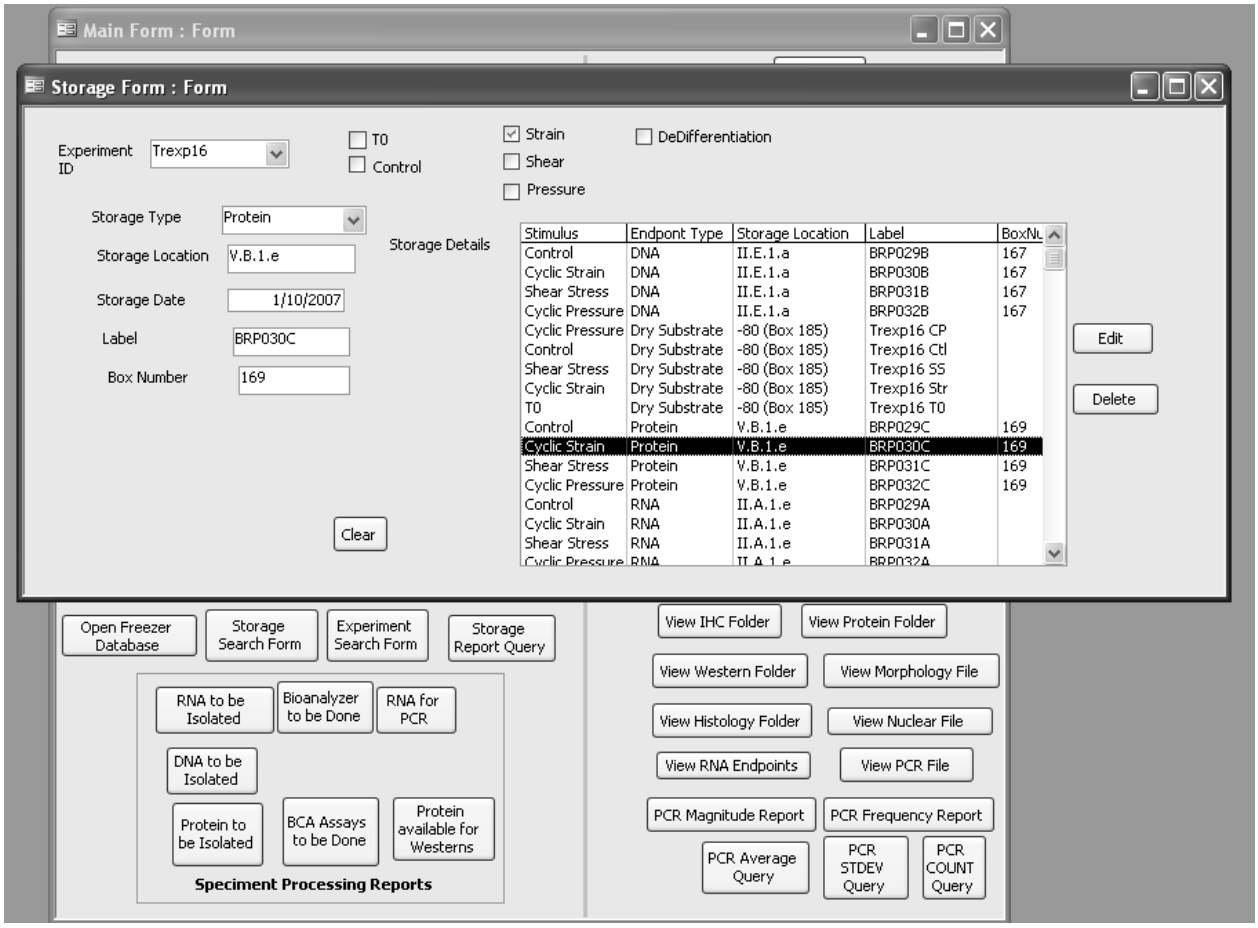

Figure E.10: The Storage Form displays the locations for biological samples generated from a given experiment.

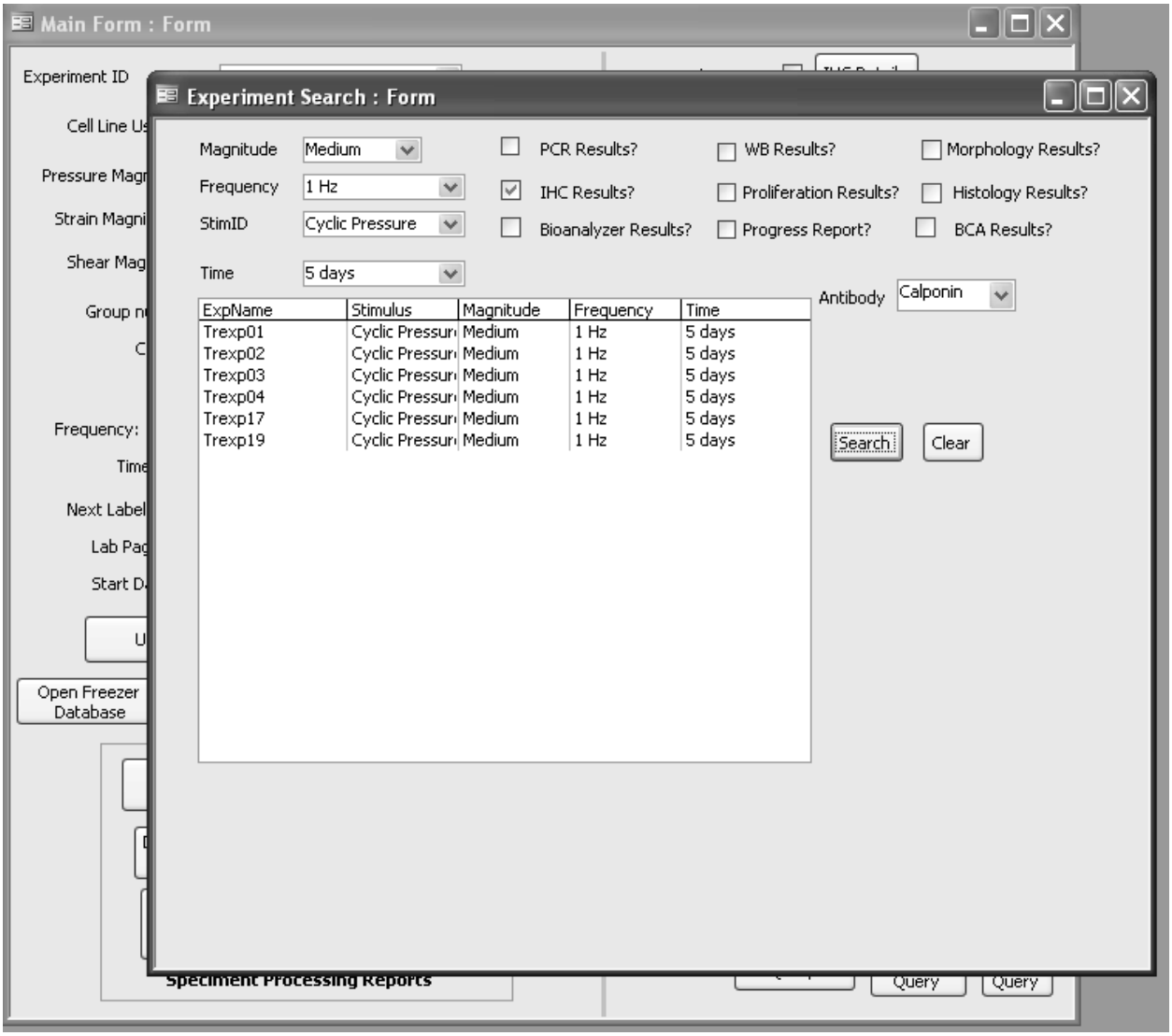

Figure E.11: The Experiment Search Form searches the database for the values in the drop-down boxes and check-boxes. Selecting any of the resulting values retrieves the data for that experiment and places it in the Main Form.

APPENDIX F

CELL CYCLE ANALYSIS

Because the decrease in cell density reported for LSS (see **Figure 3.14**) could be caused by either a true inhibition of proliferation or a selective removal of proliferating cells by the flowing media, the cell proliferation marker Ki67 was probed by immunohistochemistry.

F.1 METHODS

tBMMSCs subjected to either CS-10, CP-120, LSS-5, or control conditions were assayed for the cell proliferation marker Ki67 using immunohistochemistry protocols outlined in Section 3.2.4.4. Following termination of each stimulus, tBMMSCs were rinsed with ice cold PBS and fixed in 4% paraformaldehyde followed by 3 washes in PBS. The cell membrane was permeabilized for 15 minutes with 0.1% TritonX in PBS. Non-specific binding of the antibody was blocked using a 5% BSA solution in PBS for 1 hour at RT. The fixed and permeabilized samples were incubated with Anti-Ki67 (Santa Cruz) diluted 1:100 in PBS/BSA/Gly for 1 hour at Rt. After 3 washes in PSB/BSA/Gly, the samples were incubated for 1 hour at RT with the secondary antibody, goat anti-mouse conjugated to Alexa Fluor 488 (Sigma) diluted 1:500 in

PBS/BSA/Gly. After 3 washes of PBS/BSA/Gly, DAPI (Sigma) was added to stain the nucleus. The samples were washed 5 times in PBS and then mounted on microscope slides using gelvatol for imaging on an epifluorescent microscope (E800, Nikon). The proliferation index was calculated by counting the number of nuclei positive for Ki67 and dividing by the total number of nuclei. Five fields of view were imaged per experiment and averaged to create an average proliferation index for that experiment. A paired t-test with α=0.05 was used to compare each stimulus.

F.2 RESULTS

The average proliferation index ± SD are reported for the control (38% ± 2%, n=2), CP-120 (52% ±7%, n=2), CS-10 (35% ± 7%, n=2), and LSS-5 (5% ± 6%, n=2). Representative images are shown in **Figure F.1**. The results demonstrate that LSS has a lower proliferative index ($p<0.10$) than control, CP, or CS samples, and provides evidence tBMMSCs exposed to LSS demonstrate the majority of LSS cells were arrested in the G0 phase of the cell cycle. Although the observed drop in cell density compared to controls may have resulted from removal of proliferating cells by fluid flow, the extremely low number of cells arrested at G0 points more to a direct inhibition of proliferation by LSS.

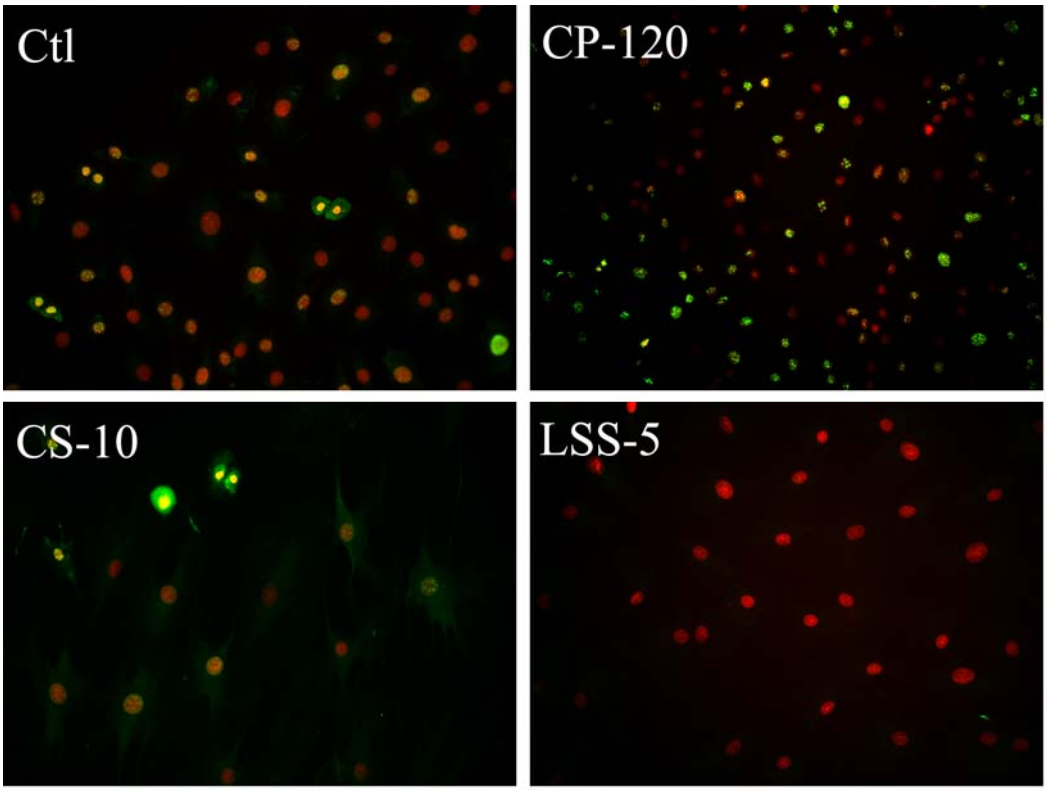

Figure F.1: Representative Ki67 staining for Mechanical Panel experiments (n=2). Green=Ki67. Red=nuclei stained with DAPI. All images taken at 100x.

APPENDIX G

EVALUATION OF 18S AS AN ENDOGENOUS CONTROL

In the TLDAs for our initial Mechanical Panel experiments (see Section 3.2.3), we utilized the expression of 18s rRNA as the endogenous control gene for several reasons, including its relative popularity in the genomic literature and the fact it was required to be present on all TLDAs produced by ABI. However, in examining two consecutive control samples, which should have behaved in a similar manner, we noticed identical C_T values for the flk-1 gene expression even though there was a large shift in the C_T for 18s. (**Figure G.1**). Because each TLDA received approximately the same cDNA mass (400ng per sample) and the change flk-1 gene expression was within 0.3 cycles, the large change in 18s rRNA prompted our deeper investigation into the validity of 18s as an endogenous control gene for our experiments involving the Mechanical Panel (see Section 4.2.2.2.1).

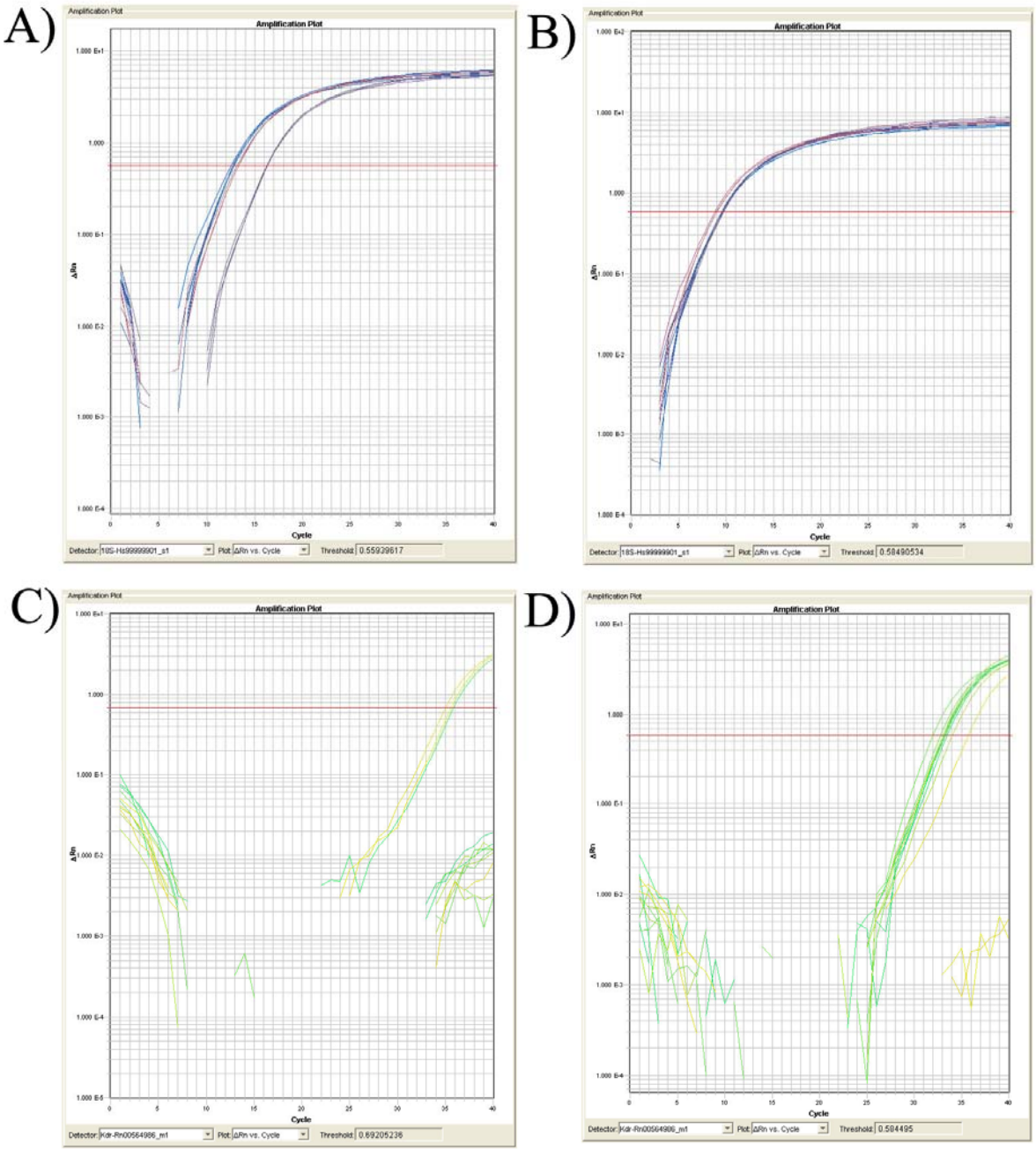

Figure G.1: ΔRn vs. cyclic time for 18s (A, B) and Flk-1 (C-D) in two control samples from Experiment 9 (A,C) and Experiment 10 (B,D). A 4 cycle shift in 18s, which translates to more than a 10-fold increase in mRNA transcripts by the $2^{\Delta\Delta Ct}$ method, did not result in a similar shift in the expression of Fkl-1.

APPENDIX H

DYNAMIC RANGE TESTING FOR TAQMAN® LOW DENSITY ARRAYS

H.1 METHODS

The dynamic range of the TaqMan® Low Density Array (TLDA) was assessed by performing the reverse transcriptase (RT) reaction with a starting mass of RNA that spanned at least 4 logs. The RNA used for the dynamic range tests was Universal Rat RNA (636658, Clontech, Mountain View, CA) to ensure that all genes queried would show detectable amplification within 40 cycles. The Universal Rat RNA is reported by the manufacturer to contain quantifiable amounts of RNA for more than 90% of the rat transcriptome. The RT reaction was initialized with 1, 10, 100, and 1000 ng of universal RNA using techniques described in Section 3.2.4.5.4 and then loaded into the TLDA and analyzed by RT-PCR (see Section 3.2.4.5.5.1).

H.2 RESULTS

The results of the dynamic range test are presented in **Figure H.1**. For each target gene, there was an approximately linear relationship between the log transformation of that starting mass

and the threshold cycle (C_T) of detection as determined by the SDS software. Based upon the curves, the mass of RNA necessary to achieve a C_T of at least 30 cycles for all target genes would require at least 100 to 1000 ng of RNA to be loaded for each sample. Therefore, whenever possible, the core facility was instructed to load 400ng of RNA per sample into the TLDA. It was also evident from these results that 18s was expressed at a much higher level than nearly all the target genes.

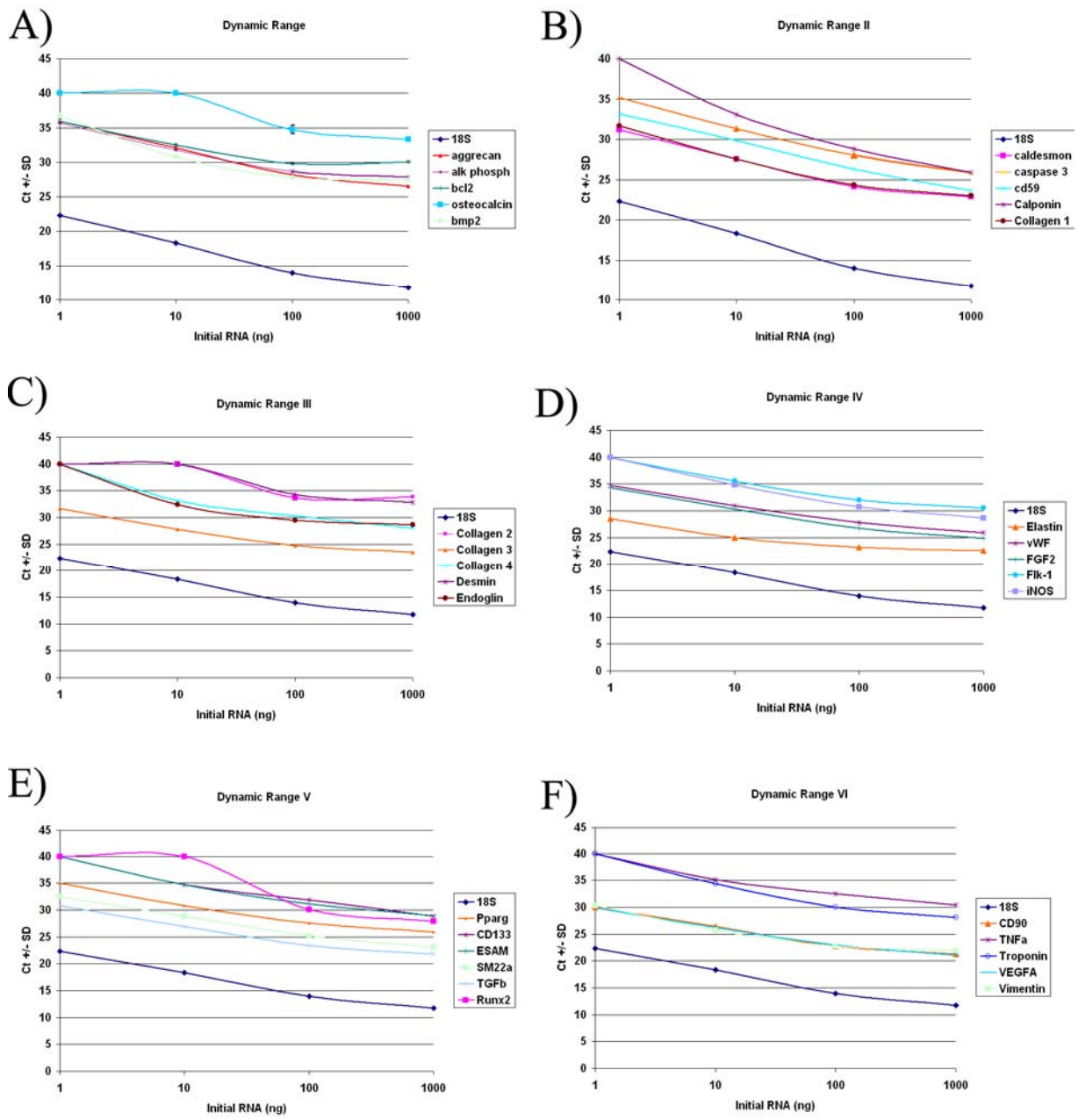

Figure H.1: Dynamic range assessment for the 32 genes chosen for the TLDA card. Each gene was tested against different starting RNA masses that spanned 4 logs.

APPENDIX I

COMPARISON OF ENDOGENOUS CONTROLS

PCR data from one experiment was analyzed by SDS software using either 18s or Gusb as the endogenous control. The RQ values for Aggrecan were compared as an example. By using 18s as the endogenous control, the RQ values for pressure and stretch were increased 88% and 40%, respectively, while the RQ values for shear stress were decreased 27% (**Table I.1**).

Table I.1: Comparison of the RQ values for Aggrecan when either 18s or Gusb are used as the endogenous control for $\Delta\Delta C_T$ evaluation. The relative change in expression is constant for all genes in a given set because all genes are normalized to the single C_T value for that stimulus.

	Gusb Endogenous			18s Endogenous		
Gene Name	Pressure	Shear	Stretch	Pressure	Shear	Stretch
Endogenous Control (C_T value)	23.10	24.44	23.59	6.75	6.73	6.81
Aggrecan	0.98	0.84	0.85	1.84	0.62	1.19
Percent difference from Gusb				+88%	-27%	+40%

APPENDIX J

WESTERN BLOT ENDPOINTS

J.1 SMOOTH MUSCLE ALPHA-ACTIN

SMA, which was successfully detected by IHC in the 5 day Mechanical Panel experiments, was proposed to be studied by Western blotting in Specific Aims 3 and 4. Following several attempts and troubleshooting steps, we have been unable to accurately, and reproducibly target SMA in a Western blot. Initial attempts using the antibody from Chemicon (MAB1536) were thought successful since only a single band appeared on the blot (**Figure J.1**). However, upon closer examination of the molecular weight of this protein, we discovered that it was much too large to be SMA. Our measurements indicated its molecular weight to be approximately 68kDa, whereas SMA has a reported molecular weight of 42 kDa. A separate SDS page gel was run, stained with Coomassie Brilliant Blue, and the 70kDa band was excised. A tryptic digestion and mass spectrometry analysis of the band was carried out by Dr. Andy Amoscato in the Department of Pathology. The resulting amino acid sequences were compared to other known sequences obtained by tryptic digestion. The tryptic digests from our sample matched to a 70kDa serum albumin precursor protein known as Phi AP3. In addition to serum albumin precursor, the first ten amino acids for SMA were also present, which helped to explain why this particular band

was staining for SMA by Western blotting at 70kDa. The presence of these two molecules has previously been identified as part of a redox sensing mechanism in SMCs [705]. We are as yet unsure why this process may be occurring in BMMSCs, since the protein band has appeared in every cell lysate from both the tBMMSC and BMMSCs isolated by Hamilton et al.[526].

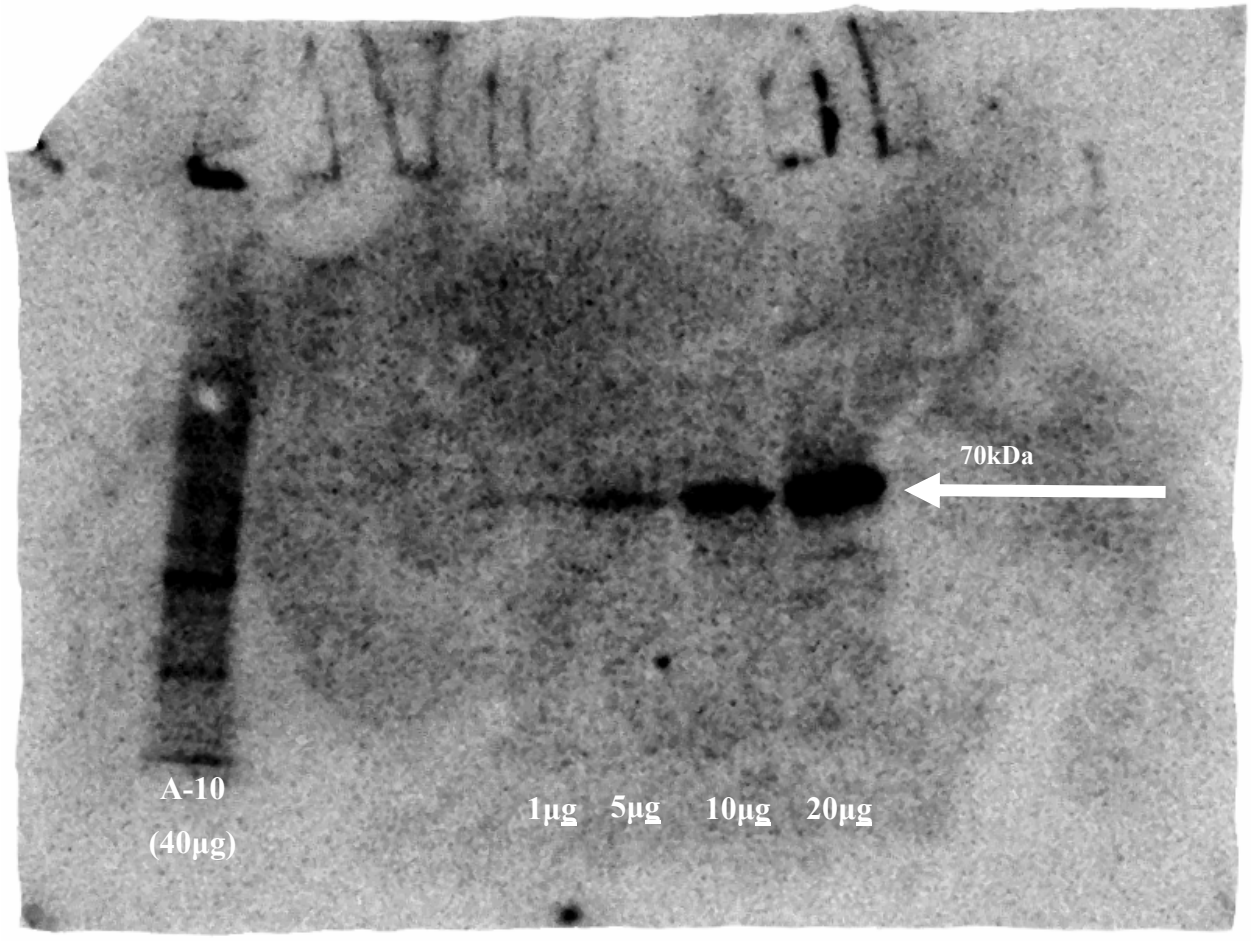

Figure J.1: Representative Western blot of SMA. The far left lane contains the A-10 cell lysate, which was used as a positive control. The remaining lanes contain increasing masses of pooled tBMMSC protein from several Mechanical Panel experiments, which was used to perform the initial Western blot testing. The arrow points to the 70kDa Phi AP3 band which appears prominently in our tBMMSCs.

In addition to the Phi AP3 band in the BMMSCs, the A-10 cell lysates displayed a constant non-specific staining the entire length of the lane. We made several attempts to inhibit this non-specific binding by changing blocking solutions, antibody concentrations, incubation temperatures, and the antibody itself. Using SuperBlock (Pierce), a 1:180,000 dilution of SMA from Sigma (clone 1A4), and a 45^{o}C primary antibody incubating temperature reduced the general non-specific staining to several distinct bands (**Figure J.2**), which was an improvement over the previous blot (**Figure J.1**). However, the strongest bands for the BMMSCs appeared at 37 kDa and 60 kDa, the positive control stained strongest at 37 kDa. These results led us to abandon our attempts to measure changes in SMA expression by Western blot.

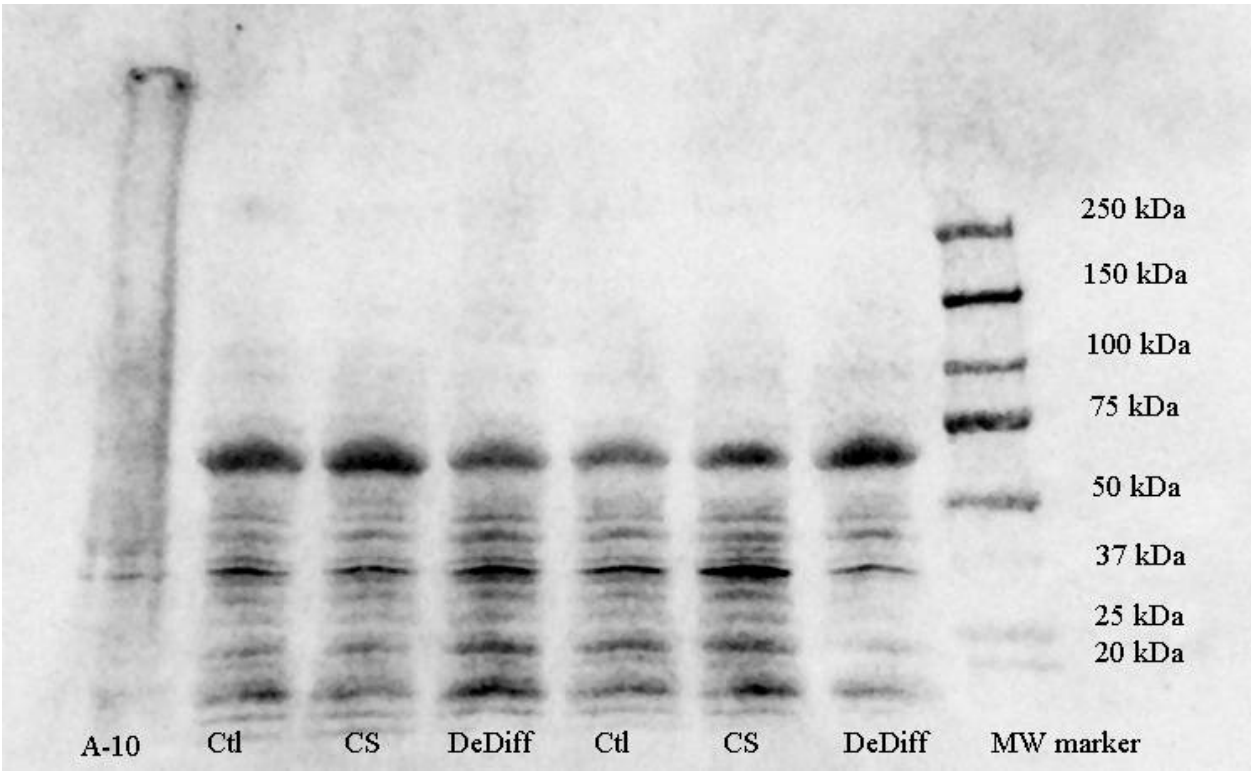

Figure J.2: Western blot for SMA depicting non-specific staining. A-10 cell lysates were used as a positive control. All lanes were loaded with 40μg of total protein.

J.2 SM-MHC

SM-MHC, which was weakly detected by IHC in the 5 day Mechanical Panel experiments, was proposed to be studied by Western blotting in Specific Aims 3 and 4. Using the same antibody from Dako, we attempted to detect SMMHC in our cyclic stretch experiments, using A-10 cell lysates as the positive control. We were unable to detect any signal from the 50μg of positive control and hypothesize that the problem rests with the transfer protocol. We have tried multiple different protocols that included high voltage transfer, addition of SDS to the transfer buffer, and extended transfer times. These changes were based upon the recommendation of the positive

control manufacturer, but have thus far been unsuccessful. A representative Western blot for SM-MHC is shown in **Figure J.3**.

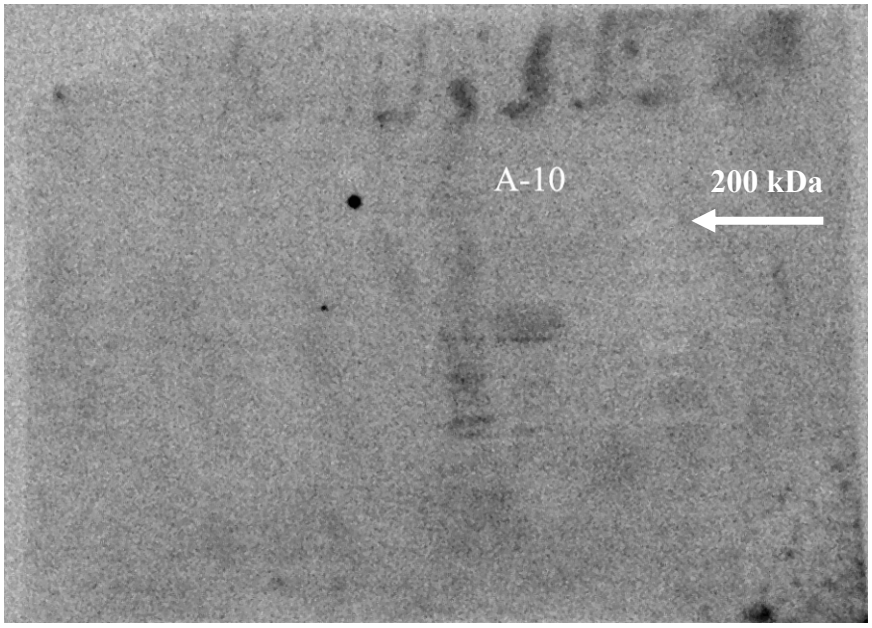

Figure J.3: Western blot for SM-MHC. The positive control (A-10) was loaded at 50µg of total protein and failed to generate any signal at 200 kDa, which is the appropriate molecular weight for SM-MHC.

J.3 PECAM

We were encouraged by the PCR results for PECAM under LSS and CP (**Table 3.6**) despite not being able to detect PECAM by IHC in our initial 5 day experiments (see **Figure 3.20**). PECAM Western blots were transferred using recommended high molecular weight protocols. Using 20 µg of the positive control (Jurkat cell lysates), we were able to detect a weak positive signal (**Figure J.4**). However, the same loading mass of our pooled experimental samples, were negative for PECAM.

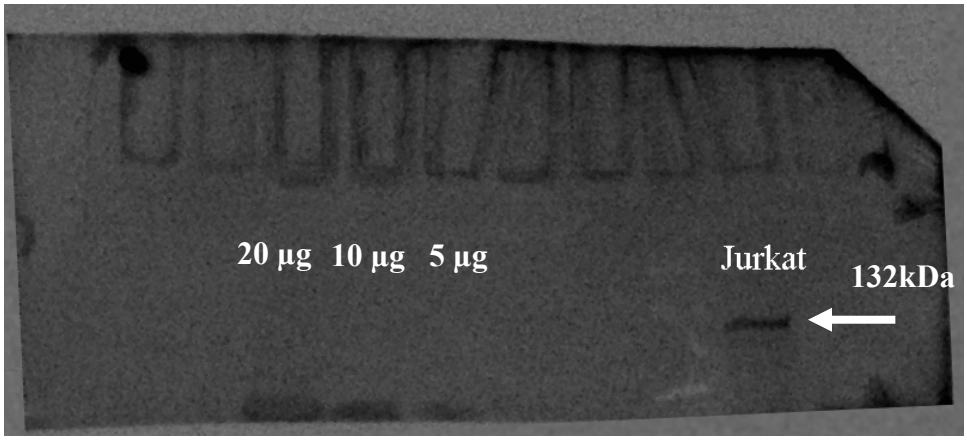

Figure J.4: Representative Western blot for PECAM using the positive control (Jurkat cell lysate) as well as pooled experimental protein. Jurkat total protein was loaded at 20µg, and the pooled expeirmental proteins were loaded at the masses indicated in the figure.

Our next step was to increase the mass of the Jurkat positive control protein to 50µg and use 40µg of the same CP and LSS samples that registered signal by PCR. This resulted in a stronger signal for the positive control, but the CP and LSS samples still did not show any signal for PECAM (**Figure J.5**). This has led us to conclude that either our experimental samples either contain very minor amounts of PECAM, or our protein extraction technique is not optimized for hydrophobic membrane-bound proteins.

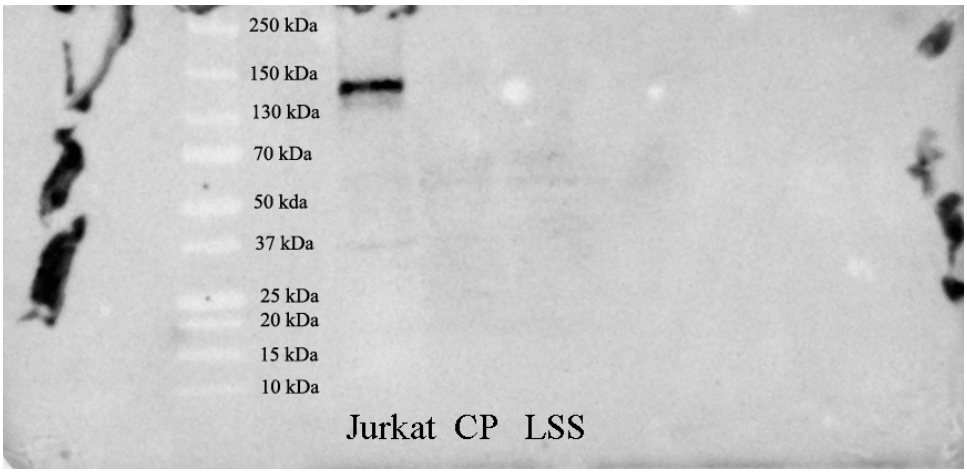

Figure J.5: Western blot for PECAM for 50µg of Jurkat, and 40µg each of the CP and LSS samples.

J.4 FLK-1

Flk-1 was the only EC-related protein detected by IHC in the 5 day experiments (**Figure 3.19**). Because it was constitutively expressed, we felt confident we could detect flk-1 by Western blot in our 24 hours and 3 day experiments. Our first Western blots for flk-1 using the positive control (ECV304 cell lysates), were successful, but the signal was extremely weak (**Figure J.6**)

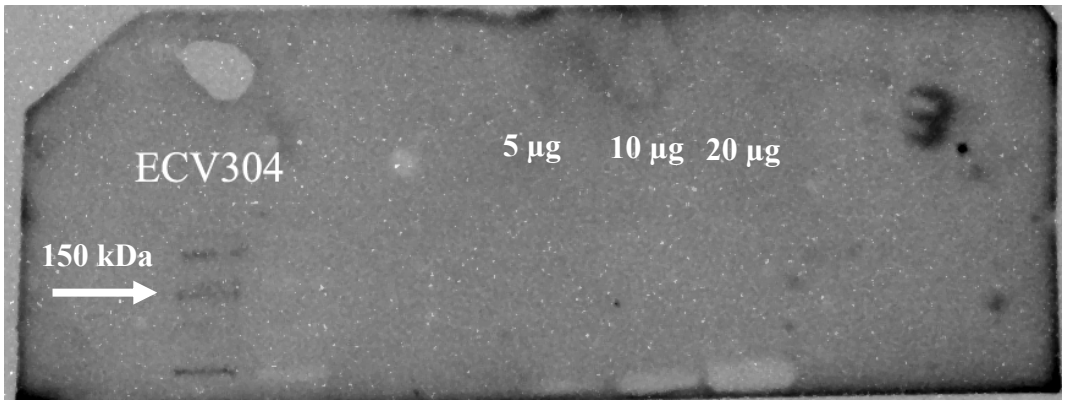

Figure J.6: Western blot for flk-1. ECV304 cell lysates were loaded at 25 µg total protein mass. Pooled experimental samples were loaded at the masses indicated in the figure.

We increased the amount of protein up to 50µg per lane and used modified transfer protocols for high molecular weight proteins (see **Table 4.5** for parameters), which was the maximum amount of protein we could reasonably load without sacrificing our ability to perform other Western blots. While the signal for the positive control sample increased, we were not able to detect any signal from our experimental samples (**Figure J.7**). Taking into consideration that flk-1 gene expression was present in these samples, that previous IHC data clearly showed constitutive expression of flk-1 protein, and that we have a good signal for the positive control (indicating the

transfer process was adequate), we conclude that our protein solubilization method was not optimized for hydrophobic proteins.

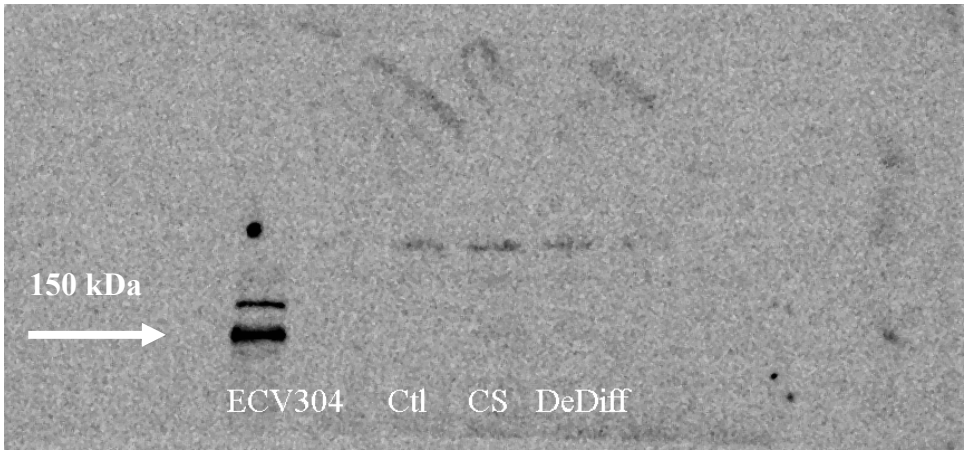

Figure J.7: Flk-1 Western blot for the positive control (ECV304) and three experimental samples. All prpotein was loaded at 50µg per lane.

J.5 SILVER STAIN

To test the hypothesis that we had difficulty solubilizing the higher molecular weight proteins, we used a silver stain (#161-0449, Bio-Rad), which is capable of detecting nanograms of protein. Approximately 20µg of protein was loaded in each lane. Three lanes were loaded with protein extracted using T-PER (#78510, Pierce), which was used in a few very early experiments. The remaining 6 lanes were loaded with protein extracted using the methods described in Section 4.2.2.3 and were representative of the various time points and stimuli used throughout this dissertation. SDS-PAGE was performed as described in Section 4.2.2.4.1, and silver staining was performed according to the manufacturer's protocols. The results of the silver stain (**Figure**

J.8) indicate that we do have some higher molecular weight protein coming into solution from the Trizol™ isolations, but it is clear that the amount of these proteins makes up a very minor fraction of the total protein. The greatest mass of protein occurs at 70k kDa, which coincides with the Phi AP3 protein identified in Section J.1. Also, 2/3 of the 3 day time point samples show almost no protein between 80 and 300 kDa. Thus, there is obvious heterogeneity in the isolation procedure. Given that transfer efficiency is always much less than 100%, it is not unreasonable to conclude that the fraction of high molecular weight protein is low enough to require greater than 50-100 μg total protein in order to transfer sufficient quantities to detect by Western blot. Loading this much protein would cause severe lane distortion because of the high mass of the Phi AP3 protein. Potential alternatives include immunoprecipitation of the desired high molecular weight protein to improve our ability to load higher quantities or immunoprecipitation of the Phi AP3 protein to remove it from the total protein before SDS-PAGE.

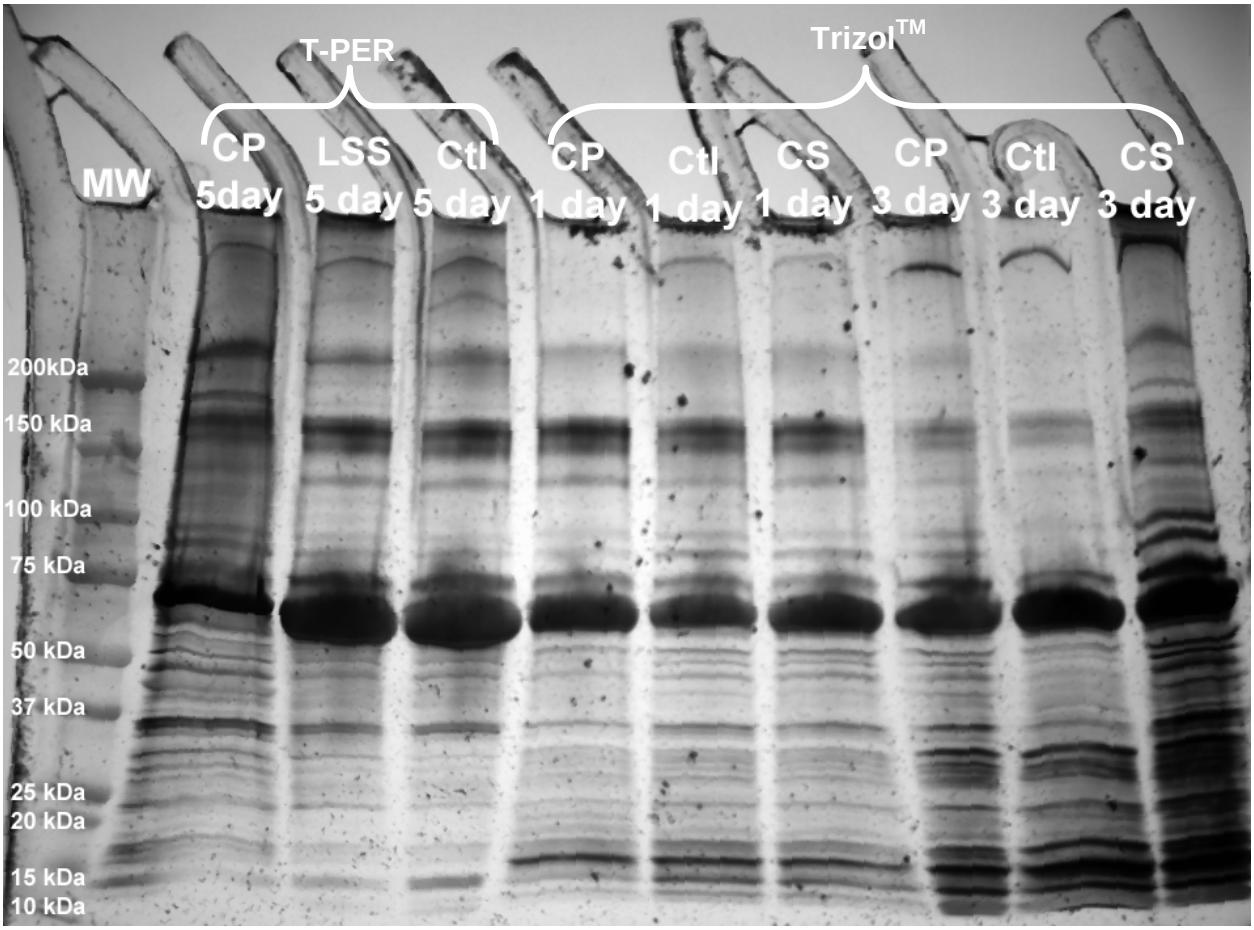

Figure J.8: Silver stained SDS page gel loaded with 20µg of total protein from various experiments.

BIBLIOGRAPHY

1. Maul, T.M., et al., *A new experimental system for the extended application of cyclic hydrostatic pressure to cell culture.* J Biomech Eng, 2007. **129**(1): p. 110-6.

2. Rosamond, W., et al., *Heart disease and stroke statistics--2007 update: a report from the American Heart Association Statistics Committee and Stroke Statistics Subcommittee.* Circulation, 2007. **115**(5): p. e69-171.

3. *Fast Stats: Inpatient Surgery*. [Web Site] 2003 November 14 [cited 2003 November 22]; Available from: http://www.cdc.gov/nchs/fastats/insurg.htm.

4. Association, A.H., *Heart Disease and Stroke Statistics-2003 Update*. 2002, American Heart Association: Dallas, TX. p. 46.

5. Ku, D.N. and R.C. Allen, *Vascular Grafts*, in *The Biomedical Engineering Handbook*, J.D. Bronzino, Editor. 1995, CRC Press: Boca Raton. p. 1871-1878.

6. Goldman, S., et al., *Long-term patency of saphenous vein and left internal mammary artery grafts after coronary artery bypass surgery: results from a Department of Veterans Affairs Cooperative Study.* J Am Coll Cardiol, 2004. **44**(11): p. 2149-56.

7. FitzGibbon, G.M., et al., *Coronary bypass graft fate. Angiographic study of 1,179 vein grafts early, one year, and five years after operation.* J Thorac Cardiovasc Surg, 1986. **91**(5): p. 773-8.

8. Weintraub, W.S., et al., *Frequency of repeat coronary bypass or coronary angioplasty after coronary artery bypass surgery using saphenous venous grafts.* Am J Cardiol, 1994. **73**(2): p. 103-12.

9. Brattich, M., *Vascular access thrombosis: etiology and prevention.* ANNA J, 1999. **26**(5): p. 537-40.

10. Hakim, R. and J. Himmelfarb, *Hemodialysis access failure: a call to action.* Kidney Int, 1998. **54**(4): p. 1029-40.

11. Johansen, K., D. Lyman, and L. Sauvage, *Biomaterials for hemodialysis access.* Blood Purif, 1994. **12**(1): p. 73-7.

12. Roy Chaudhury, P., et al., *Hemodialysis vascular access dysfunction from basic biology to clinical intervention.* Adv Ren Replace Ther, 2002. **9**(2): p. 74-84.

13. Zdrahala, R.J., *Small caliber vascular grafts. Part II: Polyurethanes revisited.* J Biomater Appl, 1996. **11**(1): p. 37-61.

14. Grigioni, M., et al., *Biomechanics and Hemodynamics of Grafting*, in *Vascular Grafts: Experiment and Modeling*, A. Tura, Editor. 2003, WIT Press: Boston. p. 41-82.

15. Davids, L., T. Dower, and P. Zilla, *The Lack of Healing in Conventional Vascular Grafts*, in *Tissue Engineering of Vascular Prosthetic Grafts*, P. Zilla and H.P. Greisler, Editors. 1999, R.G. Landes: Austin. p. 3-45.

16. Gray, J.L., et al., *FGF-1 affixation stimulates ePTFE endothelialization without intimal hyperplasia.* The Journal of Surgical Research, 1994. **57**(5): p. 596-612.

17. Greisler, H.P., *New Biologic and Synthetic Vascular Prostheses*. Medical Intelligence Unit. 1991, Autsin: R.G. Landes. 91.

18. Xue, L. and H.P. Greisler, *Biomaterials in the development and future of vascular grafts.* J Vasc Surg, 2003. **37**(2): p. 472-80.

19. Abbott, W.M., et al., *Effect of compliance mismatch on vascular graft patency.* J Vasc Surg, 1987. **5**(2): p. 376-82.

20. Saifalian, A., et al., *Noncompliance: The Silent Acceptance of a Villain*, in *Tissue Engineering of Vascular Prosthetic Grafts*, P. Zilla and H.P. Greisler, Editors. 1999, R.G. Landes: Austin. p. 45-55.

21. Stewart, S.F. and D.J. Lyman, *Effects of a vascular graft/natural artery compliance mismatch on pulsatile flow.* J Biomech, 1992. **25**(3): p. 297-310.

22. Badylak, S.F., et al., *Small intestinal submucosa as a large diameter vascular graft in the dog.* J Surg Res, 1989. **47**(1): p. 74-80.

23. McFetridge, P.S., et al., *Preparation of porcine carotid arteries for vascular tissue engineering applications.* J Biomed Mater Res A, 2004. **70**(2): p. 224-34.

24. Laub, G.W., et al., *Cryopreserved allograft veins as alternative coronary artery bypass conduits: early phase results.* Ann Thorac Surg, 1992. **54**(5): p. 826-31.

25. Cowan, D.B. and B.L. Langille, *Cellular and molecular biology of vascular remodeling.* Curr Opin Lipidol, 1996. **7**(2): p. 94-100.

26. Henry, M., et al., *State of the Art: Which Stent for Which Lesion in Peripheral Interventions.* Texas Heart Institute Journal, 2000. **27**(2): p. 119-126.

27. Kivela, A. and J. Hartikainen, *Restenosis related to percutaneous coronary intervention has been solved?* Ann Med, 2006. **38**(3): p. 173-87.

28. Bavry, A.A., et al., *Late thrombosis of drug-eluting stents: a meta-analysis of randomized clinical trials.* Am J Med, 2006. **119**(12): p. 1056-61.

29. Kandzari, D.E., *Drug-eluting stent thrombosis: it's never too late.* Nat Clin Pract Cardiovasc Med, 2006. **3**(12): p. 638-9.

30. Serruys, P.W., M.J. Kutryk, and A.T. Ong, *Coronary-artery stents.* N Engl J Med, 2006. **354**(5): p. 483-95.

31. Spertus, J.A., et al., *Prevalence, predictors, and outcomes of premature discontinuation of thienopyridine therapy after drug-eluting stent placement: results from the PREMIER registry.* Circulation, 2006. **113**(24): p. 2803-9.

32. US Food and Drug Administration. *FDA Statement on Coronary Drug-Eluting Stents*. [Web page] 2006 December 7 [cited 2006 December 15, 2006]; Available from: http://www.fda.gov/cdrh/news/091406.html.

33. Herring, M., *Endothelial Seeding Blood Flow Surfaces*, in *Vascular Grafting: Clinical Applications and Techniques*, C. Wright, Editor. 1983, PSG Inc. p. 275-314.

34. Zilla, P., et al., *Endothelial cell seeding of polytetrafluoroethylene vascular grafts in humans: a preliminary report.* J Vasc Surg, 1987. **6**(6): p. 535-41.

35. Weinberg, C.B. and E. Bell, *A blood vessel model constructed from collagen and cultured vascular cells.* Science, 1986. **231**(4736): p. 397-400.

36. Zilla, P. and H.P. Greisler, eds. *Tissue Engineering of Vascular Prosthetic Grafts*. 1999, R.G. Landes: Austin. 613.

37. Gosselin, C., et al., *ePTFE coating with fibrin glue, FGF-1 and heparin: effect on retention of seeded EC.* J Surg Res, 1996. **60**: p. 327-332.

38. L'Heureux, N., et al., *In vitro construction of a human blood vessel from cultured vascular cells: a morphologic study.* J Vasc Surg, 1993. **17**(3): p. 499-509.

39. Niklason, L.E., et al., *Functional arteries grown in vitro.* Science, 1999. **284**(5413): p. 489-93.

40. Tranquillo, R.T., et al., *Magnetically orientated tissue-equivalent tubes: application to a circumferentially orientated media-equivalent.* Biomaterials, 1996. **17**: p. 349-57.

41. Isenberg, B.C., C. Williams, and R.T. Tranquillo, *Endothelialization and flow conditioning of fibrin-based media-equivalents.* Ann Biomed Eng, 2006. **34**(6): p. 971-85.

42. Ross, J.J., et al., *Cytokine-induced differentiation of multipotent adult progenitor cells into functional smooth muscle cells.* J Clin Invest, 2006.

43. Nerem, R.M. and D. Seliktar, *Vascular tissue engineering.* Annu Rev Biomed Eng, 2001. **3**: p. 225-43.

44. Edelman, E.R., *Vascular tissue engineering : designer arteries.* Circ Res, 1999. **85**(12): p. 1115-7.

45. Ratcliffe, A., *Tissue engineering of vascular grafts.* Matrix Biology, 2000. **19**(4): p. 353-357.

46. L'Heureux, N., et al., *A completely biological tissue engineered human blood vessel.* FASEB J, 1998. **12**(1): p. 47-56.

47. Strehl, R., et al., *Proliferating cells versus differentiated cells in tissue engineering.* Tissue Eng, 2002. **8**(1): p. 37-42.

48. McKee, J.A., et al., *Human arteries engineered in vitro.* EMBO Rep, 2003. **4**(6): p. 633-8.

49. Rafii, S., et al., *Contribution of marrow-derived progenitors to vascular and cardiac regeneration.* Semin Cell Dev Biol, 2002. **13**(1): p. 61-7.

50. Sekiya, I., et al., *Expansion of human adult stem cells from bone marrow stroma: conditions that maximize the yields of early progenitors and evaluate their quality.* Stem Cells, 2002. **20**(6): p. 530-41.

51. Strauer, B.E., et al., *Repair of infarcted myocardium by autologous intracoronary mononuclear bone marrow cell transplantation in humans.* Circulation, 2002. **106**(15): p. 1913-8.

52. Iba, O., et al., *Angiogenesis by implantation of peripheral blood mononuclear cells and platelets into ischemic limbs.* Circulation, 2002. **106**(15): p. 2019-25.

53. Gojo, S., et al., *In vivo cardiovasculogenesis by direct injection of isolated adult mesenchymal stem cells.* Exp Cell Res, 2003. **288**: p. 51-59.

54. Al-Khaldi, A., et al., *Postnatal bone marrow stromal cells elicit a potent VEGF-dependent neoangiogenic response in vivo.* Gene Ther, 2003. **10**(8): p. 621-9.

55. Kadner, A., et al., *A new source for cardiovascular tissue engineering: human bone marrow stromal cells.* European Journal of Cardio-Thoracic Surgery, 2002. **21**(6): p. 1055-60.

56. Pittenger, M.F., et al., *Multilineage potential of adult human mesenchymal stem cells.* Science, 1999. **284**(5411): p. 143-7.

57. Jackson, K.A., et al., *Stem cells: a minireview.* J Cell Biochem Suppl, 2002. **38**: p. 1-6.

58. Huss, R., *Perspectives on the morphology and biology of CD34-negative stem cells.* J Hematother Stem Cell Res, 2000. **9**(6): p. 783-93.

59. Gabella, G., *Morphology of Smooth Muscle*, in *Cellular Aspects of Smooth Muscle Function*, C.Y. Kao and M.E. Carsten, Editors. 1997, Cambridge University Press: New York. p. 1-48.

60. Gilbert, S.F., *Developmental Biology*. 5th ed. 1997, Sunderland: Sinauer Associates. 918.

61. Owens, G.K., *Regulation of differentiation of vascular smooth muscle cells.* Physiol Rev, 1995. **75**(3): p. 487-517.

62. Owens, G.K., M.S. Kumar, and B.R. Wamhoff, *Molecular Regulation of Vascular Smooth Muscle Cell Differentiation in Development and Disease.* Physiol Rev, 2004. **84**(3): p. 767-801.

63. Kumar, M.S. and G.K. Owens, *Combinatorial Control of Smooth Muscle-Specific Gene Expression.* Arterioscler Thromb Vasc Biol, 2003. **23**(5): p. 737-747.

64. Hungerford, J.E., et al., *Identification of a novel marker for primordial smooth muscle and its differential expression pattern in contractile vs noncontractile cells.* J Cell Biol, 1997. **137**(4): p. 925-37.

65. Sobue, K. and J.R. Sellers, *Caldesmon, a novel regulatory protein in smooth muscle and nonmuscle actomyosin systems.* J Biol Chem, 1991. **266**(19): p. 12115-8.

66. Nieponice, A., et al. (2006) *Vascular Tissue Engineering*. Encyclopedia of Biomaterials and Biomedical Engineering **Volume**, 1-14 DOI: E-EBBE-120041896

67. Hungerford, J.E. and C.D. Little, *Developmental biology of the vascular smooth muscle cell: building a multilayered vessel wall.* J Vasc Res, 1999. **36**(1): p. 2-27.

68. Duband, J.L., et al., *Calponin and SM 22 as differentiation markers of smooth muscle: spatiotemporal distribution during avian embryonic development.* Differentiation, 1993. **55**(1): p. 1-11.

69. Fatigati, V. and R.A. Murphy, *Actin and tropomyosin variants in smooth muscles. Dependence on tissue type.* J Biol Chem, 1984. **259**(23): p. 14383-8.

70. North, A.J., et al., *Actin isoform compartments in chicken gizzard smooth muscle cells.* J Cell Sci, 1994. **107 (Pt 3)**: p. 445-55.

71. Parker, C.A., et al., *Cytoskeletal targeting of calponin in differentiated, contractile smooth muscle cells of the ferret.* J Physiol, 1998. **508 (Pt 1)**: p. 187-98.

72. Morgan, K.G. and S.S. Gangopadhyay, *Invited review: cross-bridge regulation by thin filament-associated proteins.* Journal of Applied Physiology, 2001. **91**(2): p. 953-62.

73. Word, R.A. and K.E. Kamm, *Regulation of Smooth Muscle Contraction by Myosin Phosphorylation*, in *Cellular Aspects of Smooth Muscle Function*, C.Y. Kao and M.E. Carsten, Editors. 1997, Cambridge University Press: New York. p. 209-252.

74. Zhu, P., et al., *Transdifferentiation of pulmonary arteriolar endothelial cells into smooth muscle-like cells regulated by myocardin involved in hypoxia-induced pulmonary vascular remodelling.* International Journal of Experimental Pathology, 2006. **87**(6): p. 463-74.

75. Greenberg, R.S., et al., *FAK-dependent regulation of myofibroblast differentiation.[erratum appears in FASEB J. 2006 Jul;20(9):1573].* FASEB J, 2006. **20**(7): p. 1006-8.

76. Sen, U., et al., *Homocysteine-induced myofibroblast differentiation in mouse aortic endothelial cells.* J Cell Physiol, 2006. **209**(3): p. 767-74.

77. Arciniegas, E., et al., *Transforming growth factor beta 1 promotes the differentiation of endothelial cells into smooth muscle-like cells in vitro.* J Cell Sci, 1992. **103**(Pt 2): p. 521-9.

78. Hautmann, M.B., P.J. Adam, and G.K. Owens, *Similarities and differences in smooth muscle alpha-actin induction by TGF-beta in smooth muscle versus non-smooth muscle cells.* Arterioscler Thromb Vasc Biol, 1999. **19**(9): p. 2049-58.

79. Strasser, P., et al., *Mammalian calponin : Identification and expression of genetic variants.* FEBS Letters, 1993. **330**(1): p. 13-18.

80. Winder, S.J. and M.P. Walsh, *Calponin: thin filament-linked regulation of smooth muscle contraction.* Cellular Signalling, 1993. **5**(6): p. 677-86.

81. Takeuchi, K., et al., *Co-localization of immunoreactive forms of calponin with actin cytoskeleton in platelets, fibroblasts, and vascular smooth muscle.* Journal of Biochemistry, 1991. **109**(2): p. 311-6.

82. Ogawa, Y., et al., *Immunohistochemistry of myoepithelial cells during development of the rat salivary glands.* Anat Embryol (Berl), 1999. **200**(2): p. 215-28.

83. Cevallos, M., et al., *Cyclic strain induces expression of specific smooth muscle cell markers in human endothelial cells.* Differentiation, 2006. **74**(9-10): p. 552-61.

84. Ishisaki, A., et al., *Human umbilical vein endothelium-derived cells retain potential to differentiate into smooth muscle-like cells.* J Biol Chem, 2003. **278**(2): p. 1303-9.

85. Frid, M.G., V.A. Kale, and K.R. Stenmark, *Mature vascular endothelium can give rise to smooth muscle cells via endothelial-mesenchymal transdifferentiation: in vitro analysis.* Circulation Research, 2002. **90**(11): p. 1189-96.

86. Solway, J., et al., *Structure and expression of a smooth muscle cell-specific gene, SM22 alpha.* J Biol Chem, 1995. **270**(22): p. 13460-9.

87. Fu, Y., et al., *Mutagenesis analysis of human SM22: characterization of actin binding.* Journal of Applied Physiology, 2000. **89**(5): p. 1985-90.

88. Gimona, M. and R. Mital, *The single CH domain of calponin is neither sufficient nor necessary for F-actin binding.* J Cell Sci, 1998. **111**(Pt 13): p. 1813-21.

89. Lawson, D., M. Harrison, and C. Shapland, *Fibroblast transgelin and smooth muscle SM22alpha are the same protein, the expression of which is down-regulated in many cell lines.* Cell Motility & the Cytoskeleton, 1997. **38**(3): p. 250-7.

90. Prinjha, R.K., et al., *Cloning and sequencing of cDNAs encoding the actin cross-linking protein transgelin defines a new family of actin-associated proteins.* Cell Motil Cytoskeleton, 1994. **28**(3): p. 243-55.

91. Zhang, J.C., et al., *Analysis of SM22alpha-deficient mice reveals unanticipated insights into smooth muscle cell differentiation and function.* Molecular & Cellular Biology, 2001. **21**(4): p. 1336-44.

92. Ueki, N., et al., *Expression of high and low molecular weight caldesmons during phenotypic modulation of smooth muscle cells.* Proc Natl Acad Sci U S A, 1987. **84**(24): p. 9049-53.

93. van der Loop, F.T., et al., *Smoothelin, a novel cytoskeletal protein specific for smooth muscle cells.* Journal of Cell Biology, 1996. **134**(2): p. 401-11.

94. Deruiter, M.C., et al., *Smoothelin expression during chicken embryogenesis: detection of an embryonic isoform.* Dev Dyn, 2001. **221**(4): p. 460-3.

95. Kramer, J., et al., *A novel isoform of the smooth muscle cell differentiation marker smoothelin.[see comment][erratum appears in J Mol Med 1999 Apr;77(4):399]*. Journal of Molecular Medicine, 1999. **77**(2): p. 294-8.

96. van Eys, G.J., P.M. Niessen, and S.S. Rensen, *Smoothelin in vascular smooth muscle cells.* Trends Cardiovasc Med, 2007. **17**(1): p. 26-30.

97. van der Loop, F.T., et al., *Differentiation of smooth muscle cells in human blood vessels as defined by smoothelin, a novel marker for the contractile phenotype.* Arteriosclerosis, Thrombosis & Vascular Biology, 1997. **17**(4): p. 665-71.

98. Niessen, P., et al., *Smoothelin-a is essential for functional intestinal smooth muscle contractility in mice.* Gastroenterology, 2005. **129**(5): p. 1592-601.

99. Sartore, S., et al., *Myosin gene expression and cell phenotypes in vascular smooth muscle during development, in experimental models, and in vascular disease.* Arterioscler Thromb Vasc Biol, 1997. **17**(7): p. 1210-5.

100. Shiojima, I., et al., *Embryonic smooth muscle myosin heavy chain SMemb is expressed in pressure-overloaded cardiac fibroblasts.* Japanese Heart Journal, 1999. **40**(6): p. 803-18.

101. Frangogiannis, N.G., L.H. Michael, and M.L. Entman, *Myofibroblasts in reperfused myocardial infarcts express the embryonic form of smooth muscle myosin heavy chain (SMemb).* Cardiovasc Res, 2000. **48**(1): p. 89-100.

102. Aikawa, M., et al., *Smooth muscle phenotypes in developing and atherosclerotic human arteries demonstrated by myosin expression.* Journal of Atherosclerosis & Thrombosis, 1995. **2**(1): p. 14-23.

103. Wang, D.-Z., et al., *Activation of Cardiac Gene Expression by Myocardin, a Transcriptional Cofactor for Serum Response Factor.* Cell, 2001. **105**(7): p. 851-862.

104. Li, S., et al., *The serum response factor coactivator myocardin is required for vascular smooth muscle development.* Proc Natl Acad Sci U S A, 2003. **100**(16): p. 9366-70.

105. Chen, J., et al., *Myocardin: a component of a molecular switch for smooth muscle differentiation.* J Mol Cell Cardiol, 2002. **34**(10): p. 1345-56.

106. Du, K.L., et al., *Myocardin is a critical serum response factor cofactor in the transcriptional program regulating smooth muscle cell differentiation.* Mol Cell Biol, 2003. **23**(7): p. 2425-37.

107. Yoshida, T., K. Kawai-Kowase, and G.K. Owens, *Forced expression of myocardin is not sufficient for induction of smooth muscle differentiation in multipotential embryonic cells.[see comment]*. Arteriosclerosis, Thrombosis & Vascular Biology, 2004. **24**(9): p. 1596-601.

108. Rensen, S.S., et al., *Contribution of serum response factor and myocardin to transcriptional regulation of smoothelins.* Cardiovasc Res, 2006. **70**(1): p. 136-45.

109. Heldin, C.-H. and B. Westermark, *Mechanism of Action and In Vivo Role of Platelet-Derived Growth Factor.* Physiol. Rev., 1999. **79**(4): p. 1283-1316.

110. Raines, E.W., *PDGF and cardiovascular disease.* Cytokine Growth Factor Rev, 2004. **15**(4): p. 237-254.

111. Betsholtz, C., L. Karlsson, and P. Lindahl, *Developmental roles of platelet-derived growth factors.* Bioessays, 2001. **23**(6): p. 494-507.

112. Panek, R.L., et al., *PDGF receptor protein tyrosine kinase expression in the balloon-injured rat carotid artery.* Arterioscler Thromb Vasc Biol, 1997. **17**(7): p. 1283-8.

113. Tanizawa, S., et al., *Expression of platelet derived growth factor B chain and beta receptor in human coronary arteries after percutaneous transluminal coronary angioplasty: an immunohistochemical study.* Heart, 1996. **75**(6): p. 549-56.

114. Majesky, M.W., et al., *PDGF ligand and receptor gene expression during repair of arterial injury.* J Cell Biol, 1990. **111**(5 Pt 1): p. 2149-58.

115. Sarzani, R., et al., *Effects of hypertension and aging on platelet-derived growth factor and platelet-derived growth factor receptor expression in rat aorta and heart.* Hypertension, 1991. **18**(5 Suppl): p. III93-9.

116. Tanabe, Y., et al., *Mechanical stretch augments PDGF receptor beta expression and protein tyrosine phosphorylation in pulmonary artery tissue and smooth muscle cells.* Mol Cell Biochem, 2000. **215**(1-2): p. 103-13.

117. Hu, Y., et al., *Activation of PDGF receptor alpha in vascular smooth muscle cells by mechanical stress.* FASEB J, 1998. **12**(12): p. 1135-42.

118. Rubin, K., et al., *Induction of B-type receptors for platelet-derived growth factor in vascular inflammation: possible implications for development of vascular proliferative lesions.* Lancet, 1988. **1**(8599): p. 1353-6.

119. Schollmann, C., et al., *Basic fibroblast growth factor modulates the mitogenic potency of the platelet-derived growth factor (PDGF) isoforms by specific upregulation of the PDGF alpha receptor in vascular smooth muscle cells.* J Biol Chem, 1992. **267**(25): p. 18032-9.

120. Lu, J., et al., *Coronary Smooth Muscle Differentiation from Proepicardial Cells Requires RhoA-Mediated Actin Reorganization and p160 Rho-Kinase Activity.* Dev Biol, 2001. **240**(2): p. 404-418.

121. Hellstrom, M., et al., *Role of PDGF-B and PDGFR-beta in recruitment of vascular smooth muscle cells and pericytes during embryonic blood vessel formation in the mouse.* Development, 1999. **126**(14): p. 3047-3055.

122. Brogi, E., et al., *Indirect angiogenic cytokines upregulate VEGF and bFGF gene expression in vascular smooth muscle cells, whereas hypoxia upregulates VEGF expression only.* Circulation, 1994. **90**(2): p. 649-52.

123. Winkles, J.A. and C.G. Gay, *Serum, phorbol ester, and polypeptide mitogens increase class 1 and 2 heparin-binding (acidic and basic fibroblast) growth factor gene expression in human vascular smooth muscle cells.* Cell Growth Differ, 1991. **2**(11): p. 531-40.

124. Terracio, L., et al., *Induction of platelet-derived growth factor receptor expression in smooth muscle cells and fibroblasts upon tissue culturing.* J Cell Biol, 1988. **107**(5): p. 1947-57.

125. Ferns, G.A., et al., *Inhibition of neointimal smooth muscle accumulation after angioplasty by an antibody to PDGF.* Science, 1991. **253**(5024): p. 1129-32.

126. Abedi, H. and I. Zachary, *Signalling mechanisms in the regulation of vascular cell migration.* Cardiovasc Res, 1995. **30**(4): p. 544-56.

127. Stegemann, J.P. and R.M. Nerem, *Phenotype modulation in vascular tissue engineering using biochemical and mechanical stimulation.* Ann Biomed Eng, 2003. **31**(4): p. 391-402.

128. Corjay, M.H., R.S. Blank, and G.K. Owens, *Platelet-derived growth factor-induced destabilization of smooth muscle alpha-actin mRNA.* J Cell Physiol, 1990. **145**(3): p. 391-7.

129. Corjay, M.H., et al., *Differential effect of platelet-derived growth factor- versus serum-induced growth on smooth muscle alpha-actin and nonmuscle beta-actin mRNA expression in cultured rat aortic smooth muscle cells.* J Biol Chem, 1989. **264**(18): p. 10501-6.

130. Reusch, P., et al., *Mechanical strain increases smooth muscle and decreases nonmuscle myosin expression in rat vascular smooth muscle cells.* Circ Res, 1996. **79**(5): p. 1046-53.

131. Wilson, E., et al., *Mechanical strain induces growth of vascular smooth muscle cells via autocrine action of PDGF.* J Cell Biol, 1993. **123**(3): p. 741-7.

132. Holycross, B.J., et al., *Platelet-derived growth factor-BB-induced suppression of smooth muscle cell differentiation.* Circ Res, 1992. **71**(6): p. 1525-32.

133. Okada, Y., et al., *The modulation of collagen synthesis in cultured arterial smooth muscle cells by platelet-derived growth factor.* Cell Biol Int Rep, 1992. **16**(10): p. 1015-22.

134. Okada, Y., et al., *Collagen synthesis of human arterial smooth muscle cells: effects of platelet-derived growth factor, transforming growth factor-beta 1 and interleukin-1.* Acta Pathol Jpn, 1993. **43**(4): p. 160-7.

135. Borrelli, V., et al., *Role of platelet-derived growth factor and transforming growth factor beta1 the in the regulation of metalloproteinase expressions.* Surgery, 2006. **140**(3): p. 454-63.

136. Risinger, G.M., Jr., et al., *Matrix metalloproteinase-2 expression by vascular smooth muscle cells is mediated by both stimulatory and inhibitory signals in response to growth factors.* J Biol Chem, 2006. **281**(36): p. 25915-25.

137. Massague, J., *TGF-beta signal transduction.* Annual Review of Biochemistry, 1998. **67**: p. 753-91.

138. Vargesson, N., *Vascularization of the developing chick limb bud: role of the TGFbeta signalling pathway.* J Anat, 2003. **202**(1): p. 93-103.

139. Bobik, A., *Transforming growth factor-betas and vascular disorders.* Arterioscler Thromb Vasc Biol, 2006. **26**(8): p. 1712-20.

140. Assoian, R.K., et al., *Transforming growth factor-beta in human platelets. Identification of a major storage site, purification, and characterization.* J Biol Chem, 1983. **258**(11): p. 7155-60.

141. Seay, U., et al., *Transforming growth factor-beta-dependent growth inhibition in primary vascular smooth muscle cells is p38-dependent.* Journal of Pharmacology & Experimental Therapeutics, 2005. **315**(3): p. 1005-12.

142. McCaffrey, T.A., et al., *Decreased type II/type I TGF-beta receptor ratio in cells derived from human atherosclerotic lesions. Conversion from an antiproliferative to profibrotic response to TGF-beta1.* J Clin Invest, 1995. **96**(6): p. 2667-75.

143. Iruela-Arispe, M.L. and E.H. Sage, *Endothelial cells exhibiting angiogenesis in vitro proliferate in response to TGF-beta 1.* J Cell Biochem, 1993. **52**(4): p. 414-30.

144. Pepper, M.S., *Transforming growth factor-beta: vasculogenesis, angiogenesis, and vessel wall integrity.* Cytokine Growth Factor Rev, 1997. **8**(1): p. 21-43.

145. Li, D.Y., et al., *Defective angiogenesis in mice lacking endoglin.* Science, 1999. **284**(5419): p. 1534-7.

146. Yang, X., et al., *Angiogenesis defects and mesenchymal apoptosis in mice lacking SMAD5.* Development, 1999. **126**(8): p. 1571-80.

147. Chang, H., et al., *Smad5 knockout mice die at mid-gestation due to multiple embryonic and extraembryonic defects.* Development, 1999. **126**(8): p. 1631-42.

148. Armulik, A., A. Abramsson, and C. Betsholtz, *Endothelial/pericyte interactions.* Circ Res, 2005. **97**(6): p. 512-23.

149. Sinha, S., et al., *Transforming growth factor-beta1 signaling contributes to development of smooth muscle cells from embryonic stem cells.* American Journal of Physiology - Cell Physiology, 2004. **287**(6): p. C1560-8.

150. Battegay, E.J., et al., *TGF-beta induces bimodal proliferation of connective tissue cells via complex control of an autocrine PDGF loop.* Cell, 1990. **63**(3): p. 515-24.

151. Gronwald, R.G., R.A. Seifert, and D.F. Bowen-Pope, *Differential regulation of expression of two platelet-derived growth factor receptor subunits by transforming growth factor-beta.* J Biol Chem, 1989. **264**(14): p. 8120-5.

152. Majesky, M.W., et al., *Production of transforming growth factor beta 1 during repair of arterial injury.* J Clin Invest, 1991. **88**(3): p. 904-10.

153. Grainger, D.J., et al., *Transforming growth factor beta decreases the rate of proliferation of rat vascular smooth muscle cells by extending the G2 phase of the cell cycle and delays the rise in cyclic AMP before entry into M phase.* Biochemical Journal, 1994. **299**(Pt 1): p. 227-35.

154. Singh, N.N. and D.P. Ramji, *The role of transforming growth factor-beta in atherosclerosis.* Cytokine Growth Factor Rev, 2006. **17**(6): p. 487-99.

155. Briones, V.R., et al., *Mechanism of fibroblast growth factor-binding protein 1 repression by TGF-beta.* Biochem Biophys Res Commun, 2006. **345**(2): p. 595-601.

156. Nomi, M., et al., *Principals of neovascularization for tissue engineering.* Mol Asp Med, 2002. **23**(6): p. 463-483.

157. Adam, P.J., et al., *Positive- and negative-acting Kruppel-like transcription factors bind a transforming growth factor beta control element required for expression of the smooth muscle cell differentiation marker SM22alpha in vivo.* J Biol Chem, 2000. **275**(48): p. 37798-806.

158. Hautmann, M.B., C.S. Madsen, and G.K. Owens, *A transforming growth factor beta (TGFbeta) control element drives TGFbeta-induced stimulation of smooth muscle alpha-actin gene expression in concert with two CArG elements.* J Biol Chem, 1997. **272**(16): p. 10948-56.

159. Desmouliere, A., et al., *Transforming growth factor-beta 1 induces alpha-smooth muscle actin expression in granulation tissue myofibroblasts and in quiescent and growing cultured fibroblasts.* Journal of Cell Biology, 1993. **122**(1): p. 103-11.

160. Chen, S., M. Kulik, and R.J. Lechleider, *Smad proteins regulate transcriptional induction of the SM22alpha gene by TGF-beta.* Nucleic Acids Res, 2003. **31**(4): p. 1302-10.

161. Hirschi, K.K., S.A. Rohovsky, and P.A. D'Amore, *PDGF, TGF-beta, and heterotypic cell-cell interactions mediate endothelial cell-induced recruitment of 10T1/2 cells and their differentiation to a smooth muscle fate.[erratum appears in J Cell Biol 1998 Jun 1;141(5):1287].* Journal of Cell Biology, 1998. **141**(3): p. 805-14.

162. Ninomiya, K., et al., *Transforming growth factor-beta signaling enhances transdifferentiation of macrophages into smooth muscle-like cells.* Hypertens Res, 2006. **29**(4): p. 269-76.

163. Shah, N.M., A.K. Groves, and D.J. Anderson, *Alternative neural crest cell fates are instructively promoted by TGFbeta superfamily members.* Cell, 1996. **85**(3): p. 331-43.

164. Bobik, A., et al., *Distinct patterns of transforming growth factor-beta isoform and receptor expression in human atherosclerotic lesions. Colocalization implicates TGF-beta in fibrofatty lesion development.* Circulation, 1999. **99**(22): p. 2883-91.

165. Chen, H., et al., *TGF-beta 1 attenuates myocardial ischemia-reperfusion injury via inhibition of upregulation of MMP-1.* Am J Physiol Heart Circ Physiol, 2003. **284**(5): p. H1612-7.

166. Wolff, R.A., et al., *Transforming growth factor-beta1 antisense treatment of rat vein grafts reduces the accumulation of collagen and increases the accumulation of h-caldesmon.* J Vasc Surg, 2006. **43**(5): p. 1028-36.

167. O'Callaghan, C.J. and B. Williams, *Mechanical strain-induced extracellular matrix production by human vascular smooth muscle cells: role of TGF-beta(1).* Hypertension, 2000. **36**(3): p. 319-24.

168. Kalinina, N., et al., *Smad expression in human atherosclerotic lesions: evidence for impaired TGF-beta/Smad signaling in smooth muscle cells of fibrofatty lesions.* Arteriosclerosis, Thrombosis & Vascular Biology, 2004. **24**(8): p. 1391-6.

169. Burgess, W.H. and T. Maciag, *The heparin-binding (fibroblast) growth factor family of proteins.* Annu Rev Biochem, 1989. **58**: p. 575-606.

170. Basilico, C. and D. Moscatelli, *The FGF family of growth factors and oncogenes.* Adv Cancer Res, 1992. **59**: p. 115-65.

171. Auguste, P., S. Javerzat, and A. Bikfalvi, *Regulation of vascular development by fibroblast growth factors.* Cell Tissue Res, 2003. **314**(1): p. 157-166.

172. Ornitz, D.M. and N. Itoh, *Fibroblast growth factors.* Genome biology, 2001. **2**(3): p. REVIEWS3005.

173. Baird, A. and M. Klagsbrun, *The fibroblast growth factor family.* Cancer Cells, 1991. **3**(6): p. 239-43.

174. Stavri, G.T., et al., *Basic fibroblast growth factor upregulates the expression of vascular endothelial growth factor in vascular smooth muscle cells. Synergistic interaction with hypoxia.* Circulation, 1995. **92**(1): p. 11-4.

175. Folkman, J., et al., *A heparin-binding angiogenic protein--basic fibroblast growth factor--is stored within basement membrane.* Am J Pathol, 1988. **130**(2): p. 393-400.

176. Slack, J.M., et al., *Mesoderm induction in early Xenopus embryos by heparin-binding growth factors.* Nature, 1987. **326**(6109): p. 197-200.

177. Grunz, H., et al., *Induction of mesodermal tissues by acidic and basic heparin binding growth factors.* Cell differentiation, 1988. **22**(3): p. 183-9.

178. Seed, J., B.B. Olwin, and S.D. Hauschka, *Fibroblast growth factor levels in the whole embryo and limb bud during chick development.* Dev Biol, 1988. **128**(1): p. 50-7.

179. Seed, J. and S.D. Hauschka, *Clonal analysis of vertebrate myogenesis. VIII. Fibroblasts growth factor (FGF)-dependent and FGF-independent muscle colony types during chick wing development.* Dev Biol, 1988. **128**(1): p. 40-9.

180. Ross, R., E.W. Raines, and D.F. Bowen-Pope, *The biology of platelet-derived growth factor.* Cell, 1986. **46**(2): p. 155-69.

181. Tomanek, R.J., et al., *Vascular endothelial growth factor and basic fibroblast growth factor differentially modulate early postnatal coronary angiogenesis.* Circ Res, 2001. **88**(11): p. 1135-41.

182. Winkles, J.A. and C.G. Gay, *Regulated expression of PDGF A-chain mRNA in human saphenous vein smooth muscle cells.* Biochem Biophys Res Commun, 1991. **180**(2): p. 519-24.

183. Pickering, J.G., et al., *Coordinated effects of fibroblast growth factor-2 on expression of fibrillar collagens, matrix metalloproteinases, and tissue inhibitors of matrix metalloproteinases by human vascular smooth muscle cells. Evidence for repressed collagen production and activated degradative capacity.* Arterioscler Thromb Vasc Biol, 1997. **17**(3): p. 475-82.

184. Lehoux, S., Y. Castier, and A. Tedgui, *Molecular mechanisms of the vascular responses to haemodynamic forces.* Journal of internal medicine, 2006. **259**(4): p. 381-92.

185. Dobrin, P.B., *Mechanical Factors Associated with the Development of Intimal Hyperplasia with Respect to Vascular Grafts*, in *Intimal Hyperplasia*, P.B. Dobrin, Editor. 1994, R.G. Landes: Georgetown. p. 85-104.

186. Silver, F.H., I. Horvath, and D.J. Foran, *Viscoelasticity of the vessel wall: the role of collagen and elastic fibers.* Crit Rev Biomed Eng, 2001. **29**(3): p. 279-301.

187. Faury, G., *Function-structure relationship of elastic arteries in evolution: from microfibrils to elastin and elastic fibres.* Pathologie-biologie, 2001. **49**(4): p. 310-25.

188. Sato, M. and T. Ohashi, *Biorheological views of endothelial cell responses to mechanical stimuli.* Biorheology, 2005. **42**(6): p. 421-41.

189. Williams, B., *Mechanical influences on vascular smooth muscle cell function.* J Hypertens, 1998. **16**(12 Pt 2): p. 1921-9.

190. Safar, M.E., et al., *Pulsed Doppler: diameter, blood flow velocity and volumic flow of the brachial artery in sustained essential hypertension.* Circulation, 1981. **63**(2): p. 393-400.

191. Banes, A.J., et al., *Mechanical forces and signaling in connective tissue cells: cellular mechanisms of detection, transduction, and responses to mechanical deformation.* Curr Opin Orthop, 2001. **12**(5): p. 389-396.

192. Oluwole, B.O., et al., *Gene regulation by mechanical forces.* Endothelium, 1997. **5**(2): p. 85-93.

193. Riha, G.M., et al., *Roles of hemodynamic forces in vascular cell differentiation.* Ann Biomed Eng, 2005. **33**(6): p. 772-9.

194. Lehoux, S. and A. Tedgui, *Signal transduction of mechanical stresses in the vascular wall.* Hypertension, 1998. **32**(2): p. 338-45.

195. Li, C. and Q. Xu, *Mechanical stress-initiated signal transductions in vascular smooth muscle cells.* Cellular Signalling, 2000. **12**(7): p. 435-445.

196. Campbell, J.H., et al., *Cytodifferentiation and expression of alpha-smooth muscle actin mRNA and protein during primary culture of aortic smooth muscle cells. Correlation with cell density and proliferative state.* Arteriosclerosis, 1989. **9**(5): p. 633-43.

197. Chamley, J.H., et al., *Comparison of vascular smooth muscle cells from adult human, monkey and rabbit in primary culture and in subculture.* Cell Tissue Res, 1977. **177**(4): p. 503-22.

198. Hultgardh-Nilsson, A., et al., *Expression of phenotype- and proliferation-related genes in rat aortic smooth muscle cells in primary culture.* Cardiovasc Res, 1997. **34**(2): p. 418-30.

199. Mills, I., et al., *Strain activation of bovine aortic smooth muscle cell proliferation and alignment: study of strain dependency and the role of protein kinase A and C signaling pathways.* J Cell Physiol, 1997. **170**(3): p. 228-34.

200. Hipper, A. and G. Isenberg, *Cyclic mechanical strain decreases the DNA synthesis of vascular smooth muscle cells.* Pflugers Arch, 2000. **440**(1): p. 19-27.

201. Sudhir, K., et al., *Mechanical strain and collagen potentiate mitogenic activity of angiotensin II in rat vascular smooth muscle cells.* J Clin Invest, 1993. **92**(6): p. 3003-7.

202. Li, Q., et al., *Stretch-induced proliferation of cultured vascular smooth muscle cells and a possible involvement of local renin-angiotensin system and platelet-derived growth factor (PDGF).* Hypertens Res, 1997. **20**(3): p. 217-23.

203. Standley, P.R., T.J. Obards, and C.L. Martina, *Cyclic stretch regulates autocrine IGF-I in vascular smooth muscle cells: implications in vascular hyperplasia.* Am J Physiol, 1999. **276**(4 Pt 1): p. E697-705.

204. Smith, J.D., et al., *Cyclic stretch induces the expression of vascular endothelial growth factor in vascular smooth muscle cells.* Endothelium: Journal of Endothelial Cell Research, 2001. **8**(1): p. 41-8.

205. Li, Q., et al., *Stretch-induced collagen synthesis in cultured smooth muscle cells from rabbit aortic media and a possible involvement of angiotensin II and transforming growth factor-beta.* J Vasc Res, 1998. **35**(2): p. 93-103.

206. Joki, N., et al., *Tyrosine-kinase dependent TGF-beta and extracellular matrix expression by mechanical stretch in vascular smooth muscle cells.* Hypertension Research - Clinical & Experimental, 2000. **23**(2): p. 91-9.

207. Cheng, G.C., et al., *Mechanical strain tightly controls fibroblast growth factor-2 release from cultured human vascular smooth muscle cells.* Circulation Research, 1997. **80**(1): p. 28-36.

208. Leung, D.Y., S. Glagov, and M.B. Mathews, *Cyclic stretching stimulates synthesis of matrix components by arterial smooth muscle cells in vitro.* Science, 1976. **191**(4226): p. 475-7.

209. Sumpio, B.E., et al., *Enhanced collagen production by smooth muscle cells during repetitive mechanical stretching.* Archives of Surgery, 1988. **123**(10): p. 1233-6.

210. Solan, A., et al., *Effect of pulse rate on collagen deposition in the tissue engineered blood vessel.* Tissue Eng, 2003. **9**(4): p. 579-86.

211. Sutcliffe, M.C. and J.M. Davidson, *Effect of static stretching on elastin production by porcine aortic smooth muscle cells.* Matrix, 1990. **10**(3): p. 148-53.

212. Isenberg, B.C. and R.T. Tranquillo, *Long-term cyclic distention enhances the mechanical properties of collagen-based media-equivalents.* Ann Biomed Eng, 2003. **31**(8): p. 937-49.

213. Birukov, K.G., et al., *Stretch affects phenotype and proliferation of vascular smooth muscle cells.* Mol Cell Biochem, 1995. **144**(2): p. 131-9.

214. Smith, P.G., R. Moreno, and M. Ikebe, *Strain increases airway smooth muscle contractile and cytoskeletal proteins in vitro.* Am J Physiol, 1997. **272**(1 Pt 1): p. L20-7.

215. Kanda, K. and T. Matsuda, *Mechanical stress-induced orientation and ultrastructural change of smooth muscle cells cultured in three-dimensional collagen lattices.* Cell Transplant, 1994. **3**(6): p. 481-92.

216. Wilson, E., K. Sudhir, and H.E. Ives, *Mechanical strain of rat vascular smooth muscle cells is sensed by specific extracellular matrix/integrin interactions.* J Clin Invest, 1995. **96**(5): p. 2364-72.

217. Wernig, F., M. Mayr, and Q. Xu, *Mechanical stretch-induced apoptosis in smooth muscle cells is mediated by beta1-integrin signaling pathways.* Hypertension, 2003. **41**(4): p. 903-11.

218. Nikolovski, J., B.S. Kim, and D.J. Mooney, *Cyclic strain inhibits switching of smooth muscle cells to an osteoblast-like phenotype.* FASEB J, 2003. **17**(3): p. 455-7.

219. Kanda, K., T. Matsuda, and T. Oka, *Mechanical stress induced cellular orientation and phenotypic modulation of 3-D cultured smooth muscle cells.* ASAIO J, 1993. **39**: p. M686-M690.

220. Stegemann, J.P., H. Hong, and R.M. Nerem, *Mechanical, biochemical, and extracellular matrix effects on vascular smooth muscle cell phenotype.* J Appl Physiol, 2005. **98**(6): p. 2321-2327.

221. Zhu, H.J. and A.W. Burgess, *Regulation of transforming growth factor-beta signaling.* Mol Cell Biol Res Commun, 2001. **4**(6): p. 321-30.

222. Lindner, V. and M.A. Reidy, *Proliferation of smooth muscle cells after vascular injury is inhibited by an antibody against basic fibroblast growth factor.* Proc Natl Acad Sci U S A, 1991. **88**(9): p. 3739-43.

223. Su, B.Y., et al., *The effect of phenotype on mechanical stretch-induced vascular smooth muscle cell apoptosis.* J Vasc Res, 2006. **43**(3): p. 229-37.

224. Intengan, H.D. and E.L. Schiffrin, *Vascular remodeling in hypertension: roles of apoptosis, inflammation, and fibrosis.* Hypertension, 2001. **38**(3 Pt 2): p. 581-7.

225. Watase, M., et al., *Effect of pressure on cultured smooth muscle cells.* Life Sci, 1997. **61**(10): p. 987-96.

226. Ozaki, T., et al., *Threshold-dependent DNA synthesis by pure pressure in human aortic smooth muscle cells: Gialpha-dependent and -independent pathways.* Biochem Biophys Res Commun, 1999. **256**(1): p. 212-7.

227. Franklin, S.S., et al., *The importance of pulsatile components of hypertension in predicting carotid stenosis in older adults.* J Hypertens, 1997. **15**(10): p. 1143-50.

228. Cappadona, C., et al., *Phenotype dictates the growth response of vascular smooth muscle cells to pulse pressure in vitro.* Exp Cell Res, 1999. **250**(1): p. 174-86.

229. Birney, Y.A., et al., *Pulse pressure-induced transmural fluid flux increases bovine aortic smooth muscle cell apoptosis in a mitogen activated protein kinase dependent manner.* J Vasc Res, 2004. **41**(4): p. 364-74.

230. Kibbe, M.R., et al., *Potentiation of nitric oxide-induced apoptosis in p53-/- vascular smooth muscle cells.* Am J Physiol Cell Physiol, 2002. **282**(3): p. C625-34.

231. Wang, S. and J.M. Tarbell, *Effect of fluid flow on smooth muscle cells in a 3-dimensional collagen gel model.* Arterioscler Thromb Vasc Biol, 2000. **20**(10): p. 2220-5.

232. Lee, A.A., et al., *Fluid shear stress-induced alignment of cultured vascular smooth muscle cells.* J Biomech Eng, 2002. **124**(1): p. 37-43.

233. Malek, A.M. and S. Izumo, *Mechanism of endothelial cell shape change and cytoskeletal remodeling in response to fluid shear stress.* J Cell Sci, 1996. **109**(4): p. 713-726.

234. Sterpetti, A.V., et al., *Shear stress influences the release of platelet derived growth factor and basic fibroblast growth factor by arterial smooth muscle cells. Winner of the ESVS prize for best experimental paper 1993.* Eur J Vasc Surg, 1994. **8**(2): p. 138-42.

235. Sterpetti, A.V., et al., *Modulation of arterial smooth muscle cell growth by haemodynamic forces.* Eur J Vasc Surg, 1992. **6**(1): p. 16-20.

236. Clowes, A.W., et al., *Regulation of smooth muscle cell growth in injured artery.* J Cardiovasc Pharmacol, 1989. **14 Suppl 6**: p. S12-15.

237. Civelek, M., et al., *Smooth muscle cells contract in response to fluid flow via a Ca2+-independent signaling mechanism.* J Appl Physiol, 2002. **93**(6): p. 1907-17.

238. Chapman, G.B., et al., *Physiological cyclic stretch causes cell cycle arrest in cultured vascular smooth muscle cells.* Am J Physiol Heart Circ Physiol, 2000. **278**(3): p. H748-54.

239. Ueba, H., M. Kawakami, and T. Yaginuma, *Shear stress as an inhibitor of vascular smooth muscle cell proliferation. Role of transforming growth factor-beta 1 and tissue-type plasminogen activator.* Arterioscler Thromb Vasc Biol, 1997. **17**(8): p. 1512-6.

240. Garanich, J.S., M. Pahakis, and J.M. Tarbell, *Shear stress inhibits smooth muscle cell migration via nitric oxide-mediated downregulation of matrix metalloproteinase-2 activity.* Am J Physiol Heart Circ Physiol, 2005. **288**(5): p. H2244-52.

241. Sterpetti, A.V., et al., *Growth factor release by smooth muscle cells is dependent on haemodynamic factors.* Eur J Vasc Surg, 1992. **6**(6): p. 636-8.

242. Paszkowiak, J.J. and A. Dardik, *Arterial wall shear stress: observations from the bench to the bedside.* 2003. **37**(1): p. 47-57.

243. Wang, H., et al., *Shear stress induces endothelial transdifferentiation from mouse smooth muscle cells.* Biochemical & Biophysical Research Communications, 2006. **346**(3): p. 860-5.

244. Chien, S., *Molecular basis of rheological modulation of endothelial functions: importance of stress direction.* Biorheology, 2006. **43**(2): p. 95-116.

245. Rossant, J. and L. Howard, *Signaling pathways in vascular development.* Annu Rev Cell Dev Biol, 2002. **18**: p. 541-73.

246. Ferguson, J.E., 3rd, R.W. Kelley, and C. Patterson, *Mechanisms of endothelial differentiation in embryonic vasculogenesis.* Arterioscler Thromb Vasc Biol, 2005. **25**(11): p. 2246-54.

247. Risau, W. and I. Flamme, *Vasculogenesis.* Annu Rev Cell Dev Biol, 1995. **11**: p. 73-91.

248. le Noble, F., et al., *Control of arterial branching morphogenesis in embryogenesis: go with the flow.* Cardiovasc Res, 2005. **65**(3): p. 619-28.

249. Tang, D.G. and C.J. Conti, *Endothelial cell development, vasculogenesis, angiogenesis, and tumor neovascularization: an update.* Seminars in thrombosis and hemostasis, 2004. **30**(1): p. 109-17.

250. Nishikawa, S.I., et al., *Progressive lineage analysis by cell sorting and culture identifies FLK1+VE-cadherin+ cells at a diverging point of endothelial and hemopoietic lineages.* Development, 1998. **125**(9): p. 1747-57.

251. Shalaby, F., et al., *Failure of blood-island formation and vasculogenesis in Flk-1-deficient mice.* Nature, 1995. **376**(6535): p. 62-6.

252. Shalaby, F., et al., *A requirement for Flk1 in primitive and definitive hematopoiesis and vasculogenesis.* Cell, 1997. **89**(6): p. 981-90.

253. Roy, H., S. Bhardwaj, and S. Yla-Herttuala, *Biology of vascular endothelial growth factors.* FEBS Lett, 2006. **580**(12): p. 2879-87.

254. Carmeliet, P., et al., *Targeted deficiency or cytosolic truncation of the VE-cadherin gene in mice impairs VEGF-mediated endothelial survival and angiogenesis.* Cell, 1999. **98**(2): p. 147-57.

255. Takahashi, T. and M. Shibuya, *The 230 kDa mature form of KDR/Flk-1 (VEGF receptor-2) activates the PLC-gamma pathway and partially induces mitotic signals in NIH3T3 fibroblasts.* Oncogene, 1997. **14**(17): p. 2079-89.

256. Conway, E.M., D. Collen, and P. Carmeliet, *Molecular mechanisms of blood vessel growth.* Cardiovasc Res, 2001. **49**(3): p. 507-521.

257. Meirer, R., R. Gurunluoglu, and M. Siemionow, *Neurogenic perspective on vascular endothelial growth factor: review of the literature.* Journal of reconstructive microsurgery, 2001. **17**(8): p. 625-30.

258. Ogunshola, O.O., et al., *Paracrine and autocrine functions of neuronal vascular endothelial growth factor (VEGF) in the central nervous system.* J Biol Chem, 2002. **277**(13): p. 11410-5.

259. Yang, X. and C.L. Cepko, *Flk-1, a receptor for vascular endothelial growth factor (VEGF), is expressed by retinal progenitor cells.* J Neurosci, 1996. **16**(19): p. 6089-99.

260. Yamashita, J., et al., *Flk1-positive cells derived from embryonic stem cells serve as vascular progenitors.* Nature, 2000. **408**(6808): p. 92-6.

261. Asashima, T., et al., *Rat brain pericyte cell lines expressing beta2-adrenergic receptor, angiotensin II receptor type 1A, klotho, and CXCR4 mRNAs despite having endothelial cell markers.* J Cell Physiol, 2003. **197**(1): p. 69-76.

262. Simper, D., et al., *Smooth muscle progenitor cells in human blood.* Circulation, 2002. **106**(10): p. 1199-204.

263. Goede, V., et al., *Analysis of blood vessel maturation processes during cyclic ovarian angiogenesis.* Lab Invest, 1998. **78**(11): p. 1385-94.

264. Shweiki, D., et al., *Vascular endothelial growth factor induced by hypoxia may mediate hypoxia-initiated angiogenesis.* Nature, 1992. **359**(6398): p. 843-5.

265. Naganuma, Y., et al., *Cleavage of platelet endothelial cell adhesion molecule-1 (PECAM-1) in platelets exposed to high shear stress.* J Thromb Haemost, 2004. **2**(11): p. 1998-2008.

266. Baldwin, H.S., et al., *Platelet endothelial cell adhesion molecule-1 (PECAM-1/CD31): alternatively spliced, functionally distinct isoforms expressed during mammalian cardiovascular development.* Development, 1994. **120**(9): p. 2539-53.

267. Vittet, D., et al., *Embryonic stem cells differentiate in vitro to endothelial cells through successive maturation steps.* Blood, 1996. **88**(9): p. 3424-3431.

268. Albelda, S.M., et al., *Molecular and cellular properties of PECAM-1 (endoCAM/CD31): a novel vascular cell-cell adhesion molecule.* J Cell Biol, 1991. **114**(5): p. 1059-68.

269. Muller, W.A., et al., *A human endothelial cell-restricted, externally disposed plasmalemmal protein enriched in intercellular junctions.* J Exp Med, 1989. **170**(2): p. 399-414.

270. Newman, P.J., et al., *PECAM-1 (CD31) cloning and relation to adhesion molecules of the immunoglobulin gene superfamily.* Science, 1990. **247**(4947): p. 1219-22.

271. Piali, L., et al., *Murine platelet endothelial cell adhesion molecule (PECAM-1)/CD31 modulates beta 2 integrins on lymphokine-activated killer cells.* European journal of immunology, 1993. **23**(10): p. 2464-71.

272. Tanaka, Y., et al., *CD31 expressed on distinctive T cell subsets is a preferential amplifier of beta 1 integrin-mediated adhesion.* J Exp Med, 1992. **176**(1): p. 245-53.

273. Sato, T.N., et al., *Tie-1 and tie-2 define another class of putative receptor tyrosine kinase genes expressed in early embryonic vascular system.* Proc Natl Acad Sci U S A, 1993. **90**(20): p. 9355-8.

274. Dumont, D.J., et al., *Vascularization of the mouse embryo: a study of flk-1, tek, tie, and vascular endothelial growth factor expression during development.* Dev Dyn, 1995. **203**(1): p. 80-92.

275. Papapetropoulos, A., et al., *Angiopoietin-1 inhibits endothelial cell apoptosis via the Akt/survivin pathway.* J Biol Chem, 2000. **275**(13): p. 9102-5.

276. Folkman, J. and P.A. D'Amore, *Blood vessel formation: what is its molecular basis?* Cell, 1996. **87**(7): p. 1153-5.

277. Suri, C., et al., *Increased vascularization in mice overexpressing angiopoietin-1.* Science, 1998. **282**(5388): p. 468-71.

278. Drake, C.J. and C.D. Little, *Exogenous vascular endothelial growth factor induces malformed and hyperfused vessels during embryonic neovascularization.* Proc Natl Acad Sci U S A, 1995. **92**(17): p. 7657-61.

279. Carmeliet, P. and D. Collen, *Molecular basis of angiogenesis. Role of VEGF and VE-cadherin.* Ann N Y Acad Sci, 2000. **902**: p. 249-62; discussion 262-4.

280. Lampugnani, M.G., et al., *A novel endothelial-specific membrane protein is a marker of cell-cell contacts.* J Cell Biol, 1992. **118**(6): p. 1511-22.

281. Gory-Faure, S., et al., *Role of vascular endothelial-cadherin in vascular morphogenesis.* Development, 1999. **126**(10): p. 2093-2102.

282. Fujimoto, T., et al., *Step-wise divergence of primitive and definitive haematopoietic and endothelial cell lineages during embryonic stem cell differentiation.* Genes Cells, 2001. **6**(12): p. 1113-27.

283. Breier, G., et al., *Molecular cloning and expression of murine vascular endothelial-cadherin in early stage development of cardiovascular system.* Blood, 1996. **87**(2): p. 630-41.

284. Matsuyoshi, N., et al., *In vivo evidence of the critical role of cadherin-5 in murine vascular integrity.* Proceedings of the Association of American Physicians, 1997. **109**(4): p. 362-71.

285. Nishikawa, S.I., et al., *In vitro generation of lymphohematopoietic cells from endothelial cells purified from murine embryos.* Immunity, 1998. **8**(6): p. 761-9.

286. Vittet, D., et al., *Targeted null-mutation in the vascular endothelial-cadherin gene impairs the organization of vascular-like structures in embryoid bodies.* Proc Natl Acad Sci U S A, 1997. **94**(12): p. 6273-8.

287. Hirashima, M., et al., *Maturation of embryonic stem cells into endothelial cells in an in vitro model of vasculogenesis.* Blood, 1999. **93**(4): p. 1253-63.

288. Ogawa, M., et al., *Expression of alpha4-integrin defines the earliest precursor of hematopoietic cell lineage diverged from endothelial cells.* Blood, 1999. **93**(4): p. 1168-77.

289. Otrock, Z.K., et al., *Understanding the biology of angiogenesis: Review of the most important molecular mechanisms.* Blood Cells, Molecules, and Diseases, 2007. **In Press, Corrected Proof**.

290. Nelson, C.M. and C.S. Chen, *VE-cadherin simultaneously stimulates and inhibits cell proliferation by altering cytoskeletal structure and tension.* J Cell Sci, 2003. **116**(Pt 17): p. 3571-81.

291. Blann, A.D., *Plasma von Willebrand factor, thrombosis, and the endothelium: the first 30 years.* Thromb Haemost, 2006. **95**(1): p. 49-55.

292. Coffin, J.D., et al., *Angioblast differentiation and morphogenesis of the vascular endothelium in the mouse embryo.* Dev Biol, 1991. **148**(1): p. 51-62.

293. Jaffe, E.A., *Endothelial cells and the biology of factor VIII.* N Engl J Med, 1977. **296**(7): p. 377-83.

294. Wagner, D.D., *Cell biology of von Willebrand factor.* Annual review of cell biology, 1990. **6**: p. 217-46.

295. Rand, J.H., et al., *Localization of factor-VIII-related antigen in human vascular subendothelium.* Blood, 1980. **55**(5): p. 752-6.

296. Dejana, E., et al., *Von Willebrand factor promotes endothelial cell adhesion via an Arg-Gly-Asp-dependent mechanism.* J Cell Biol, 1989. **109**(1): p. 367-75.

297. Bahnak, B.R., et al., *Expression of von Willebrand factor in porcine vessels: heterogeneity at the level of von Willebrand factor mRNA.* J Cell Physiol, 1989. **138**(2): p. 305-10.

298. Rand, J.H., et al., *Distribution of von Willebrand factor in porcine intima varies with blood vessel type and location.* Arteriosclerosis, 1987. **7**(3): p. 287-91.

299. Wagner, C.T., et al., *Hemodynamic forces induce the expression of heme oxygenase in cultured vascular smooth muscle cells.* J Clin Invest, 1997. **100**(3): p. 589-96.

300. Ferrara, N., H.P. Gerber, and J. LeCouter, *The biology of VEGF and its receptors.* Nat Med, 2003. **9**(6): p. 669-76.

301. Poole, T.J., E.B. Finkelstein, and C.M. Cox, *The role of FGF and VEGF in angioblast induction and migration during vascular development.* Dev Dyn, 2001. **220**(1): p. 1-17.

302. Riese, J., R. Zeller, and R. Dono, *Nucleo-cytoplasmic translocation and secretion of fibroblast growth factor-2 during avian gastrulation.* Mech Dev, 1995. **49**(1-2): p. 13-22.

303. Fong, G.H., et al., *Increased hemangioblast commitment, not vascular disorganization, is the primary defect in flt-1 knock-out mice.* Development, 1999. **126**(13): p. 3015-25.

304. Gerber, H.P., V. Dixit, and N. Ferrara, *Vascular endothelial growth factor induces expression of the antiapoptotic proteins Bcl-2 and A1 in vascular endothelial cells.* J Biol Chem, 1998. **273**(21): p. 13313-6.

305. Hood, J.D., et al., *VEGF upregulates ecNOS message, protein, and NO production in human endothelial cells.* Am J Physiol, 1998. **274**(3 Pt 2): p. H1054-8.

306. He, H., et al., *Vascular endothelial growth factor signals endothelial cell production of nitric oxide and prostacyclin through flk-1/KDR activation of c-Src.* J Biol Chem, 1999. **274**(35): p. 25130-5.

307. Maxwell, P.H. and P.J. Ratcliffe, *Oxygen sensors and angiogenesis.* Semin Cell Dev Biol, 2002. **13**(1): p. 29-37.

308. Conklin, B.S., et al., *Shear stress regulates occludin and VEGF expression in porcine arterial endothelial cells.* J Surg Res, 2002. **102**(1): p. 13-21.

309. Ferrara, N. and T. Davis-Smyth, *The biology of vascular endothelial growth factor.* Endocr Rev, 1997. **18**(1): p. 4-25.

310. Senger, D.R., et al., *Tumor cells secrete a vascular permeability factor that promotes accumulation of ascites fluid.* Science, 1983. **219**(4587): p. 983-5.

311. Wang, J. and R. Milner, *Fibronectin promotes brain capillary endothelial cell survival and proliferation through alpha5beta1 and alphavbeta3 integrins via MAP kinase signalling.* Journal of neurochemistry, 2006. **96**(1): p. 148-59.

312. Wilson, S.H., et al., *Fibronectin fragments promote human retinal endothelial cell adhesion and proliferation and ERK activation through alpha5beta1 integrin and PI 3-kinase.* Invest Ophthalmol Vis Sci, 2003. **44**(4): p. 1704-15.

313. Clark, R.A., et al., *Blood vessel fibronectin increases in conjunction with endothelial cell proliferation and capillary ingrowth during wound healing.* J Invest Dermatol, 1982. **79**(5): p. 269-76.

314. Lamoreaux, W.J., et al., *Vascular endothelial growth factor increases release of gelatinase A and decreases release of tissue inhibitor of metalloproteinases by microvascular endothelial cells in vitro.* Microvasc Res, 1998. **55**(1): p. 29-42.

315. Pepper, M.S., et al., *Vascular endothelial growth factor (VEGF) induces plasminogen activators and plasminogen activator inhibitor-1 in microvascular endothelial cells.* Biochem Biophys Res Commun, 1991. **181**(2): p. 902-6.

316. Mandriota, S.J., et al., *Vascular endothelial growth factor increases urokinase receptor expression in vascular endothelial cells.* J Biol Chem, 1995. **270**(17): p. 9709-16.

317. Unemori, E.N., et al., *Vascular endothelial growth factor induces interstitial collagenase expression in human endothelial cells.* J Cell Physiol, 1992. **153**(3): p. 557-62.

318. Barbara, N.P., J.L. Wrana, and M. Letarte, *Endoglin is an accessory protein that interacts with the signaling receptor complex of multiple members of the transforming growth factor-beta superfamily.* J Biol Chem, 1999. **274**(2): p. 584-94.

319. Letamendia, A., et al., *Role of endoglin in cellular responses to transforming growth factor-beta. A comparative study with betaglycan.* J Biol Chem, 1998. **273**(49): p. 33011-9.

320. Letterio, J.J., et al., *Maternal rescue of transforming growth factor-beta 1 null mice.* Science, 1994. **264**(5167): p. 1936-8.

321. Arthur, H.M., et al., *Endoglin, an ancillary TGFbeta receptor, is required for extraembryonic angiogenesis and plays a key role in heart development.* Dev Biol, 2000. **217**(1): p. 42-53.

322. Larsson, J., et al., *Abnormal angiogenesis but intact hematopoietic potential in TGF-beta type I receptor-deficient mice.* EMBO J, 2001. **20**(7): p. 1663-73.

323. Dickson, M.C., et al., *Defective haematopoiesis and vasculogenesis in transforming growth factor-beta 1 knock out mice.* Development, 1995. **121**(6): p. 1845-54.

324. Oh, S.P., et al., *Activin receptor-like kinase 1 modulates transforming growth factor-beta 1 signaling in the regulation of angiogenesis.* Proc Natl Acad Sci U S A, 2000. **97**(6): p. 2626-31.

325. Bertolino, P., et al., *Transforming growth factor-beta signal transduction in angiogenesis and vascular disorders.* Chest, 2005. **128**(6 Suppl): p. 585S-590S.

326. Qiu, P., X.H. Feng, and L. Li, *Interaction of Smad3 and SRF-associated complex mediates TGF-beta1 signals to regulate SM22 transcription during myofibroblast differentiation.* J Mol Cell Cardiol, 2003. **35**(12): p. 1407-20.

327. Heimark, R.L., D.R. Twardzik, and S.M. Schwartz, *Inhibition of endothelial regeneration by type-beta transforming growth factor from platelets.* Science, 1986. **233**(4768): p. 1078-80.

328. Muller, G., et al., *Inhibitory action of transforming growth factor beta on endothelial cells.* Proc Natl Acad Sci U S A, 1987. **84**(16): p. 5600-4.

329. Lee, N.Y. and G.C. Blobe, *The interaction of endoglin with beta -arrestin2 regulates transforming growth factor-beta -mediated ERK activation and migration in endothelial cells.* J Biol Chem, 2007.

330. Castanares, C., et al., *Signaling by ALK5 mediates TGF-beta-induced ET-1 expression in endothelial cells: a role for migration and proliferation.* J Cell Sci, 2007. **120**(Pt 7): p. 1256-66.

331. Lee, Y.H., et al., *TGF-{beta}1 Effects on Endothelial Monolayer Permeability Involve FAK/Src.* Am J Respir Cell Mol Biol, 2007.

332. Yang, E.Y. and H.L. Moses, *Transforming growth factor beta 1-induced changes in cell migration, proliferation, and angiogenesis in the chicken chorioallantoic membrane.* J Cell Biol, 1990. **111**(2): p. 731-41.

333. Li, C., et al., *Angiogenesis in breast cancer: the role of transforming growth factor beta and CD105.* Microscopy research and technique, 2001. **52**(4): p. 437-49.

334. Schwarte-Waldhoff, I., et al., *Smad4/DPC4-mediated tumor suppression through suppression of angiogenesis.* Proc Natl Acad Sci U S A, 2000. **97**(17): p. 9624-9.

335. Munoz-Chapuli, R., et al., *Cellular precursors of the coronary arteries.* Texas Heart Institute Journal, 2002. **29**(4): p. 243-9.

336. Chamley-Campbell, J., G.R. Campbell, and R. Ross, *The smooth muscle cell in culture.* Physiol Rev, 1979. **59**(1): p. 1-61.

337. Ferns, G.A., A.L. Stewart-Lee, and E.E. Anggard, *Arterial response to mechanical injury: balloon catheter de-endothelialization.* Atherosclerosis, 1992. **92**(2-3): p. 89-104.

338. Schwartz, S.M., R.L. Heimark, and M.W. Majesky, *Developmental mechanisms underlying pathology of arteries.* Physiol Rev, 1990. **70**(4): p. 1177-209.

339. Flamme, I. and W. Risau, *Induction of vasculogenesis and hematopoiesis in vitro.* Development, 1992. **116**(2): p. 435-9.

340. Cross, M.J. and L. Claesson-Welsh, *FGF and VEGF function in angiogenesis: signalling pathways, biological responses and therapeutic inhibition.* Trends in pharmacological sciences, 2001. **22**(4): p. 201-7.

341. Deng, C.X., et al., *Murine FGFR-1 is required for early postimplantation growth and axial organization.* Genes Dev, 1994. **8**(24): p. 3045-57.

342. Flamme, I., G. Breier, and W. Risau, *Vascular endothelial growth factor (VEGF) and VEGF receptor 2 (flk-1) are expressed during vasculogenesis and vascular differentiation in the quail embryo.* Dev Biol, 1995. **169**(2): p. 699-712.

343. Wanaka, A., J. Milbrandt, and E.M. Johnson, Jr., *Expression of FGF receptor gene in rat development.* Development, 1991. **111**(2): p. 455-68.

344. Peters, K.G., et al., *Two FGF receptor genes are differentially expressed in epithelial and mesenchymal tissues during limb formation and organogenesis in the mouse.* Development, 1992. **114**(1): p. 233-43.

345. Lindner, V., R.A. Majack, and M.A. Reidy, *Basic fibroblast growth factor stimulates endothelial regrowth and proliferation in denuded arteries.* J Clin Invest, 1990. **85**(6): p. 2004-8.

346. Mignatti, P., et al., *In vitro angiogenesis on the human amniotic membrane: requirement for basic fibroblast growth factor-induced proteinases.* J Cell Biol, 1989. **108**(2): p. 671-82.

347. Gospodarowicz, D., *Expression and control of vascular endothelial cells: proliferation and differentiation by fibroblast growth factors.* J Invest Dermatol, 1989. **93**(2 Suppl): p. 39S-47S.

348. Kanda, S., et al., *Signaling via fibroblast growth factor receptor-1 is dependent on extracellular matrix in capillary endothelial cell differentiation.* Exp Cell Res, 1999. **248**(1): p. 203-13.

349. Terranova, V.P., et al., *Human endothelial cells are chemotactic to endothelial cell growth factor and heparin.* J Cell Biol, 1985. **101**(6): p. 2330-4.

350. Partridge, C.R., J.R. Hawker, Jr., and R. Forough, *Overexpression of a secretory form of FGF-1 promotes MMP-1-mediated endothelial cell migration.* J Cell Biochem, 2000. **78**(3): p. 487-99.

351. Eliceiri, B.P., et al., *Integrin alphavbeta3 requirement for sustained mitogen-activated protein kinase activity during angiogenesis.* J Cell Biol, 1998. **140**(5): p. 1255-63.

352. Schwartz, M.A. and M.H. Ginsberg, *Networks and crosstalk: integrin signaling spreads.* Nat Cell Biol, 2002. **4**(4): p. E65-8.

353. Sastry, S.K., et al., *Integrin alpha subunit ratios, cytoplasmic domains, and growth factor synergy regulate muscle proliferation and differentiation.* J Cell Biol, 1996. **133**(1): p. 169-84.

354. Forsberg, K., et al., *Platelet-derived growth factor (PDGF) in oncogenesis: development of a vascular connective tissue stroma in xenotransplanted human melanoma producing PDGF-BB.* Proc Natl Acad Sci U S A, 1993. **90**(2): p. 393-7.

355. Battegay, E.J., et al., *PDGF-BB modulates endothelial proliferation and angiogenesis in vitro via PDGF beta-receptors.* J Cell Biol, 1994. **125**(4): p. 917-28.

356. Bar, R.S., et al., *The effects of platelet-derived growth factor in cultured microvessel endothelial cells.* Endocrinology, 1989. **124**(4): p. 1841-8.

357. Nicosia, R.F., S.V. Nicosia, and M. Smith, *Vascular endothelial growth factor, platelet-derived growth factor, and insulin-like growth factor-1 promote rat aortic angiogenesis in vitro.* Am J Pathol, 1994. **145**(5): p. 1023-9.

358. Chien, S., *Mechanotransduction and endothelial cell homeostasis: the wisdom of the cell.* Am J Physiol Heart Circ Physiol, 2007. **292**(3): p. H1209-24.

359. Iba, T., et al., *Effect of cyclic stretch on endothelial cells from different vascular beds.* Circulatory shock, 1991. **35**(4): p. 193-8.

360. Resnick, N., et al., *Fluid shear stress and the vascular endothelium: for better and for worse.* Prog Biophys Mol Biol, 2003. **81**(3): p. 177-99.

361. Papadaki, M. and S.G. Eskin, *Effects of fluid shear stress on gene regulation of vascular cells.* Biotechnology Progress, 1997. **13**(3): p. 209-21.

362. Howard, A.B., et al., *Cyclic strain induces an oxidative stress in endothelial cells.* Am J Physiol, 1997. **272**(2 Pt 1): p. C421-7.

363. Chien, S., S. Li, and Y.J. Shyy, *Effects of mechanical forces on signal transduction and gene expression in endothelial cells.* Hypertension, 1998. **31**(1 Pt 2): p. 162-9.

364. Hishikawa, K. and T.F. Luscher, *Pulsatile stretch stimulates superoxide production in human aortic endothelial cells.* Circulation, 1997. **96**(10): p. 3610-6.

365. Awolesi, M.A., et al., *Cyclic strain increases endothelial nitric oxide synthase activity.* Surgery, 1994. **116**(2): p. 439-44; discussion 444-5.

366. Upchurch, G.R., Jr., et al., *Nitric Oxide Alters Human Microvascular Endothelial Cell Response to Cyclic Strain.* J Cardiovasc Pharmacol Ther, 1998. **3**(2): p. 135-142.

367. Wung, B.S., et al., *Cyclical strain increases monocyte chemotactic protein-1 secretion in human endothelial cells.* Am J Physiol, 1996. **270**(4 Pt 2): p. H1462-8.

368. Kobayashi, S., et al., *Stretch-induced IL-6 secretion from endothelial cells requires NF-kappaB activation.* Biochem Biophys Res Commun, 2003. **308**(2): p. 306-12.

369. Wang, D.L., et al., *Mechanical strain increases endothelin-1 gene expression via protein kinase C pathway in human endothelial cells.* J Cell Physiol, 1995. **163**(2): p. 400-6.

370. Sumpio, B.E. and M.D. Widmann, *Enhanced production of endothelium-derived contracting factor by endothelial cells subjected to pulsatile stretch.* Surgery, 1990. **108**(2): p. 277-81; discussion 281-2.

371. Macarthur, H., et al., *Endothelin-1 release from endothelial cells in culture is elevated both acutely and chronically by short periods of mechanical stretch.* Biochem Biophys Res Commun, 1994. **200**(1): p. 395-400.

372. Cheng, J.J., et al., *Cyclic strain-induced plasminogen activator inhibitor-1 (PAI-1) release from endothelial cells involves reactive oxygen species.* Biochem Biophys Res Commun, 1996. **225**(1): p. 100-5.

373. Barron, V., et al., *The effect of physiological cyclic stretch on the cell morphology, cell orientation and protein expression of endothelial cells.* J Mater Sci Mater Med, 2007.

374. Krizbai, I.A., et al., *Effect of oxidative stress on the junctional proteins of cultured cerebral endothelial cells.* Cell Mol Neurobiol, 2005. **25**(1): p. 129-39.

375. Larsson, P.T., et al., *Circulating markers of inflammation are related to carotid artery atherosclerosis.* Int Angiol, 2005. **24**(1): p. 43-51.

376. Iba, T., et al., *Stimulation of endothelial secretion of tissue-type plasminogen activator by repetitive stretch.* J Surg Res, 1991. **50**(5): p. 457-60.

377. Matsumoto, T., et al., *Mechanical strain regulates endothelial cell patterning in vitro.* Tissue Eng, 2007. **13**(1): p. 207-17.

378. Sumpio, B.E., et al., *Mechanical stress stimulates aortic endothelial cells to proliferate.* J Vasc Surg, 1987. **6**(3): p. 252-6.

379. Busse, R. and I. Fleming, *Pulsatile stretch and shear stress: physical stimuli determining the production of endothelium-derived relaxing factors.* J Vasc Res, 1998. **35**(2): p. 73-84.

380. Chang, H., et al., *Cyclical mechanical stretch enhances angiopoietin-2 and Tie2 receptor expression in cultured human umbilical vein endothelial cells.* Clin Sci (Lond), 2003. **104**(4): p. 421-8.

381. Liu, X.M., et al., *Physiologic cyclic stretch inhibits apoptosis in vascular endothelium.* FEBS Lett, 2003. **541**(1-3): p. 52-6.

382. Millgard, J. and L. Lind, *Acute hypertension impairs endothelium-dependent vasodilation.* 1998. **94**(6): p. 601-7.

383. Wolinsky, H., *Response of the rat aortic media to hypertension. Morphological and chemical studies.* Circulation Research, 1970. **26**(4): p. 507-22.

384. Tokunaga, O. and T. Watanabe, *Properties of endothelial cell and smooth muscle cell cultured in ambient pressure.* In Vitro Cell Dev Biol, 1987. **23**(8): p. 528-34.

385. Tokunaga, O., J.L. Fan, and T. Watanabe, *Atherosclerosis and endothelium. Part II. Properties of aortic endothelial and smooth muscle cells cultured at various ambient pressures.* Acta Pathol Jpn, 1989. **39**(6): p. 356-62.

386. Sumpio, B.E., et al., *Increased ambient pressure stimulates proliferation and morphologic changes in cultured endothelial cells.* J Cell Physiol, 1994. **158**(1): p. 133-9.

387. Kato, S., et al., *Ambient pressure stimulates immortalized human aortic endothelial cells to increase DNA synthesis and matrix metalloproteinase 1 (tissue collagenase) production.* Virchows Arch, 1994. **425**(4): p. 385-90.

388. Vouyouka, A.G., et al., *Ambient pulsatile pressure modulates endothelial cell proliferation.* J Mol Cell Cardiol, 1998. **30**(3): p. 609-15.

389. Shin, H.Y., M.E. Gerritsen, and R. Bizios, *Regulation of endothelial cell proliferation and apoptosis by cyclic pressure.* Ann Biomed Eng, 2002. **30**(3): p. 297-304.

390. Hasel, C., et al., *Pathologically elevated cyclic hydrostatic pressure induces CD95-mediated apoptotic cell death in vascular endothelial cells.* Am J Physiol Cell Physiol, 2005. **289**(2): p. C312-22.

391. Nosaka, S., et al., *The effects of transmural pressure on prostacyclin release from porcine endocardial endothelial cells--comparison with vascular endothelial cells.* Pflugers Arch, 1997. **433**(6): p. 848-50.

392. Hishikawa, K., et al., *Pressure enhances endothelin-1 release from cultured human endothelial cells.* Hypertension, 1995. **25**(3): p. 449-52.

393. Shin, H.Y., R. Bizios, and M.E. Gerritsen, *Cyclic pressure modulates endothelial barrier function.* Endothelium, 2003. **10**(3): p. 179-87.

394. Shin, H.Y., et al., *VEGF-C mediates cyclic pressure-induced endothelial cell proliferation.* Physiological Genomics, 2002. **11**(3): p. 245-51.

395. Shin, H.Y., et al., *Receptor-mediated basic fibroblast growth factor signaling regulates cyclic pressure-induced human endothelial cell proliferation.* Endothelium, 2004. **11**(5-6): p. 285-91.

396. Ohashi, T., et al., *Hydrostatic pressure influences morphology and expression of VE-cadherin of vascular endothelial cells.* J Biomech, 2007. **40**(11): p. 2399-2405.

397. Wajant, H., K. Pfizenmaier, and P. Scheurich, *Non-apoptotic Fas signaling.* Cytokine Growth Factor Rev, 2003. **14**(1): p. 53-66.

398. Heine, U.I., et al., *Effects of retinoid deficiency on the development of the heart and vascular system of the quail embryo.* Virchows Archiv, 1985. **50**(2): p. 135-52.

399. Broekhuizen, M.L., et al., *Altered hemodynamics in chick embryos after extraembryonic venous obstruction.* Ultrasound Obstet Gynecol, 1999. **13**(6): p. 437-45.

400. Hogers, B., et al., *Extraembryonic venous obstructions lead to cardiovascular malformations and can be embryolethal.* Cardiovasc Res, 1999. **41**(1): p. 87-99.

401. Hogers, B., et al., *Unilateral vitelline vein ligation alters intracardiac blood flow patterns and morphogenesis in the chick embryo.* Circ Res, 1997. **80**(4): p. 473-81.

402. Resnick, N. and M.A. Gimbrone, *Hemodynamic forces are complex regulators of endothelial gene expression.* FASEB J, 1995. **9**(10): p. 874-82.

403. Nerem, R.M., M.J. Levesque, and J.F. Cornhill, *Vascular endothelial morphology as an indicator of the pattern of blood flow.* J Biomech Eng, 1981. **103**(3): p. 172-6.

404. Malek, A.M. and S. Izumo, *Molecular aspects of signal transduction of shear stress in the endothelial cell.* J Hypertens, 1994. **12**(9): p. 989-99.

405. Akimoto, S., et al., *Laminar shear stress inhibits vascular endothelial cell proliferation by inducing cyclin-dependent kinase inhibitor p21(Sdi1/Cip1/Waf1).* Circulation Research, 2000. **86**(2): p. 185-90.

406. Davies, P.F., et al., *Turbulent fluid shear stress induces vascular endothelial cell turnover in vitro.* Proc Natl Acad Sci U S A, 1986. **83**(7): p. 2114-7.

407. Chen, B.P., et al., *DNA microarray analysis of gene expression in endothelial cells in response to 24-h shear stress.* Physiol Genomics, 2001. **7**(1): p. 55-63.

408. Hsieh, H.J., N.Q. Li, and J.A. Frangos, *Shear stress increases endothelial platelet-derived growth factor mRNA levels.* Am J Physiol, 1991. **260**(2 Pt 2): p. H642-6.

409. Hsieh, H.J., N.Q. Li, and J.A. Frangos, *Shear-induced platelet-derived growth factor gene expression in human endothelial cells is mediated by protein kinase C.* J Cell Physiol, 1992. **150**(3): p. 552-8.

410. Malek, A.M., et al., *Fluid shear stress differentially modulates expression of genes encoding basic fibroblast growth factor and platelet-derived growth factor B chain in vascular endothelium.* J Clin Invest, 1993. **92**(4): p. 2013-21.

411. Diamond, S.L., et al., *Tissue plasminogen activator messenger RNA levels increase in cultured human endothelial cells exposed to laminar shear stress.* J Cell Physiol, 1990. **143**(2): p. 364-71.

412. Shyy, Y.J., et al., *Fluid shear stress induces a biphasic response of human monocyte chemotactic protein 1 gene expression in vascular endothelium.* Proc Natl Acad Sci U S A, 1994. **91**(11): p. 4678-82.

413. Sampath, R., et al., *Shear stress-mediated changes in the expression of leukocyte adhesion receptors on human umbilical vein endothelial cells in vitro.* Ann Biomed Eng, 1995. **23**(3): p. 247-56.

414. Nagel, T., et al., *Shear stress selectively upregulates intercellular adhesion molecule-1 expression in cultured human vascular endothelial cells.* J Clin Invest, 1994. **94**(2): p. 885-91.

415. Schwachtgen, J.L., et al., *Fluid shear stress activation of egr-1 transcription in cultured human endothelial and epithelial cells is mediated via the extracellular signal-related kinase 1/2 mitogen-activated protein kinase pathway.* J Clin Invest, 1998. **101**(11): p. 2540-9.

416. Khachigian, L.M., et al., *Egr-1 is activated in endothelial cells exposed to fluid shear stress and interacts with a novel shear-stress-response element in the PDGF A-chain promoter.* Arterioscler Thromb Vasc Biol, 1997. **17**(10): p. 2280-6.

417. Resnick, N., et al., *Endothelial gene regulation by laminar shear stress.* Advances in experimental medicine and biology, 1997. **430**: p. 155-64.

418. Fisslthaler, B., et al., *Identification of a cis-element regulating transcriptional activity in response to fluid shear stress in bovine aortic endothelial cells.* Endothelium, 2003. **10**(4-5): p. 267-75.

419. Topper, J.N., et al., *Identification of vascular endothelial genes differentially responsive to fluid mechanical stimuli: cyclooxygenase-2, manganese superoxide dismutase, and endothelial cell nitric oxide synthase are selectively up-regulated by steady laminar shear stress.* Proc Natl Acad Sci U S A, 1996. **93**(19): p. 10417-22.

420. Bao, X., C. Lu, and J.A. Frangos, *Temporal gradient in shear but not steady shear stress induces PDGF-A and MCP-1 expression in endothelial cells: role of NO, NF kappa B, and egr-1.* Arterioscler Thromb Vasc Biol, 1999. **19**(4): p. 996-1003.

421. White, C.R., et al., *Temporal gradients in shear, but not spatial gradients, stimulate ERK1/2 activation in human endothelial cells.* Am J Physiol Heart Circ Physiol, 2005. **289**(6): p. H2350-5.

422. Walpola, P.L., et al., *Expression of ICAM-1 and VCAM-1 and monocyte adherence in arteries exposed to altered shear stress.* Arterioscler Thromb Vasc Biol, 1995. **15**(1): p. 2-10.

423. Cho, A., et al., *Effects of changes in blood flow rate on cell death and cell proliferation in carotid arteries of immature rabbits.* Circ Res, 1997. **81**(3): p. 328-37.

424. Cho, A., D.W. Courtman, and B.L. Langille, *Apoptosis (programmed cell death) in arteries of the neonatal lamb.* Circ Res, 1995. **76**(2): p. 168-75.

425. Tardy, Y., et al., *Shear stress gradients remodel endothelial monolayers in vitro via a cell proliferation-migration-loss cycle.* Arterioscler Thromb Vasc Biol, 1997. **17**(11): p. 3102-6.

426. Collins, T. and M.I. Cybulsky, *NF-kappaB: pivotal mediator or innocent bystander in atherogenesis?* J Clin Invest, 2001. **107**(3): p. 255-64.

427. Cybulsky, M.I., et al., *A major role for VCAM-1, but not ICAM-1, in early atherosclerosis.* J Clin Invest, 2001. **107**(10): p. 1255-62.

428. Hajra, L., et al., *The NF-kappa B signal transduction pathway in aortic endothelial cells is primed for activation in regions predisposed to atherosclerotic lesion formation.* Proc Natl Acad Sci U S A, 2000. **97**(16): p. 9052-7.

429. Noris, M., et al., *Nitric oxide synthesis by cultured endothelial cells is modulated by flow conditions.* Circ Res, 1995. **76**(4): p. 536-43.

430. Ando, J., et al., *Differential display and cloning of shear stress-responsive messenger RNAs in human endothelial cells.* Biochem Biophys Res Commun, 1996. **225**(2): p. 347-51.

431. Ando, J., et al., *Down-regulation of vascular adhesion molecule-1 by fluid shear stress in cultured mouse endothelial cells.* Ann N Y Acad Sci, 1995. **748**: p. 148-56; discussion 156-7.

432. De Keulenaer, G.W., et al., *Oscillatory and steady laminar shear stress differentially affect human endothelial redox state: role of a superoxide-producing NADH oxidase.* Circ Res, 1998. **82**(10): p. 1094-101.

433. DePaola, N., et al., *Vascular endothelium responds to fluid shear stress gradients.* Arterioscler Thromb, 1992. **12**(11): p. 1254-7.

434. Brooks, A.R., P.I. Lelkes, and G.M. Rubanyi, *Gene expression profiling of human aortic endothelial cells exposed to disturbed flow and steady laminar flow.* Physiol Genomics, 2002. **9**(1): p. 27-41.

435. Taylor, C.A., T.J. Hughes, and C.K. Zarins, *Effect of exercise on hemodynamic conditions in the abdominal aorta.* J Vasc Surg, 1999. **29**(6): p. 1077-89.

436. Kuchan, M.J., H. Jo, and J.A. Frangos, *Role of G proteins in shear stress-mediated nitric oxide production by endothelial cells.* Am J Phys, 1994. **267**(3 Pt 1): p. C753-8.

437. Ranjan, V., Z. Xiao, and S.L. Diamond, *Constitutive NOS expression in cultured endothelial cells is elevated by fluid shear stress.* Am J Physiol Heart Circ Physiol, 1995. **269**(2 Pt 2): p. H550-5.

438. Uematsu, M., et al., *Regulation of endothelial cell nitric oxide synthase mRNA expression by shear stress.* Am J Physiol Cell Physiol, 1995. **269**(6 Pt 1): p. C1371-8.

439. Sharefkin, J.B., et al., *Fluid flow decreases preproendothelin mRNA levels and suppresses endothelin-1 peptide release in cultured human endothelial cells.* J Vasc Surg, 1991. **14**(1): p. 1-9.

440. Malek, A. and S. Izumo, *Physiological fluid shear stress causes downregulation of endothelin-1 mRNA in bovine aortic endothelium.* Am J Physiol, 1992. **263**(2 Pt 1): p. C389-96.

441. Morita, T., et al., *Disruption of cytoskeletal structures mediates shear stress-induced endothelin-1 gene expression in cultured porcine aortic endothelial cells.* J Clin Invest, 1993. **92**(4): p. 1706-12.

442. Kuchan, M.J. and J.A. Frangos, *Shear stress regulates endothelin-1 release via protein kinase C and cGMP in cultured endothelial cells.* Am J Physiol Heart Circ Physiol, 1993. **264**(1 Pt 2): p. H150-6.

443. Eskin, S.G., N.A. Turner, and L.V. McIntire, *Endothelial cell cytochrome P450 1A1 and 1B1: up-regulation by shear stress.* Endothelium, 2004. **11**(1): p. 1-10.

444. Yoshizumi, M., et al., *Hemodynamic shear stress stimulates endothelin production by cultured endothelial cells.* Biochem Biophys Res Commun, 1989. **161**(2): p. 859-64.

445. Frangos, J.A., et al., *Flow effects on prostacyclin production by cultured human endothelial cells.* Science, 1985. **227**(4693): p. 1477-9.

446. Okahara, K., B. Sun, and J. Kambayashi, *Upregulation of prostacyclin synthesis-related gene expression by shear stress in vascular endothelial cells.* Arterioscler Thromb Vasc Biol, 1998. **18**(12): p. 1922-6.

447. Grabowski, E.F., E.A. Jaffe, and B.B. Weksler, *Prostacyclin production by cultured endothelial cell monolayers exposed to step increases in shear stress.* The Journal of laboratory and clinical medicine, 1985. **105**(1): p. 36-43.

448. Resnick, N., et al., *Platelet-derived growth factor B chain promoter contains a cis-acting fluid shear-stress-responsive element.* Proc Natl Acad Sci U S A, 1993. **90**(10): p. 4591-5.

449. Aromatario, C., et al., *Fluid shear stress increases the release of platelet derived growth factor BB (PDGF BB) by aortic endothelial cells.* Minerva cardioangiologica, 1997. **45**(1-2): p. 1-7.

450. Khachigian, L.M., et al., *Nuclear factor-kappa B interacts functionally with the platelet-derived growth factor B-chain shear-stress response element in vascular endothelial cells exposed to fluid shear stress.* J Clin Invest, 1995. **96**(2): p. 1169-75.

451. Ohno, M., et al., *Fluid shear stress induces endothelial transforming growth factor beta-1 transcription and production. Modulation by potassium channel blockade.* J Clin Invest, 1995. **95**(3): p. 1363-9.

452. Cucina, A., et al., *Shear stress induces transforming growth factor-beta 1 release by arterial endothelial cells.* Surgery, 1998. **123**(2): p. 212-7.

453. Tsuboi, H., et al., *Flow stimulates ICAM-1 expression time and shear stress dependently in cultured human endothelial cells.* Biochem Biophys Res Commun, 1995. **206**(3): p. 988-96.

454. Shyy, J.Y., et al., *The cis-acting phorbol ester "12-O-tetradecanoylphorbol 13-acetate"-responsive element is involved in shear stress-induced monocyte chemotactic protein 1 gene expression.* Proc Natl Acad Sci U S A, 1995. **92**(17): p. 8069-73.

455. Fernandez, P., et al., *Gene Response in Endothelial Cells Cultured on Engineered Surfaces Is Regulated by Shear Stress.* Tissue Eng, 2007.

456. Vara, D.S., et al., *The effect of shear stress on human endothelial cells seeded on cylindrical viscoelastic conduits: an investigation of gene expression.* Biotechnology and applied biochemistry, 2006. **45**(Pt 3): p. 119-30.

457. Yao, Y., A. Rabodzey, and C.F. Dewey, *Glycocalyx modulates the motility and proliferative response of vascular endothelium to fluid shear stress.* Am J Physiol Heart Circ Physiol, 2007.

458. Noria, S., et al., *Transient and steady-state effects of shear stress on endothelial cell adherens junctions.* Circ Res, 1999. **85**(6): p. 504-14.

459. Lin, M.C., et al., *Shear stress induction of the tissue factor gene.* J Clin Invest, 1997. **99**(4): p. 737-44.

460. Malek, A.M., et al., *Endothelial expression of thrombomodulin is reversibly regulated by fluid shear stress.* Circ Res, 1994. **74**(5): p. 852-60.

461. Takada, Y., et al., *Fluid shear stress increases the expression of thrombomodulin by cultured human endothelial cells.* Biochem Biophys Res Commun, 1994. **205**(2): p. 1345-52.

462. Westmuckett, A.D., et al., *Fluid flow induces upregulation of synthesis and release of tissue factor pathway inhibitor in vitro.* Arterioscler Thromb Vasc Biol, 2000. **20**(11): p. 2474-82.

463. Inoue, H., et al., *Transcriptional and posttranscriptional regulation of cyclooxygenase-2 expression by fluid shear stress in vascular endothelial cells.* Arterioscler Thromb Vasc Biol, 2002. **22**(9): p. 1415-20.

464. Inoue, N., et al., *Shear stress modulates expression of Cu/Zn superoxide dismutase in human aortic endothelial cells.* Circ Res, 1996. **79**(1): p. 32-7.

465. Cohnheim, J., Arch Path Anat Physiol Klin Med, 1867. **40**: p. 1.

466. Friedenstein, A.J., *Precursor cells of mechanocytes.* Int Rev Cytol, 1976. **47**: p. 327-59.

467. Friedenstein, A.J., *Stromal Mechanisms of Bone Marrow: Cloning in vitro and Retransplantation in vivo*, in *Immunology of Bone Marrow Transplantation*, S. Thienfelder, H. Rodt, and H.J. Kolb, Editors. 1980, Springer-Verlag: Berlin. p. 19-20.

468. Friedenstein, A.J., et al., *Stromal cells responsible for transferring the microenvironment of the hemopoietic tissues. Cloning in vitro and retransplantation in vivo.* Transplantation, 1974. **17**(4): p. 331-40.

469. Friedenstein, A.J., et al., *Heterotopic of bone marrow. Analysis of precursor cells for osteogenic and hematopoietic tissues.* Transplantation, 1968. **6**(2): p. 230-47.

470. Dexter, T.M., et al., *Stimulation of differentiation and proliferation of haemopoietic cells in vitro.* J Cell Physiol, 1973. **82**(3): p. 461-73.

471. Dexter, T.M. and L.G. Lajtha, *Proliferation of haemopoietic stem cells in vitro.* Br J Haematol, 1974. **28**(4): p. 525-30.

472. Dexter, T.M., et al., *Congenital and induced defects in haemopoietic environments, stem cell proliferation and differentiation.* Hamatol Bluttransfus, 1979. **24**: p. 73-8.

473. Lee, J.Y., et al., *Clonal isolation of muscle-derived cells capable of enhancing muscle regeneration and bone healing.* J Cell Biol, 2000. **150**(5): p. 1085-100.

474. Lee, J.Y., et al., *Effect of bone morphogenetic protein-2-expressing muscle-derived cells on healing of critical-sized bone defects in mice.* J Bone Joint Surg Am, 2001. **83-A**(7): p. 1032-9.

475. Van Epps, D.E., et al., *Harvesting, characterization, and culture of CD34+ cells from human bone marrow, peripheral blood, and cord blood.* Blood Cells, 1994. **20**(2-3): p. 411-23.

476. Fliedner, T.M., *The role of blood stem cells in hematopoietic cell renewal.* Stem Cells, 1998. **16 Suppl 1**: p. 13-29.

477. Huss, R., *Isolation of Primary and Immortalized CD34- Hematopoietic and Mesenchymal Stem Cells from Various Sources.* Stem Cells, 2000. **18**(1): p. 1-9.

478. Fukuda, J., et al., *Direct measurement of CD34+ blood stem cell absolute counts by flow cytometry.* Stem Cells, 1998. **16**(4): p. 294-300.

479. Koizumi, K., et al., *In vitro expansion of CD34+/CD41+ cells from human peripheral blood CD34+/CD41- cells: role of cytokines for in vitro proliferation and differentiation of megakaryocytic progenitors.* Exp Hematol, 1998. **26**(12): p. 1140-7.

480. Bojanic, I. and B. Golubic Cepulic, *[Umbilical cord blood as a source of stem cells].* Acta Med Croatica, 2006. **60**(3): p. 215-25.

481. Lu, L.L., et al., *Isolation and characterization of human umbilical cord mesenchymal stem cells with hematopoiesis-supportive function and other potentials.* Haematologica, 2006. **91**(8): p. 1017-26.

482. Zuk, P.A., et al., *Multilineage cells from human adipose tissue: implications for cell-based therapies.* Tissue Eng, 2001. **7**(2): p. 211-28.

483. Cao, Y., et al., *Human adipose tissue-derived stem cells differentiate into endothelial cells in vitro and improve postnatal neovascularization in vivo*
Human adipose tissue as a source of Flk-1+ cells: new method of differentiation and expansion. Biochem Biophys Res Commun, 2005. **332**(2): p. 370-9.

484. Martinez-Estrada, O.M., et al., *Human adipose tissue as a source of Flk-1+ cells: new method of differentiation and expansion.* Cardiovasc Res, 2005. **65**(2): p. 328-33.

485. Rodriguez, L.V., et al., *Clonogenic multipotent stem cells in human adipose tissue differentiate into functional smooth muscle cells.* Proc Natl Acad Sci U S A, 2006. **103**(32): p. 12167-72.

486. Igura, K., et al., *Isolation and characterization of mesenchymal progenitor cells from chorionic villi of human placenta*
Mesengenic progenitor cells derived from human placenta. Cytotherapy, 2004. **6**(6): p. 543-53.

487. Wulf, G.G., et al., *Mesengenic progenitor cells derived from human placenta.* Tissue Eng, 2004. **10**(7-8): p. 1136-47.

488. Jiang, Y., et al., *Multipotent progenitor cells can be isolated from postnatal murine bone marrow, muscle, and brain.* Exp Hematol, 2002. **30**(8): p. 896-904.

489. Gritti, A., A.L. Vescovi, and R. Galli, *Adult neural stem cells: plasticity and developmental potential.* J Physiol Paris, 2002. **96**(1-2): p. 81-90.

490. Jackson, K.A., et al., *Regeneration of ischemic cardiac muscle and vascular endothelium by adult stem cells.* J Clin Invest, 2001. **107**(11): p. 1395-402.

491. Foster, L.J., et al., *Differential expression profiling of membrane proteins by quantitative proteomics in a human mesenchymal stem cell line undergoing osteoblast differentiation.* Stem Cells, 2005. **23**(9): p. 1367-77.

492. Gronthos, S., et al., *Molecular and cellular characterisation of highly purified stromal stem cells derived from human bone marrow.* J Cell Sci, 2003. **116**(Pt 9): p. 1827-35.

493. Jiang, Y., et al., *Pluripotency of mesenchymal stem cells derived from adult marrow.* Nature, 2002. **418**(6893): p. 41-9.

494. Deans, R.J. and A.B. Moseley, *Mesenchymal stem cells: biology and potential clinical uses.* Exp Hematol, 2000. **28**(8): p. 875-84.

495. Burger, P.E., et al., *Fibroblast growth factor receptor-1 is expressed by endothelial progenitor cells.* Blood, 2002. **100**(10): p. 3527-35.

496. Ashman, L.K., *The biology of stem cell factor and its receptor C-kit.* Int J Biochem Cell Biol, 1999. **31**(10): p. 1037-51.

497. Mohle, R., R. Haas, and W. Hunstein, *Expression of adhesion molecules and c-kit on CD34+ hematopoietic progenitor cells: comparison of cytokine-mobilized blood stem cells with normal bone marrow and peripheral blood.* J Hematother, 1993. **2**(4): p. 483-9.

498. Hill, B., et al., *High-level expression of a novel epitope of CD59 identifies a subset of CD34+ bone marrow cells highly enriched for pluripotent stem cells.* Exp Hematol, 1996. **24**(8): p. 936-43.

499. Reyes, M., et al., *Origin of endothelial progenitors in human postnatal bone marrow.* J Clin Invest, 2002. **109**(3): p. 337-46.

500. Salven, P., et al., *VEGFR-3 and CD133 identify a population of CD34+ lymphatic/vascular endothelial precursor cells.* Blood, 2003. **101**(1): p. 168-72.

501. Gehling, U.M., et al., *In vitro differentiation of endothelial cells from AC133-positive progenitor cells.* Blood, 2000. **95**(10): p. 3106-12.

502. Akhouayri, O., et al., *Effects of static or dynamic mechanical stresses on osteoblast phenotype expression in three-dimensional contractile collagen gels.* J Cell Biochem, 1999. **76**(2): p. 217-30.

503. Nomura, S. and T. Takano-Yamamoto, *Molecular events caused by mechanical stress in bone.* Matrix Biol, 2000. **19**(2): p. 91-6.

504. Okano, T., et al., *Tissue engineering of skeletal muscle. Highly dense, highly oriented hybrid muscular tissues biomimicking native tissues.* ASAIO J, 1997. **43**(5): p. M749-53.

505. Smith, R.L., et al., *In vitro stimulation of articular chondrocyte mRNA and extracellular matrix synthesis by hydrostatic pressure.* J Orthop Res, 1996. **14**(1): p. 53-60.

506. Zeichen, J., M. van Griensven, and U. Bosch, *The proliferative response of isolated human tendon fibroblasts to cyclic biaxial mechanical strain.* Am J Sports Med, 2000. **28**(6): p. 888-92.

507. Altman, G.H., et al., *Cell differentiation by mechanical stress.* FASEB J, 2002. **16**(2): p. 270-2.

508. Gomes, M.E., et al., *In Vitro Localization of Bone Growth Factors in Constructs of Biodegradable Scaffolds Seeded with Marrow Stromal Cells and Cultured in a Flow Perfusion Bioreactor.* Tissue Eng, 2006.

509. Friedenstein, A.J., *Marrow stromal fibroblasts.* Calcif Tissue Int, 1995. **56 Suppl 1**: p. S17.

510. Caplan, A.I., *Mesenchymal stem cells.* J Orthop Res, 1991. **9**(5): p. 641-50.

511. Conget, P.A. and J.J. Minguell, *Phenotypical and functional properties of human bone marrow mesenchymal progenitor cells.* J Cell Physiol, 1999. **181**(1): p. 67-73.

512. Bruder, S.P., D.J. Fink, and A.I. Caplan, *Mesenchymal stem cells in bone development, bone repair, and skeletal regeneration therapy.* J Cell Biochem, 1994. **56**(3): p. 283-94.

513. Prockop, D.J., *Marrow stromal cells as stem cells for nonhematopoietic tissues.* Science, 1997. **276**(5309): p. 71-4.

514. Lanotte, M., et al., *Clonal preadipocyte cell lines with different phenotypes derived from murine marrow stroma: factors influencing growth and adipogenesis in vitro.* J Cell Physiol, 1982. **111**(2): p. 177-86.

515. Friedenstein, A.J., R.K. Chailakhyan, and U.V. Gerasimov, *Bone marrow osteogenic stem cells: in vitro cultivation and transplantation in diffusion chambers.* Cell Tissue Kinet, 1987. **20**(3): p. 263-72.

516. Simmons, P.J. and B. Torok-Storb, *CD34 expression by stromal precursors in normal human adult bone marrow.* Blood, 1991. **78**(11): p. 2848-53.

517. Simmons, P.J. and B. Torok-Storb, *Identification of stromal cell precursors in human bone marrow by a novel monoclonal antibody, STRO-1.* Blood, 1991. **78**(1): p. 55-62.

518. Caplan, A.I., *Review: mesenchymal stem cells: cell-based reconstructive therapy in orthopedics.* Tissue Eng, 2005. **11**(7-8): p. 1198-211.

519. Solchaga, L.A., et al., *Generation of pluripotent stem cells and their differentiation to the chondrocytic phenotype.* Methods Mol Med, 2004. **100**: p. 53-68.

520. Goodell, M.A., et al., *Stem cell plasticity in muscle and bone marrow.* Ann N Y Acad Sci, 2001. **938**: p. 208-18; discussion 218-20.

521. Grounds, M.D., et al., *The role of stem cells in skeletal and cardiac muscle repair.* The Journal of Histochemistry and Cytochemistry, 2002. **50**(5): p. 589-610.

522. Bayes-Genis, A., et al., *Identification of cardiomyogenic lineage markers in untreated human bone marrow-derived mesenchymal stem cells.* Transplant Proc, 2005. **37**(9): p. 4077-9.

523. Zhang, S., et al., *Purified human bone marrow multipotent mesenchymal stem cells regenerate infarcted myocardium in experimental rats.* Cell Transplant, 2005. **14**(10): p. 787-98.

524. Shim, W.S., et al., *Ex vivo differentiation of human adult bone marrow stem cells into cardiomyocyte-like cells.* Biochem Biophys Res Commun, 2004. **324**(2): p. 481-8.

525. Makino, S., et al., *Cardiomyocytes can be generated from marrow stromal cells in vitro.* J Clin Invest, 1999. **103**(5): p. 697-705.

526. Hamilton, D.W., T.M. Maul, and D.A. Vorp, *Characterization of the Response of Bone Marrow Derived Progenitor Cells to Cyclic Strain: Implications for Vascular Tissue Engineering Applications.* Tissue Eng, 2004. **10**(3/4): p. 361-70.

527. Park, J.S., et al., *Differential effects of equiaxial and uniaxial strain on mesenchymal stem cells.* Biotechnol Bioeng, 2004. **88**(3): p. 359-68.

528. Galmiche, M.C., et al., *Stromal cells from human long-term marrow cultures are mesenchymal cells that differentiate following a vascular smooth muscle differentiation pathway.* Blood, 1993. **82**(1): p. 66-76.

529. Arakawa, E., et al., *A mouse bone marrow stromal cell line, TBR-B, shows inducible expression of smooth muscle-specific genes.* FEBS Letters, 2000. **481**(2): p. 193-6.

530. Kobayashi, N., et al., *Mechanical stress promotes the expression of smooth muscle-like properties in marrow stromal cells.* Exp Hematol, 2004. **32**(12): p. 1238-45.

531. Kinner, B., J.M. Zaleskas, and M. Spector, *Regulation of smooth muscle actin expression and contraction in adult human mesenchymal stem cells.* Exp Cell Res, 2002. **278**(1): p. 72-83.

532. Takahashi, T., et al., *Ischemia- and cytokine-induced mobilization of bone marrow-derived endothelial progenitor cells for neovascularization.* Nat Med, 1999. **5**(4): p. 434-8.

533. Oswald, J., et al., *Mesenchymal stem cells can be differentiated into endothelial cells in vitro.* Stem Cells, 2004. **22**(3): p. 377-84.

534. Fujiyama, S., et al., *Bone marrow monocyte lineage cells adhere on injured endothelium in a monocyte chemoattractant protein-1-dependent manner and accelerate reendothelialization as endothelial progenitor cells.* Circ Res, 2003. **93**(10): p. 980-9.

535. Tropel, P., et al., *Functional neuronal differentiation of bone marrow-derived mesenchymal stem cells.* Stem Cells, 2006.

536. Zemchikhina, V.N. and O.N. Golubeva, *The capacity of mesenchymal stem cells for neural differentiation in vitro.* Tsitologiia, 2005. **47**(7): p. 644-8.

537. Wakitani, S., T. Saito, and A.I. Caplan, *Myogenic cells derived from rat bone marrow mesenchymal stem cells exposed to 5-azacytidine.* Muscle and Nerve, 1995. **18**(12): p. 1417-26.

538. Maniatopoulos, C., J. Sodek, and A.H. Melcher, *Bone formation in vitro by stromal cells obtained from bone marrow of young adult rats.* Cell Tissue Res, 1988. **254**(2): p. 317-30.

539. Locklin, R.M., et al., *In vitro effects of growth factors and dexamethasone on rat marrow stromal cells.* Clin Orthop, 1995(313): p. 27-35.

540. Jaiswal, N., et al., *Osteogenic differentiation of purified, culture-expanded human mesenchymal stem cells in vitro.* J Cell Biochem, 1997. **64**(2): p. 295-312.

541. Rabbany, S.Y., et al., *Molecular pathways regulating mobilization of marrow-derived stem cells for tissue revascularization.* Trends Mol Med, 2003. **9**(3): p. 109-17.

542. Quirici, N., et al., *Differentiation and expansion of endothelial cells from human bone marrow CD133(+) cells.* Br J Haematol, 2001. **115**(1): p. 186-94.

543. Caplice, N.M. and B. Doyle, *Vascular progenitor cells: origin and mechanisms of mobilization, differentiation, integration, and vasculogenesis.* Stem Cells Dev, 2005. **14**(2): p. 122-39.

544. Iwaguro, H., et al., *Endothelial progenitor cell vascular endothelial growth factor gene transfer for vascular regeneration.* Circulation, 2002. **105**(6): p. 732-8.

545. Wijelath, E.S., et al., *Fibronectin promotes VEGF-induced CD34 cell differentiation into endothelial cells.* J Vasc Surg, 2004. **39**(3): p. 655-60.

546. Li, T.S., et al., *Improved angiogenic potency by implantation of ex vivo hypoxia prestimulated bone marrow cells in rats.* Am J Physiol Heart Circ Physiol, 2002. **283**(2): p. H468-73.

547. Asahara, T., et al., *Isolation of putative progenitor endothelial cells for angiogenesis.* Science, 1997. **275**(5302): p. 964-7.

548. Asahara, T., et al., *VEGF contributes to postnatal neovascularization by mobilizing bone marrow-derived endothelial progenitor cells.* EMBO J, 1999. **18**(14): p. 3964-72.

549. Broxmeyer, H.E., et al., *Myeloid progenitor cell regulatory effects of vascular endothelial cell growth factor.* Int J Hematol, 1995. **62**(4): p. 203-15.

550. Marcelin-Jimenez, G. and B. Escalante, *Functional and cellular interactions between nitric oxide and prostacyclin.* 2001. **129**(4): p. 349-59.

551. Kim, D.H., et al., *Gene expression profile of cytokine and growth factor during differentiation of bone marrow-derived mesenchymal stem cell.* Cytokine, 2005. **31**(2): p. 119-26.

552. Charbord, P., et al., *The cytoskeleton of stromal cells from human bone marrow cultures resembles that of cultured smooth muscle cells.* Exp Hematol, 1990. **18**(4): p. 276-82.

553. Shoji, M., et al., *Temporal and spatial characterization of cellular constituents during neointimal hyperplasia after vascular injury: Potential contribution of bone-marrow-derived progenitors to arterial remodeling.* Cardiovasc Pathol, 2004. **13**(6): p. 306-12.

554. Cogan, J.G., et al., *Vascular Smooth Muscle alpha -Actin Gene Transcription during Myofibroblast Differentiation Requires Sp1/3 Protein Binding Proximal to the MCAT Enhancer.* J. Biol. Chem., 2002. **277**(39): p. 36433-36442.

555. Jerareungrattan, A., M. Sila-asna, and A. Bunyaratvej, *Increased smooth muscle actin expression from bone marrow stromal cells under retinoic acid treatment: an attempt for autologous blood vessel tissue engineering.* Asian Pacific journal of allergy and immunology / launched by the Allergy and Immunology Society of Thailand, 2005. **23**(2-3): p. 107-13.

556. Barry, F., et al., *Chondrogenic differentiation of mesenchymal stem cells from bone marrow: differentiation-dependent gene expression of matrix components.* Exp Cell Res, 2001. **268**(2): p. 189-200.

557. Nieponice, A., et al., *Mechanical stimulation induces morphological and phenotypic changes in bone marrow-derived progenitor cells within a three-dimensional fibrin matrix.* J Biomed Mater Res A, 2006.

558. Kurpinski, K., et al., *Anisotropic mechanosensing by mesenchymal stem cells.* Proc Natl Acad Sci U S A, 2006. **103**(44): p. 16095-100.

559. Song, G., et al., *Mechanical stretch promotes proliferation of rat bone marrow mesenchymal stem cells.* Colloids and surfaces, 2007. **58**(2): p. 271-7.

560. Thomas, G.P. and A.J. el-Haj, *Bone marrow stromal cells are load responsive in vitro.* Calcif Tissue Int, 1996. **58**(2): p. 101-8.

561. Ku, C.H., et al., *Collagen synthesis by mesenchymal stem cells and aortic valve interstitial cells in response to mechanical stretch.* Cardiovasc Res, 2006. **71**(3): p. 548-56.

562. David, V., et al., *Mechanical Loading Down-Regulates Peroxisome Proliferator-Activated Receptor {gamma} in Bone Marrow Stromal Cells and Favors Osteoblastogenesis at the Expense of Adipogenesis.* Endocrinology, 2007. **148**(5): p. 2553-2562.

563. Yoshikawa, T., et al., *Biochemical analysis of the response in rat bone marrow cell cultures to mechanical stimulation.* Biomed Mater Eng, 1997. **7**(6): p. 369-77.

564. Jagodzinski, M., et al., *Effects of cyclic longitudinal mechanical strain and dexamethasone on osteogenic differentiation of human bone marrow stromal cells.* European cells & materials, 2004. **7**: p. 35-41; discussion 41.

565. Jing, Y., et al., *The effect of mechanical strain on proliferation and osteogenic differentiation of bone marrow mesenchymal stem cells from rats.* Sheng wu yi xue gong cheng xue za zhi = Journal of biomedical engineering = Shengwu yixue gongchengxue zazhi, 2006. **23**(3): p. 542-5.

566. Engelmayr, G.C., Jr., et al., *Cyclic flexure and laminar flow synergistically accelerate mesenchymal stem cell-mediated engineered tissue formation: Implications for engineered heart valve tissues.* Biomaterials, 2006. **27**(36): p. 6083-95.

567. Yamamoto, K., et al., *Fluid shear stress induces differentiation of Flk-1-positive embryonic stem cells into vascular endothelial cells in vitro.* Am J Physiol Heart Circ Physiol, 2005. **288**(4): p. H1915-24.

568. Wang, H., et al., *Shear stress induces endothelial differentiation from a murine embryonic mesenchymal progenitor cell line.* Arterioscler Thromb Vasc Biol, 2005. **25**(9): p. 1817-23.

569. Huang, H., et al., *Differentiation from embryonic stem cells to vascular wall cells under in vitro pulsatile flow loading.* J Artif Organs, 2005. **8**(2): p. 110-8.

570. Li, Y.J., et al., *Oscillatory fluid flow affects human marrow stromal cell proliferation and differentiation.* J Orthop Res, 2004. **22**(6): p. 1283-9.

571. Kreke, M.R. and A.S. Goldstein, *Hydrodynamic shear stimulates osteocalcin expression but not proliferation of bone marrow stromal cells.* Tissue Eng, 2004. **10**(5-6): p. 780-8.

572. Kreke, M.R., W.R. Huckle, and A.S. Goldstein, *Fluid flow stimulates expression of osteopontin and bone sialoprotein by bone marrow stromal cells in a temporally dependent manner.* Bone, 2005. **36**(6): p. 1047-55.

573. Holtorf, H.L., J.A. Jansen, and A.G. Mikos, *Flow perfusion culture induces the osteoblastic differentiation of marrow stroma cell-scaffold constructs in the absence of dexamethasone.* J Biomed Mater Res A, 2005. **72**(3): p. 326-34.

574. Roelofsen, J., J. Klein Nulend, and E.H. Burger, *Mechanical stimulation by intermittent hydrostatic compression promotes bone-specific gene expression in vitro.* J Biomech, 1995. **28**(12): p. 1493-503.

575. Kim, S.H., et al., *ERK 1/2 activation in enhanced osteogenesis of human mesenchymal stem cells in poly(lactic-glycolic acid) by cyclic hydrostatic pressure.* J Biomed Mater Res A, 2007. **80**(4): p. 826-36.

576. Nagatomi, J., et al., *Effects of cyclic pressure on bone marrow cell cultures.* J Biomech Eng, 2002. **124**(3): p. 308-14.

577. Rubin, J., et al., *Pressure regulates osteoclast formation and MCSF expression in marrow culture.* J Cell Physiol, 1997. **170**(1): p. 81-7.

578. Angele, P., et al., *Cyclic hydrostatic pressure enhances the chondrogenic phenotype of human mesenchymal progenitor cells differentiated in vitro.* J Orthop Res, 2003. **21**(3): p. 451-7.

579. Elder, S.H., K.S. Fulzele, and W.R. McCulley, *Cyclic hydrostatic compression stimulates chondroinduction of C3H/10T1/2 cells.* Biomech Model Mechanobiol, 2005. **3**(3): p. 141-6.

580. Miyanishi, K., et al., *Effects of hydrostatic pressure and transforming growth factor-beta 3 on adult human mesenchymal stem cell chondrogenesis in vitro.* Tissue Eng, 2006. **12**(6): p. 1419-28.

581. Finger, A.R., et al., *Differential effects on messenger ribonucleic acid expression by bone marrow-derived human mesenchymal stem cells seeded in agarose constructs due to ramped and steady applications of cyclic hydrostatic pressure.* Tissue Eng, 2007. **13**(6): p. 1151-8.

582. Elder, S.H., et al., *Chondrocyte differentiation is modulated by frequency and duration of cyclic compressive loading.* Ann Biomed Eng, 2001. **29**(6): p. 476-82.

583. Abbott, B.L., *ABCG2 (BCRP) expression in normal and malignant hematopoietic cells.* Hematol Oncol, 2003. **21**(3): p. 115-30.

584. Azuma, N., et al., *Endothelial cell response to different mechanical forces.* J Vasc Surg, 2000. **32**(4): p. 789-94.

585. Garcia-Cardena, G., et al., *Biomechanical activation of vascular endothelium as a determinant of its functional phenotype.* Proc Natl Acad Sci U S A, 2001. **98**(8): p. 4478-85.

586. Joe, P., et al., *Effects of mechanical factors on growth and maturation of the lung in fetal sheep.* Am J Phys, 1997. **272**(1 Pt 1): p. L95-105.

587. Skalak, T.C., R.J. Price, and P.J. Zeller, *Where do new arterioles come from? Mechanical forces and microvessel adaptation.* Microcirculation, 1998. **5**(2-3): p. 91-4.

588. Zhao, S., et al., *Synergistic effects of fluid shear stress and cyclic circumferential stretch on vascular endothelial cell morphology and cytoskeleton.* Arterioscler Thromb Vasc Biol, 1995. **15**(10): p. 1781-6.

589. Han, C.I., G.R. Campbell, and J.H. Campbell, *Circulating bone marrow cells can contribute to neointimal formation.* J Vasc Res, 2001. **38**(2): p. 113-9.

590. Hirschi, K.K. and M.A. Goodell, *Hematopoietic, vascular and cardiac fates of bone marrow-derived stem cells.* Gene Ther, 2002. **9**(10): p. 648-52.

591. Hirschi, K. and M. Goodell, *Common origins of blood and blood vessels in adults?* Differentiation, 2001. **68**(4-5): p. 186-92.

592. Asahara, T. and A. Kawamoto, *Endothelial progenitor cells for postnatal vasculogenesis.* Am J Physiol Cell Physiol, 2004. **287**(3): p. C572-9.

593. Drab, M., et al., *From totipotent embryonic stem cells to spontaneously contracting smooth muscle cells: a retinoic acid and db-cAMP in vitro differentiation model.* FASEB J, 1997. **11**(11): p. 905-15.

594. Skaletz-Rorowski, A., et al., *Protein Kinase C Mediates Basic Fibroblast Growth Factor–Induced Proliferation Through Mitogen-Activated Protein Kinase in Coronary Smooth Muscle Cells.* Arterioscler Thromb Vasc Biol, 1999. **19**(7): p. 1608-1614.

595. Suzuki, T., et al., *Preferential Differentiation of P19 Mouse Embryonal Carcinoma Cells Into Smooth Muscle Cells : Use of Retinoic Acid and Antisense Against the Central Nervous System–Specific POU Transcription Factor Brn-2.* Circ Res, 1996. **78**(3): p. 395-404.

596. Parkkinen, J.J., et al., *Influence of short-term hydrostatic pressure on organization of stress fibers in cultured chondrocytes.* J Orthop Res, 1995. **13**(4): p. 495-502.

597. Hasel, C., et al., *A cell-culture system for long-term maintenance of elevated hydrostatic pressure with the option of additional tension.* J Biomech, 2002. **35**(5): p. 579-84.

598. Pugin, J., et al., *Activation of human macrophages by mechanical ventilation in vitro.* Am J Physiol, 1998. **275**(6 Pt 1): p. L1040-50.

599. Banes, A.J., et al., *Culturing cells in a mechanically active environment.* Am Biotechnol Lab, 1990. **8**(7): p. 12-22.

600. Blackman, B.R., K.A. Barbee, and L.E. Thibault, *In vitro cell shearing device to investigate the dynamic response of cells in a controlled hydrodynamic environment.* Ann Biomed Eng, 2000. **28**(4): p. 363-72.

601. Chiu, J.-J., et al., *A model for studying the effect of shear stress on interactions between vascular endothelial cells and smooth muscle cells.* J Biomech, 2004. **37**(4): p. 531-539.

602. Archambault, J.M., et al., *Rabbit tendon cells produce MMP-3 in response to fluid flow without significant calcium transients.* J Biomech, 2002. **35**(3): p. 303-9.

603. Xing, Y., et al., *Cyclic pressure affects the biological properties of porcine aortic valve leaflets in a magnitude and frequency dependent manner.* Ann Biomed Eng, 2004. **32**(11): p. 1461-70.

604. Williams, R., et al., *Relationship between the humidity and temperature of inspired gas and the function of the airway mucosa.* Crit Care Med, 1996. **24**(11): p. 1920-9.

605. Miller, G., *Handbook of Research Methods in Public Administration*. 1999, New York: Marcel Dekker Inc. 657.

606. *CFD-ACE(U) Modules*. 2002, CFDRC Research Corporation: Huntsville, AL. p. 1-25.

607. Kute, S.M. and D.A. Vorp, *The effect of proximal artery flow on the hemodynamics at the distal anastomosis of a vascular bypass graft: computational study.* J Biomech Eng, 2001. **123**(3): p. 277-83.

608. *ABL 5 Reference Manual*. 1999, Radiometer: Copenhagen, Denmark. p. 3.3.3.

609. Billecocq, A., et al., *1 alpha,25-dihydroxyvitamin D3 regulates the expression of carbonic anhydrase II in nonerythroid avian bone marrow cells.* Proc Natl Acad Sci U S A, 1990. **87**(16): p. 6470-4.

610. Nave, C.R. and B.C. Nave, *Physics for the Health Sciences*. 3rd Ed. ed. 1985, Philadelphia: W. B. Saunders. 430.

611. Parkkinen, J.J., et al., *Effects of cyclic hydrostatic pressure on proteoglycan synthesis in cultured chondrocytes and articular cartilage explants.* Arch Biochem Biophys, 1993. **300**(1): p. 458-65.

612. Whaley, L. and D. Wong, *Nursing Care of Infants and Children*. 5th ed, ed. N. Kline. 1999, St. Louis: Mosby. 1994.

613. Javazon, E.H., et al., *Rat Marrow Stromal Cells are More Sensitive to Plating Density and Expand More Rapidly from Single-Cell-Derived Colonies than Human Marrow Stromal Cells.* Stem Cells, 2001. **19**(3): p. 219-225.

614. Simione, F.P., *Cryopreservation Manual*. 1998, Nalge Nunc International. p. 15.

615. Li, C., et al., *Cyclic strain stress-induced mitogen-activated protein kinase (MAPK) phosphatase 1 expression in vascular smooth muscle cells is regulated by Ras/Rac-MAPK pathways.* J Biol Chem, 1999. **274**(36): p. 25273-80.

616. Sumpio, B.E. and A.J. Banes, *Prostacyclin synthetic activity in cultured aortic endothelial cells undergoing cyclic mechanical deformation.* Surgery, 1988. **104**(2): p. 383-9.

617. Sumpio, B.E., et al., *Modulation of endothelial cell phenotype by cyclic stretch: inhibition of collagen production.* The Journal of Surgical Research, 1990. **48**(5): p. 415-20.

618. Sumpio, B.E., et al., *Regulation of tPA in endothelial cells exposed to cyclic strain: role of CRE, AP-2, and SSRE binding sites.* Am J Physiol, 1997. **273**(5 Pt 1): p. C1441-8.

619. Sun, H.B., et al., *Model-based analysis of matrix metalloproteinase expression under mechanical shear.* Ann Biomed Eng, 2003. **31**(2): p. 171-80.

620. Elfervig, M.K., et al., *IL-1beta sensitizes intervertebral disc annulus cells to fluid-induced shear stress.* J Cell Biochem, 2001. **82**(2): p. 290-8.

621. Lennon, D.P., J.M. Edmison, and A.I. Caplan, *Cultivation of Rat Marrow-Derived Mesenchymal Stem Cells in Reduced Oxygen Tension: Effects on In Vitro and In Vivo Osteochondrogenesis.* J Cell Physiol, 2001. **187**: p. 345-355.

622. Ishikawa, Y. and T. Ito, *Kinetics of hemopoietic stem cells in a hypoxic culture.* Eur J Haematol, 1988. **40**(2): p. 126-9.

623. Annabi, B., et al., *Hypoxia promotes murine bone-marrow-derived stromal cell migration and tube formation.* Stem Cells, 2003. **21**(3): p. 337-47.

624. Salasznyk, R.M., et al., *Adhesion to Vitronectin and Collagen I Promotes Osteogenic Differentiation of Human Mesenchymal Stem Cells.* J Biomed Biotechnol, 2004. **2004**(1): p. 24-34.

625. Davis, G.E. and D.R. Senger, *Endothelial extracellular matrix: biosynthesis, remodeling, and functions during vascular morphogenesis and neovessel stabilization.* Circ Res, 2005. **97**(11): p. 1093-107.

626. Lan, C.W., F.F. Wang, and Y.J. Wang, *Osteogenic enrichment of bone-marrow stromal cells with the use of flow chamber and type I collagen-coated surface.* J Biomed Mater Res A, 2003. **66**(1): p. 38-46.

627. Lan, C.W. and Y.J. Wang, *Collagen as an immobilization vehicle for bone marrow stromal cells enriched with osteogenic potential.* Artif Cells Blood Substit Immobil Biotechnol, 2003. **31**(1): p. 59-68.

628. Hamilton, D.W., et al. *Characterization of rabbit bone marrow stromal cells for use in vascular tissue engineering*. in *Engineering Tissue Growth Conference and Exposition*. 2001. Marriott Hotel, Pittsburgh, PA.

629. Hamilton, D.W., et al., *The response of primary articular chondrocytes to micrometric surface topography and sulphated hyaluronic acid-based matrices.* Cell Biol Int, 2005. **29**(8): p. 605-15.

630. Hamilton, D.W., et al., *Articular chondrocyte passage number: influence on adhesion, migration, cytoskeletal organisation and phenotype in response to nano- and micro-metric topography.* Cell Biol Int, 2005. **29**(6): p. 408-21.

631. Kataoka, N., S. Ujita, and M. Sato, *Effect of flow direction on the morphological responses of cultured bovine aortic endothelial cells.* Med Biol Eng Comput, 1998. **36**(1): p. 122-8.

632. Sugaya, Y., et al., *Elongation and random orientation of bovine endothelial cells in response to hydrostatic pressure: comparison with response to shear stress.* JSME Int. J., Ser C, 2003. **46**: p. 1248–1255.

633. Chomczynski, P., *A reagent for the single-step simultaneous isolation of RNA, DNA and proteins from cell and tissue samples.* BioTechniques, 1993. **15**(3): p. 532-4, 536-7.

634. Chomczynski, P. and N. Sacchi, *Single-step method of RNA isolation by acid guanidinium thiocyanate-phenol-chloroform extraction.* Anal Biochem, 1987. **162**(1): p. 156-9.

635. *RNeasy Mini Handbook*. 2006, Qiagen. p. 88.

636. Livak, K.J. and T.D. Schmittgen, *Analysis of Relative Gene Expression Data Using Real-Time Quantitative PCR and the 2-[Delta][Delta]CT Method.* Methods, 2001. **25**(4): p. 402-408.

637. Kent, W., *A Simple Guide to Five Normal Forms in Relational Database Theory.* Communications of the ACM, 1983. **26**(2): p. 120-125.

638. Rosner, B., *Fundamentals of Biostatistics*. 5th ed. 2000, Pacific Grove, CA: Duxbury. 792.

639. Keppel, G. and T.D. Wickens, *Design and analysis: A researchers handbook*. 4th ed. 2004, Upper Saddle River, NJ: Pearson.

640. Moore, B.R., *A Modification of the Rayleigh Test for Vector Data.* Biometrika, 1980. **67**(1.): p. 175-180.

641. Naruse, K., T. Yamada, and M. Sokabe, *Involvement of SA channels in orienting response of cultured endothelial cells to cyclic stretch.* Am J Physiol Heart Circ Physiol, 1998. **274**(5): p. H1532-1538.

642. Poole, K., et al., *Molecular-scale Topographic Cues Induce the Orientation and Directional Movement of Fibroblasts on Two-dimensional Collagen Surfaces.* Journal of Molecular Biology, 2005. **349**(2): p. 380-386.

643. Johnson, E.C., et al., *Global Changes in Optic Nerve Head Gene Expression after Exposure to Elevated Intraocular Pressure in a Rat Glaucoma Model.* Invest. Ophthalmol. Vis. Sci., 2007. **48**(7): p. 3161-3177.

644. Hammond, J.P., et al., *Using genomic DNA-based probe-selection to improve the sensitivity of high-density oligonucleotide arrays when applied to heterologous species.* Plant Methods, 2005. **1**(1): p. 10.

645. Stover, J. and J. Nagatomi, *Cyclic Pressure Stimulates DNA Synthesis through the PI3K/Akt Signaling Pathway in Rat Bladder Smooth Muscle Cells.* Ann Biomed Eng, 2007. **35**(9): p. 1585-94.

646. Schwartz, E.A., et al., *Exposure of human vascular endothelial cells to sustained hydrostatic pressure stimulates proliferation. Involvement of the alphaV integrins.* Circ Res, 1999. **84**(3): p. 315-22.

647. Lee, W.C., et al., *Effects of uniaxial cyclic strain on adipose-derived stem cell morphology, proliferation, and differentiation.* Biomech Model Mechanobiol, 2006.

648. Kanda, K. and T. Matsuda, *Behavior of arterial wall cells cultured on periodically stretched substrates.* Cell Transplant, 1993. **2**(6): p. 475-84.

649. Wasserman, S.M., et al., *Gene expression profile of human endothelial cells exposed to sustained fluid shear stress.* Physiol Genomics, 2002. **12**(1): p. 13-23.

650. Riha, G.M., et al., *Cyclic strain induces vascular smooth muscle cell differentiation from murine embryonic mesenchymal progenitor cells.* Surgery, 2007. **141**(3): p. 394-402.

651. Yamamoto, K., et al., *Proliferation, differentiation, and tube formation by endothelial progenitor cells in response to shear stress.* J Appl Physiol, 2003. **95**(5): p. 2081-8.

652. Yamashita, J.K., *Differentiation and diversification of vascular cells from embryonic stem cells.* Int J Hematol, 2004. **80**(1): p. 1-6.

653. Kurpinski, K., et al., *Regulation of vascular smooth muscle cells and mesenchymal stem cells by mechanical strain.* Mol Cell Biomech, 2006. **3**(1): p. 21-34.

654. Liu, Y., et al., *Kruppel-like factor 4 abrogates myocardin-induced activation of smooth muscle gene expression.* J Biol Chem, 2005. **280**(10): p. 9719-27.

655. Yoshida, T., et al., *Platelet-derived growth factor-BB represses smooth muscle cell marker genes via changes in binding of MKL factors and histone deacetylases to their promoters.* Am J Physiol Cell Physiol, 2007. **292**(2): p. C886-95.

656. Wang, Z., et al., *Myocardin and ternary complex factors compete for SRF to control smooth muscle gene expression.* Nature, 2004. **428**(6979): p. 185-9.

657. Vandesompele, J., et al., *Accurate normalization of real-time quantitative RT-PCR data by geometric averaging of multiple internal control genes.* Genome biology, 2002. **3**(7): p. RESEARCH0034.

658. Balharry, D., V. Oreffo, and R. Richards, *Use of toxicogenomics for identifying genetic markers of pulmonary oedema.* Toxicology and Applied Pharmacology, 2005. **204**(2): p. 101-108.

659. Murray, T.R., B.E. Marshall, and E.J. Macarak, *Contraction of vascular smooth muscle in cell culture.* J Cell Physiol, 1990. **143**(1): p. 26-38.

660. Perlingeiro, R.C.R., *Endoglin is required for hemangioblast and early hematopoietic development.* Development, 2007. **134**(16): p. 3041-3048.

661. Wu, Y., et al., *TGF[beta]1 regulation of vimentin gene expression during differentiation of the C2C12 skeletal myogenic cell line requires Smads, AP-1 and Sp1 family members.* Biochimica et Biophysica Acta (BBA) - Molecular Cell Research, 2007. **1773**(3): p. 427-439.

662. Ito, M., *Factors controlling cyclin B expression.* Plant molecular biology, 2000. **43**(5-6): p. 677-90.

663. Dheda, K., et al., *The implications of using an inappropriate reference gene for real-time reverse transcription PCR data normalization.* Anal Biochem, 2005. **344**(1): p. 141-143.

664. Adam, P.J., G.J. Clesham, and P.L. Weissberg, *Expression of endoglin mRNA and protein in human vascular smooth muscle cells.* Biochem Biophys Res Commun, 1998. **247**(1): p. 33-7.

665. Conley, B.A., et al., *Endoglin, a TGF-beta receptor-associated protein, is expressed by smooth muscle cells in human atherosclerotic plaques.* Atherosclerosis, 2000. **153**(2): p. 323-35.

666. Rodriguez-Barbero, A., et al., *Endoglin expression in human and rat mesangial cells and its upregulation by TGF-beta1.* Biochem Biophys Res Commun, 2001. **282**(1): p. 142-7.

667. Sauvage, M., et al., *Localization of elastin mRNA and TGF-beta1 in rat aorta and caudal artery as a function of age.* Cell Tissue Res, 1998. **291**(2): p. 305-14.

668. Massague, J., *The TGF-beta family of growth and differentiation factors.* Cell, 1987. **49**(4): p. 437-8.

669. Massague, J. and R.R. Gomis, *The logic of TGFbeta signaling.* FEBS Lett, 2006. **580**(12): p. 2811-20.

670. Isoda, K., et al., *Osteopontin plays an important role in the development of medial thickening and neointimal formation.* Circ Res, 2002. **91**(1): p. 77-82.

671. Xie, Z., et al., *Regulation of angiotensin II-stimulated osteopontin expression in cardiac microvascular endothelial cells: role of p42/44 mitogen-activated protein kinase and reactive oxygen species.* J Cell Physiol, 2001. **188**(1): p. 132-8.

672. Ikeda, T., et al., *Osteopontin mRNA is expressed by smooth muscle-derived foam cells in human atherosclerotic lesions of the aorta.* J Clin Invest, 1993. **92**(6): p. 2814-20.

673. Butler, W.T., *The nature and significance of osteopontin.* Connective tissue research, 1989. **23**(2-3): p. 123-36.

674. Ruoslahti, E., *Fibronectin and its receptors.* Annu Rev Biochem, 1988. **57**: p. 375-413.

675. Liao, X.D., et al., *Mechanical stretch induces mitochondria-dependent apoptosis in neonatal rat cardiomyocytes and G2/M accumulation in cardiac fibroblasts.* Cell research, 2004. **14**(1): p. 16-26.

676. Garcia-Cardena, G., et al., *Biomechanical activation of vascular endothelium as a determinant of its functional phenotype.* Proc Natl Acad Sci U S A, 2001. **98**(8): p. 4478-85.

677. Wasserman, S.M. and J.N. Topper, *Adaptation of the endothelium to fluid flow: in vitro analyses of gene expression and in vivo implications.* Vascular medicine (London, England), 2004. **9**(1): p. 35-45.

678. Hegner, B., et al., *Differential regulation of smooth muscle markers in human bone marrow-derived mesenchymal stem cells.* J Hypertens, 2005. **23**(6): p. 1191-202.

679. Remy Martin, J.P., et al., *Vascular smooth muscle differentiation of murine stroma: a sequential model.* Exp Hematol, 1999. **27**(12): p. 1782-95.

680. Ding, R., et al., *Endothelial-mesenchymal interactions in vitro reveal molecular mechanisms of smooth muscle/pericyte differentiation.* Stem Cells Dev, 2004. **13**(5): p. 509-20.

681. Zeng, X., et al., *TGF-beta1 perturbs vascular development and inhibits epithelial differentiation in fetal lung in vivo.* Dev Dyn, 2001. **221**(3): p. 289-301.

682. Minami, T., R.D. Rosenberg, and W.C. Aird, *Transforming growth factor-beta 1-mediated inhibition of the flk-1/KDR gene is mediated by a 5'-untranslated region palindromic GATA site.* J Biol Chem, 2001. **276**(7): p. 5395-402.

683. Mandriota, S.J., P.A. Menoud, and M.S. Pepper, *Transforming growth factor beta 1 down-regulates vascular endothelial growth factor receptor 2/flk-1 expression in vascular endothelial cells.* J Biol Chem, 1996. **271**(19): p. 11500-5.

684. Nieponice, A., et al., *Development of a Tissue-engineered Vascular Graft Combining a Biodegradable Elastomeric Scaffold, Muscle-derived Stem Cells and In-vivo Remodeling in a Rat Model* in *Tissue Engineering and Regenerative Medicine International Society, North America*. 2007: Toronto, Canada.

685. Tian, Q., et al., *Integrated genomic and proteomic analyses of gene expression in Mammalian cells.* Mol Cell Proteomics, 2004. **3**(10): p. 960-9.

686. Grove, A.D., et al., *Both protein activation and gene expression are involved in early vascular tube formation in vitro.* Clin Cancer Res, 2002. **8**(9): p. 3019-26.

687. Unwin, R.D., et al., *Quantitative proteomics reveals posttranslational control as a regulatory factor in primary hematopoietic stem cells.* Blood, 2006. **107**(12): p. 4687-94.

688. Pratt, J.M., et al., *Dynamics of protein turnover, a missing dimension in proteomics.* Mol Cell Proteomics, 2002. **1**(8): p. 579-91.

689. Williams, D.F., *To engineer is to create: the link between engineering and regeneration.* Trends Biotechnol, 2006. **24**(1): p. 4-8.

690. Tamama, K., et al., *Epidermal growth factor as a candidate for ex vivo expansion of bone marrow-derived mesenchymal stem cells.* Stem Cells, 2006. **24**(3): p. 686-95.

691. Janes, K.A., et al., *A systems model of signaling identifies a molecular basis set for cytokine-induced apoptosis.* Science, 2005. **310**(5754): p. 1646-53.

692. Janes, K.A., et al., *Cue-signal-response analysis of TNF-induced apoptosis by partial least squares regression of dynamic multivariate data.* J Comput Biol, 2004. **11**(4): p. 544-61.

693. Hautaniemi, S., et al., *Modeling of signal-response cascades using decision tree analysis.* Bioinformatics, 2005. **21**(9): p. 2027-35.

694. Janes, K.A., et al., *A high-throughput quantitative multiplex kinase assay for monitoring information flow in signaling networks: application to sepsis-apoptosis.* Mol Cell Proteomics, 2003. **2**(7): p. 463-73.

695. Kopf, E. and D. Zharhary, *Antibody Arrays - An Emerging Tool in Cancer Proteomics.* Int J Biochem Cell Biol. **In Press, Accepted Manuscript**(39): p. 7-8.

696. Tannu, N.S. and S.E. Hemby, *Methods for proteomics in neuroscience.* Progress in brain research, 2006. **158**: p. 41-82.

697. Wang, D., et al., *Proteomic profiling of bone marrow mesenchymal stem cells upon TGF-beta stimulation.* J Biol Chem, 2004. **9**: p. 9.

698. Nielsen, U.B., et al., *Profiling receptor tyrosine kinase activation by using Ab microarrays.* Proc Natl Acad Sci U S A, 2003. **100**(16): p. 9330-5.

699. Schmidt, B.T., et al., *Robotic Cell culture System for Stem Cell Assays.* Industrial Robot, 2007. **In Press**.

700. Deasy, B.M., et al., *Mechanisms of muscle stem cell expansion with cytokines.* Stem Cells, 2002. **20**(1): p. 50-60.

701. Deasy, B.M., et al., *A role for cell sex in stem cell-mediated skeletal muscle regeneration: female cells have higher muscle regeneration efficiency.* J Cell Biol, 2007. **177**(1): p. 73-86.

702. Deasy, B.M., et al., *Modeling stem cell population growth: incorporating terms for proliferative heterogeneity.* Stem Cells, 2003. **21**(5): p. 536-45.

703. Jankowski, R.J., et al., *The role of CD34 expression and cellular fusion in the regeneration capacity of myogenic progenitor cells.* J Cell Sci, 2002. **115**(Pt 22): p. 4361-74.

704. Becker, S.A., *Developing Quality Complex Database Systems: Practices, Techniques and Technologies*. 2001, Hershey, PA: Idea Group Publishing. 374.

705. Holderman, M.T., et al., *Identification of albumin precursor protein, Phi AP3, and alpha-smooth muscle actin as novel components of redox sensing machinery in vascular smooth muscle cells.* Molecular pharmacology, 2002. **61**(5): p. 1174-83.